

Autophagy: Molecular insights into its role and therapeutic potential in bladder cancer and neurodegeneration

Inaugural-Dissertation

zur Erlangung des Doktorgrades
der Mathematisch-Naturwissenschaftlichen Fakultät
der Heinrich-Heine-Universität Düsseldorf

vorgelegt von

David Schlütermann

aus Lüdinghausen

Düsseldorf, Dezember 2020

aus dem Institut für Molekulare Medizin I
der Heinrich-Heine-Universität Düsseldorf

Gedruckt mit der Genehmigung der
Mathematisch-Naturwissenschaftlichen Fakultät der
Heinrich-Heine-Universität Düsseldorf

Berichtersteller:

1. Univ.-Prof. Dr. Björn Stork
2. Univ.-Prof. Dr. Holger Stark

Tag der mündlichen Prüfung:

25.02.2021

Eidesstattliche Erklärung

Ich versichere an Eides Statt, dass die Dissertation von mir selbständig und ohne unzulässige fremde Hilfe unter Beachtung der „Grundsätze zur Sicherung guter wissenschaftlicher Praxis an der Heinrich-Heine-Universität Düsseldorf“ erstellt worden ist. Die vorliegende Arbeit wurde von mir selbständig verfasst und keine anderen als die angegebenen Hilfsmittel verwendet. Alle wörtlich oder inhaltlich übernommenen Stellen habe ich als solche gekennzeichnet. Zudem versichere ich, dass ich die vorliegende Dissertation nur in diesem und keinem anderen Promotionsverfahren eingereicht habe und diesem kein früheres Promotionsverfahren vorausgegangen ist.

Ort, Datum

David Schlütermann

Acknowledgement

An dieser Stelle möchte ich allen Beteiligten, die mich bei der Erstellung meiner Dissertation unterstützt haben, meine große Dankbarkeit aussprechen.

Ganz besonders bedanken möchte ich mich bei meinem Doktorvater Prof. Björn Stork für die hervorragende Betreuung, zahlreiche konstruktive Diskussionen und seinen steten Optimismus. Vielen Dank für die uneingeschränkte Unterstützung während der gesamten Zeit meiner Promotion, auch wenn mal ein Derby verloren ging.

Weiterhin möchte ich mich bei Prof. Holger Stark für die Betreuung und Begutachtung dieser Dissertation als Zweitgutachter bedanken.

Mein herzlicher Dank gilt auch Prof. Sebastian Wesselborg, der mir die Möglichkeit und sein Vertrauen gab, meine Dissertation in seinem Institut für Molekulare Medizin I realisieren zu dürfen.

In addition, I would like to thank all the co-authors and collaborators who contributed substantially to the manuscripts presented in this dissertation. Vor allem PD Dr. Michèle Hoffmann und Margaretha Skowron (Forschungslabor der Klinik für Urologie), Dr. Ute Fischer und Cyrill Schipp (Klinik für Kinder-Onkologie, -Hämatologie und Klinische Immunologie) möchte ich für die gemeinsame Zusammenarbeit danken.

Mein Dank gilt auch dem Graduiertenkolleg (GRK) 2158 und der Düsseldorf School of Oncology (DSO) für die finanzielle und fachliche Unterstützung. Im Besonderen danke ich Dr. Martina Holz und Dr. Cornelia Höhner.

Außerdem möchte ich mich bei allen aktuellen und ehemaligen Mitgliedern der Molekularen Medizin I und der Molekularen Radioonkologie für die Unterstützung und die sehr schöne Zeit nicht nur im Labor bedanken. Ihr habt mir die Arbeit auch an langen Laborabenden erleichtert und mich auch aufgebaut und motiviert, wenn es nötig war. Darüber hinaus sorgten unsere gemeinsamen Journal Clubs in und um Düsseldorf auch für die nötige Ablenkung und ich bin sehr froh, dass sich im Laufe der Zeit auch einige persönliche Freundschaften daraus entwickelt haben. Thank you so much!

Zu guter Letzt danke ich meinen Eltern, sowie meinen Geschwistern Lukas und Helena, dass ihr immer für mich da wart und mich bei allem unterstützt habt.

Abbreviations

| | |
|-----------|--|
| 3-MA | 3-methyladenine |
| ALS | amyotrophic lateral sclerosis |
| AMP | adenosine monophosphate |
| AMPK | AMP-activated protein kinase |
| ATG | Autophagy-related |
| ATP | adenosine triphosphate |
| AZI2/NAP1 | 5-azacytidine-induced protein 2 |
| BAK | Bcl-2 antagonist/killer |
| BAX | Bcl-2-associated X protein |
| BC | bladder cancer |
| Bcl-2 | B-cell lymphoma 2 |
| Bim | Bcl2-interacting mediator of cell death |
| CC | coiled coil |
| cGAS | cyclic GMP-AMP synthase |
| CMA | chaperone-mediated autophagy |
| DFCP | double FYVE domain containing protein |
| DNA | deoxyribonucleic acid |
| EBV | Epstein–Barr virus |
| ER | endoplasmic reticulum |
| FIP200 | focal adhesion kinase-interacting protein of 200 kDa |
| FIR | FIP200-interacting region |
| FTD | frontotemporal dementia |
| GABARAP | GABA type A receptor-associated protein |
| GMP | guanosine monophosphate |
| HORMA | Hop1p, Rev7p and MAD2 |

| | |
|----------|--|
| HSC70 | heat shock-cognate protein of 70 kDa |
| HSE | childhood herpes simplex encephalitis |
| IFN | interferon |
| IRF3 | interferon regulatory factor 3 |
| KO | knockout |
| LAMP2A | lysosome-associated membrane protein 2 A |
| LC3 | (microtubule associated protein 1) light chain 3 |
| LIR | LC3-interacting region |
| LPS | lipopolysaccharide |
| MAVS | mitochondrial antiviral signaling protein |
| MDA5 | melanoma differentiation-associated protein 5 |
| MIC26/27 | MICOS complex subunit MIC26/27 |
| mTOR | mechanistic target of rapamycin |
| mTORC1 | mTOR complex 1 |
| MyD88 | myeloid differentiation primary response 88 |
| NBR1 | neighbor of BRCA1 gene 1 |
| NDP52 | nuclear dot protein 52 kDa |
| NRBF2 | nuclear receptor-binding factor 2 |
| NTG | normal tension glaucoma |
| OPTN | optineurin |
| OXPHOS | oxidative phosphorylation |
| PAMP | pathogen-associated molecular pattern |
| PB1 | Phox and Bem1 |
| PE | phosphatidylethanolamine |
| PRR | pattern recognition receptor |
| PtdIns3K | phosphatidylinositol 3-kinase |
| PtdIns3P | phosphatidylinositol 3-phosphate |

| | |
|----------------|--|
| Raptor | regulatory-associated protein of mTOR |
| RIG-I | retinoic acid-inducible gene I |
| RIPK1 | receptor-interacting serine/threonine-protein kinase 1 |
| RLR | RIG-I-like receptor |
| RNA | ribonucleic acid |
| SAR | selective autophagy receptor |
| SKICH | SKIP carboxyl homology |
| SLR | SQSTM1/p62-like receptor |
| snRNP | small nuclear Ribonucleoprotein Particle |
| SQSTM1/p62 | sequestosome 1 |
| STING | stimulator of interferon genes |
| STK4 | serine/threonine-protein kinase 4 |
| STX17 | syntaxin 17 |
| TAX1BP1 | Tax1 binding protein 1 |
| TBK1 | TANK-binding kinase 1 |
| TBKBP1/SINTBAD | TBK1-binding protein 1 |
| TLR3/4 | toll-like receptor 3/4 |
| TNF | tumor necrosis factor |
| TRAF3 | TNF receptor associated factor |
| TRIF | TIR-domain-containing adapter-inducing interferon- β |
| UBA | ubiquitin-associated |
| UBZ | ubiquitin binding zinc finger |
| ULK1/2 | UNC-51-like kinase 1/2 |
| UPS | ubiquitin-proteasome system |
| VPS34 | vacuolar protein sorting 34 |
| WIPI | WD repeat domain phosphoinositide-interacting protein |
| ZZ | ZZ-type zinc finger |

Amino acids

| | | |
|---------------|---|-----|
| Alanine | A | Ala |
| Cysteine | C | Cys |
| Aspartic acid | D | Asp |
| Glutamic acid | E | Glu |
| Phenylalanine | F | Phe |
| Glycine | G | Gly |
| Histidine | H | His |
| Isoleucine | I | Ile |
| Lysine | K | Lys |
| Leucine | L | Leu |
| Methionine | M | Met |
| Asparagine | N | Asn |
| Proline | P | Pro |
| Glutamine | Q | Gln |
| Arginine | R | Arg |
| Serine | S | Ser |
| Threonine | T | Thr |
| Valine | V | Val |
| Tryptophan | W | Trp |
| Tyrosine | Y | Tyr |

Table of Contents

| | |
|--|----|
| Acknowledgement..... | I |
| Abbreviations | II |
| Amino acids..... | V |
| Summary | 1 |
| Zusammenfassung..... | 2 |
| 1 Introduction | 3 |
| 1.1 The process of (macro-)autophagy | 3 |
| 1.1.1 Initiation of autophagy | 4 |
| 1.1.2 Two ubiquitin-like conjugation systems..... | 6 |
| 1.1.3 Selective autophagy..... | 8 |
| 1.1.4 Origination, Expansion and Degradation of Autophagosomes | 10 |
| 1.2 Cross-talk between autophagy, apoptosis, and innate immune signaling | 10 |
| 1.2.1 Apoptosis..... | 10 |
| 1.2.2 Innate immune response | 11 |
| 1.3 Autophagy in diseases | 12 |
| 1.3.1 Bladder cancer | 13 |
| 1.3.2 Neurodegenerative diseases..... | 14 |
| 2 Aims of this work..... | 15 |
| 3 Summary of publications..... | 16 |
| 3.1 Publications within the scope of this dissertation..... | 16 |
| 3.2 Publications beyond the scope of this dissertation | 19 |
| 4 Discussion | 22 |
| 4.1 Autophagy modulation as a therapeutic approach in BC | 22 |
| 4.2 Targeting autophagy on the level of the ULK1 complex | 23 |
| 4.3 FIP200 – A new player in TBK1 regulation | 24 |
| 5 References | 28 |
| Licensing & Copyright..... | 40 |
| Appendix | 41 |

Summary

Autophagy is an evolutionary conserved recycling process that degrades long-lived or aggregated proteins and organelles, thereby maintaining cellular homeostasis. During autophagy, the cargo is engulfed by autophagosomes and transported to lysosomes for degradation. The recognition of the cargo can be either non-selective or selective, the latter including e.g. the specific degradation of protein aggregates. The initiation of autophagy is centrally regulated by two kinase complexes: (1) the ULK1 protein kinase complex containing the kinase ULK1 and the adapter proteins ATG13, ATG101 and FIP200, and (2) the class III PtdIns3K lipid kinase complex I. Alterations in autophagy are associated with the development and promotion of diseases such as cancer and neurodegeneration. Therefore, the characterization and modulation of autophagy in disease situations is of great importance.

Cisplatin resistance is a major obstacle in the treatment of bladder cancer and the mechanisms underlying this resistance are not yet clearly understood. We have provided evidence that the cytoprotective function of autophagy may contribute to its development, but more importantly, inhibition of autophagy sensitized cisplatin-sensitive and resistant bladder cancer cells to cisplatin treatment. In particular, the class III PtdIns3K complex appears to be a suitable target for overcoming cisplatin resistance in bladder cancer.

Another major problem, however, is that highly specific autophagy inhibitors are lacking for clinical use. Therefore, we aimed to investigate the interaction interfaces of ATG13, which might be ideal targets for specific autophagy inhibition, since ATG13 is required for the formation of the ULK1 complex. We identified four residues within ATG13 that are responsible for the binding to ATG101, and inhibition of the ATG13-ATG101 interaction abolished autophagy. Therefore, we propose small compounds that disrupt this interaction as valuable drugs for clinical use.

Neurodegenerative diseases are still incurable today and their development is associated with dysregulated TBK1 activation and protein aggregation, frequently caused by defective autophagy. We observed that defective autophagy leads to accumulation of the autophagy receptors SQSTM1/p62 and TAX1BP1 together with TBK1, which is activated within these aggregates. Active TBK1 then phosphorylates SQSTM1/p62 at serine 403. However, if FIP200 cannot be recruited to these aggregates by TAX1BP1, the activation of TBK1 and the aggregation of SQSTM1/p62 are aberrantly enhanced. Therefore, we suggest that the enforced recruitment of FIP200 to these aggregates represents a promising therapeutic approach for neurodegenerative diseases.

Zusammenfassung

Autophagie ist ein evolutionär konservierter Recyclingprozess, der langlebige oder aggregierte Proteine und Organelle abbaut und dadurch die zelluläre Homöostase aufrechterhält. Während der Autophagie werden die abzubauenen Zellbestandteile von Autophagosomen umhüllt und zum Abbau zu Lysosomen transportiert. Man unterscheidet dabei zwischen einer nicht-selektiven und einer selektiven Form der Autophagie, wobei letztere z.B. den spezifischen Abbau von Proteinaggregaten beinhaltet. Die Initiierung der Autophagie wird zentral durch zwei Proteinkomplexe reguliert: (1) der ULK1-Komplex, der die Proteinkinase ULK1 und die Adapterproteine ATG13, ATG101 und FIP200 enthält, und (2) der Klasse III PtdIns3K-Komplex. Ein gestörter Ablauf der Autophagie kann die Entwicklung von Krankheiten wie Krebs und Neurodegeneration fördern. Daher ist die Charakterisierung und Modulation der Autophagie in Krankheitssituationen von großer Bedeutung.

Bei der Behandlung von Blasenkrebs stellt die Cisplatin-Resistenz ein zentrales Problem dar, jedoch sind die ihr zugrunde liegenden Mechanismen noch nicht klar verstanden. Wir gehen davon aus, dass die zytoprotektive Funktion der Autophagie zu ihrer Entwicklung beiträgt. Darüber hinaus konnten wir durch die Hemmung der Autophagie Cisplatin-sensitive und resistente Blasenkrebszellen für die Cisplatin-Behandlung sensitivieren. Insbesondere der Klasse III PtdIns3K-Komplex scheint dabei ein geeignetes Ziel für die Überwindung der Cisplatin-Resistenz bei Blasenkrebs zu sein.

Ein weiteres Problem ist jedoch, dass hochspezifische Autophagie-Inhibitoren für die klinische Verwendung fehlen. Deshalb charakterisierten wir die Interaktionsstellen von ATG13. Diese könnten ein ideales Ziel für die spezifische Inhibition der Autophagie sein, da ATG13 für die Bildung des ULK1-Komplexes erforderlich ist. Wir identifizierten vier Aminosäurereste innerhalb von ATG13, die für die Interaktion mit ATG101 verantwortlich sind, und die Hemmung dieser Interaktion blockte die Autophagie. Daher schlagen wir niedermolekulare Verbindungen, die diese Interaktion stören, als hilfreiche Medikamente für die klinische Anwendung vor.

Neurodegenerative Erkrankungen sind auch heute noch unheilbar. Sie entstehen u.a. durch eine gestörte TBK1-Aktivierung oder durch Proteinaggregate, die hauptsächlich durch eine fehlerhafte selektive Autophagie verursacht werden. Wir beobachteten, dass bei einer defekten Autophagie TBK1 zusammen mit den Autophagie-Rezeptoren SQSTM1/p62 und TAX1BP1 akkumuliert. TBK1 wird innerhalb dieser Aggregate aktiviert und phosphoryliert dann SQSTM1/p62 an Serin 403. Wenn FIP200 jedoch nicht von TAX1BP1 zu diesen Aggregaten rekrutiert werden kann, wird die Aktivierung von TBK1 und die Akkumulation von SQSTM1/p62 stark erhöht. Daher schlagen wir vor, dass die forcierte Rekrutierung von FIP200 an diese Aggregate ein vielversprechender therapeutischer Ansatz für neurodegenerative Erkrankungen sein könnte.

1 Introduction

Autophagy is an evolutionary conserved recycling process that contributes to waste management within a cell and thereby maintains cellular homeostasis. The term autophagy was first introduced in 1963 by Christian De Duve at a conference on lysosomes. Autophagy is derived from the Greek words “*αυτός*” meaning “self” and “*φαγεῖν*” meaning “to eat”. During autophagy, long-lived or aggregated proteins and organelles are degraded within lysosomes to recycle them into new energy sources such as amino acids and lipids. Autophagy is classified into three different groups, depending on how the cargo is delivered to lysosomes. Microautophagy describes the direct incorporation of small cytosolic portions into lysosomes (Li et al., 2012). During Chaperone-mediated autophagy (CMA), proteins containing the pentapeptide motif KFERQ are selectively recognized by the cytosolic chaperone heat shock-cognate protein of 70 kDa (HSC70) and directly transported into the lumen of lysosomes by lysosome-associated membrane protein 2 A (LAMP2A) (Kaushik and Cuervo, 2012). The third mode of autophagy is macroautophagy, which is also the most studied. During macroautophagy, cytosolic cargo gets engulfed by double-membraned vesicles called autophagosomes, which transport the cargo to lysosomes (Yin et al., 2016). The fusion of autophagosomes with lysosomes leads to the formation of autolysosomes, in which the cargo is finally degraded.

Besides autophagy, the ubiquitin-proteasome system (UPS) is the second important degradation system that contributes to cellular homeostasis (Pohl and Dikic, 2019). The UPS mainly degrades short-lived proteins and cooperates with the autophagy signaling pathway (Ji and Kwon, 2017). Dysregulated autophagy, however, cannot be completely compensated by the UPS and is associated with various diseases such as cancer or neurodegeneration (Ji and Kwon, 2017; Komatsu et al., 2006; Qu et al., 2003). Therefore, autophagy must be strictly regulated to ensure cellular health and homeostasis.

1.1 The process of (macro-)autophagy

(Macro-)autophagy can be divided into five distinct steps: initiation of autophagy, elongation of the isolation membrane (also called phagophore), maturation of the autophagosome, fusion of autophagosome with lysosome, and finally the degradation of autophagic cargo within the autolysosome (Yin et al., 2016). Autophagy-related (ATG) proteins are building the core autophagic machinery and can be classified into six functional groups: (i) the UNC-51-like kinase 1 (ULK1) protein kinase complex, (ii) the class III phosphatidylinositol 3-kinase (PtdIns3K) lipid kinase complex, (iii) the transmembrane protein ATG9, (iv) the WD repeat domain phosphoinositide-interacting protein (WIPI) complex, (v) the ATG5–ATG12 conjugation system, (vi) and the ATG8–phosphatidylethanolamine (PE) conjugation system (Suzuki et al., 2017).

1.1.1 Initiation of autophagy

To maintain homeostasis, autophagy occurs in most cell types at low basal levels. Nevertheless, autophagy can be induced by many stimuli including amino acid or growth factor withdrawal, DNA damage, hypoxia, protein aggregates, damaged organelles, or even intracellular pathogens (Kroemer et al., 2010). The ULK1 protein kinase complex containing the Ser/Thr kinase ULK1 and the adapter proteins ATG13, ATG101 and focal adhesion kinase-interacting protein of 200 kDa (FIP200) is the most upstream signaling node within the autophagy pathway. To ensure signal transduction, the loss of ULK1 can be partially compensated by its homolog ULK2 (Lee and Tournier, 2011). Normally, however, they appear to act independently of each other (Joo et al., 2011; Joshi et al., 2016). The formation of the ULK1 complex is modulated by the scaffold protein ATG13, and deficiency for ATG13 inhibits the formation of the ULK1 complex (Hosokawa et al., 2009; Kaizuka and Mizushima, 2016). ATG13 can be roughly divided into an intrinsically disordered region in the C terminus and a structured N terminus containing a highly conserved HORMA domain (Fujioka et al., 2014; Mei et al., 2014). ATG101 also contains a HORMA domain, which complements the HORMA domain of ATG13 and enables the heterodimerization of these two proteins (Michel et al., 2015; Qi et al., 2015; Suzuki et al., 2015). Moreover, this interaction is crucial for the integration of ATG101 into the ULK1 complex (Suzuki et al., 2015). However, the function of ATG101 within the ULK1 complex is still not completely understood. One function might be that the unique WF finger within the HORMA domain recruits downstream effector proteins (Suzuki et al., 2015). Unlike ATG101, ULK1 and FIP200 bind to the C terminus of ATG13 (Jung et al., 2009). Deletion of the last three amino acids of ATG13 was sufficient to block ULK1-ATG13 interaction (Hieke et al., 2015), while the FIP200 binding platform was mapped to a 26 amino acid stretch (Alers et al., 2011). Recently, it has been shown that the N terminus of FIP200 builds a C-shaped dimer that binds ATG13 (Shi et al., 2020). This C-shaped dimer is probably the center around which the entire ULK1 complex is organized, since ATG13 further recruits ATG101 and ULK1 to it (Shi et al., 2020). Surprisingly, interruption of ULK1-ATG13 binding had only minor effects on starvation-induced autophagy, although complex formation was disrupted (Hieke et al., 2015). Normally in vertebrates, unlike in yeast, the ULK1 complex is constitutively assembled and its activation is only controlled by phosphorylation events (Hosokawa et al., 2009; Kamada et al., 2000).

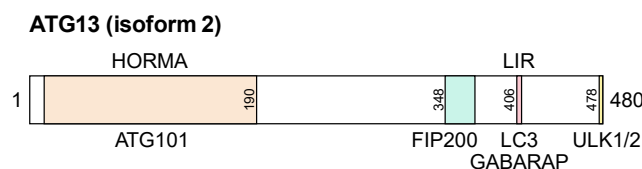


Figure 1: Domain structure and interaction interfaces of ATG13. Schematic overview of human ATG13 (isoform 2). ATG13 comprises an N-terminal HORMA domain that mediates interaction with ATG101. The C terminus of ATG13 includes interaction interfaces for FIP200 and ULK1/2 and a LIR motif that mediates binding to LC3 and GABARAP.

The activity of the ULK1 complex is strictly regulated by two energy-sensing kinases: mechanistic target of rapamycin (mTOR) (Hosokawa et al., 2009) and AMP-activated protein kinase (AMPK) (Mack et

al., 2012). Under growth conditions, the mTOR complex 1 (mTORC1), containing the regulatory-associated protein of mTOR (Raptor), associates with the ULK1 complex leading to its inactivation by mTOR dependent phosphorylation of ULK1 and ATG13 (Ganley et al., 2009; Hosokawa et al., 2009; Jung et al., 2009). Under nutrient withdrawal, however, mTORC1 is inactivated and dissociates from the ULK1 complex. This dissociation enables ULK1 to auto-phosphorylate and trans-phosphorylate ATG13 and FIP200, which ultimately leads to the activation of the ULK1 complex (Alers et al., 2012; Jung et al., 2009). ULK1 dependent phosphorylation of ATG101 has also been proposed, but its function has not yet been clarified (Egan et al., 2015). The activity of mTOR can also be inhibited by certain compounds such as Rapamycin (Ravikumar et al., 2004) or Torin 2 (Wang et al., 2015), which leads to activation of autophagy. The other energy sensor, AMPK, senses the ATP:AMP ratio within a cell. A low ratio means that the cell lacks energy resulting in the activation of AMPK. Active AMPK further activates the ULK1 complex directly by phosphorylating ULK1 (Mack et al., 2012) and indirectly by phosphorylating Raptor, which inactivates mTORC1 activity (Gwinn et al., 2008).

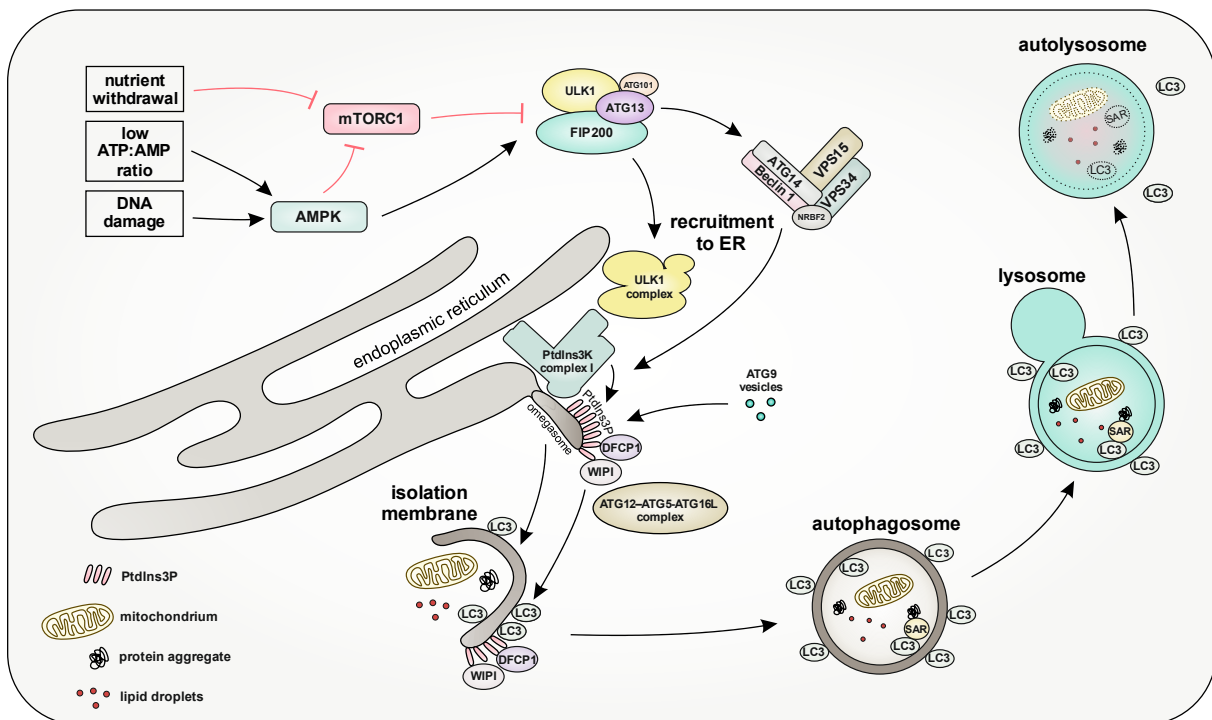


Figure 2: (Macro-)autophagy at a glance. Cellular stress such as nutrient withdrawal, a low ATP:AMP ratio or DNA damage activates the ULK1 complex, consisting of ULK1, ATG13, ATG101, and FIP200, via the two energy-sensors mTORC1 and AMPK. After activation, the ULK1 complex activates the class III PtdIns3K complex I, consisting of VPS34, VPS15, ATG14, Beclin 1, and NRBF2, and both complexes translocate to the endoplasmic reticulum (ER). The class III PtdIns3K complex I then generates PtdIns3P, which accumulates at evaginations of the ER, so-called omegasomes, resulting in the recruitment of the downstream targets DFCP1 and WIPI1 proteins. The omegasome is the origin of the isolation membrane, which is decorated on the inner and outer membrane with LC3 by the ATG12–ATG5–ATG16L complex. This complex in turn is recruited by WIPI2. The isolation membrane then elongates and engulfs cytosolic components such as mitochondria, protein aggregates, and lipid droplets. ATG9-containing vesicles support membrane elongation by delivering lipids. The closure of the isolation membrane results in the formation of an autophagosome. Engulfed cargo can also be attached to the inner site of the autophagosomal membrane via selective autophagy receptors (SARs). The autophagosome finally fuses with a lysosome, forming an autolysosome in which the cargo is degraded together with LC3 and SARs by lysosomal hydrolases to produce new energy sources. In contrast, LC3 attached to the outer site of the autophagosome is recycled.

Besides the ULK1 complex, the class III PtdIns3K lipid kinase complex I is the second initiator complex regulating the induction of autophagy (Wesselborg and Stork, 2015). It consists of the catalytic subunit

vacuolar protein sorting 34 (VPS34) and the associated proteins VPS15, Beclin 1, ATG14, and nuclear receptor-binding factor 2 (NRBF2). The class III PtdIns3K complex I translocates together with the activated ULK1 complex to the autophagosome formation site (Itakura and Mizushima, 2010; Matsunaga et al., 2010). ULK1-dependent phosphorylation of Beclin 1 is required to activate the lipid kinase VPS34 (Park et al., 2018; Russell et al., 2013) and phosphorylation of ATG14 further enhances the activity of VPS34 (Park et al., 2016; Wold et al., 2016). Once activated, VPS34 phosphorylates phosphoinositide at position 3' of the inositol ring and produces phosphatidylinositol 3-phosphate (PtdIns3P), which accumulates on the isolation membrane to recruit further downstream effectors such as double FYVE domain containing protein (DFCP) or WIPI1/2 (Axe et al., 2008; Proikas-Cezanne et al., 2015).

1.1.2 Two ubiquitin-like conjugation systems

The recruitment of the PtdIns3P-binding proteins WIPI1/2 to the isolation membrane is crucial for the biogenesis of autophagosomes (Polson et al., 2010; Proikas-Cezanne et al., 2015). WIPI2, for example, binds to ATG16L and links the downstream autophagy machinery, two ubiquitin-like conjugation systems, to autophagosomes (Dooley et al., 2014).

Ubiquitination is a posttranslational protein modification in which ubiquitin is covalently bound to a target protein, e.g. to mark it for degradation (Liebl and Hoppe, 2016). This conjugation mechanism involves three types of enzymes: (i) the ubiquitin-activating enzyme E1, (ii) the ubiquitin-carrier enzyme E2, (iii) and the ubiquitin protein ligase E3 (Weissmann, 2001). During autophagy, this multistep mechanism is used to attach ATG12 to ATG5 and later ATG8 family proteins to PE (Mizushima, 2020). The ATG8 family proteins are ubiquitin-like and include the two subfamilies (i) microtubule associated protein 1 light chain 3 (LC3), and (ii) GABA type A receptor-associated protein (GABARAP) (Shpilka et al., 2011). In a first step, the E1-like enzyme ATG7 binds ATG12 in an ATP-dependent manner by forming a thiol-ester bond with the C-terminal glycine of ATG12 (Mizushima et al., 1998a). Afterwards, ATG7 transfers ATG12 to the E2-like enzyme ATG10 (Kaiser et al., 2012). Finally, ATG12 is conjugated to ATG5 via an isopeptide bond (Mizushima et al., 1998b). ATG5–ATG12 conjugates bind to ATG16L resulting in a large complex after dimerization of ATG16L (Fujioka et al., 2010; Mizushima et al., 2003). The ATG12–ATG5–ATG16L complexes have E3-like functions for the second ubiquitin-like system, which involves the lipidation of LC3 or GABARAP (Otomo et al., 2013). First, LC3 is cleaved by ATG4 to expose a glycine residue at its C terminus (Kirisako et al., 2000). Cleaved LC3 is termed LC3-I. LC3-I is activated by ATG7, as well (Noda et al., 2011). LC3-I is then transferred to the E2-like enzyme ATG3, which conjugates LC3-I to PE (Kaiser et al., 2012; Taherbhoy et al., 2011). Lipidated LC3 is termed LC3-II. Binding of ATG12 to ATG3 enables the E3-like ATG12–ATG5–ATG16L complex to promote LC3–PE conjugation (Metlagel et al., 2013). ATG16L does not have E3-like functions, but localizes the machinery on WIPI2 positive membranes, such as isolation membranes, in which LC3-II is anchored by its lipid tail (Dooley et al., 2014).

The integration of lipidated proteins of the ATG8 family into the inner and outer layers of autophagosomal membranes is essential for the expansion and closure of autophagosomes (Fujita et al., 2008; Nakatogawa et al., 2007; Xie et al., 2008). If lipidation is inhibited, e.g. by knocking out ATG3 or ATG5, autophagy is completely blocked (Fujita et al., 2008; Kuma et al., 2004). On autophagosomes, ATG8 family proteins act as a binding platform for the core autophagic machinery and downstream targets (Kraft et al., 2012; Lee and Lee, 2016). Many ATG proteins, like ATG13 and ULK1, as well as selective autophagy receptors (SARs) contain a LC3-interacting region (LIR) motif, which allows them to bind LC3 and GABARAP (Birgisdottir et al., 2013). SARs connect the cargo with autophagosomes and function in various selective autophagy pathways (Kirkin and Rogov, 2019).

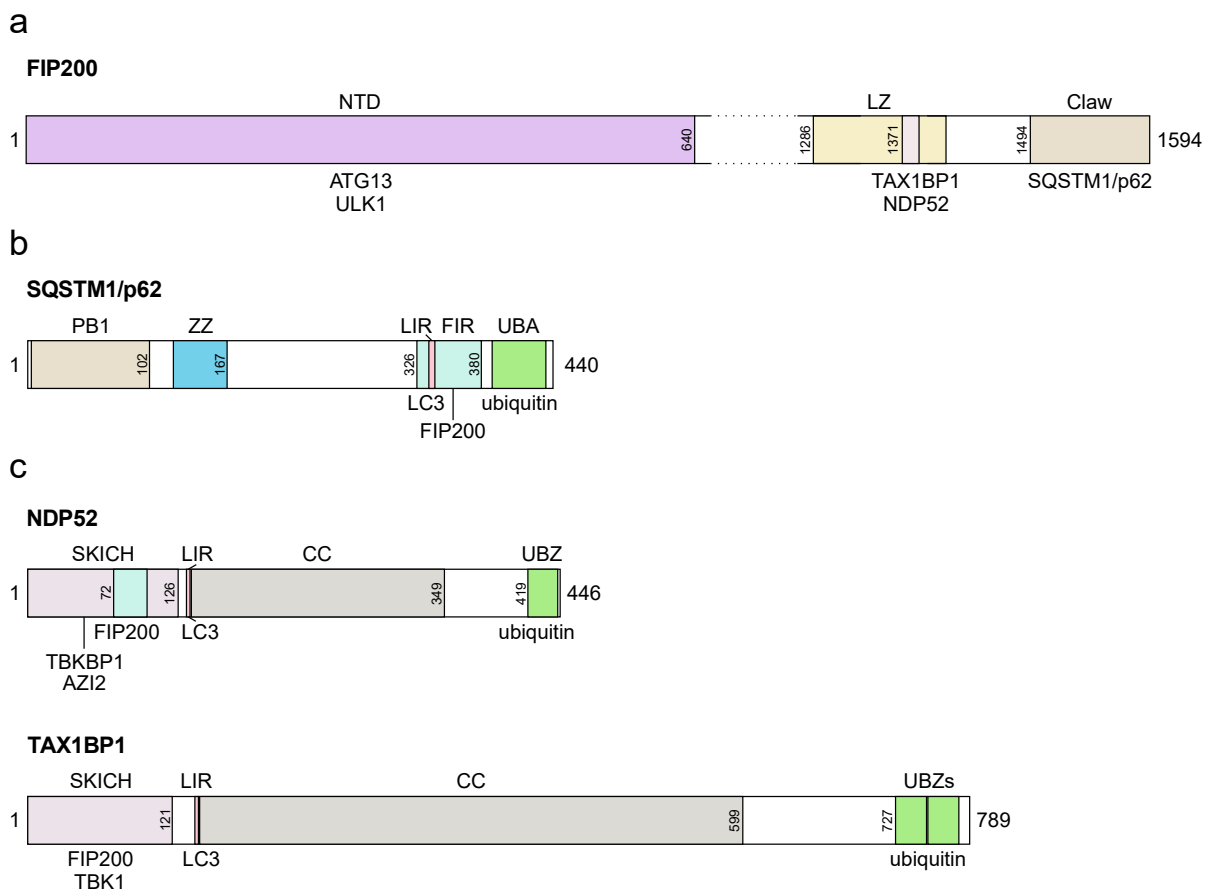


Figure 3: Domain structures and interaction interfaces of FIP200 and the SARs SQSTM1/p62, NDP52, and TAX1BP1. (a) Schematic overview of human FIP200. The N-terminal domain (NTD) of FIP200 is required to form the ULK1 complex. It forms a C-shaped dimer that mediates binding to ATG13 and ULK1. The C terminus of FIP200, however, is responsible to recruit FIP200 to the cargo. It contains a leucine zipper and a Claw region mediating interaction with TAX1BP1, NDP52 or SQSTM1/p62, respectively. (b) Schematic overview of human SQSTM1/p62. The N terminus of SQSTM1/p62 contains a Phox and Bem1 (PB1) domain that enables polymerization, followed by a ZZ-type zinc finger (ZZ). The C-terminal LC3-interacting region (LIR), FIP200-interacting region (FIR) and the ubiquitin-associated (UBA) domain mediate the binding to LC3, FIP200 and ubiquitin, respectively. The binding to LC3 and FIP200 is mutually exclusive. (c) Schematic overview of human NDP52 and TAX1BP1. Both SARs are structurally similar and contain an N-terminal SKIP carboxyl homology (SKICH) domain, followed by a LIR domain, a large coiled coil (CC) region in the middle, and one or two C-terminal ubiquitin binding zinc fingers (UBZs). The SKICH domain enables binding to FIP200 and to TBK1. The binding to TBK1 is either direct (for TAX1BP1) or indirect via TBKBP1 or AZI2 (for NDP52). In summary, SARs function as a bridge between the cargo (via ubiquitin), the ULK1 complex (via FIP200) and the autophagosome (via LC3).

1.1.3 Selective autophagy

As mentioned above, autophagy can be induced by various stimuli that determine which cargo is degraded. When a cell starves, cargo gets randomly engulfed by autophagosomes. During selective autophagy, however, the cargo is specifically targeted by SARs and linked to autophagosomes for their degradation (Johansen and Lamark, 2020; Rogov et al., 2014). The specific recognition of cargo allows a highly selective degradation of cellular components. Selective autophagy is classified in different types based on the recognized and degraded cargo, including for example protein aggregates (aggrephagy), cytosolic pathogens (xenophagy), or damaged mitochondria (mitophagy). Specificity is regulated by different types of SARs, which are either soluble or membrane-bound (Johansen and Lamark, 2020). The sequestosome 1 (SQSTM1/p62)-like receptor (SLR) family is the best-studied family of soluble SARs and include SQSTM1/p62, neighbor of BRCA1 gene 1 (NBR1), nuclear dot protein 52 kDa (NDP52), Tax1 binding protein 1 (TAX1BP1), and optineurin (OPTN) (Kirkin and Rogov, 2019).

The recognized cargoes of the individual SLRs are highly diverse, e.g. SQSTM1/p62 detects misfolded proteins, protein aggregates, damaged organelles, or cytosolic pathogens (Kirkin and Rogov, 2019). An important function of SQSTM1/p62 is that it can polymerize via its Phox and Bem1 (PB1) domain (Wilson et al., 2003), which leads to phase separation into large condensates when mixed with ubiquitin chains (Sun et al., 2018; Zaffagnini et al., 2018). SQSTM1/p62 binds ubiquitin chains via its ubiquitin-associated (UBA) domain (Isogai et al., 2011). The structure of NBR1 is similar to SQSTM1/p62 and also contains an N-terminal PB1 and a C-terminal UBA domain (Kim et al., 2016). In contrast, NDP52 and TAX1BP1 contain a SKIP carboxyl homology (SKICH) domain at their N terminus and C-terminal ubiquitin binding zinc fingers (UBZs) (Johansen and Lamark, 2020). In addition to ubiquitin binding domains, all SLRs contain a LIR domain that enables interaction with LC3 and thus the recruitment of the cargo to autophagosomes (Kim et al., 2016). Recently, SLRs have also been shown to bind the C terminus of FIP200, which contains a large coiled-coil region including a leucine zipper motif (Chano et al., 2002) and a dimeric globular domain termed the Claw (Turco et al., 2019). SQSTM1/p62 binds the Claw region of FIP200, which decreased phase separation of ubiquitinated proteins in a reconstituted system (Turco et al., 2019). Interestingly, the interactions with FIP200 and LC3 are mutually exclusive since both bind to the LIR domain of SQSTM1/p62 (Turco et al., 2019). In addition, NDP52 interacts with the leucine zipper motif of FIP200 through its SKICH domain, thereby recruiting the ULK1 complex to damaged mitochondria (Vargas et al., 2019) and cytosolic pathogens (Ravenhill et al., 2019). Recruitment of the ULK1 complex via FIP200 is facilitated by the TANK-binding kinase 1 (TBK1) and is essential for the induction of selective autophagy, as demonstrated in both cases (Ravenhill et al., 2019; Vargas et al., 2019). The involvement of the Ser/Thr kinase TBK1 in autophagy signaling has attracted more attention in recent years, although it is mainly known as the central regulator of the innate immune response. During autophagy, TBK1 is recruited by SLRs which bind TBK1 either directly (Vargas et al., 2019) or indirectly via TBK1-binding protein 1 (TBKBP1/SINTBAD) (Ravenhill et al.,

2019) or 5-azacytidine-induced protein 2 (AZI2/NAP1) (Fu et al., 2018). Local clustering leads to activation of TBK1 by trans-autophosphorylation of TBK1 dimers at serine 172 (Helgason et al., 2013; Ma et al., 2012). Active TBK1 is required to facilitate the recruitment of the ULK1 complex to mitochondria or cytosolic pathogens, although the exact mechanism is not yet fully understood (Ravenhill et al., 2019; Vargas et al., 2019). However, it is known that TBK1 phosphorylates several SARs to modulate their binding affinities, including SQSTM1/p62 and TAX1BP1 (Fu et al., 2018; Pilli et al., 2012; Richter et al., 2016; Wild et al., 2011). For example, TBK1 dependent phosphorylation of the UBA domain of SQSTM1/p62 at serine 403 strongly increases its affinity for ubiquitin binding (Matsumoto et al., 2011; Pilli et al., 2012). Ubiquitin binding is also increased by ULK1-dependent phosphorylation of SQSTM1/p62 at serine 409, and deficiency of this phosphorylation blocks degradation of ubiquitinated proteins and leads to accumulation of SQSTM1/p62 (Lim et al., 2015).

Since all SLRs are involved in different types of selective autophagy and all bind to ubiquitin and LC3, the question arises whether they have specific or redundant roles during selective autophagy. However, it is still not well understood whether and how SLRs work together.

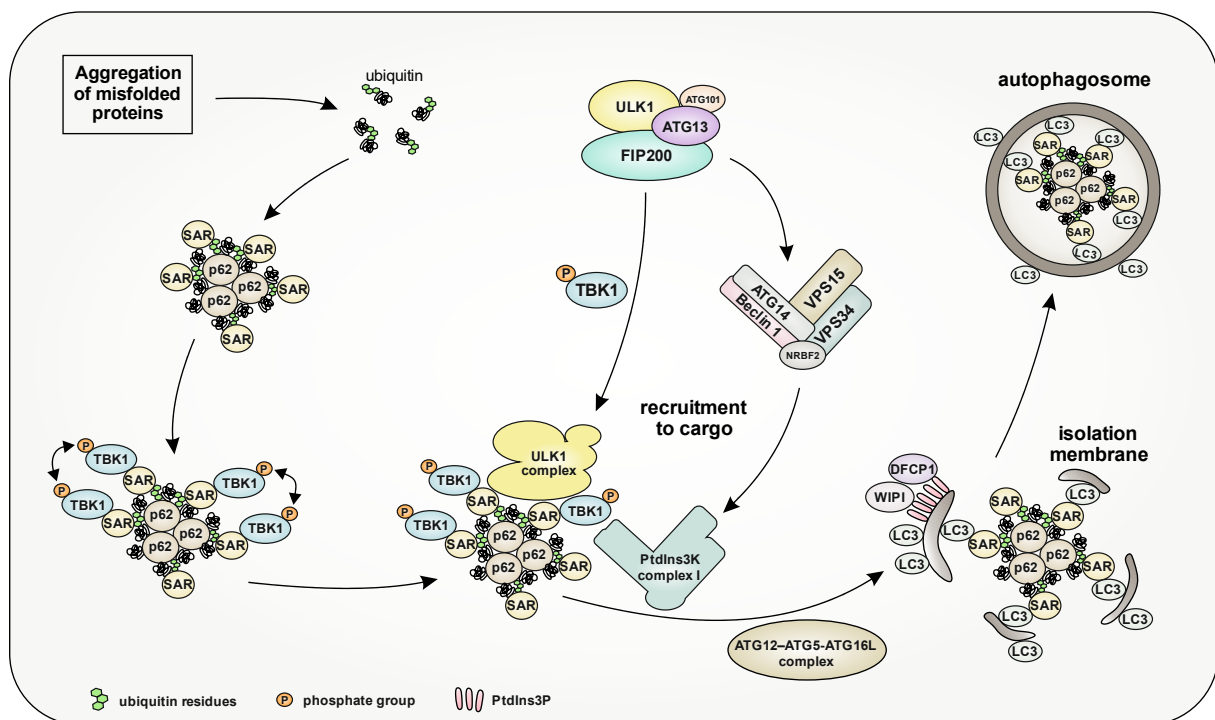


Figure 4: Aggrephagy at a glance. Aggrephagy describes the selective autophagic degradation of aggregates that can result from misfolded proteins. Aggregates within a cell are ubiquitinated, and ubiquitinated aggregates are then detected by selective autophagy receptors (SARs) such as TAX1BP1 and SQSTM1/p62. When mixed with ubiquitin, SQSTM1/p62 polymerizes, resulting in phase separation of the aggregates. TBK1 is then recruited to the cargo and local clustering of TBK1 leads to its trans-autophosphorylation and activation. After activation, TBK1 facilitates the recruitment of the ULK1 complex to the cargo via binding of FIP200 to SARs. Further recruitment of class III PtdIns3K complex I leads to the generation of PtdIns3P, which accumulates on isolation membranes that are formed directly around the cargo, resulting in the recruitment of further downstream targets such as DFCP1, WIPI proteins and the ATG12-ATG5-ATG16L complex. Decoration of the isolation membranes with LC3 then leads to their elongation and subsequently to their fusion and formation of an autophagosome. The final steps, fusion of an autophagosome with a lysosome and the degradation of the cargo within autolysosomes are similar to (macro-)autophagy (see Figure 2).

1.1.4 Origination, Expansion and Degradation of Autophagosomes

During starvation-induced autophagy, the ULK1 complex translocates together with ATG9 positive vesicles to the endoplasmic reticulum (ER) (Karanasios et al., 2016), and after activation of the class III PtdIns3K complex, PtdIns3P is synthesized at evaginations of the ER-mitochondria-contact sites, which are termed omegasomes due to their shape (Axe et al., 2008). These structures are the origin of the isolation membrane, which expands after LC3 decoration (Xie et al., 2008). During selective autophagy, isolation membranes can be generated at different locations directly around the cargo and eventually fuse into one large autophagosome (Walker and Ktistakis, 2019). The origin of the lipids required for expansion is still controversial, and it appears that various lipid sources, such as ER, Golgi, mitochondria, and endosomes are involved (Walker and Ktistakis, 2019).

After expansion and engulfment of the cytosolic cargo, the autophagosome matures and ATG proteins located on the outer side of the autophagosomal membrane are released due to ATG4-dependent cleavage of lipidated LC3 (Nakatogawa et al., 2014). To prevent premature release or incorporation of LC3 into non-autophagosomal membranes, ATG4 activity is inactivated by ULK1-dependent phosphorylation (Pengo et al., 2017; Sánchez-Wandelmer et al., 2017). The matured autophagosome is then transported along microtubule structures to lysosomes for fusion (Geeraert et al., 2010; Jahreiss et al., 2008; Nakamura and Yoshimori, 2017). The resulting autolysosomes degrade the cargo along with LC3 and autophagic receptors attached to the inner site of the membrane by lysosomal hydrolases, and finally new energy sources are available (Yim and Mizushima, 2020).

1.2 Cross-talk between autophagy, apoptosis, and innate immune signaling

Many ATG proteins have autophagy dependent and independent functions (Galluzzi and Green, 2019). Besides autophagy, FIP200 is also involved in cell growth, cell proliferation, cell survival, and embryogenesis (Gan and Guan, 2008). The loss of FIP200 causes embryonic lethality (Gan et al., 2006), while *Atg5*- or *Atg7*-deficient mice die shortly after birth due to lack of autophagy (Komatsu et al., 2005; Kuma et al., 2004), which underscores the importance of the autophagy independent functions of FIP200. In addition, some autophagy independent functions of ATG proteins connect autophagy with other signaling pathways, such as apoptosis or innate immune responses, thus enabling cross-talk between them (Galluzzi and Green, 2019).

1.2.1 Apoptosis

Apoptosis describes a form of programmed cell death that normally occurs during development and aging or as a defense mechanism after infection (Elmore, 2007). Apoptosis is classified in two major pathways depending on its induction. The extrinsic pathway is activated by death receptors after ligand

binding (Scott et al., 2009). The intrinsic pathway, however, is induced by intracellular stress, like DNA damage, followed by the permeabilization of the mitochondrial membrane and cytochrome c release (Elmore, 2007; Hu et al., 1999). Both pathways are based on the activation of an irreversible caspase cascade. Caspases are cysteine proteases that cleave target proteins following aspartic acid residues (Elmore, 2007). Cytosolic cytochrome c results in the cleavage and thus activation of the initiator caspase 9 (Hu et al., 1999; Li et al., 1997). Initiator caspases further activate effector caspases, such as caspase 3, to trigger the caspase cascade that ultimately causes programmed cell death (Elmore, 2007). To prevent inflammation, the intracellular components are engulfed in plasma membranes and quickly removed by macrophages (Peter et al., 2010; Savill and Fadok, 2000).

Stress conditions induce autophagy and apoptosis, and cross-talk between these two pathways determines cell fate, since autophagy promotes survival and apoptosis induces cell death (Mukhopadhyay et al., 2014). The cross-talk between these two pathways, amongst others, involves the proteins of the B-cell lymphoma 2 (Bcl-2) family. During apoptosis they act pro- or anti-apoptotically and regulate its induction. The pro-apoptotic Bcl-2 family members Bcl-2-associated X protein (BAX) and Bcl-2 antagonist/killer (BAK) build pores within the outer mitochondrial membrane, resulting in cytochrome c release (Dewson and Kluck, 2009; Eskes et al., 2000). Other pro-apoptotic family members, such as Bcl-2-interacting mediator of cell death (Bim), bind the anti-apoptotic family member BCL-2, which is the link between apoptosis and autophagy (Mukhopadhyay et al., 2014). BCL-2 localizes to mitochondria and the ER, where it binds and inactivates BAX (Bender et al., 2012) or Beclin 1, respectively (Feng et al., 2007; Marquez and Xu, 2012). Under stress conditions, BCL-2 is first released from Beclin 1 due to a weak binding affinity, which induces autophagy (Mukhopadhyay et al., 2014). Autophagy itself has an anti-apoptotic effect by degrading damaged mitochondria or caspases. However, severe stress conditions also lead to disruption of the BCL-2-BAX complex and induction of apoptosis. (Mukhopadhyay et al., 2014). In addition, the active caspase 3 cleaves Beclin 1 and ATG4, which further induces mitochondrial apoptosis and inhibits autophagy, further promoting cell death (Betin and Lane, 2009; Wirawan et al., 2010; Zhu et al., 2010).

1.2.2 Innate immune response

The innate immune response is the first line of defense against pathogens. Specific patterns on bacterial or viral components are recognized by pattern recognition receptors (PRRs), which eventually lead to the production of pro-inflammatory cytokines and chemokines to prevent bacterial or viral replication (Koyama et al., 2008). PRRs are divided into different groups that differ in their localization and recognition of pathogen-associated molecular patterns (PAMPs). The group of toll-like receptors (TLRs) includes TLR3 and TLR4, which localize to endosomes or the cell membrane, respectively (El-Zayat et al., 2019). TLR3 recognizes double-stranded RNA, while TLR4 detects extracellular and intracellular bacterial or viral material, such as the bacterial cell wall component lipopolysaccharide (LPS) (El-Zayat et al., 2019). Viral RNA is also recognized by retinoic acid-inducible gene I (RIG-I)

and melanoma differentiation-associated protein 5 (MDA5), which belong to the RIG-I-like receptors (RLRs) (Eisenacher and Krug, 2012). Another group includes cytosolic DNA receptors such as cyclic GMP-AMP synthase (cGAS) (Motwani et al., 2019). Upon ligand binding, TLR3/4, RIG-I and cGAS signal through binding to the adaptor proteins TIR-domain-containing adapter-inducing interferon- β (TRIF), mitochondrial antiviral signaling protein (MAVS), and stimulator of interferon genes (STING), respectively (Liu et al., 2015). PRRs bound to TRIF, MAVS or STING mediate the recruitment of TBK1, followed by TBK1 activation through local clustering and trans-autophosphorylation (Helgason et al., 2013; Liu et al., 2015; Ma et al., 2012). Once activated, TBK1 phosphorylates the adaptors TRIF, MAVS or STING, which leads to the recruitment of interferon regulatory factor 3 (IRF3) (Liu et al., 2015). TBK1 then phosphorylates IRF3 at serine 396, thereby inducing its dimerization and nuclear translocation. Inside the nucleus, IRF3 activates type I interferon (IFN) gene expression (Tamura et al., 2008). Generally, type I IFNs, including IFN- α and IFN- β , are produced by any nucleated cell. In contrast, IFN- γ , which is the only type II IFN, is produced exclusively by specific immune cells (Koyama et al., 2008).

In addition to the innate immune response, autophagy is also activated during pathogen infections (Sumpter and Levine, 2010). During TLR signaling, the adaptor proteins TRIF and myeloid differentiation primary response 88 (MyD88) bind to Beclin 1, thereby reducing the binding of Beclin 1 to its inhibitory regulator BCL-2 (Pattingre et al., 2005; Shi and Kehrl, 2008). Cytosolic pathogens are then degraded during the selective autophagy process xenophagy, which enables cell-autonomous immunity (Randow et al., 2013). In addition, autophagy is important for fine-tuning the innate immune response and protects the cell from excessive inflammation through various anti-inflammatory mechanisms (Galluzzi and Green, 2019; Sumpter and Levine, 2010). One mechanism involves the association of ATG5–ATG12 conjugates to RIG-I and MAVS, which prevents further signaling (Jounai et al., 2007). Another mechanism is the selective autophagic degradation of proteins involved during innate immunity, e.g. TLR3/4 signaling is inhibited by TAX1BP1-dependent degradation of TRIF (Yang et al., 2017). In addition, TAX1BP1 and A20 target TBK1, which leads to the disruption of the TNF receptor associated factor (TRAF3)-TBK1 signaling complex, thereby reducing inflammation (Prabakaran et al., 2018).

All mechanisms described above demonstrate the importance of cross-talks between autophagy and other signaling pathways, especially to ensure cellular homeostasis and prevent the development of diseases.

1.3 Autophagy in diseases

Cancer and neurodegenerative diseases are closely connected with changes in autophagic signal transduction. Defective autophagy causes protein aggregation, which is known to be responsible for the development of some neurodegenerative diseases (Hara et al., 2006; Komatsu et al., 2006; Mallucci et

al., 2020). In the case of cancer, autophagy is like a double-edged sword, since it can both inhibit or promote tumor progression (Ávalos et al., 2014). On the one hand, basal autophagy removes oncogenic factors such as misfolded proteins, damaged organelles, or reactive oxygen species and thus reduces tumor development. This is perfectly shown by alterations in Beclin 1 expression. Ectopic overexpression reduces breast cancer cell proliferation (Liang et al., 1999), while the monoallelic deletion of the mammalian gene encoding Beclin 1 promotes tumorigenesis in mice and has been found in 40-75% of cases of human ovarian, sporadic breast, and prostate cancer (Qu et al., 2003). However, once the tumor is established, autophagy has a tumor-promoting effect, as autophagy provides nutrients for malignant cells in hypoxic regions (Degenhardt et al., 2006). In addition, anticancer therapies often induce autophagy, which contributes to chemoresistance (Amaravadi and Thompson, 2007; Rebecca and Amaravadi, 2016). Consequently, autophagy inhibiting drugs are currently being tested in clinical trials. They are being combined with various anticancer drugs to increase their cytotoxic potential and minimize the development of chemoresistance. Chloroquine/hydroxychloroquine is used in several of these trials. It inhibits autophagy by raising the lysosomal pH, thereby inhibiting the fusion of autophagosomes and lysosomes (Rebecca and Amaravadi, 2016). In contrast to chloroquine/hydroxychloroquine, the compounds MRT68921 and SAR405 inhibit autophagy more specifically by targeting ULK1 and VPS34, respectively, and inhibiting their kinase activities (Petherick et al., 2015; Ronan et al., 2014). So far, however, they have only been investigated in preclinical studies.

1.3.1 Bladder cancer

Bladder cancer (BC) is the tenth most common cancer worldwide, with approximately 549,000 newly diagnosed cases and 200,000 deaths in 2018 (Bray et al., 2018). BC is more common in men than in women. For men, BC is the sixth most common cancer and the ninth most common cause of cancer death worldwide (Bray et al., 2018). The highest burden currently falls on Europe and North America and thus on the most developed countries across the globe (Richters et al., 2020). Cigarette smoking and occupational exposure to chemical or water contaminants are the main risk factors for BC (Bray et al., 2018). Histologically BCs are classified into muscle-invasive and non-muscle-invasive (Knowles, 2006). Both subtypes differ at the molecular level and in clinical behavior. At initial diagnosis, 20-30% of BCs are already diagnosed as muscle invasive (Yuk et al., 2019). Muscle-invasive BCs often develop into a metastatic disease and patients face a poor prognosis with a survival rate of only 50% to 60% after 5 years. (Witjes et al., 2017). Cisplatin- or carboplatin-based neoadjuvant chemotherapy is the first line treatment for muscle-invasive and metastatic BCs (Witjes et al., 2017). The anticancer effect of cisplatin is mainly based on the cross-linking of DNA strands that block transcription and replication (Galluzzi et al., 2012). Subsequently generated DNA double-strand breaks stimulate the response to DNA damage and finally induce apoptosis (Roos and Kaina, 2013). Unfortunately, cisplatin treatment often results in the development of chemoresistance (Drayton and Catto, 2013). The molecular mechanisms of cisplatin resistance are manifold including dysregulated apoptosis signaling, DNA repair or drug transport, as

well as phenotype plasticity (Galluzzi et al., 2012; Höhn et al., 2016; Skowron et al., 2015). However, the mechanisms underlying the cisplatin resistance of BC cells are not yet clearly understood and avoiding or overcoming chemoresistance in BC therapy remains a major challenge.

1.3.2 Neurodegenerative diseases

As the world's population continues to age, neurodegenerative diseases are likely to be the leading cause of death in the future and are still incurable today (Mallucci et al., 2020). Several neurodegenerative diseases such as childhood herpes simplex encephalitis (HSE), amyotrophic lateral sclerosis (ALS), frontotemporal dementia (FTD), and normal tension glaucoma (NTG) are associated with dysregulated TBK1 and develop after accumulation of disease-specific proteins or infection of neuronal cells (Ahmad et al., 2016; Mallucci et al., 2020). Loss-of-function mutations in the human gene coding for TBK1 can cause ALS and FTD (Freischmidt et al., 2015), mainly due to the impaired autophagic removal of protein aggregates (Forman et al., 2004; Neumann et al., 2006). However, duplication of the *TBK1* gene was observed in patients with NTG (Ahmad et al., 2016). Besides *TBK1*, mutations in the genes of two SARs, *OPTN* and *SQSTM1/p62*, were found in patients with neurodegenerative diseases (Fecto et al., 2011; Maruyama et al., 2010; Pottier et al., 2015). In neuronal cells of NTG patients, the E50K *OPTN* mutant forms protein aggregates due to enhanced binding to TBK1, which ultimately drives *OPTN* into insolubility (Minegishi et al., 2013). Accordingly, the modulation of TBK1 could be an option to reduce protein aggregation and thus prevent neurodegenerative diseases. However, the regulation of TBK1 during selective autophagy requires additional clarification first.

2 Aims of this work

The main aims of this dissertation were to study the role of autophagy in disease settings and whether the modulation of autophagy can contribute to the prevention or cure of disease. These aims have been pursued in several (cooperation) projects that have been published or are being prepared for publication.

In the first project, the autophagy signaling pathway was characterized in cisplatin-sensitive and -resistant bladder cancer cells. In a next step, autophagy-modulating compounds were used in mono- and combination therapy together with cisplatin in order to prevent or overcome cisplatin resistance.

In the second project, new ways to specifically inhibit autophagy were investigated, as clinics lack highly specific autophagy inhibitors. Therefore, the interaction interfaces of ATG13 were analyzed regarding ULK1 complex formation and autophagy induction.

A third project investigated the formation of protein aggregates and the dysregulation of TBK1 in cells incapable of autophagy signaling. This could help to better understand the development of neurodegenerative diseases and to optimize treatment options.

3 Summary of publications

3.1 Publications within the scope of this dissertation

The full original texts of these manuscripts can be found in the appendix of this dissertation.

Publication 1

Targeting urothelial carcinoma cells by combining cisplatin with a specific inhibitor of the autophagy-inducing class III PtdIns3K complex

David Schlütermann, Margaretha A. Skowron, Niklas Berleth, Philip Böhrer, Jana Deitersen, Fabian Stuhldreier, Nora Wallot-Hieke, Wenxian Wu, Christoph Peter, Michèle J. Hoffmann, Günter Niegisch, Björn Stork

Urologic Oncology: Seminars and Original Investigations, volume 36, issue 4, pages 160.e1-160.e13, April 2018

DOI: 10.1016/j.urolonc.2017.11.021

Cisplatin resistance is a major obstacle to bladder cancer therapies, and autophagy is linked to the development of drug resistance in cancer. By analyzing the autophagy signaling pathway in cisplatin-sensitive and -resistant bladder cancer cells, we found that some ATG proteins, such as LC3, ULK1, FIP200, ATG13, and Beclin 1, are up-regulated in cells resistant to cisplatin. We therefore inhibited autophagy using the compounds chloroquine, 3-methyladenine (3-MA) and SAR405 in mono- and combination therapy together with cisplatin. Inhibition of autophagy sensitized both sensitive and resistant bladder cancer cells to treatment with cisplatin by inducing apoptosis. In particular, the class III PtdIns3K complex, which is targeted by 3-MA and SAR405, appears to be an appropriate target for increasing the efficacy of cisplatin to prevent or overcome cisplatin resistance in bladder cancer.

Author contribution:

The author of this dissertation designed the experiments, performed cell viability and caspase-3 activity assays, and performed immunoblot analyses. In addition, the author analyzed and interpreted the data and wrote the manuscript.

Relative contribution: about 80%.

Publication 2

Systematic analysis of ATG13 domain requirements for autophagy induction

Nora Wallot-Hieke, Neha Verma, David Schlütermann, Niklas Berleth, Jana Deitersen, Philip Böhrer, Fabian Stuhldreier, Wenxian Wu, Sabine Seggewiß, Christoph Peter, Holger Gohlke, Noboru Mizushima, Björn Stork

Autophagy, volume 14, issue 5, pages 743-763, March 2018

DOI: 10.1080/15548627.2017.1387342

ATG13 is a key protein for the induction of autophagy as it recruits ULK1, ATG101, and FIP200 into a ULK1 core complex and binds phospholipids and proteins of the ATG8 family. This makes ATG13 an attractive target for regulating autophagy. We found that binding of ATG13 to ATG101 is central for the induction of autophagy following amino acid starvation or mTOR inhibition. In contrast, the interactions of ATG13 with ULK1 or FIP200 were not mandatory, at least for starvation-induced autophagy, although ULK1 complex formation was disturbed in all cases. In addition, the interaction of ATG13 with phospholipids or proteins of the ATG8 family was not absolutely necessary to induce autophagy. These results suggest that the interaction of ATG13 with ATG101 could be a promising target in disease situations where inhibition of autophagy is desired.

Author contribution:

The author of this dissertation contributed some ideas to the project, gave technical support, discussed the results, and commented on the manuscript.

Relative contribution: about 5%.

Publication 3

FIP200 controls TBK1 activation threshold at SQSTM1/p62-positive condensates

David Schlütermann, Niklas Berleth, Jana Deitersen, Nora Wallot-Hieke, Olena Friesen, Wenxian Wu, Fabian Stuhldreier, Yadong Sun, Lena Berning, Annabelle Friedrich, María José Mendiburo, Christoph Peter, Constanze Wiek, Helmut Hanenberg, Anja Stefanski, Kai Stühler, Björn Stork

Manuscript in preparation

Autophagy is responsible for the removal of protein aggregates, and FIP200 has been shown to be essential for selective autophagy as it recruits the ULK1 complex to the cargo. We found that in cells deficient for autophagy in general or FIP200 in particular, aggregates containing TBK1, TAX1BP1 and SQSTM1/p62 develop. In these aggregates TBK1 is activated by trans-autophosphorylation, then phosphorylates SQSTM1/p62 at serine 403 and thus probably regulates the efficient engulfment and degradation of these aggregates. TAX1BP1 mediates the recruitment of TBK1 to these aggregates and this recruitment is further enhanced when FIP200 is absent or unable to bind to TAX1BP1. This indicates that FIP200 hampers aberrant TBK1 activation and, more importantly, the further accumulation of SQSTM1/p62 aggregates. Since dysregulated TBK1 activity and protein aggregates are a key feature in neurodegenerative diseases, we suggest that the enforced recruitment of FIP200 to these aggregates could be a promising therapeutic approach.

Author contribution:

The author of this dissertation designed the experiments, performed mutagenesis, generated cell lines (FIP200+ULK1), performed immunofluorescence, and immunoblot analyses, and supported RT-qPCR analyses. In addition, the author analyzed and interpreted the data and wrote the manuscript.

Relative contribution: about 75%.

3.2 Publications beyond the scope of this dissertation

The author of this dissertation has contributed to several additional publications. However, these are not discussed here or attached to this work, as they would go beyond the scope of this dissertation.

Publication 4

The mycotoxin phomoxanthone A disturbs the form and function of the inner mitochondrial membrane

Philip Böhler, Fabian Stuhldreier, Ruchika Anand, Arun Kumar Kondadi, David Schlütermann, Niklas Berleth, Jana Deitersen, Nora Wallot-Hieke, Wenxian Wu, Marian Frank, Hendrik Niemann, Elisabeth Wesbuer, Andreas Barbian, Tomas Luyten, Jan B. Parys, Stefanie Weidtkamp-Peters, Andrea Borchardt, Andreas S. Reichert, Aida Peña-Blanco, Ana J. García-Sáez, Samuel Itskanov, Alexander M. Van Der Blik, Peter Proksch, Sebastian Wesselborg, Björn Stork

Cell Death & Disease, volume 9, article 286, February 2018

DOI: 10.1080/15548627.2017.1387342

Author contribution:

The author of this dissertation has done some preliminary work, contributed several ideas to the project, gave technical support, discussed the results, and commented on the manuscript.

Relative contribution: about 5%.

Publication 5

EBV Negative Lymphoma and Autoimmune Lymphoproliferative Syndrome Like Phenotype Extend the Clinical Spectrum of Primary Immunodeficiency Caused by STK4 Deficiency

Cyrrill Schipp, David Schlütermann, Andrea Hönscheid, Schafiq Nabhani, Jessica Holl, Prasad T. Oommen, Sebastian Ginzler, Bernhard Fleckenstein, Björn Stork, Arndt Borkhardt, Polina Stepensky, Ute Fischer

Frontiers in Immunology, volume 9, article 2400, October 2018

DOI: 10.3389/fimmu.2018.02400

Author contribution:

The author of this dissertation performed laboratory work, designed research, analyzed data, and participated in writing the paper.

Relative contribution: about 5%.

Publication 6

The Autophagy-Initiating Kinase ULK1 Controls RIPK1-Mediated Cell Death

Wenxian Wu, Xiaojing Wang, Niklas Berleth, Jana Deitersen, Nora Wallot-Hieke, Philip Böhler, David Schlütermann, Fabian Stuhldreier, Jan Cox, Katharina Schmitz, Sabine Seggewiß, Christoph Peter, Gary Kasof, Anja Stefanski, Kai Stühler, Astrid Tschapek, Axel Gödecke, Björn Stork

Cell Reports, volume 31, issue 3, article 107547, April 2020

DOI: 10.1016/j.celrep.2020.107547

Author contribution:

The author of this dissertation gave technical support, discussed the results, and commented on the manuscript.

Relative contribution: about 2%.

Publication 7

MIC26 and MIC27 cooperate to regulate cardiolipin levels and the landscape of OXPPOS complexes

Ruchika Anand, Arun Kumar Kondadi, Jana Meisterknecht, Mathias Golombek, Oliver Nortmann, Julia Riedel, Leon Peifer-Weiß, Nahal Brocke-Ahmadinejad, David Schlütermann, Björn Stork, Thomas O. Eichmann, Ilka Wittig, Andreas S. Reichert

Life Science Alliance, volume 3, issue 10, August 2020

DOI: 10.26508/lsa.202000711

Author contribution:

The author of this dissertation gave technical support and commented on the manuscript.

Relative contribution: about 1%

Publication 8

TNF-induced necroptosis initiates early autophagy events via RIPK3-dependent AMPK

Activation, but inhibits late autophagy

Wenxian Wu, Xiaojing Wang, Yadong Sun, Niklas Berleth, Jana Deitersen, David Schlütermann, Fabian Stuhldreier, Nora Wallot-Hieke, María José Mendiburo, Jan Cox, Christoph Peter, Ann Kathrin Bergmann, Björn Stork

Manuscript in preparation

Author contribution:

The author of this dissertation gave technical support, discussed the results, and commented on the manuscript.

Relative contribution: about 2%

Publication 9

An Essential Role of the Autophagy Activating Kinase ULK1 in snRNP Biogenesis

Katharina Schmitz, Jan Cox, Lea Marie Esser, Martin Voss, Katja Sander, Antje Löffler, Frank Hillebrand, Steffen Erkelenz, Heiner Schaal, Thilo Kähne, Stefan Klinker, Tao Zhang, Luitgard Nagel-Steger, Dieter Willbold, Sabine Seggewiß, David Schlütermann, Björn Stork, Matthias Grimmler, Sebastian Wesselborg, Christoph Peter

Manuscript in preparation

Author contribution:

The author of this dissertation executed the domain analysis of ULK1, analyzed the autophagic capacity of cells, gave technical support, discussed the results, and commented on the manuscript.

Relative contribution: about 4%

4 Discussion

As understanding of the molecular mechanism of autophagy progresses, several studies have highlighted the role of altered autophagy signaling in human diseases. Therefore, the characterization and modulation of autophagy in disease settings is of great importance. The projects presented in this dissertation contributed in different ways to a better understanding of both aspects. After analyzing the autophagy signaling pathway in cisplatin-sensitive and -resistant bladder cancer (BC) cells, we found that autophagy is enhanced in cisplatin resistant cells. As a result, we were able to sensitize both cisplatin-sensitive and -resistant cells to cisplatin by inhibiting autophagy. We also highlighted the ATG13-ATG101 interaction as a promising new target for specific autophagy inhibition. In addition, we demonstrated the importance of FIP200 in preventing the development of aberrant TBK1 activation and SQSTM1/p62 aggregation, both associated with neurodegenerative diseases.

4.1 Autophagy modulation as a therapeutic approach in BC

Cisplatin-based chemotherapy is the first-line treatment for muscle-invasive and metastatic BCs according to European guidelines (Witjes et al., 2017). However, the development of cisplatin resistance is still the cause of high mortality. The cyto-protective function of autophagy has been suggested as a possible off-target mechanism for cisplatin resistance in cancer cells (Galluzzi et al., 2012; Mani et al., 2015; Xiao et al., 2016; Yu et al., 2014). In fact, enhanced autophagy was found in several cancer cells resistant to cisplatin, and resistant cells could be sensitized to cisplatin treatment by inhibiting the autophagic pathway (Bao et al., 2015; Hu et al., 2020; Su et al., 2016; Wang and Wu, 2014; Yu et al., 2011). In line with these studies, we found increased expression of various ATG proteins in different cisplatin-resistant BC cells, suggesting higher basal autophagic flux. In addition, autophagy inhibition by 3-MA or SAR405, both of which inhibit VPS34, increased the efficacy of cisplatin to induce apoptosis in those cells. Supportingly, Lin et al. (Lin et al., 2017) showed that treatment with cisplatin upregulates Beclin 1 expression in BC cells. Beclin 1 and VPS34 both belong to the class III PtdIns3K complex, and inhibition of this complex has already been shown to sensitize cisplatin-resistant ovarian cancer (Bao et al., 2015; He et al., 2015; Hu et al., 2020) and lung adenocarcinoma cells (Ren et al., 2010). We therefore hypothesize that the class III PtdIns3K complex appears to be a suitable target for overcoming cisplatin resistance also in BC.

Nonetheless, the modulation of autophagy as an effective anticancer therapy depends on the stage and type of cancer. In contrast to our results, other studies have shown that autophagy is reduced in cisplatin resistant lung cancer (García-Cano et al., 2015; Sirichanchuen et al., 2012) and gastric cancer (Gu et al., 2020) cells and that induction of autophagy increased cisplatin efficacy. In addition, it has been shown that autophagy deficiency in mice increases liver tumor development in early stages (Takamura et al., 2011). But it is also controversial for BC how autophagy should be modulated to overcome cisplatin

resistance, since some studies suggest inhibition (Mani et al., 2015; Ojha et al., 2014) and others induction (Li et al., 2013; Pinto-Leite et al., 2013) of autophagy. In our study, we used different cisplatin-resistant BC cells and inhibition of VPS34 was most effective in cells with high ULK1 expression. However, whether a high ULK1 expression is indeed needed has to be tested in future studies. All these observations highlight the importance of characterizing the autophagy signaling pathway in different types of cancer in order to decide whether and at what stage autophagy should be modulated in each individual cancer therapy.

4.2 Targeting autophagy on the level of the ULK1 complex

The autophagy inhibitor chloroquine/hydroxychloroquine is currently being tested in several clinical trials (Liu et al., 2020). Our and other studies showed that chloroquine was also able to overcome cisplatin resistance in various cancer cells (Fukuda et al., 2015; Qu et al., 2017; Zhu et al., 2017). However, chloroquine does not specifically target autophagy and it is doubtful that its anti-cancer effect is solely due to the inhibition of autophagy (Eng et al., 2015; Maycotte et al., 2012). Compounds that specifically target ULK1 or VPS34 and inhibit their kinase activities are currently being investigated in preclinical studies (Dowdle et al., 2014; Egan et al., 2015; Petherick et al., 2015; Ronan et al., 2014). This includes the inhibitor SAR405 used in this study. However, both kinases have additional functions outside the autophagy pathway that may also be affected (Bechtel et al., 2013; Parekh et al., 2017; Yuan et al., 2019). Therefore, kinase inhibition might also not be the ideal way to specifically modulate autophagy.

Preclinical studies are still aiming to identify highly specific autophagy inhibitors for clinical use. Besides the inhibition of kinase activities, another possibility is to target the interaction sites of ATG proteins, which could inhibit autophagy and ensure the non-autophagic functions of the targeted proteins. The assembly of the ULK1 complex is highly dependent on ATG13, which recruits ULK1, FIP200 and ATG101 to form the core complex. Therefore, the interaction interfaces of ATG13 could be an ideal target for the modulation of autophagy. In our study, however, the disruption of the ULK1-ATG13 interaction had only a mild effect on starvation-induced autophagy, although formation of the complex was disrupted. This was also shown in a previous study (Hieke et al., 2015), and it is not surprising, as some studies reported ULK1-independent autophagy pathways (Alers et al., 2011; Cheong et al., 2011; Choi et al., 2016; Gao et al., 2016; Manzoni et al., 2016).

Recently, Shi et al. reported that ATG13 assembles the core ULK1 complex at a C-shaped dimer of an N-terminal region of FIP200 (Shi et al., 2020). Accordingly, in our study the ATG13-FIP200 interaction was mandatory for ULK1 complex formation. But unexpectedly, we did not see an effect on autophagy induction after amino acid starvation or mTOR inhibition. We speculate that, in this case, the members of the ULK1 complex might be recruited to the isolation membrane independently, thus maintaining autophagy. In contrast, our group previously reported that in DT40 chicken B cells the deletion of the

FIP200 interaction site in ATG13 leads to the inhibition of autophagy (Alers et al., 2011). In addition, Chen et al. expressed a FIP200 variant in mice that cannot bind ATG13, resulting also in the suppression of autophagy (Chen et al., 2016). The discrepancy to our results might be explained by different model systems or autophagy readouts. In addition, it was recently reported that FIP200 is mandatory for selective autophagy by recruiting the ULK1 complex to the cargo (Ravenhill et al., 2019; Turco et al., 2020; Vargas et al., 2019). However, selective autophagy was not investigated in the mentioned studies. Therefore, the relevance of the ATG13-FIP200 interaction has to be further clarified with respect to its significance for the induction of autophagy.

So far it has been shown that ATG13 interacts with ATG101 via their HORMA domains (Qi et al., 2015; Suzuki et al., 2015). We identified the four amino acid residues I131, R133, V134, and Y138 within the HORMA domain of ATG13 as mandatory for binding ATG101 and mutation of this interaction motif suppressed autophagy. In accordance with our observations, Suzuki et al. mutated the ATG13 binding motif in ATG101, which also resulted in defective autophagy (Suzuki et al., 2015). They suggested two reasons why autophagy is inhibited. First, the protein levels of ATG13 and ATG101 were strongly reduced when binding is inhibited, which is consistent to our observations (Kaizuka and Mizushima, 2016; Suzuki et al., 2015). Second, the unique WF finger in the HORMA domain of ATG101 could be required to recruit adaptor proteins that are important for the induction of autophagy, although these proteins have not yet been identified (Qi et al., 2015; Suzuki et al., 2015). However, future studies will have to assess whether the reduced stability of ATG13 might also affect its non-autophagic functions, e.g. in pathogen control (Mauthe et al., 2016). Furthermore, it is not clear whether selective autophagy is also dependent on the ATG13-ATG101 interaction since we analyzed autophagy only after amino acid starvation or mTOR inhibition. Nonetheless, we suspect that the interaction of ATG13 with ATG101 is a promising target for the specific inhibition of autophagy and that small molecule compounds that interfere with this interaction could be valuable drugs for clinical use.

4.3 FIP200 – A new player in TBK1 regulation

Medically effective therapies are also urgently needed for neurodegenerative diseases. However, these therapies have so far been very difficult to implement, so that neurodegeneration is still considered incurable today. The reasons for their development are diverse, including the dysregulation of TBK1 and the accumulation of disease-specific protein aggregates, which is mainly caused by defective autophagy. In our study we give evidence that FIP200 plays a major role in controlling TBK1 activation and SQSTM1/p62 aggregation. We found that TAX1BP1 mediates the recruitment of TBK1 to SQSTM1/p62 aggregates, and when FIP200 is absent or unable to bind TAX1BP1, aggregation of TBK1 and SQSTM1/p62 is aberrantly enhanced. In line with our results, studies with conditional FIP200 KO mice showed that the loss of FIP200 leads to defective autophagy and accumulation of SQSTM1/p62 aggregates in different cell types (Liu et al., 2013; Wei et al., 2011; Yao et al., 2015). Similarly, Turco

et al. reported that knockdown of FIP200 increases both the numbers and volume of SQSTM1/p62 aggregates (Turco et al., 2019). In addition, they also demonstrated that the Claw region, which is located within the C terminus of FIP200, is needed to degrade SQSTM1/p62 aggregates, as it binds SQSTM1/p62, thereby promoting the formation of autophagosomes (Turco et al., 2019). Besides SQSTM1/p62, TAX1BP1 and NDP52 also bind to the C terminus of FIP200, but apparently outside the Claw region (Ravenhill et al., 2019). Recent reports indicate that NDP52 is responsible for the recruitment of the ULK1 complex to damaged mitochondria or intracellular pathogens via binding to FIP200 (Ravenhill et al., 2019; Vargas et al., 2019). Interestingly, we have observed that TAX1BP1 and not NDP52 is recruited to SQSTM1/p62 aggregates. Our observations are consistent with a manuscript reporting that the clearance of aggregates is mediated by TAX1BP1 (Sarraf et al., 2020). Generally, the binding of FIP200 to TAX1BP1 and SQSTM1/p62 may not be mutually exclusive, as their binding regions differ (Ravenhill et al., 2019; Turco et al., 2019). However, our results clearly show that TAX1BP1 is responsible for the recruitment of TBK1 to SQSTM1/p62 aggregates, which in turn leads to activation of TBK1 and phosphorylation of SQSTM1/p62 within these aggregates.

So far, TBK1 has been described to function during selective autophagy by controlling several components of the autophagy signaling pathway (Kumar et al., 2019; Matsumoto et al., 2015; Pilli et al., 2012; Richter et al., 2016; Wild et al., 2011; Zhao et al., 2018) and facilitating the recruitment of the ULK1 complex to the cargo (Ravenhill et al., 2019; Vargas et al., 2019). However, its regulation during selective autophagy is only marginally understood. We observed that inhibition of autophagy at different stages increased TBK1 activation. In addition, starvation-induced autophagy reduced TBK1 activation, but only in cells with functional autophagy. Yang et al. also observed that TBK1 activation is increased when autophagy is blocked and decreased during starvation-induced autophagy. In line with our observations, Yang et al. (Yang et al., 2016) also observed that starvation-induced autophagy decreased TBK1 activation while inhibition increased its activity. These observations indicate that TBK1 activation is controlled by autophagy.

Besides the general control of TBK1 activity during autophagy, we observed that FIP200 has an additional influence on TBK1 activation, which seems to be independent of its autophagic functions. This is supported by two observations. First, TBK1 aggregation and activation are more prominent in FIP200 KO cells than in other autophagy deficient cell lines, which is consistent with a report by Goodwin et al. (Goodwin et al., 2017). They suggest a compensatory relationship between the ULK1 complex and TBK1 at least for lysosomal ferritin flux (Goodwin et al., 2017). Second, the deletion of the C terminus of FIP200 is already sufficient to increase TBK1 activation, although starvation-induced autophagy is still functional. However, the C terminus is required for the recruitment of FIP200 to the cargo during selective autophagy (Ravenhill et al., 2019; Turco et al., 2019; Vargas et al., 2019). Surprisingly, in the case of SQSTM1/p62 aggregates, FIP200 does not appear to be required for the recruitment of the upstream autophagy machinery such as ULK1, but rather for PtdIns3P formation, ATG16L and WIPI2 recruitment, and activation of ULK1 (Turco et al., 2020; Turco et al., 2019). In

addition, we have shown that FIP200 is also required for the regulation of TBK1 activation in SQSTM1/p62 aggregates and that the other members of the ULK1 complex or high TBK1 activity cannot compensate the absence of FIP200.

We clearly show that FIP200 regulates the activity of TBK1, but further clarification is needed to mechanistically understand this regulation. The removal of TBK1 or the steric hindrance of TBK1 trans-autophosphorylation could be possible ways to achieve this. Okamoto et al. (Okamoto et al., 2020) also reported that FIP200 is involved in the regulation of TBK1 activation. They showed that FIP200 can limit the AZI2/NAP1-TBK1-IRF signaling pathway independently of its autophagic functions to control inflammatory responses (Okamoto et al., 2020; Yeo et al., 2020). In line with this, Saul et al. showed that cellular stress triggers the TBK1 adapters TBKBP1/SINTBAD and AZI2/NAP1 to be incorporated into membraneless organelles to control TBK1 activation (Saul et al., 2019). We cannot say from our data whether the SQSTM1/p62 aggregates observed in our study represent different or identical condensates. However, we did not observe a difference in IFN- β production but in SQSTM1/p62 phosphorylation, specifically at serine 403.

The phosphorylation of SQSTM1/p62 at serine 403 has been linked to the selective autophagic clearance of ubiquitinated proteins and aggregates (Matsumoto et al., 2011). Later it has been shown that this phosphorylation is catalyzed by TBK1 and required for efficient autophagosomal engulfment of mitochondria (Matsumoto et al., 2015; Pilli et al., 2012). In general, SQSTM1/p62 mediates the phase separation of ubiquitinated proteins into larger condensates (Turco et al., 2019) and proteotoxic stress can lead to insolubility of SQSTM1/p62 and TAX1BP1 (Sarraf et al., 2020). Furthermore, Cho et al. (Cho et al., 2018) reported that inhibition of TBK1 prevented the generation of insoluble protein aggregates in hepatocytes. Therefore, we suggest a TAX1BP1-TBK1-SQSTM1/p62 feed-forward loop to ensure efficient engulfment of SQSTM1/p62 aggregates. In addition, the presence of FIP200 on these aggregates appears to be important to recruit the downstream autophagy machinery and to control TBK1 activation and SQSTM1/p62 phosphorylation, otherwise uncontrolled TBK1 activation would excessively increase the size of these aggregates.

As mentioned above, dysregulated TBK1 activity and protein aggregates are closely associated with neurodegenerative diseases. For example, ALS-associated *TBK1* mutations affect phosphorylation of different autophagy receptors such as SQSTM1/p62 (Ye et al., 2019), and inhibition of TBK1 abolished the aberrant insolubility of an OPTN mutant (E50K) found in patients with NTG (Minegishi et al., 2013). Besides TBK1 and SQSTM1/p62, FIP200 was also found to play a role in neuronal homeostasis. Liang et al. (Liang et al., 2010) reported that neural-specific loss of FIP200 in mice causes accumulation of SQSTM1/p62 and ubiquitinated proteins, ultimately leading to cerebellar degeneration. Interestingly, the observed phenotypes were earlier and partially more severe in mice with neural-specific loss of FIP200 than in mice with loss of Atg5 or Atg7 (Liang et al., 2010). We speculate that the FIP200-dependent regulation of TBK1 activity at SQSTM1/p62 aggregates might contribute to these

observations. In addition, we suggest that besides the pharmacological regulation of TBK1 activity, the enforced recruitment of FIP200 to these aggregates may be a promising therapeutic approach.

In summary, we propose the inhibition of autophagy as a possible approach to prevent or overcome cisplatin resistance in bladder cancer and recommend targeting the interaction of ATG13 and ATG101 for specific inhibition of autophagy in certain disease settings. In addition, we suspect that FIP200 may be involved in the development of neurodegenerative diseases. All in all, this dissertation provided molecular insights into the role of autophagy and its therapeutic potential in bladder cancer and neurodegeneration.

5 References

- Ahmad, L., Zhang, S.Y., Casanova, J.L., and Sancho-Shimizu, V. (2016). Human TBK1: A Gatekeeper of Neuroinflammation. *Trends in Molecular Medicine* 22, 511-527.
- Alers, S., Loffler, A.S., Paasch, F., Dieterle, A.M., Keppeler, H., Lauber, K., Campbell, D.G., Fehrenbacher, B., Schaller, M., Wesselborg, S., *et al.* (2011). Atg13 and FIP200 act independently of Ulk1 and Ulk2 in autophagy induction. *Autophagy* 7, 1423-1433.
- Alers, S., Loffler, A.S., Wesselborg, S., and Stork, B. (2012). Role of AMPK-mTOR-Ulk1/2 in the regulation of autophagy: cross talk, shortcuts, and feedbacks. *Mol Cell Biol* 32, 2-11.
- Amaravadi, R.K., and Thompson, C.B. (2007). The roles of therapy-induced autophagy and necrosis in cancer treatment. *Clin Cancer Res* 13, 7271-7279.
- Ávalos, Y., Canales, J., Bravo-Sagua, R., Criollo, A., Lavandero, S., and Quest, A.F.G. (2014). Tumor Suppression and Promotion by Autophagy. *BioMed Research International* 2014.
- Axe, E.L., Walker, S.A., Manifava, M., Chandra, P., Roderick, H.L., Habermann, A., Griffiths, G., and Ktistakis, N.T. (2008). Autophagosome formation from membrane compartments enriched in phosphatidylinositol 3-phosphate and dynamically connected to the endoplasmic reticulum. *Journal of Cell Biology* 182, 685-701.
- Bao, L., Jaramillo, M., Zhang, Y., Zheng, Y., Yao, M., Zhang, D., and Yi, X. (2015). Induction of autophagy contributes to cisplatin resistance in human ovarian cancer cells. *Mol Med Rep* 11, 91-98.
- Bechtel, W., Helmstadter, M., Balica, J., Hartleben, B., Kiefer, B., Hrnjic, F., Schell, C., Kretz, O., Liu, S., Geist, F., *et al.* (2013). Vps34 deficiency reveals the importance of endocytosis for podocyte homeostasis. *J Am Soc Nephrol* 24, 727-743.
- Bender, C.E., Fitzgerald, P., Tait, S.W.G., Llambi, F., McStay, G.P., Tupper, D.O., Pellettieri, J., Sánchez Alvarado, A., Salvesen, G.S., and Green, D.R. (2012). Mitochondrial pathway of apoptosis is ancestral in metazoans. *Proceedings of the National Academy of Sciences of the United States of America* 109, 4904-4909.
- Betin, V.M.S., and Lane, J.D. (2009). Caspase cleavage of Atg4D stimulates GABARAP-L1 processing and triggers mitochondrial targeting and apoptosis. *Journal of Cell Science* 122, 2554-2566.
- Birgisdottir, A.B., Lamark, T., and Johansen, T. (2013). The LIR motif - crucial for selective autophagy. *J Cell Sci* 126, 3237-3247.
- Bray, F., Ferlay, J., Soerjomataram, I., Siegel, R.L., Torre, L.A., and Jemal, A. (2018). Global cancer statistics 2018: GLOBOCAN estimates of incidence and mortality worldwide for 36 cancers in 185 countries. *CA Cancer J Clin* 68, 394-424.
- Chano, T., Ikegawa, S., Saito-Ohara, F., Inazawa, J., Mabuchi, A., Saeki, Y., and Okabe, H. (2002). Isolation, characterization and mapping of the mouse and human RB1CC1 genes. *Gene* 291, 29-34.
- Chen, S., Wang, C., Yeo, S., Liang, C.C., Okamoto, T., Sun, S., Wen, J., and Guan, J.L. (2016). Distinct roles of autophagy-dependent and -independent functions of FIP200 revealed by generation and analysis of a mutant knock-in mouse model. *Genes Dev* 30, 856-869.
- Cheong, H., Lindsten, T., Wu, J., Lu, C., and Thompson, C.B. (2011). Ammonia-induced autophagy is independent of ULK1/ULK2 kinases. *Proc Natl Acad Sci U S A* 108, 11121-11126.
- Cho, C.S., Park, H.W., Ho, A., Semple, I.A., Kim, B., Jang, I., Park, H., Reilly, S., Saltiel, A.R., and Lee, J.H. (2018). Lipotoxicity induces hepatic protein inclusions through TANK binding kinase 1-mediated p62/sequestosome 1 phosphorylation. *Hepatology* 68, 1331-1346.

- Choi, H., Merceron, C., Mangiavini, L., Seifert, E.L., Schipani, E., Shapiro, I.M., and Risbud, M.V. (2016). Hypoxia promotes noncanonical autophagy in nucleus pulposus cells independent of mTOR and HIF1A signaling. *Autophagy* *12*, 1631-1646.
- Degenhardt, K., Mathew, R., Beaudoin, B., Bray, K., Anderson, D., Chen, G., Mukherjee, C., Shi, Y., Gelinas, C., Fan, Y., *et al.* (2006). Autophagy promotes tumor cell survival and restricts necrosis, inflammation, and tumorigenesis. *Cancer Cell* *10*, 51-64.
- Dewson, G., and Kluck, R.M. (2009). Mechanisms by which Bak and Bax permeabilise mitochondria during apoptosis. *Journal of Cell Science* *122*, 2801-2808.
- Dooley, H.C., Razi, M., Polson, H.E., Girardin, S.E., Wilson, M.I., and Tooze, S.A. (2014). WIPI2 links LC3 conjugation with PI3P, autophagosome formation, and pathogen clearance by recruiting Atg12-5-16L1. *Mol Cell* *55*, 238-252.
- Dowdle, W.E., Nyfeler, B., Nagel, J., Elling, R.a., Liu, S., Triantafellow, E., Menon, S., Wang, Z., Honda, A., Pardee, G., *et al.* (2014). Selective VPS34 inhibitor blocks autophagy and uncovers a role for NCOA4 in ferritin degradation and iron homeostasis in vivo. *Nature Cell Biology* *16*.
- Drayton, R.M., and Catto, J.W.F. (2013). Molecular mechanisms of cisplatin resistance in bladder cancer. *Expert Rev Anticancer Ther* *12*, 1-4.
- Egan, D.F., Chun, M.G., Vamos, M., Zou, H., Rong, J., Miller, C.J., Lou, H.J., Raveendra-Panickar, D., Yang, C.C., Sheffler, D.J., *et al.* (2015). Small Molecule Inhibition of the Autophagy Kinase ULK1 and Identification of ULK1 Substrates. *Mol Cell* *59*, 285-297.
- Eisenacher, K., and Krug, A. (2012). Regulation of RLR-mediated innate immune signaling--it is all about keeping the balance. *Eur J Cell Biol* *91*, 36-47.
- El-Zayat, S.R., Sibaii, H., and Mannaa, F.A. (2019). Toll-like receptors activation, signaling, and targeting: an overview. *Bulletin of the National Research Centre* *43*.
- Elmore, S. (2007). Apoptosis: A Review of Programmed Cell Death. *Toxicol Pathol* *35*, 495-516.
- Eng, C.H., Wang, Z., Tkach, D., Toral-Barza, L., Ugwonali, S., Liu, S., Fitzgerald, S.L., George, E., Frias, E., Cochran, N., *et al.* (2015). Macroautophagy is dispensable for growth of KRAS mutant tumors and chloroquine efficacy. *PNAS* *113*, 182-187.
- Eskes, R., Desagher, S., Antonsson, B., and Martinou, J.C. (2000). Bid induces the oligomerization and insertion of Bax into the outer mitochondrial membrane. *Molecular and cellular biology* *20*, 929-935.
- Fecto, F., Yan, J., Vemula, S.P., Liu, E., Yang, Y., Chen, W., Zheng, J.G., Shi, Y., Siddique, N., Arrat, H., *et al.* (2011). SQSTM1 Mutations in Familial and Sporadic Amyotrophic Lateral Sclerosis. *Archives of neurology* *68*.
- Feng, W., Huang, S., Wu, H., and Zhang, M. (2007). Molecular Basis of Bcl-xL's Target Recognition Versatility Revealed by the Structure of Bcl-xL in Complex with the BH3 Domain of Beclin-1. *Journal of Molecular Biology* *372*, 223-235.
- Forman, M.S., Trojanowski, J.Q., and Lee, V.M.-Y. (2004). Neurodegenerative diseases: a decade of discoveries paves the way for therapeutic breakthroughs. *Nature Medicine* *10*, 1055-1063(2004).
- Freischmidt, A., Wieland, T., Richter, B., Ruf, W., Schaeffer, V., Müller, K., Marroquin, N., Nordin, F., Hübers, A., Weydt, P., *et al.* (2015). Haploinsufficiency of TBK1 causes familial ALS and frontotemporal dementia. *Nature Neuroscience* *18*, 631-636.
- Fu, T., Liu, J., Wang, Y., Xie, X., Hu, S., and Pan, L. (2018). Mechanistic insights into the interactions of NAP1 with the SKICH domains of NDP52 and TAX1BP1. *Proceedings of the National Academy of Sciences of the United States of America* *115*, E11651-E11660.
- Fujioka, Y., Noda, N.N., Nakatogawa, H., Ohsumi, Y., and Inagaki, F. (2010). Dimeric coiled-coil structure of *Saccharomyces cerevisiae* Atg16 and its functional significance in autophagy. *J Biol Chem* *285*, 1508-1515.

- Fujioka, Y., Suzuki, S.W., Yamamoto, H., Kondo-Kakuta, C., Kimura, Y., Hirano, H., Akada, R., Inagaki, F., Ohsumi, Y., and Noda, N.N. (2014). Structural basis of starvation-induced assembly of the autophagy initiation complex. *Nat Struct Mol Biol* *21*, 513-521.
- Fujita, N., Hayashi-Nishino, M., Fukumoto, H., Omori, H., Yamamoto, A., Noda, T., and Yoshimori, T. (2008). An Atg4B Mutant Hampers the Lipidation of LC3 Paralogues and Causes Defects in Autophagosome Closure. *Molecular Biology of the Cell* *19*, 4545-5029.
- Fukuda, T., Oda, K., Wada-Hiraike, O., Sone, K., Inaba, K., Ikeda, Y., Miyasaka, A., Kashiyama, T., Tanikawa, M., Arimoto, T., *et al.* (2015). The anti-malarial chloroquine suppresses proliferation and overcomes cisplatin resistance of endometrial cancer cells via autophagy inhibition. *Gynecol Oncol* *137*, 538-545.
- Galluzzi, L., and Green, D.R. (2019). Autophagy-Independent Functions of the Autophagy Machinery. *Cell* *177*, 1682-1699.
- Galluzzi, L., Senovilla, L., Vitale, I., Michels, J., Martins, I., Kepp, O., Castedo, M., and Kroemer, G. (2012). Molecular mechanisms of cisplatin resistance. *Oncogene* *31*, 1869-1883.
- Gan, B., and Guan, J.L. (2008). FIP200, a key signaling node to coordinately regulate various cellular processes. *Cellular Signalling* *20*, 787-794.
- Gan, B., Peng, X., Nagy, T., Alcaraz, A., Gu, H., and Guan, J.L. (2006). Role of FIP200 in cardiac and liver development and its regulation of TNFalpha and TSC-mTOR signaling pathways. *J Cell Biol* *175*, 121-133.
- Ganley, I.G., Lam du, H., Wang, J., Ding, X., Chen, S., and Jiang, X. (2009). ULK1.ATG13.FIP200 complex mediates mTOR signaling and is essential for autophagy. *J Biol Chem* *284*, 12297-12305.
- Gao, Y., Liu, Y., Hong, L., Yang, Z., Cai, X., Chen, X., Fu, Y., Lin, Y., Wen, W., Li, S., *et al.* (2016). Golgi-associated LC3 lipidation requires V-ATPase in noncanonical autophagy. *Cell Death Dis* *7*, e2330.
- García-Cano, J., Ambroise, G., Pascual-Serra, R., Carrión, M.C., Serrano-Oviedo, L., Ortega-Muelas, M., Cimas, F.J., Sabater, S., Ruiz-Hidalgo, M.J., Sanchez Perez, I., *et al.* (2015). Exploiting the potential of autophagy in cisplatin therapy: A new strategy to overcome resistance. *Oncotarget* *6*.
- Geeraert, C., Ratier, A., Pfisterer, S.G., Perdiz, D., Cantaloube, I., Rouault, A., Patingre, S., Proikas-Cezanne, T., Codogno, P., and Pous, C. (2010). Starvation-induced hyperacetylation of tubulin is required for the stimulation of autophagy by nutrient deprivation. *J Biol Chem* *285*, 24184-24194.
- Goodwin, J.M., Dowdle, W.E., DeJesus, R., Wang, Z., Bergman, P., Kobylarz, M., Lindeman, A., Xavier, R.J., McAllister, G., Nyfeler, B., *et al.* (2017). Autophagy-Independent Lysosomal Targeting Regulated by ULK1/2-FIP200 and ATG9. *Cell Reports* *20*, 2341-2356.
- Gu, Y., Fei, Z., and Zhu, R. (2020). miR-21 modulates cisplatin resistance of gastric cancer cells by inhibiting autophagy via the PI3K/Akt/mTOR pathway. *Anticancer Drugs* *31*, 385-393.
- Gwinn, D.M., Shackelford, D.B., Egan, D.F., Mihaylova, M.M., Mery, A., Vasquez, D.S., Turk, B.E., and Shaw, R.J. (2008). AMPK phosphorylation of raptor mediates a metabolic checkpoint. *Mol Cell* *30*, 214-226.
- Hara, T., Nakamura, K., Matsui, M., Yamamoto, A., Nakahara, Y., Suzuki-Migishima, R., Yokoyama, M., Mishima, K., Saito, I., Okano, H., *et al.* (2006). Suppression of basal autophagy in neural cells causes neurodegenerative disease in mice. *Nature* *441*, 885-889.
- He, J., Yu, J.J., Xu, Q., Wang, L., Zheng, J.Z., Liu, L.Z., and Jiang, B.H. (2015). Downregulation of ATG14 by EGR1-MIR152 sensitizes ovarian cancer cells to cisplatin-induced apoptosis by inhibiting cyto-protective autophagy. *Autophagy* *11*, 373-384.
- Helgason, E., Phung, Q.T., and Dueber, E.C. (2013). Recent insights into the complexity of Tank-binding kinase 1 signaling networks: The emerging role of cellular localization in the activation and substrate specificity of TBK1. *FEBS Letters* *587*, 1230-1237.

- Hieke, N., Löffler, A.S., Kaizuka, T., Berleth, N., Bohler, P., Driessen, S., Stuhldreier, F., Friesen, O., Assani, K., Schmitz, K., *et al.* (2015). Expression of a ULK1/2 binding-deficient ATG13 variant can partially restore autophagic activity in ATG13-deficient cells. *Autophagy* *11*, 1471-1483.
- Höhn, A., Krüger, K., Skowron, M.A., Bormann, S., Schumacher, L., Schulz, W.A., Hoffmann, M.J., Niegisch, G., and Fritz, G. (2016). Distinct mechanisms contribute to acquired cisplatin resistance of urothelial carcinoma cells. *Oncotarget* *7*, 41320–41335.
- Hosokawa, N., Hara, T., Kaizuka, T., Kishi, C., Takamura, A., Miura, Y., Iemura, S.-i., Natsume, T., Takehana, K., Yamada, N., *et al.* (2009). Nutrient-dependent mTORC1 Association with the ULK1–Atg13–FIP200 Complex Required for Autophagy. *Molecular Biology of the Cell* *20*, 1891-2129.
- Hu, Y., Benedict, M.A., Ding, L., and Núñez, G. (1999). Role of cytochrome c and dATP/ATP hydrolysis in Apaf-1-mediated caspase-9 activation and apoptosis. *The EMBO journal* *18*, 3586-3595.
- Hu, Z., Cai, M., Zhang, Y., Tao, L., and Guo, R. (2020). miR-29c-3p inhibits autophagy and cisplatin resistance in ovarian cancer by regulating FOXP1/ATG14 pathway. *Cell Cycle* *19*, 193-206.
- Isogai, S., Morimoto, D., Arita, K., Unzai, S., Tenno, T., Hasegawa, J., Sou, Y.S., Komatsu, M., Tanaka, K., Shirakawa, M., *et al.* (2011). Crystal structure of the ubiquitin-associated (UBA) domain of p62 and its interaction with ubiquitin. *J Biol Chem* *286*, 31864-31874.
- Itakura, E., and Mizushima, N. (2010). Characterization of autophagosome formation site by a hierarchical analysis of mammalian Atg proteins. *Autophagy* *6*, 764-776.
- Jahreiss, L., Menzies, F.M., and Rubinsztein, D.C. (2008). The itinerary of autophagosomes: from peripheral formation to kiss-and-run fusion with lysosomes. *Traffic* *9*, 574-587.
- Ji, C.H., and Kwon, Y.T. (2017). Crosstalk and Interplay between the Ubiquitin-Proteasome System and Autophagy. *Mol Cells* *40*, 441-449.
- Johansen, T., and Lamark, T. (2020). Selective Autophagy: ATG8 Family Proteins, LIR Motifs and Cargo Receptors. *J Mol Biol* *432*, 80-103.
- Joo, J.H., Dorsey, F.C., Joshi, A., Hennessy-Walters, K.M., Rose, K.L., McCastlain, K., Zhang, J., Iyengar, R., Jung, C.H., Suen, D.F., *et al.* (2011). Hsp90-Cdc37 chaperone complex regulates Ulk1- and Atg13-mediated mitophagy. *Mol Cell* *43*, 572-585.
- Joshi, A., Iyengar, R., Joo, J.H., Li-Harms, X.J., Wright, C., Marino, R., Winborn, B.J., Phillips, A., Temirov, J., Sciarretta, S., *et al.* (2016). Nuclear ULK1 promotes cell death in response to oxidative stress through PARP1. *Cell Death Differ* *23*, 216-230.
- Jounai, N., Takeshita, F., Kobiyama, K., Sawano, A., Miyawaki, A., Xin, K.Q., Ishii, K.J., Kawai, T., Akira, S., Suzuki, K., *et al.* (2007). The Atg5 Atg12 conjugate associates with innate antiviral immune responses. *Proc Natl Acad Sci U S A* *104*, 14050-14055.
- Jung, C.H., Bong Jun, C., Ro, S.-H., Kim, Y.-M., Otto, N.M., Cao, J., Kundu, M., and Kim, D.-H. (2009). ULK-Atg13-FIP200 Complexes Mediate mTOR Signaling to the Autophagy Machinery. *Molecular Biology of the Cell* *20*, 1992–2003.
- Kaiser, S.E., Mao, K., Taherbhoy, A.M., Yu, S., Olszewski, J.L., Duda, D.M., Kurinov, I., Deng, A., Fenn, T.D., Klionsky, D.J., *et al.* (2012). Noncanonical E2 recruitment by the autophagy E1 revealed by Atg7-Atg3 and Atg7-Atg10 structures. *Nat Struct Mol Biol* *19*, 1242-1249.
- Kaizuka, T., and Mizushima, N. (2016). Atg13 Is Essential for Autophagy and Cardiac Development in Mice. *Mol Cell Biol* *36*, 585-595.
- Kamada, Y., Funakoshi, T., Shintani, T., Nagano, K., Ohsumi, M., and Ohsumi, Y. (2000). Tor-Mediated Induction of Autophagy via an Apg1 Protein Kinase Complex. *Journal of Cell Biology* *150*, 1507–1513.
- Karanasios, E., Walker, S.A., Okkenhaug, H., Manifava, M., Hummel, E., Zimmermann, H., Ahmed, Q., Domart, M.-C., Collinson, L., and Ktistakis, N.T. (2016). Autophagy initiation by ULK

- complex assembly on ER tubulovesicular regions marked by ATG9 vesicles. *Nature Communications* 7.
- Kaushik, S., and Cuervo, A.M. (2012). Chaperone-mediated autophagy: a unique way to enter the lysosome world. *Trends Cell Biol* 22, 407-417.
- Kim, B.W., Kwon, D.H., and Song, H.K. (2016). Structure biology of selective autophagy receptors. *BMB Rep* 49, 73-80.
- Kirisako, T., Ichimura, Y., Okada, H., Kabeya, Y., Mizushima, N., Yoshimori, T., Ohsumi, M., Takao, T., Noda, T., and Ohsumi, Y. (2000). The Reversible Modification Regulates the Membrane-Binding State of Apg8/Aut7 Essential for Autophagy and the Cytoplasm to Vacuole Targeting Pathway. *Journal of Cell Biology* 151, 263–276.
- Kirkin, V., and Rogov, V.V. (2019). A Diversity of Selective Autophagy Receptors Determines the Specificity of the Autophagy Pathway. *Molecular Cell* 76, 268-285.
- Knowles, M.A. (2006). Molecular subtypes of bladder cancer: Jekyll and Hyde or chalk and cheese? *Carcinogenesis* 27, 361-373.
- Komatsu, M., Waguri, S., Chiba, T., Murata, S., Iwata, J., Tanida, I., Ueno, T., Koike, M., Uchiyama, Y., Kominami, E., *et al.* (2006). Loss of autophagy in the central nervous system causes neurodegeneration in mice. *Nature* 441, 880-884.
- Komatsu, M., Waguri, S., Ueno, T., Iwata, J., Murata, S., Tanida, I., Ezaki, J., Mizushima, N., Ohsumi, Y., Uchiyama, Y., *et al.* (2005). Impairment of starvation-induced and constitutive autophagy in Atg7-deficient mice. *J Cell Biol* 169, 425-434.
- Koyama, S., Ishii, K.J., Coban, C., and Akira, S. (2008). Innate immune response to viral infection. *Cytokine* 43, 336-341.
- Kraft, C., Kijanska, M., Kalie, E., Siergiejuk, E., Lee, S.S., Semplicio, G., Stoffel, I., Brezovich, A., Verma, M., Hansmann, I., *et al.* (2012). Binding of the Atg1/ULK1 kinase to the ubiquitin-like protein Atg8 regulates autophagy. *EMBO Journal* 31, 3691-3703.
- Kroemer, G., Marino, G., and Levine, B. (2010). Autophagy and the integrated stress response. *Mol Cell* 40, 280-293.
- Kuma, A., Hatano, M., Matsui, M., Yamamoto, A., Nakaya, H., Yoshimori, T., Ohsumi, Y., Tokuhisa, T., and Mizushima, N. (2004). The role of autophagy during the early neonatal starvation period. *Nature* 432, 1032–1036.
- Kumar, S., Gu, Y., Abudu, Y.P., Bruun, J.A., Jain, A., Farzam, F., Mudd, M., Anonsen, J.H., Rusten, T.E., Kasof, G., *et al.* (2019). Phosphorylation of Syntaxin 17 by TBK1 Controls Autophagy Initiation. *Developmental Cell* 49, 130-144.e136.
- Lee, E.J., and Tournier, C. (2011). The requirement of uncoordinated 51-like kinase 1 (ULK1) and ULK2 in the regulation of autophagy. *Autophagy* 7, 689-695.
- Lee, Y.K., and Lee, J.A. (2016). Role of the mammalian ATG8/LC3 family in autophagy: differential and compensatory roles in the spatiotemporal regulation of autophagy. *BMB Rep* 49, 424-430.
- Li, J.R., Cheng, C.L., Yang, C.R., Ou, Y.C., Wu, M.J., and Ko, J.L. (2013). Dual inhibitor of phosphoinositide 3-kinase/mammalian target of rapamycin NVP-BEZ235 effectively inhibits cisplatin-resistant urothelial cancer cell growth through autophagic flux. *Toxicol Lett* 220, 267-276.
- Li, P., Nijhawan, D., Budihardjo, I., Srinivasula, S.M., Ahmad, M., Alnemri, E.S., and Wang, X. (1997). Cytochrome c and dATP-dependent formation of Apaf-1/caspase-9 complex initiates an apoptotic protease cascade. *Cell* 91, 479-489.
- Li, W.W., Li, J., and Bao, J.K. (2012). Microautophagy: lesser-known self-eating. *Cell Mol Life Sci* 69, 1125-1136.

- Liang, C.C., Wang, C., Peng, X., Gan, B., and Guan, J.L. (2010). Neural-specific deletion of FIP200 leads to cerebellar degeneration caused by increased neuronal death and axon degeneration. *J Biol Chem* 285, 3499-3509.
- Liang, X.H., Jackson, S., Seaman, M., Brown, K., Kempkes, B., Hibshoosh, H., and Levine, B. (1999). Induction of autophagy and inhibition of tumorigenesis by *beclin 1*. *Nature* 402, 672-676.
- Liebl, M.P., and Hoppe, T. (2016). It's all about talking: two-way communication between proteasomal and lysosomal degradation pathways via ubiquitin. *Am J Physiol Cell Physiol* 311, C166-178.
- Lim, J., Lachenmayer, M.L., Wu, S., Liu, W., Kundu, M., Wang, R., Komatsu, M., Oh, Y.J., Zhao, Y., and Yue, Z. (2015). Proteotoxic stress induces phosphorylation of p62/SQSTM1 by ULK1 to regulate selective autophagic clearance of protein aggregates. *PLoS Genet* 11, e1004987.
- Lin, J.-F., Lin, Y.-C., Tsai, T.-F., Chen, H.-E., Chou, K.-Y., and Hwang, I.S. (2017). Cisplatin induces protective autophagy through activation of BECN1 in human bladder cancer cells. *Drug Design, Development and Therapy Volume 11*, 1517-1533.
- Liu, F., Fang, F., Yuan, H., Yang, D., Chen, Y., Williams, L., Goldstein, S.A., Krebsbach, P.H., and Guan, J.-L. (2013). Suppression of autophagy by FIP200 deletion leads to osteopenia in mice through the inhibition of osteoblast terminal differentiation. *Journal of Bone and Mineral Research* 28, 2414-2430.
- Liu, S., Cai, X., Wu, J., Cong, Q., Chen, X., Li, T., Du, F., Ren, J., Wu, Y.T., Grishin, N.V., *et al.* (2015). Phosphorylation of innate immune adaptor proteins MAVS, STING, and TRIF induces IRF3 activation. *Science* 347, aaa2630-aaa2630.
- Liu, T., Zhang, J., Li, K., Deng, L., and Wang, H. (2020). Combination of an Autophagy Inducer and an Autophagy Inhibitor: A Smarter Strategy Emerging in Cancer Therapy. *Front Pharmacol* 11, 408.
- Ma, X., Helgason, E., Phung, Q.T., Quan, C.L., Iyer, R.S., Lee, M.W., Bowman, K.K., Starovasnik, M.a., and Dueber, E.C. (2012). Molecular basis of Tank-binding kinase 1 activation by transautophosphorylation. *Proceedings of the National Academy of Sciences* 109, 9378-9383.
- Mack, H.I., Zheng, B., Asara, J.M., and Thomas, S.M. (2012). AMPK-dependent phosphorylation of ULK1 regulates ATG9 localization. *Autophagy* 8, 1197-1214.
- Mallucci, G.R., Klenerman, D., and Rubinsztein, D.C. (2020). Developing Therapies for Neurodegenerative Disorders: Insights from Protein Aggregation and Cellular Stress Responses. *Annu Rev Cell Dev Biol* 36, 165-189.
- Mani, J., Vallo, S., Rakel, S., Antonietti, P., Gessler, F., Blaheta, R., Bartsch, G., Michaelis, M., Cinatl, J., Haferkamp, A., *et al.* (2015). Chemoresistance is associated with increased cytoprotective autophagy and diminished apoptosis in bladder cancer cells treated with the BH3 mimetic (-)-Gossypol (AT-101). *BMC Cancer* 15, 1-14.
- Manzoni, C., Mamais, A., Roosen, D.A., Dihanich, S., Soutar, M.P., Plun-Favreau, H., Bandopadhyay, R., Hardy, J., Tooze, S.A., Cookson, M.R., *et al.* (2016). mTOR independent regulation of macroautophagy by Leucine Rich Repeat Kinase 2 via Beclin-1. *Sci Rep* 6, 35106.
- Marquez, R.T., and Xu, L.G. (2012). Bcl-2:Beclin 1 complex: multiple, mechanisms regulating autophagy/apoptosis toggle switch. *American Journal of Cancer Research* 2, 214-221.
- Maruyama, H., Morino, H., Ito, H., Izumi, Y., Kato, H., Watanabe, Y., Kinoshita, Y., Kamada, M., Nodera, H., Suzuki, H., *et al.* (2010). Mutations of optineurin in amyotrophic lateral sclerosis. *Nature* 465, 223-226.
- Matsumoto, G., Shimogori, T., Hattori, N., and Nukina, N. (2015). TBK1 controls autophagosomal engulfment of polyubiquitinated mitochondria through p62/SQSTM1 phosphorylation. *Human molecular genetics* 24, 4429-4442.

- Matsumoto, G., Wada, K., Okuno, M., Kurosawa, M., and Nukina, N. (2011). Serine 403 phosphorylation of p62/SQSTM1 regulates selective autophagic clearance of ubiquitinated proteins. *Mol Cell* *44*, 279-289.
- Matsunaga, K., Morita, E., Saitoh, T., Akira, S., Ktistakis, N.T., Izumi, T., Noda, T., and Yoshimori, T. (2010). Autophagy requires endoplasmic reticulum targeting of the PI3-kinase complex via Atg14L. *J Cell Biol* *190*, 511-521.
- Mauthe, M., Langereis, M., Jung, J., Zhou, X., Jones, A., Omta, W., Tooze, S.A., Stork, B., Paludan, S.R., Ahola, T., *et al.* (2016). An siRNA screen for ATG protein depletion reveals the extent of the unconventional functions of the autophagy proteome in virus replication. *Journal of Cell Biology* *214*, 619-635.
- Maycotte, P., Aryal, S., Cummings, C.T., Thorburn, J., Morgan, M.J., and Thorburn, A. (2012). Chloroquine sensitizes breast cancer cells to chemotherapy independent of autophagy. *Autophagy* *8*, 200-212.
- Mei, Y., Su, M., Soni, G., Salem, S., Colbert, C.L., and Sinha, S.C. (2014). Intrinsically disordered regions in autophagy proteins. *Proteins* *82*, 565-578.
- Metlagel, Z., Otomo, C., Takaesu, G., and Otomo, T. (2013). Structural basis of ATG3 recognition by the autophagic ubiquitin-like protein ATG12. *PNAS* *110*, 18844-18849.
- Michel, M., Schwarten, M., Decker, C., Nagel-Steger, L., Willbold, D., and Weiergraber, O.H. (2015). The mammalian autophagy initiator complex contains 2 HORMA domain proteins. *Autophagy* *11*, 2300-2308.
- Minegishi, Y., Iejima, D., Kobayashi, H., Chi, Z.L., Kawase, K., Yamamoto, T., Seki, T., Yuasa, S., Fukuda, K., and Iwata, T. (2013). Enhanced optineurin E50K-TBK1 interaction evokes protein insolubility and initiates familial primary open-angle glaucoma. *Hum Mol Genet* *22*, 3559-3567.
- Mizushima, N. (2020). The ATG conjugation systems in autophagy. *Current Opinion in Cell Biology* *63*, 1-10.
- Mizushima, N., Kuma, A., Kobayashi, Y., Yamamoto, A., Matsubae, M., Takao, T., Natsume, T., Ohsumi, Y., and Yoshimori, T. (2003). Mouse Apg16L, a novel WD-repeat protein, targets to the autophagic isolation membrane with the Apg12-Apg5 conjugate. *Journal of Cell Science* *116*, 1679-1688.
- Mizushima, N., Noda, T., Yoshimori, T., Tanaka, Y., Ishii, T., George, M.D., Klionsky, D.J., Ohsumi, M., and Ohsumi, Y. (1998a). A protein conjugation system essential for autophagy. *Nature* *395*, 395-398.
- Mizushima, N., Sugita, H., Yoshimori, T., and Ohsumi, Y. (1998b). A new protein conjugation system in human. The counterpart of the yeast Apg12p conjugation system essential for autophagy. *The Journal of Biological Chemistry* *273*, 33889-33892.
- Motwani, M., Pesiridis, S., and Fitzgerald, K.A. (2019). DNA sensing by the cGAS-STING pathway in health and disease. *Nat Rev Genet* *20*, 657-674.
- Mukhopadhyay, S., Panda, P.K., Sinha, N., Das, D.N., and Bhutia, S.K. (2014). Autophagy and apoptosis: where do they meet? *Apoptosis* *19*, 555-566.
- Nakamura, S., and Yoshimori, T. (2017). New insights into autophagosome-lysosome fusion. *J Cell Sci* *130*, 1209-1216.
- Nakatogawa, H., Ichimura, Y., and Ohsumi, Y. (2007). Atg8, a ubiquitin-like protein required for autophagosome formation, mediates membrane tethering and hemifusion. *Cell* *130*, 165-178.
- Nakatogawa, H., Ishii, J., Asai, E., and Ohsumi, Y. (2014). Atg4 recycles inappropriately lipidated Atg8 to promote autophagosome biogenesis. *Autophagy* *8*, 177-186.
- Neumann, M., Sampathu, D.M., Kwong, L.K., Truax, A.C., Micsenyi, M.C., Chou, T.T., Bruce, J., Schuck, T., Grossman, M., Clark, C.M., *et al.* (2006). Ubiquitinated TDP-43 in Frontotemporal Lobar Degeneration and Amyotrophic Lateral Sclerosis. *Science* *314*.

- Noda, N.N., Satoo, K., Fujioka, Y., Kumeta, H., Ogura, K., Nakatogawa, H., Ohsumi, Y., and Inagaki, F. (2011). Structural basis of Atg8 activation by a homodimeric E1, Atg7. *Mol Cell* *44*, 462-475.
- Ojha, R., Singh, S.K., Bhattacharyya, S., Dhanda, R.S., Rakha, A., Mandal, A.K., and Jha, V. (2014). Inhibition of grade dependent autophagy in urothelial carcinoma increases cell death under nutritional limiting condition and potentiates the cytotoxicity of chemotherapeutic agent. *Journal of Urology* *191*, 1889-1898.
- Okamoto, T., Yeo, S.K., Hao, M., Copley, M.R., Haas, M.A., Chen, S., and Guan, J.L. (2020). FIP200 Suppresses Immune Checkpoint Therapy Responses in Breast Cancers by Limiting AZI2/TBK1/IRF Signaling Independent of Its Canonical Autophagy Function. *Cancer Res* *80*, 3580-3592.
- Otomo, C., Metlagel, Z., Takaesu, G., and Otomo, T. (2013). Structure of the human ATG12~ATG5 conjugate required for LC3 lipidation in autophagy. *Nat Struct Mol Biol* *20*, 59-66.
- Parekh, V.V., Pabbisetty, S.K., Wu, L., Sebzda, E., Martinez, J., Zhang, J., and Van Kaer, L. (2017). Autophagy-related protein Vps34 controls the homeostasis and function of antigen cross-presenting CD8alpha(+) dendritic cells. *Proc Natl Acad Sci U S A* *114*, E6371-E6380.
- Park, J.M., Jung, C.H., Seo, M., Otto, N.M., Grunwald, D., Kim, K.H., Moriarity, B., Kim, Y.M., Starker, C., Nho, R.S., *et al.* (2016). The ULK1 complex mediates MTORC1 signaling to the autophagy initiation machinery via binding and phosphorylating ATG14. *Autophagy* *12*, 547-564.
- Park, J.M., Seo, M., Jung, C.H., Grunwald, D., Stone, M., Otto, N.M., Toso, E., Ahn, Y., Kyba, M., Griffin, T.J., *et al.* (2018). ULK1 phosphorylates Ser30 of BECN1 in association with ATG14 to stimulate autophagy induction. *Autophagy* *14*, 584-597.
- Pattingre, S., Tassa, A., Qu, X., Garuti, R., Liang, X.H., Mizushima, N., Packer, M., Schneider, M.D., and Levine, B. (2005). Bcl-2 antiapoptotic proteins inhibit Beclin 1-dependent autophagy. *Cell* *122*, 927-939.
- Pengo, N., Agrotis, A., Prak, K., Jones, J., and Ketteler, R. (2017). A reversible phospho-switch mediated by ULK1 regulates the activity of autophagy protease ATG4B. *Nature Communications* *8*.
- Peter, C., Wesselborg, S., Herrmann, M., and Lauber, K. (2010). Dangerous attraction: phagocyte recruitment and danger signals of apoptotic and necrotic cells. *Apoptosis : an international journal on programmed cell death* *15*, 1007-1028.
- Petherick, K.J., Conway, O.J.L., Mpamhanga, C., Osborne, S.a., Kamal, A., Saxty, B., and Ganley, I.G. (2015). Pharmacological Inhibition of ULK1 Blocks mTOR-Dependent Autophagy. *Journal of Biological Chemistry* *290*, 11376-11383.
- Pilli, M., Arko-Mensah, J., Ponpuak, M., Roberts, E., Master, S., Mandell, M.A., Dupont, N., Ornatowski, W., Jiang, S., Bradfute, S.B., *et al.* (2012). TBK-1 Promotes Autophagy-Mediated Antimicrobial Defense by Controlling Autophagosome Maturation. *Immunity* *37*, 223-234.
- Pinto-Leite, R., Arantes-Rodrigues, R., Palmeira, C., Colaço, B., Lopes, C., Colaço, A., Costa, C., da Silva, V.M., Oliveira, P., and Santos, L. (2013). Everolimus combined with cisplatin has a potential role in treatment of urothelial bladder cancer. *Biomedicine & Pharmacotherapy* *67*, 116-121.
- Pohl, C., and Dikic, I. (2019). Cellular quality control by the ubiquitin-proteasome system and autophagy. *Science* *366*, 818-822.
- Polson, H.E., de Lartigue, J., Rigden, D.J., Reedijk, M., Urbe, S., Clague, M.J., and Tooze, S.A. (2010). Mammalian Atg18 (WIPI2) localizes to omegasome-anchored phagophores and positively regulates LC3 lipidation. *Autophagy* *6*, 506-522.
- Pottier, C., Bieniek, K.F., Finch, N., van de Vorst, M., Baker, M., Perkersen, R., Brown, P., Ravenscroft, T., van Blitterswijk, M., Nicholson, A.M., *et al.* (2015). Whole-genome sequencing reveals

- important role for TBK1 and OPTN mutations in frontotemporal lobar degeneration without motor neuron disease. *Acta Neuropathologica* *130*, 77-92.
- Prabakaran, T., Bodda, C., Krapp, C., Zhang, B.-C., Christensen, M.H., Sun, C., Reinert, L., Cai, Y., Jensen, S.B., Skouboe, M.K., *et al.* (2018). Attenuation of cGAS-STING signaling is mediated by a p62/SQSTM1-dependent autophagy pathway activated by TBK1. *The EMBO Journal*.
- Proikas-Cezanne, T., Takacs, Z., Donnes, P., and Kohlbacher, O. (2015). WIPI proteins: essential PtdIns3P effectors at the nascent autophagosome. *J Cell Sci* *128*, 207-217.
- Qi, S., Kim, D.J., Stjepanovic, G., and Hurley, J.H. (2015). Structure of the Human Atg13-Atg101 HORMA Heterodimer: an Interaction Hub within the ULK1 Complex. *Structure* *23*, 1848-1857.
- Qu, X., Sheng, J., Shen, L., Su, J., Xu, Y., Xie, Q., Wu, Y., Zhang, X., and Sun, L. (2017). Autophagy inhibitor chloroquine increases sensitivity to cisplatin in QBC939 cholangiocarcinoma cells by mitochondrial ROS. *PLoS One* *12*, e0173712.
- Qu, X., Yu, J., Bhagat, G., Furuya, N., Hibshoosh, H., Troxel, A., Rosen, J., Eskelinen, E.-L., Mizushima, N., Ohsumi, Y., *et al.* (2003). Promotion of tumorigenesis by heterozygous disruption of the beclin 1 autophagy gene. *Journal of Clinical Investigation* *112*, 1809-1820.
- Randow, F., MacMicking, J.D., and James, L.C. (2013). Cellular Self-Defense. How Cell-Autonomous Immunity Protects Against Pathogens. *Science* *340*, 701-706.
- Ravenhill, B.J., Boyle, K.B., von Muhlinen, N., Ellison, C.J., Masson, G.R., Otten, E.G., Foeglein, A., Williams, R., and Randow, F. (2019). The Cargo Receptor NDP52 Initiates Selective Autophagy by Recruiting the ULK Complex to Cytosol-Invading Bacteria. *Molecular Cell* *74*, 320-329.e326.
- Ravikumar, B., Vacher, C., Berger, Z., Davies, J.E., Luo, S., Oroz, L.G., Scaravilli, F., Easton, D.F., Duden, R., O'Kane, C.J., *et al.* (2004). Inhibition of mTOR induces autophagy and reduces toxicity of polyglutamine expansions in fly and mouse models of Huntington disease. *Nat Genet* *36*, 585-595.
- Rebecca, V.W., and Amaravadi, R.K. (2016). Emerging strategies to effectively target autophagy in cancer. *Oncogene* *35*, 1-11.
- Ren, J.-H., He, W.-S., Nong, L., Zhu, Q.-Y., Hu, K., Zhang, R.-G., Huang, L.-L., Zhu, F., and Wu, G. (2010). Acquired Cisplatin Resistance in Human Lung Adenocarcinoma Cells Is Associated with Enhanced Autophagy. *Cancer Biotherapy and Radiopharmaceuticals* *25*.
- Richter, B., Sliter, D.A., Herhaus, L., Stolz, A., Wang, C., Beli, P., Zaffagnini, G., Wild, P., Martens, S., Wagner, S.A., *et al.* (2016). Phosphorylation of OPTN by TBK1 enhances its binding to Ub chains and promotes selective autophagy of damaged mitochondria. *Proceedings of the National Academy of Sciences*, 201523926-201523926.
- Richters, A., Aben, K.K.H., and Kiemeny, L. (2020). The global burden of urinary bladder cancer: an update. *World J Urol* *38*, 1895-1904.
- Rogov, V., Dotsch, V., Johansen, T., and Kirkin, V. (2014). Interactions between autophagy receptors and ubiquitin-like proteins form the molecular basis for selective autophagy. *Mol Cell* *53*, 167-178.
- Ronan, B., Flamand, O., Vescovi, L., Dureuil, C., Durand, L., Fassy, F., Bachelot, M.-f., Lamberton, A., Mathieu, M., Bertrand, T., *et al.* (2014). A highly potent and selective Vps34 inhibitor alters vesicle trafficking and autophagy. *Nat Chem Biol* *10*, 1013-1019.
- Roos, W.P., and Kaina, B. (2013). DNA damage-induced cell death: from specific DNA lesions to the DNA damage response and apoptosis. *Cancer Lett* *332*, 237-248.
- Russell, R.C., Tian, Y., Yuan, H., Park, H.W., Chang, Y.Y., Kim, J., Kim, H., Neufeld, T.P., Dillin, A., and Guan, K.L. (2013). ULK1 induces autophagy by phosphorylating Beclin-1 and activating VPS34 lipid kinase. *Nat Cell Biol* *15*, 741-750.

- Sánchez-Wandelmer, J., Kriegenburg, F., Rohringer, S., Schuschnig, M., Gómez-Sánchez, R., Zens, B., Abreu, S., Hardenberg, R., Hollenstein, D., Gao, J., *et al.* (2017). Atg4 proteolytic activity can be inhibited by Atg1 phosphorylation. *Nature Communications* 8.
- Sarraf, S.A., Shah, H.V., Kanfer, G., Pickrell, A.M., Holtzclaw, L.A., Ward, M.E., and Youle, R.J. (2020). Loss of TAX1BP1-Directed Autophagy Results in Protein Aggregate Accumulation in the Brain. *Molecular Cell*.
- Saul, V.V., Seibert, M., Krüger, M., Jeratsch, S., Kracht, M., and Schmitz, M.L. (2019). ULK1/2 Restricts the Formation of Inducible SINT-Speckles, Membraneless Organelles Controlling the Threshold of TBK1 Activation. *iScience* 19, 527-544.
- Savill, J., and Fadok, V. (2000). Corpse clearance defines the meaning of cell death. *Nature* 407, 784-788.
- Scott, F.L., Stec, B., Pop, C., Dobaczewska, M.K., Lee, J.J., Monosov, E., Robinson, H., Salvesen, G.S., Schwarzenbacher, R., and Riedl, S.J. (2009). The Fas-FADD death domain complex structure unravels signalling by receptor clustering. *Nature* 457, 1019-1022.
- Shi, C.S., and Kehrl, J.H. (2008). MyD88 and Trif target Beclin 1 to trigger autophagy in macrophages. *J Biol Chem* 283, 33175-33182.
- Shi, X., Yokom, A.L., Wang, C., Young, L.N., Youle, R.J., and Hurley, J.H. (2020). ULK complex organization in autophagy by a C-shaped FIP200 N-terminal domain dimer. *J Cell Biol* 219.
- Shpilka, T., Weidberg, H., Pietrokovski, S., and Elazar, Z. (2011). Atg8: an autophagy-related ubiquitin-like protein family. *Genome Biology* 12, 226.
- Sirichanchuen, B., Pengsuparp, T., and Chanvorachote, P. (2012). Long-term cisplatin exposure impairs autophagy and causes cisplatin resistance in human lung cancer cells. *Mol Cell Biochem* 364, 11-18.
- Skowron, M.A., Niegisch, G., Fritz, G., Arent, T., van Roermund, J.G., Romano, A., Albers, P., Schulz, W.A., and Hoffmann, M.J. (2015). Phenotype plasticity rather than repopulation from CD90/CK14+ cancer stem cells leads to cisplatin resistance of urothelial carcinoma cell lines. *J Exp Clin Cancer Res* 34, 144.
- Su, Y.C., Davuluri, G.V., Chen, C.H., Shiau, D.C., Chen, C.C., Chen, C.L., Lin, Y.S., and Chang, C.P. (2016). Galectin-1-Induced Autophagy Facilitates Cisplatin Resistance of Hepatocellular Carcinoma. *PLoS One* 11, e0148408.
- Sumpter, R., and Levine, B. (2010). Autophagy and innate immunity: Triggering, targeting and tuning. *Seminars in Cell and Developmental Biology* 21, 699-711.
- Sun, D., Wu, R., Zheng, J., Li, P., and Yu, L. (2018). Polyubiquitin chain-induced p62 phase separation drives autophagic cargo segregation. *Cell Res* 28, 405-415.
- Suzuki, H., Kaizuka, T., Mizushima, N., and Noda, N.N. (2015). Structure of the Atg101-Atg13 complex reveals essential roles of Atg101 in autophagy initiation. *Nat Struct Mol Biol* 22, 572-580.
- Suzuki, H., Osawa, T., Fujioka, Y., and Noda, N.N. (2017). Structural biology of the core autophagy machinery. *Current Opinion in Structural Biology* 43, 10-17.
- Taherbhoy, A.M., Tait, S.W., Kaiser, S.E., Williams, A.H., Deng, A., Nourse, A., Hammel, M., Kurinov, I., Rock, C.O., Green, D.R., *et al.* (2011). Atg8 transfer from Atg7 to Atg3: a distinctive E1-E2 architecture and mechanism in the autophagy pathway. *Mol Cell* 44, 451-461.
- Takamura, A., Komatsu, M., Hara, T., Sakamoto, A., Kishi, C., Waguri, S., Eishi, Y., Hino, O., Tanaka, K., and Mizushima, N. (2011). Autophagy-deficient mice develop multiple liver tumors. *Genes Dev* 25, 795-800.
- Tamura, T., Yanai, H., Savitsky, D., and Taniguchi, T. (2008). The IRF family transcription factors in immunity and oncogenesis. *Annu Rev Immunol* 26, 535-584.

- Turco, E., Fischer, I., and Martens, S. (2020). FIP200 organizes the autophagy machinery at p62-ubiquitin condensates beyond activation of the ULK1 kinase, M.P.L. Department of Biochemistry and Cell Biology, University of Vienna, Vienna, Austria, ed. (bioRxiv).
- Turco, E., Witt, M., Abert, C., Bock-Bierbaum, T., Su, M.Y., Trapannone, R., Sztacho, M., Danieli, A., Shi, X., Zaffagnini, G., *et al.* (2019). FIP200 Claw Domain Binding to p62 Promotes Autophagosome Formation at Ubiquitin Condensates. *Molecular Cell* *74*, 330-346.e311.
- Vargas, J.N.S., Wang, C., Bunker, E., Hao, L., Maric, D., Schiavo, G., Randow, F., and Youle, R.J. (2019). Spatiotemporal Control of ULK1 Activation by NDP52 and TBK1 during Selective Autophagy. *Molecular Cell* *74*, 347-362.e346.
- Walker, S.A., and Ktistakis, N.T. (2019). Autophagosome Biogenesis Machinery. *Journal of Molecular Biology*.
- Wang, C., Wang, X., Su, Z., Fei, H., Liu, X., and Pan, Q. (2015). The novel mTOR inhibitor Torin-2 induces autophagy and downregulates the expression of UHRF1 to suppress hepatocarcinoma cell growth. *Oncol Rep* *34*, 1708-1716.
- Wang, J., and Wu, G.S. (2014). Role of autophagy in cisplatin resistance in ovarian cancer cells. *J Biol Chem* *289*, 17163-17173.
- Wei, H., Wei, S., Gan, B., Peng, X., Zou, W., and Guan, J.-L. (2011). Suppression of autophagy by FIP200 deletion inhibits mammary tumorigenesis. *Genes & Development*.
- Weissmann, A.M. (2001). Themes and variations on ubiquitylation. *Nature Reviews Molecular Cell Biology* *2*, 169–178.
- Wesselborg, S., and Stork, B. (2015). Autophagy signal transduction by ATG proteins: from hierarchies to networks. *Cellular and Molecular Life Sciences*.
- Wild, P., Farhan, H., McEwan, D.G., Wagner, S., Rogov, V.V., Brady, N.R., Richter, B., Korac, J., Waidmann, O., Choudhary, C., *et al.* (2011). Phosphorylation of the autophagy receptor optineurin restricts Salmonella growth. *Science* *333*, 228-233.
- Wilson, M.I., Gill, D.J., Perisic, O., Quinn, M.T., and Williams, R.L. (2003). PB1 Domain-Mediated Heterodimerization in NADPH Oxidase and Signaling Complexes of Atypical Protein Kinase C with Par6 and p62. *Molecular Cell* *12*, 39-50.
- Wirawan, E., Vande Walle, L., Kersse, K., Cornelis, S., Claerhout, S., Vanoverberghe, I., Roelandt, R., De Rycke, R., Verspurten, J., Declercq, W., *et al.* (2010). Caspase-mediated cleavage of Beclin-1 inactivates Beclin-1-induced autophagy and enhances apoptosis by promoting the release of proapoptotic factors from mitochondria. *Cell Death & Disease* *1*, e18-e18.
- Witjes, J.A., Leuret, T., Comperat, E.M., Cowan, N.C., De Santis, M., Bruins, H.M., Hernandez, V., Espinos, E.L., Dunn, J., Rouanne, M., *et al.* (2017). Updated 2016 EAU Guidelines on Muscle-invasive and Metastatic Bladder Cancer. *Eur Urol* *71*, 462-475.
- Wold, M.S., Lim, J., Lachance, V., Deng, Z., and Yue, Z. (2016). ULK1-mediated phosphorylation of ATG14 promotes autophagy and is impaired in Huntington's disease models. *Mol Neurodegener* *11*, 76.
- Xiao, L., Shi, X.Y., Zhang, Y., Zhu, Y., Zhu, L., Tian, W., Zhu, B.K., and Wei, Z.L. (2016). YAP induces cisplatin resistance through activation of autophagy in human ovarian carcinoma cells. *Onco Targets Ther* *9*, 1105-1114.
- Xie, Z., Nair, U., and Klionsky, D.J. (2008). Atg8 Controls Phagophore Expansion during Autophagosome Formation. *Molecular Biology of the Cell* *19*, 3179-3613.
- Yang, Q., Liu, T.T., Lin, H., Zhang, M., Wei, J., Luo, W.W., Hu, Y.H., Zhong, B., Hu, M.M., and Shu, H.B. (2017). TRIM32-TAX1BP1-dependent selective autophagic degradation of TRIF negatively regulates TLR3/4-mediated innate immune responses. *PLoS Pathogens* *13*, 1-21.

- Yang, S., Imamura, Y., Jenkins, R.W., Canadas, I., Kitajima, S., Aref, A., Brannon, A., Oki, E., Castoreno, A., Zhu, Z., *et al.* (2016). Autophagy Inhibition Dysregulates TBK1 Signaling and Promotes Pancreatic Inflammation. *Cancer Immunology Research* 4, 520-530.
- Yao, J., Jia, L., Khan, N., Lin, C., Mitter, S.K., Boulton, M.E., Dunaief, J.L., Klionsky, D.J., Guan, J.L., Thompson, D.A., *et al.* (2015). Deletion of autophagy inducer RB1CC1 results in degeneration of the retinal pigment epithelium. *Autophagy* 11, 939-953.
- Ye, J., Cheung, J., Gerbino, V., Ahlsen, G., Zimanyi, C., Hirsh, D., and Maniatis, T. (2019). Effects of ALS-associated TANK binding kinase 1 mutations on protein-protein interactions and kinase activity. *Proc Natl Acad Sci U S A* 116, 24517-24526.
- Yeo, S.K., Wang, C., and Guan, J.L. (2020). Role of FIP200 in inflammatory processes beyond its canonical autophagy function. *Biochem Soc Trans* 48, 1599-1607.
- Yim, W.W.Y., and Mizushima, N. (2020). Lysosome biology in autophagy. *Cell Discovery* 6.
- Yin, Z., Pascual, C., and Klionsky, D.J. (2016). Autophagy: machinery and regulation. *Microb Cell* 3, 588-596.
- Yu, H., Su, J., Xu, Y., Kang, J., Li, H., Zhang, L., Yi, H., Xiang, X., Liu, F., and Sun, L. (2011). P62/SQSTM1 involved in cisplatin resistance in human ovarian cancer cells by clearing ubiquitinated proteins. *European Journal of Cancer* 47, 1585-1594.
- Yu, L., Gu, C., Zhong, D., Shi, L., Kong, Y., Zhou, Z., and Liu, S. (2014). Induction of autophagy counteracts the anticancer effect of cisplatin in human esophageal cancer cells with acquired drug resistance. *Cancer Lett* 355, 34-45.
- Yuan, F., Jin, X., Li, D., Song, Y., Zhang, N., Yang, X., Wang, L., Zhu, W.G., Tian, C., and Zhao, Y. (2019). ULK1 phosphorylates Mad1 to regulate spindle assembly checkpoint. *Nucleic Acids Res* 47, 8096-8110.
- Yuk, H.D., Jeong, C.W., Kwak, C., Kim, H.H., Moon, K.C., and Ku, J.H. (2019). Clinical outcomes of muscle invasive bladder Cancer according to the BASQ classification. *BMC Cancer* 19, 897.
- Zaffagnini, G., Savova, A., Danieli, A., Romanov, J., Tremel, S., Ebner, M., Peterbauer, T., Sztacho, M., Trapannone, R., Tarafder, A.K., *et al.* (2018). P62 Filaments Capture and Present Ubiquitinated Cargos for Autophagy. *The EMBO Journal* 37, 1-21.
- Zhao, P., Wong, K.i., Sun, X., Reilly, S.M., Uhm, M., Liao, Z., Skorobogatko, Y., and Saltiel, A.R. (2018). TBK1 at the Crossroads of Inflammation and Energy Homeostasis in Adipose Tissue. *Cell* 172, 731-743.
- Zhu, J., Zheng, Y., Zhang, H., Zhu, J., and Sun, H. (2017). Low concentration of chloroquine enhanced efficacy of cisplatin in the treatment of human ovarian cancer dependent on autophagy. *Am J Transl Res* 9, 4046-4058.
- Zhu, Y., Zhao, L., Liu, L., Gao, P., Tian, W., Wang, X., Jin, H., Xu, H., and Chen, Q. (2010). Beclin 1 cleavage by caspase-3 inactivates autophagy and promotes apoptosis. *Protein & Cell* 1, 468-477.

Licensing & Copyright

I hereby grant anyone the right to reuse any part of this dissertation, including figures 1 to 4, which I have created myself, that is not subject to explicit copyright, as long as credit is given (license CC BY 4.0). Please cite as follows:

Schlütermann, David (2020) *Autophagy: Molecular insights into its role and therapeutic potential in bladder cancer and neurodegeneration*. Heinrich Heine University, Düsseldorf.

All non-copyrighted parts of this work are licensed under the Creative Commons Attribution 4.0 International License. To view a copy of this license, visit <http://creativecommons.org/licenses/by/4.0/> or send a letter to Creative Commons, PO Box 1866, Mountain View, CA 94042, USA.

The following parts of this dissertation are protected by copyright and have been reprinted unchanged:

Manuscript “Targeting urothelial carcinoma cells by combining cisplatin with a specific inhibitor of the autophagy-inducing class III PtdIns3K complex”:

Copyright Schlütermann et al. 2018 (DOI: 10.1016/j.urolonc.2017.11.021)

Reprinted under the Creative Commons CC-BY-NC-ND 4.0 license (as indicated by Elsevier).

Manuscript “Systematic analysis of ATG13 domain requirements for autophagy induction”:

Copyright Wallot-Hieke et al. 2018 (DOI: 10.1080/15548627.2017.1387342)

Reprinted under the Creative Commons CC-BY-NC-ND 4.0 license (as indicated by Taylor & Francis Group).

Manuscript “FIP200 controls TBK1 activation threshold at SQSTM1/p62-positive condensates”:

Copyright Schlütermann et al. 2020

Reprinted with the copyright as author and protected by the German copyright laws (including § 16, § 17, § 18, § 19a UrhG). Any reproduction of any parts of this manuscript in any form is not permitted without the explicit permission of the authors.

Appendix

Publication 1

Targeting urothelial carcinoma cells by combining cisplatin with a specific inhibitor of the autophagy-inducing class III PtdIns3K complex

David Schlütermann, Margaretha A. Skowron, Niklas Berleth, Philip Böhler, Jana Deitersen, Fabian Stuhldreier, Nora Wallot-Hieke, Wenxian Wu, Christoph Peter, Michèle J. Hoffmann, Günter Niegisch, Björn Stork

Urologic Oncology: Seminars and Original Investigations, volume 36, issue 4, pages 160.e1-160.e13, April 2018

DOI: 10.1016/j.urolonc.2017.11.021

Original article

Targeting urothelial carcinoma cells by combining cisplatin with a specific inhibitor of the autophagy-inducing class III PtdIns3K complex

David Schlütermann, M.Sc.^a, Margaretha A. Skowron, M.Sc.^b, Niklas Berleth, M.Sc.^a, Philip Böhrer, M.Sc.^a, Jana Deitersen, M.Sc.^a, Fabian Stuhldreier, M.Sc.^a, Nora Wallot-Hieke, Ph.D.^a, Wenxian Wu, M.Sc.^a, Christoph Peter, Ph.D.^a, Michèle J. Hoffmann, Ph.D.^b, Günter Niegisch, M.D.^b, Björn Stork, Ph.D.^{a,*}

^a Institute of Molecular Medicine I, Medical Faculty, Heinrich Heine University Düsseldorf, Düsseldorf, Germany

^b Department of Urology, Medical Faculty, Heinrich Heine University Düsseldorf, Düsseldorf, Germany

Received 7 June 2017; received in revised form 31 October 2017; accepted 30 November 2017

Abstract

Background: Cisplatin-based regimens are routinely employed for the treatment of urothelial carcinoma. However, therapeutic success is hampered by the primary presence of or the development of cisplatin resistance. This chemoresistance is executed by multiple cellular pathways. In recent years, the cellular process of autophagy has been identified as a prosurvival pathway of cancer cells. On the one hand, autophagy enables cancer cells to survive conditions of low oxygen or nutrient supply, frequently found in tumors. On the other hand, autophagy supports chemoresistance of cancer cells. Here, we aimed at investigating the involvement of autophagy for cisplatin resistance in different urothelial carcinoma cell lines.

Materials & Methods: We analyzed the expression levels of different autophagy-related proteins in cisplatin-sensitive and cisplatin-resistant urothelial carcinoma cell lines. Furthermore, we performed cell viability assays and caspase activity assays with cells treated with cisplatin, non-specific or specific autophagy inhibitors (chloroquine, 3-methyladenine, SAR405) or combinations thereof.

Results: We found that autophagy-related proteins are up-regulated in different cisplatin-resistant urothelial carcinoma cells compared to the sensitive parental cell lines. Furthermore, inhibition of autophagy, in general, or of the autophagy-inducing class III PtdIns3K complex, in particular, sensitized both sensitive and resistant urothelial carcinoma cells to cisplatin-induced cytotoxic effects.

Conclusion: We propose that targeting the autophagic machinery might represent a suitable approach to complement or even increase cisplatin efficacy in order to overcome cisplatin resistance in urothelial carcinoma. © 2017 The Authors. Published by Elsevier Inc. This is an open access article under the CC BY-NC-ND license (<http://creativecommons.org/licenses/by-nc-nd/4.0/>).

Keywords: Autophagy; Cisplatin; Urothelial carcinoma; VPS34; Chemoresistance

1. Introduction

Bladder cancer (BC) is the fifth most common cancer in the developed world, with approximately 400,000 new cases diagnosed per year and 150,000 deaths worldwide [1]. In industrial countries, about 90% of BCs are urothelial carcinomas (UC) which may be further classified into muscle-invasive and non-muscle-invasive cancers. These UC subtypes are distinct in clinical behavior and molecular alterations [2]. Comprising up to one-third of UC, muscle-invasive tumors often progress to metastatic disease and

patients face a poor prognosis with only 50% to 60% survival after 5 years [3]. Although platinum-based chemotherapy is the standard first-line treatment for advanced UC, its impact on cancer-specific survival is limited [4]. Despite frequent initial treatment responses, overall survival does not exceed 12 to 16 months in metastatic patients [5]. Its anticancer efficacy mainly originates from the formation of bivalent DNA intrastrand crosslinks blocking transcription and replication [6,7]. Subsequently generated DNA double-strand breaks stimulate DNA damage response and initiate the intrinsic mitochondrial apoptosis pathway [8–10]. However, cisplatin treatment frequently leads to the development of chemoresistance, and the molecular mechanisms of resistance are multifaceted [8]. Several factors have been

*Corresponding author. Tel.: +49 211 81 11954; fax: +49 211 81 14103.
E-mail address: bjoern.stork@uni-duesseldorf.de (B. Stork).

suggested to determine the response to cisplatin treatment, including factors regulating mechanisms of apoptosis, DNA repair and transport, as well as phenotype plasticity [8,11,12]. However, the mechanisms underlying cisplatin resistance of UC cells have not been clearly identified yet, and current preclinical research aims at increasing efficacy of cisplatin treatment or re-sensitizing cisplatin-resistant cells for cytotoxic effects.

In recent years, autophagy has emerged as an attractive target for cancer therapy [13–15]. During autophagy, intracellular cargo becomes engulfed by double-membraned vesicles termed autophagosomes. Autophagosomes fuse with lysosomes, and within the resulting autolysosomes, the engulfed cargo becomes degraded [16]. Autophagy occurs at basal levels in most cell types, but can also be actively induced upon stress conditions like nutrient deprivation or treatment with anticancer drugs. The induction of autophagy is centrally regulated by 2 kinase complexes: (1) the ULK1 protein kinase complex consisting of the Ser/Thr protein kinase unc51-like kinase 1 (ULK1) and the interacting proteins autophagy-related (ATG) protein 13 (ATG13), ATG101, and RB1-inducible coiled-coil 1 (RB1CC1; alternatively termed FAK family kinase-interacting protein of 200 kDa, FIP200) and (2) the class III phosphatidylinositol 3-kinase (PtdIns3K) lipid kinase complex consisting of the catalytic subunit vacuolar protein sorting 34 (VPS34; alternatively termed phosphatidylinositol 3-kinase catalytic subunit type 3, PIK3C3) and the interacting proteins VPS15/PIK3R4, Beclin 1, ATG14, and nuclear receptor-binding factor 2 (NRBF2) [16,17]. The activation of these 2 complexes initiates autophagosome biogenesis, most likely at specific subdomains of the endoplasmic reticulum (ER) [18]. Several additional ATG proteins are involved in the formation of autophagosomes; among them the ubiquitin-like protein microtubule-associated proteins 1A/1B light chain 3 (MAP1LC3 or briefly LC3), which can be conjugated to phosphatidylethanolamine and thus be recruited to the autophagosomal membrane [19]. Anticancer therapies frequently induce autophagy as a prosurvival response that contributes to chemoresistance [14,20]. Consequently, drugs that inhibit autophagy are tested in clinical trials in combination with different anticancer drugs to increase their cytotoxic potential. Several of these trials make use of chloroquine/hydroxychloroquine, which raise the lysosomal pH and thus block fusion of autophagosomes and lysosomes [14]. So far, more specific inhibitors targeting the kinase activities of ULK1 or VPS34 have only been assessed in preclinical studies. These inhibitors include the ULK1 inhibitor MRT68921 or the VPS34 inhibitor SAR405 [21,22].

In this study, we made use of the urothelial carcinoma cell line (UCC) RT-112 and its respective cisplatin-resistant subline RT-112^{CisPt-R} [12]. We observed that the expression levels of several autophagy-related proteins are increased in RT-112^{CisPt-R} cells compared to the parental line. Furthermore, it appears that basal autophagy is increased in the resistant cells, but they still remain responsive to autophagy-inducing stimuli. The inhibition of autophagy either by

chloroquine or the VPS34-Beclin 1 complex-targeting inhibitors 3-MA or SAR405 complemented or even increased the cytotoxic effects of cisplatin in both parental and RT-112^{CisPt-R} cells. Furthermore, we obtained similar results with other UCCs representing the heterogeneity of this disease. Accordingly, we hypothesize that the inhibition of the autophagy-inducing VPS34-Beclin 1 complex represents a promising approach to increase the efficacy of cisplatin or to overcome cisplatin resistance in UC.

2. Material and methods

2.1. Antibodies and reagents

Antibodies against β -actin (clone AC-74, Sigma-Aldrich, #A5316), ATG13 (Sigma-Aldrich, #SAB4200100), ATG14 (MBL, #PD026), Beclin 1 (Santa Cruz, #sc-11427 or Sigma-Aldrich, #B6186), Caspase-3 (R&D Systems, #AF-605-NA), GAPDH (Abcam, #ab8245), LC3B (Cell Signaling Technology, #2775), PARP (Enzo, #BML-SA250), RB1CC1 (Bethyl Laboratories, #A301-574A), α -Tubulin (Sigma-Aldrich, #T5168), ULK1 (clone D8H5, Cell Signaling Technology, #8054), and VPS34 (Thermo Fisher Scientific, #PA1-46456) were used. IRDye 800- or IRDye 680-conjugated secondary antibodies were purchased from LI-COR Biosciences (926-68070, 926-68071 and 926-32211). Other reagents used were 3-MA (Sigma-Aldrich, #M9281), Bafilomycin A₁ (Sigma-Aldrich, #B1793), Chloroquine (Sigma-Aldrich, #C6628), Cisplatin (Accord Healthcare GmbH, PZN: 00370955), DMSO (Sigma-Aldrich, #D4540), Q-VD-OPh (MP Biomedicals, #03OPH109), and SAR405 (Selleck Chemicals, #7682).

2.2. Cell lines and cell culture

All cell lines were cultured in Dulbecco's Modified Eagle Medium (DMEM) containing 10% FCS and 4.5 g/l D-glucose in a humidified atmosphere at 37°C and 5% CO₂. The Cisplatin-resistant sublines were generated over several months by increasing dosages of cisplatin added with every passage up to concentrations of 12, 1, 2, 7, 3.5, or 1.5 μ g/ml to RT-112, J82, 253J, T24, 5637, and SW-1710 cells, respectively. Accordingly, the respective concentration of cisplatin was added to the media of the cisplatin-resistant sublines with every passage. For amino acid starvation, RT-112 cells were washed once with PBS and incubated for 2 hours in EBSS (Gibco, #24010-043).

2.3. Microscopy

RT-112 and RT-112^{CisPt-R} cells were cultured in regular medium or medium containing 12 μ g/ml cisplatin, respectively. Phase contrast images were captured using an Axio Observer A1 microscope (Carl Zeiss) with a magnification of 200 \times (Objective: ZEISS, LD A-Plan 20 \times /0.30 Ph1).

2.4. Cell viability assay

RT-112, J82, 253J or T24 cells were seeded in 96-well plates with a density of 1×10^4 cells/well. For combination analysis, the cell density of J82, 253J, and T24 cells was reduced to 0.5×10^4 . The following day, the cells were treated with cisplatin and autophagy inhibitors for 72 hours. Cell viability was determined by using an MTT assay. Briefly, MTT (Calbiochem, #475989) was added to the cells and incubated at 37°C for 1 hour. Afterwards, the plates were centrifuged at 600 rcf and 4°C for 5 minutes, and cells were lysed in DMSO for 20 minutes in the dark. Finally, the absorbance was measured at 570 nm and 650 nm for reference, using a microplate reader (BioTek, Synergy Mx). The mean of the absorbance of the control samples was set as 100%.

2.5. Caspase activity assay

1×10^4 RT-112 or RT-112^{CisPt-R} cells were seeded in 96-well plates, and the following day, the cells were treated with cisplatin and autophagy inhibitors for 48 hours. After treatment, plates were centrifuged at 600 rcf and 4°C for 5 minutes, quickly frozen at –80°C, and cells were lysed in lysis buffer (20 mM HEPES, 84 mM KCl, 10 mM MgCl₂, 200 μM EDTA, 200 μM EGTA, 0.5% NP-40, 1 μg/ml Leupeptin, 1 μg/ml Pepstatin, and 5 μg/ml Aprotinin) for 10 minutes on ice. Subsequently, reaction buffer (50 mM HEPES, 100 mM NaCl, 10% Sucrose, 0.1% CHAPS [Carl Roth GmbH & Co., #1479.3], 2 mM CaCl₂, 13.35 mM DTT, and 70 μM Ac-DEVD-AMC [Biomol, #ABD-13402]) was added to the lysates and fluorescence (with an excitation of 360 nm, and an emission of 450 nm) was measured every 2 minutes over a period of 2.5 hours at 37°C, using a microplate reader (BioTek, Synergy Mx). Caspase-3 activity was measured by the cleavage of the substrate Ac-DEVD-AMC and the following release of the fluorophore AMC (7-amido-4-methylcoumarin). For evaluation, the rise of the linear sector of the resulting curve was determined and the mean of the control samples was set as “1.”

2.6. Immunoblotting

Cells were harvested by scraping, pelletized at 600 rcf and 4°C for 5 minutes, quickly frozen in liquid nitrogen and lysed in lysis buffer (50 mM Tris-HCl, pH 7.5, 150 mM NaCl, 1 mM EDTA, 1 mM EGTA, 10 μM Na₂MoO₄, 1 mM Na₃VO₄, 50 mM NaF, 5 mM Na₄P₂O₇, 1% [v/v] Triton X-100 [Carl Roth GmbH & Co., #3051.2], and protease inhibitor cocktail [Sigma-Aldrich, #P2714]) for 30 minutes on ice. Lysates were cleared by centrifugation at 18,000 rcf and 4°C for 15 minutes. Equal protein amounts were determined by Bradford assay, prepared by addition of sample buffer (125 mM Tris-HCl, pH 6.8, 17.2% [v/v] glycerol, 4.1% [w/v] SDS [AppliChem GmbH, #A7249], 200 μg/ml

bromophenol blue, and 2% [v/v] β-mercaptoethanol) and heated at 95°C for 5 minutes. Proteins were separated on SDS-PAGE, transferred to PVDF membranes (Merck, Millipore, IPFL00010), and analyzed using the indicated primary antibodies and appropriate IRDye 800- or IRDye 680-conjugated secondary antibodies (LI-COR Biosciences). Signals were detected by using an Odyssey Infrared Imaging system (LI-COR Biosciences). Quantifications were performed with Image Studio (LI-COR Biosciences).

2.7. Statistical analysis

IC₅₀ values were calculated using GraphPad Prism 7.01. For isobologram analysis, CompuSyn 1.0 was used, which also allows a computerized simulation of synergism, additivism, and antagonism at any effect level [23]. The resulting Combination Index (CI) values represent synergism (CI < 1), additivism (CI = 1), and antagonism (CI > 1). For immunoblotting, the density of each protein band was divided by the average of the density of all bands from the same protein on the membrane. The ratios of the proteins of interest were normalized to the loading control, and fold changes were calculated by dividing each normalized density ratio by the average of the density ratios of the wild type control lane (control lane: fold change = 1.00, $n \geq 3$). For all analyses, results are shown as mean ± standard deviation, and *P* values were determined by two-way ANOVA and are given in the bar diagrams.

3. Results

In order to analyze the effect of autophagy modulation on the efficacy of cisplatin treatment, we first generated a cisplatin-resistant subline of the UCC RT-112. Cisplatin resistance was confirmed by a cell viability assay (Fig. 1). Notably, cisplatin-resistant RT-112 cells (RT-112^{CisPt-R}) revealed morphologic alterations, including increased cell size and number of protrusions (Fig. S1), which is in accordance with previous observations [11,12].

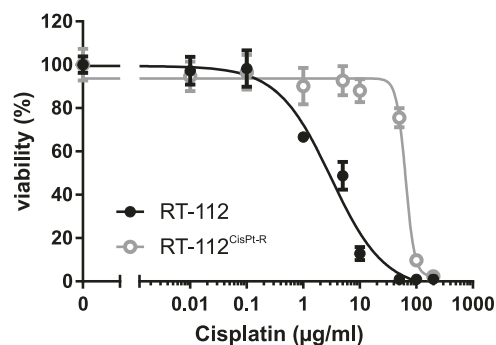


Fig. 1. Characterization of RT-112 and RT-112^{CisPt-R} cells. RT-112 and RT-112^{CisPt-R} cells were treated with different concentrations of cisplatin (0.01–200 μg/ml) for 72 hours. After treatment, cell viability was measured using an MTT assay. The results are shown as means ± standard deviation of 3 independent experiments which were performed in triplicates.

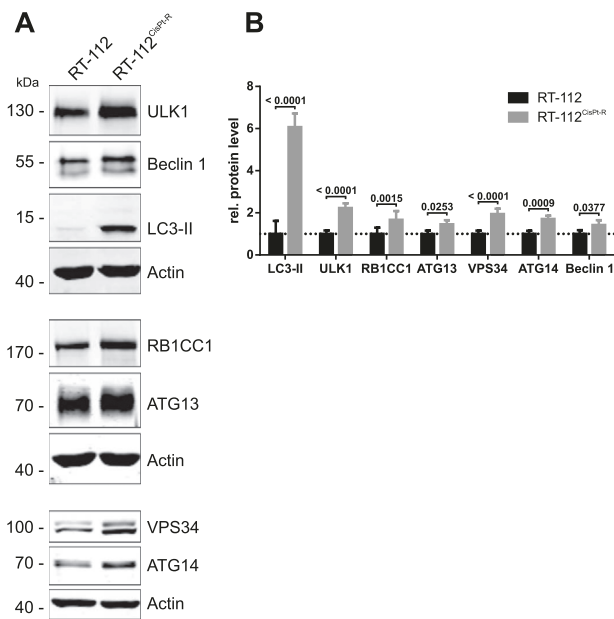


Fig. 2. ATG proteins are differentially expressed in RT-112 and RT-112^{CisPt-R} cells. (A) RT-112 and RT-112^{CisPt-R} cells were lysed and cleared cellular lysates were subjected to SDS-PAGE and immunoblotting for ULK1, Beclin 1, LC3, RB1CC1, ATG13, VPS34, ATG14, and Actin. One representative immunoblot is shown. (B) The densities of bands on immunoblots of at least 3 independent experiments were quantified using Image Studio (LI-COR Biosciences) and normalized to Actin. The mean of the resulting values for RT-112 cells were set as “1” for each protein. Then, the values of RT-112^{CisPt-R} cells were normalized to the values of RT-112 cells. The bars represent the means + standard deviation. A two-way ANOVA was used to compare the differences in protein expression between RT-112 and RT-112^{CisPt-R} cells. The respective *P* values are depicted in the diagram.

3.1. Autophagy-related (ATG) proteins are up-regulated in RT-112^{CisPt-R} cells

Next we aimed at investigating whether cisplatin resistance affects expression levels of different autophagy-related (ATG) proteins. As determined by immunoblotting, several subunits of the autophagy-inducing ULK1 and VPS34-Beclin 1 complexes were significantly up-regulated, including the catalytic subunits ULK1 and VPS34 as well as the associated proteins RB1CC1, ATG13, Beclin 1, and ATG14 (Fig. 2). Additionally, expression of the ubiquitin-like autophagy marker protein LC3-II was strongly increased in RT-112^{CisPt-R} cells (Fig. 2, *P* < 0.0001). Although the up-regulation of ATG proteins might indicate an increased potential to execute autophagy, this upregulation is not sufficient evidence of increased autophagy [24]. This is best exemplified by LC3-II, which is increasingly generated during autophagy induction and at the same time accumulates during autophagy inhibition [24]. In order to investigate whether autophagy is functional in RT-112^{CisPt-R} cells, we performed an LC3 turnover assay using starvation as proautophagic stimulus. In this assay, lysosomal degradation is blocked by the V-ATPase inhibitor bafilomycin A₁, which ultimately blocks the fusion of autophagosomes with

lysosomes [24]. We detected LC3 turnover by immunoblotting and observed increased LC3-II levels in RT-112^{CisPt-R} cells under all conditions (Fig. S2). Nevertheless, the RT-112^{CisPt-R} remained responsive to starvation by incubation in Earle’s Balanced Salt Solution (EBSS). Collectively, these data suggest that RT-112^{CisPt-R} cells possess an enhanced capacity for basal autophagy but can still respond to proautophagic stimuli.

3.2. Inhibition of autophagy complements or increases cisplatin-mediated cytotoxicity in both RT-112^{CisPt-R} and parental cells

The increased protein expression of several ATG proteins in RT-112^{CisPt-R} cells and the possibly increased potential to execute autophagy led us to hypothesize that targeting the autophagy machinery might be a reasonable approach to increase the efficacy of cisplatin treatment. To date, most clinical studies investigating the effects of autophagy inhibition rely on the usage of chloroquine, a lysosomotropic compound that raises the lysosomal pH and thus inhibits the fusion between autophagosomes and lysosomes [24]. First, we confirmed the autophagy-inhibiting properties of chloroquine in RT-112 and RT-112^{CisPt-R} cells by an LC3 turnover assay. We observed that LC3-II accumulated in EBSS-treated cells upon co-incubation with chloroquine (Figure S3A). In order to investigate whether cisplatin and chloroquine exhibit a combined effect on cell viability in these two cell lines, the effect of chloroquine treatment alone (Fig. 3A) or in combination with cisplatin was analyzed, and isobologram analysis was performed (Fig. 3B and C; the corresponding isobologram is shown in Fig. S4A). For this analysis, concentrations of 0.25×, 0.5× or 1× of the IC₅₀ values of the individual compounds (cisplatin or chloroquine) were applied. As can be deduced from the combination index plot, in RT-112 cells, the combination of cisplatin and chloroquine was synergistic (CI < 1) if used at concentrations of 1× IC₅₀. In RT-112^{CisPt-R} cells, the effect was rather additive at high effect levels. These results indicate that inhibition of autophagy might indeed represent a suitable tool to increase cisplatin efficacy in responsive UCCs or to target resistant UCCs, respectively.

3.3. Inhibition of the VPS34-Beclin 1 complex sensitizes RT-112^{CisPt-R} and parental cells to cisplatin treatment

We observed that general inhibition of autophagy supports cisplatin-mediated cytotoxicity in UCCs. However, chloroquine is not a specific autophagy inhibitor. Additionally, it has recently been suggested that the enhanced drug efficacy of anticancer therapeutics in combination with chloroquine might be due to lysosomal cell death rather than to regulation of autophagy [25]. Taken these drawbacks of chloroquine together, we analyzed whether the direct and specific inhibition of the autophagy-inducing

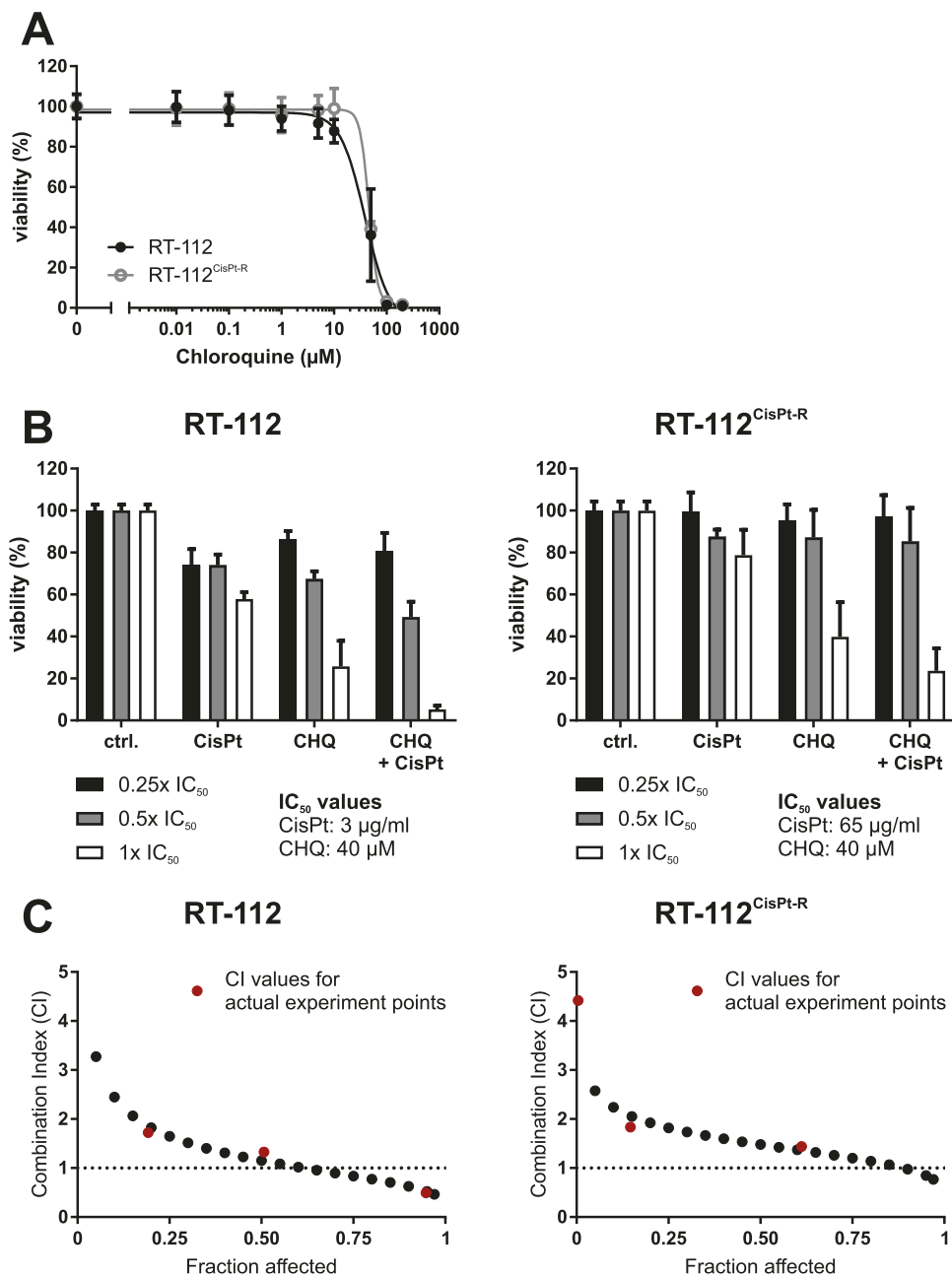


Fig. 3. Chloroquine complements or increases cisplatin-mediated cytotoxicity in both RT-112^{CisPt-R} and parental cells. (A and B) RT-112 and RT-112^{CisPt-R} cells were treated with different concentrations of chloroquine (CHQ; 0.01–200 μM) (A) or with cisplatin, chloroquine, or a combination of both (B) for 72 hours. For combination analysis (B), IC₅₀ values of 3 $\mu\text{g/ml}$ (RT-112) or 65 $\mu\text{g/ml}$ (RT-112^{CisPt-R}) cisplatin and 40 μM chloroquine (RT-112 and RT-112^{CisPt-R}) were used. After treatment, cell viability was measured using an MTT assay. At least 3 independent experiments were performed in triplicates. The results are shown as means \pm or + standard deviations of the independent experiments. For all experiments, 0.1% DMSO was used as control. For 1 \times IC₅₀, 0.5 \times IC₅₀, and 0.25 \times IC₅₀ in Figs. 3B, 4B, and 5B, the same controls are shown for each cell line. (C) Combination Index (CI) values were calculated using the software CompuSyn in order to determine synergistic (CI < 1), additive (CI = 1), or antagonistic (CI > 1) effects for the combination of cisplatin and chloroquine. CompuSyn uses algorithms for a computerized simulation to show synergism, additivism, and antagonism at any effect level.

VPS34-Beclin 1 complex can phenocopy the effect of chloroquine. We interfered with the VPS34-Beclin 1 complex using the class III PtdIns3K inhibitor 3-methyladenine (3-MA). Again, we confirmed the autophagy-inhibitory potential of 3-MA in our cellular model systems. Cells treated with 3-MA did not accumulate LC3-II upon bafilomycin A₁ treatment, verifying that 3-MA blocks an early step of the autophagic pathway (Fig. S3B). Next, we

performed cell viability assays using individual (Fig. 4A) and combined treatments (Fig. 4B and C). As shown in the CI plots, we found that 3-MA synergistically sensitizes both parental and RT-112^{CisPt-R} cells to cisplatin-induced cell death. In RT-112 cells, this was the case for all applied concentrations; for the RT-112^{CisPt-R} cells, the synergistic effect could be observed for concentrations in the range of the IC₅₀ (Fig. 4B and C; the corresponding isobologram is

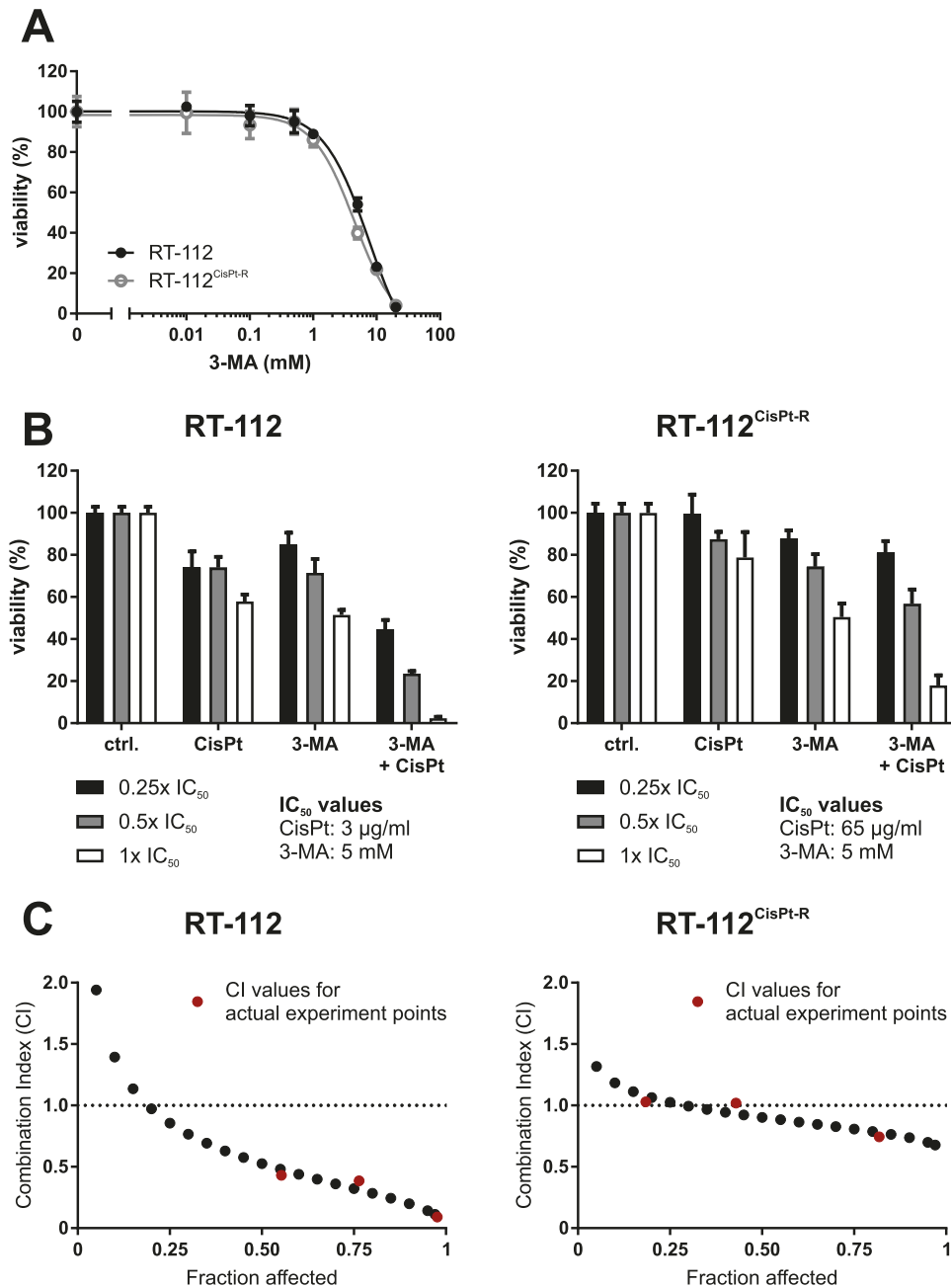


Fig. 4. The PtdIns3K inhibitor 3-MA sensitizes both RT-112 and RT-112^{CisPt-R} cells to cisplatin-induced cell death. (A and B) RT-112 and RT-112^{CisPt-R} cells were treated with different concentrations of 3-methyladenine (3-MA; 0.01–20 mM) (A) or with cisplatin, 3-MA or a combination of both (B) for 72 hours. For combination analyses (B), IC₅₀ values of 3 µg/ml (RT-112) or 65 µg/ml (RT-112^{CisPt-R}) cisplatin and 5 mM 3-MA (RT-112 and RT-112^{CisPt-R}) were used. After treatment, cell viability was measured using an MTT assay. At least 3 independent experiments were performed in triplicates. The results are shown as means ± or + standard deviations of the independent experiments. For all experiments, 0.1% DMSO was used as control. For 1× IC₅₀, 0.5× IC₅₀, and 0.25× IC₅₀ in Figs. 3B, 4B, and 5B, the same controls are shown for each cell line. (C) Combination Index (CI) values were calculated using the software CompuSyn in order to determine synergistic (CI < 1), additive (CI = 1), or antagonistic (CI > 1) effects for the combination of cisplatin and 3-MA. CompuSyn uses algorithms for a computerized simulation to show synergism, additivism, and antagonism at any effect level.

shown in Fig. S4B). It has been reported that 3-MA inhibits both class I and class III PtdIns3Ks with different kinetics, and that 3-MA can indeed promote autophagy in long-term experiments [26]. Accordingly, we also tested the recently described VPS34-specific inhibitor SAR405 [22]. Of note, the IC₅₀ of SAR405 alone was 5 to 7 times lower in RT-112^{CisPt-R} cells compared to the parental RT-112 cell line,

indicating a clearly increased sensitivity toward VPS34 inhibition in the cisplatin-resistant cell line (Fig. 5A). This observation is in line with our analysis of autophagy inhibition using SAR405 in both cell lines. In RT-112^{CisPt-R} cells, SAR405 efficiently inhibited autophagy at concentrations of 0.5 µM, whereas 5 µM were necessary in parental RT-112 cells (Fig. S3C). Again, we performed

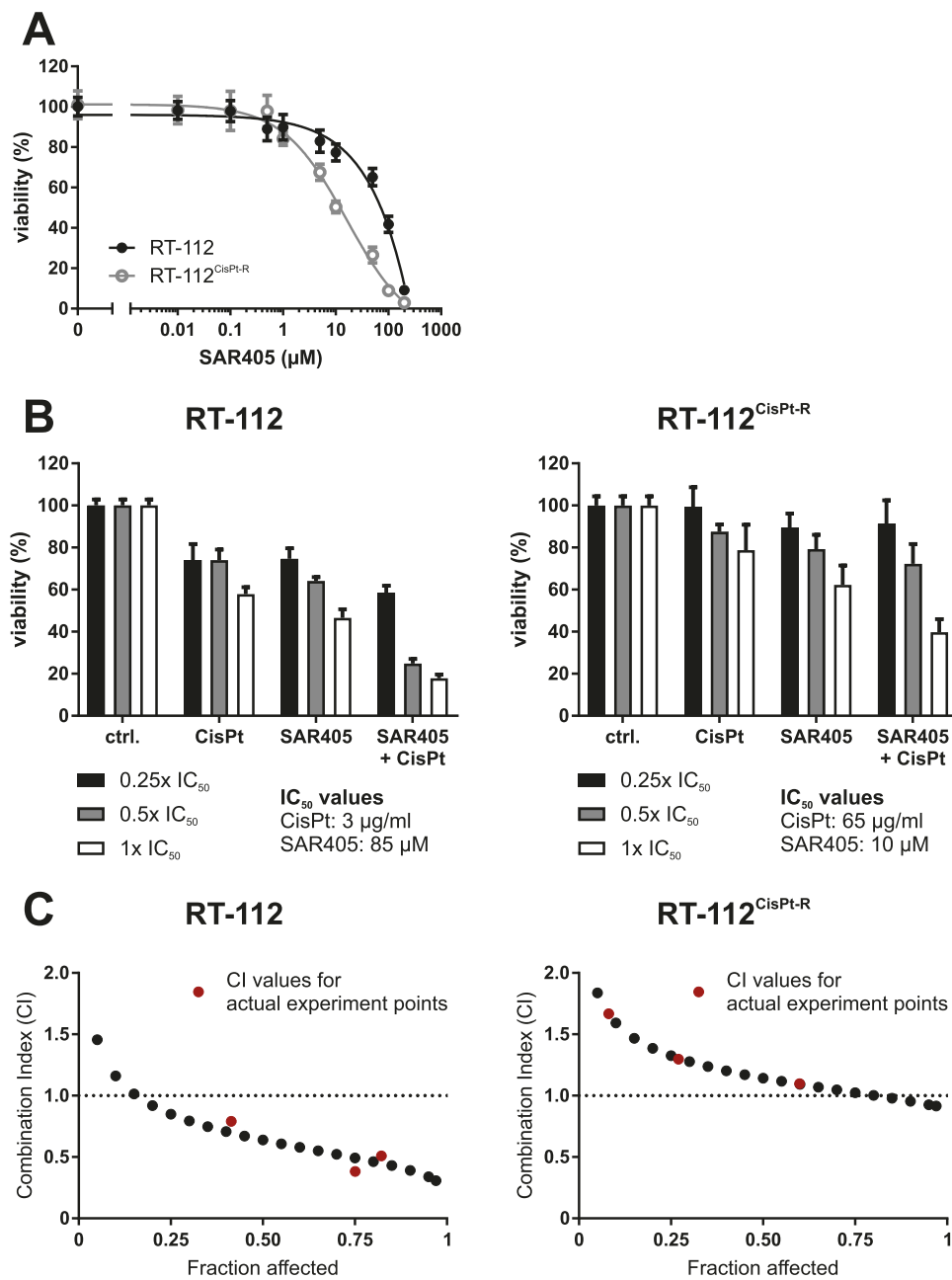


Fig. 5. The VPS34-specific inhibitor SAR405 supports cisplatin-induced cell death in both RT-112 and RT-112^{CisPt-R} cells. (A and B) RT-112 and RT-112^{CisPt-R} cells were treated with different concentrations of SAR405 (0.01–200 μM) (A) or with cisplatin, SAR405 or a combination of both (B) for 72 hours. For combination analyses (B), IC₅₀ values of 3 $\mu\text{g/ml}$ (RT-112) or 65 $\mu\text{g/ml}$ (RT-112^{CisPt-R}) cisplatin and 85 μM (RT-112) or 10 μM (RT-112^{CisPt-R}) SAR405 were used. After treatment, cell viability was measured using an MTT assay. At least 3 independent experiments were performed in triplicates. The results are shown as means \pm or + standard deviations of the independent experiments. For all experiments, 0.1% DMSO was used as control. For 1 \times IC₅₀, 0.5 \times IC₅₀, and 0.25 \times IC₅₀ in Figs. 3B, 4B, and 5B, the same controls are shown for each cell line. (C) Combination Index (CI) values were calculated using the software CompuSyn in order to determine synergistic (CI < 1), additive (CI = 1), or antagonistic (CI > 1) effects for the combination of cisplatin and SAR405. CompuSyn uses algorithms for a computerized simulation to show synergism, additivism, and antagonism at any effect level.

combination treatments with subsequent isobologram analyses. In RT-112 cells, SAR405 and cisplatin exhibit a synergistic interaction for all concentrations analyzed. In RT-112^{CisPt-R} cells, the effect was additive if concentrations were used in the range of the IC₅₀ of the individual compounds (Fig. 5B and C; the corresponding isobologram is shown in Fig. S4C). The presence of an additive effect

instead of synergism might be partly caused by the increased cytotoxicity of SAR405 alone in RT-112^{CisPt-R} cells. Accordingly, the combination of cisplatin with SAR405 concentrations of approximately 10 μM might open a valuable therapeutic window. In a next step, we wanted to confirm the results of the cell viability assay by an assay detecting caspase activity. For that, 0.5 \times IC₅₀ or

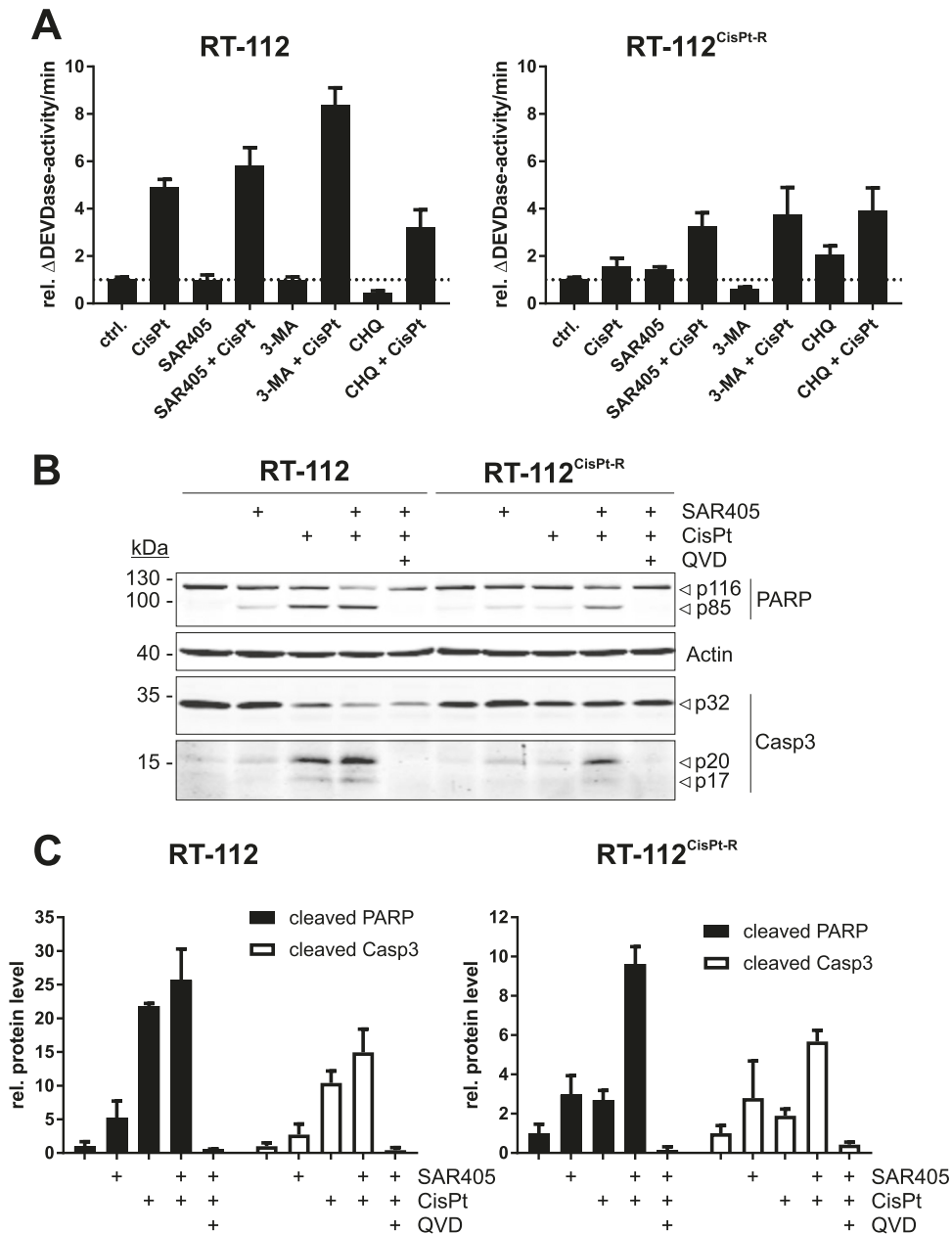


Fig. 6. The combination of cisplatin and SAR405 induces apoptosis in RT-112 and RT-112^{CisPt-R} cells. (A) RT-112 and RT-112^{CisPt-R} cells were treated with cisplatin, SAR405, 3-MA, or chloroquine (CHQ) alone or in combination. The concentrations used are the IC₅₀ or half IC₅₀ values for RT-112^{CisPt-R} and RT-112, respectively (Figs. 3–5). Caspase-3 activity was measured after 48 hours using a DEVD assay. The obtained values were normalized to the mean of the control values of each cell line. The results are shown as means + standard deviation of 3 independent experiments which were performed in triplicates. For all experiments, 0.1% DMSO was used as control. (B) RT-112 and RT-112^{CisPt-R} cells were treated with cisplatin, SAR405, and a combination of both in absence and presence of QVD (10 μ M). Again, the concentrations used were the IC₅₀ or half IC₅₀ values for RT-112^{CisPt-R} and RT-112, respectively (Figs. 3–5). After 48 hours, the cells were lysed, and cleared cellular lysates were subjected to SDS-PAGE and immunoblotting for PARP, caspase-3 (Casp3), and Actin. One representative immunoblot is shown. (C) The densities of bands on immunoblots of at least 3 independent experiments were quantified using Image Studio (LI-COR Biosciences) and normalized to Actin. The mean of the resulting control values for each cell line were set as “1” for each protein. The bars represent the means + standard deviation.

1 \times IC₅₀ of each compound were used in RT-112 or RT-112^{CisPt-R} cells, respectively. Of note, caspase activity was increased in parental and resistant cells if cisplatin was combined with either 3-MA or SAR405 compared to cisplatin alone (Fig. 6A). We also investigated caspase activation by immunoblot analysis detecting the cleavage of either the caspase-3 substrate poly (ADP-ribose)

polymerase (PARP) or caspase-3 itself, respectively (Fig. 6B and C). Increased PARP and caspase-3 cleavage was especially evident in RT-112^{CisPt-R} cells using SAR405 in combination with cisplatin compared to the individual treatments. Both PARP cleavage and caspase-3 activation could be inhibited using the caspase-inhibitor QVD, confirming that these treatments induce apoptosis. Collectively,

it appears that inhibition of the VPS34-Beclin 1 complex can sensitize both cisplatin-responsive and -resistant cells to cisplatin-induced cell death. Additionally, treatment with a VPS34-specific inhibitor such as SAR405 in a monotherapy might be a reasonable therapeutic approach in a setting with acquired cisplatin resistance.

3.4. VPS34 inhibition supports cisplatin-induced cell death in various UCC lines

RT-112 cells represent a UC with the histological grade G2. In order to investigate the general validity of our observations, we included several additional cell lines representing the heterogeneity of UC in our analyses, including epithelial-like 5637 and mesenchymal-like J82, 253J, T24, and SW-1710. Similar to RT-112 cells, we analyzed the expression levels of several ATG proteins in cisplatin-sensitive and -resistant cell pairs. Again, we observed the up-regulation of different ATG proteins in cisplatin-resistant derivatives (Fig. 7). Subsequently, we determined the IC₅₀ values for cisplatin and SAR405 within the cell lines J82, 253J, and T24 (Fig. S5A, S5B and S5C), and repeated the above described combination experiments for the cisplatin-sensitive and -resistant variants. In all cell lines except for T24^{CisPt-R}, the combination of cisplatin and SAR405 resulted in the highest reduction of cell viability (Fig. 8). For J82^{CisPt-R} and 253J^{CisPt-R} cells, isobologram analysis allowed the generation of CI plots. Whereas the combination was synergistic in J82^{CisPt-R} cells for concentrations in the range of the IC₅₀, it was rather additive for 253J^{CisPt-R} cells (Fig. 8D). Clearly, in J82^{CisPt-R} cells, the synergistic effect was most prominent. Like in RT-112^{CisPt-R} cells, J82^{CisPt-R} cells reveal an increased expression of ULK1 (Figs 2 and 7), which is a central regulator of the VPS34-Beclin 1 complex [17]. Accordingly, we hypothesize that the combination of cisplatin with a VPS34-specific inhibitor might be especially effective in UCCs with increased expression of components of both the VPS34 and the ULK1 complex.

4. Discussion

The European Association of Urology recommends cisplatin-based chemotherapy as upfront treatment in advanced and metastatic urothelial carcinoma, whenever not precluded by comorbidities. For perioperative systemic therapy, cisplatin-based chemotherapy is likewise the treatment of choice in eligible patients [27]. However, both the primary presence of or the development of chemoresistance are major obstacles for successful therapies. In this study, we characterized the autophagy signaling pathway as an appropriate target to increase cisplatin efficacy or to resensitize resistant cells. We found that several ATG proteins are up-regulated in various cisplatin-resistant UCC lines, suggesting that basal autophagy is increased in these cells. Nevertheless, they still respond to proautophagic conditions. Furthermore, we inhibited the autophagic

pathway by different pharmacological inhibitors and found synergistic or additive cytotoxic effects when combined with cisplatin compared to control conditions. Therefore, we propose that the efficacy of cisplatin-based therapy might be enhanced by combination with autophagy-inhibiting compounds. Under certain circumstances, the approach of autophagy inhibition might also be effective as monotherapy.

Current translational research aims at identifying and characterizing specific autophagy-modulating compounds. To date, chloroquine and hydroxychloroquine are still the substances of choice in the clinic if inhibition of autophagy is desired. However, there is an urgent need for more specific inhibitors of the autophagic pathway. The autophagy-inducing protein and lipid kinase complexes based on ULK1 and VPS34 are druggable targets, and recently some specific inhibitors targeting these kinases have been reported [21,22,28–30]. Interestingly, we observed that VPS34 inhibition was especially effective in cells with high ULK1 expression, i.e., RT-112^{CisPt-R} and J82^{CisPt-R} cells. There exists a strong crosstalk between these 2 complexes, but future studies have to assess whether an effective application of SAR405 requires high ULK1 expression.

We observed that both cisplatin-responsive and -resistant cells were sensitized for cisplatin-mediated effects by autophagy inhibition. This indicates that autophagy plays a central role for cytoprotection during de novo cisplatin treatment and during acquired cisplatin resistance. The dependency of cisplatin-resistant cells on autophagy is especially evident from the SAR405 experiments where mono-treatment with SAR405 was sufficient to significantly reduce cell viability of resistant cells. Hence, basal and constitutive autophagy is essential for supporting survival of resistant cells and/or for maintaining their resistant phenotype. However, these observations were not made for chloroquine or 3-MA as mono-treatment. Accordingly, we speculate that—next to autophagy—additional VPS34- or PtdIns3P-dependent processes might contribute to the establishment of cisplatin resistance, which are not efficiently targeted by chloroquine or 3-MA, respectively.

Among several molecular mechanisms of cisplatin resistance, autophagy has been suggested as one mode of off-target resistance [8]. Off-target resistance mechanisms describe cellular processes which are not directly engaged by cisplatin, but interfere with its lethal outcome [8]. The involvement of autophagy in cisplatin resistance has been shown for several cancer entities, and accordingly inhibition of autophagy sensitized resistant cells to cisplatin-induced cytotoxic effects [31–37]. However, it should be noted that also mTOR inhibition, which induces rather than inhibits autophagy, has been shown to be effective for overcoming cisplatin resistance [38–43]. Of note, Garcia-Cano et al. [44] reported that monoplatin, which promotes autophagy, is able to promote cell death of both cisplatin-sensitive and -resistant cells. In an analogous manner, conflicting results of autophagy modulation have been proposed with regard to

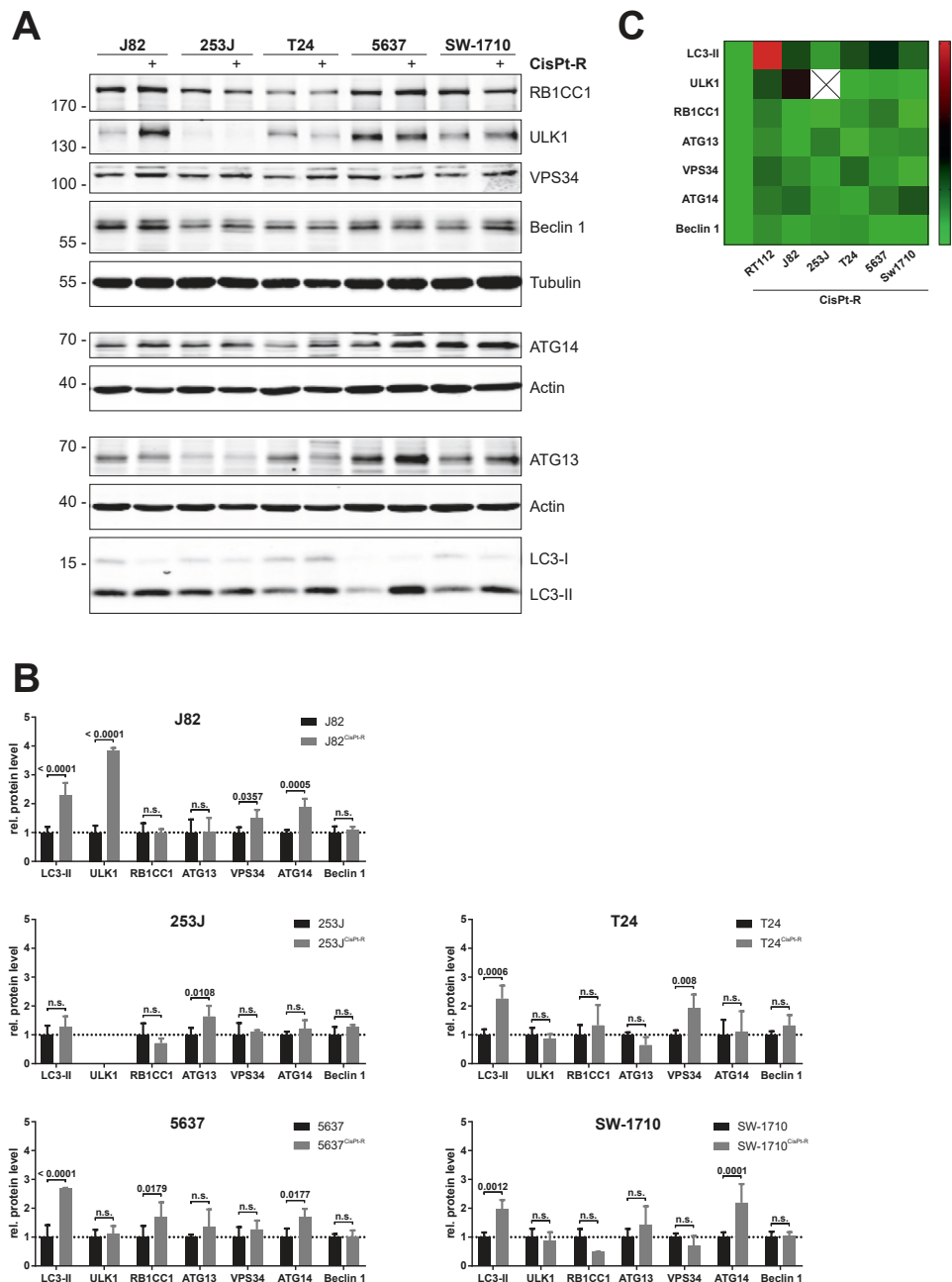


Fig. 7. ATG proteins are differentially expressed in various cisplatin-sensitive and -resistant UCCs. (A) Cells from various cisplatin-sensitive and -resistant UCCs (J82, 253J, T24, 5637, and SW-1710) were lysed and cleared cellular lysates were subjected to SDS-PAGE and immunoblotting for ULK1, Beclin 1, LC3, RB1CC1, ATG13, VPS34, ATG14, Actin, and Tubulin. One representative immunoblot is shown. (B) The densities of bands on immunoblots of at least 3 independent experiments were quantified using Image Studio (LI-COR Biosciences) and normalized to Actin or Tubulin. The mean of the resulting values for each cisplatin-sensitive cell line was set as “1” for each protein. Then, the values of the cisplatin-resistant cell lines were normalized to the values of their parental cells. The bars represent the means + standard deviation. A two-way ANOVA was used to compare the differences in protein expression between cisplatin-sensitive and -resistant cells. The respective *P* values are depicted in the diagram. (C) The expression of ATG proteins in cisplatin-resistant UCCs normalized to the expression in their parental cells (Figs. 2B and 7B) are summarized in a Heat Map. Please note, 253J cells lack quantifiable levels of ULK1 expression.

UC (reviewed in Ref. [45]). Ojija et al. [46] observed that inhibition of autophagy by chloroquine potentiates the cytotoxicity of cisplatin. Along these lines, Mani et al. suggested that enhanced autophagy might play an important role for the chemoresistant phenotype of bladder cancer. They observed a significant increase in apoptosis in cisplatin-

resistant UCCs treated with the BH3-mimetic (–)-gossypol upon knockdown of ATG5 or 3-MA treatment [47]. In contrast to these findings, Li et al. [48] reported that inhibition of the autophagic flux by chloroquine appears to be a survival mechanism of UCCs. Additionally, Pinto-Leite et al. [49] suggested using a combination of the mTOR

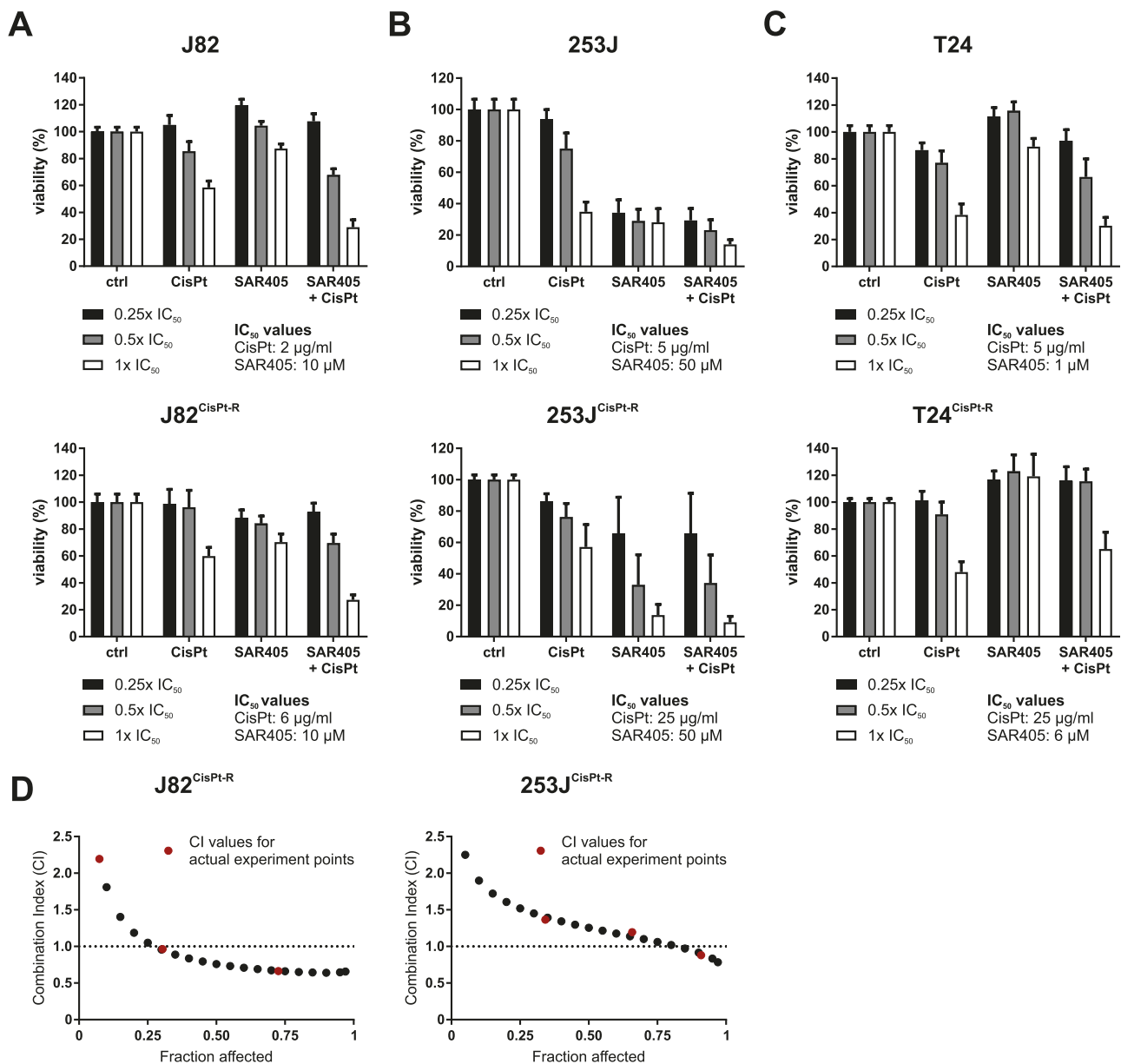


Fig. 8. Combination of cisplatin and SAR405 in various UCCs. (A–C) Cisplatin-sensitive and -resistant J82 (A), 253J (B), and T24 (C) cells were treated with cisplatin, SAR405, or a combination of both for 72 hours. The IC₅₀ values used for the combination treatment are shown in the figure. After treatment, cell viability was measured using an MTT assay. At least 3 independent experiments were performed in triplicates. The results are shown as means + standard deviations of the independent experiments. For all experiments, 0.1% DMSO was used as control. For 1× IC₅₀, 0.5× IC₅₀, and 0.25× IC₅₀, the same controls are shown for each cell line. (D) Combination Index (CI) values for J82^{CisPt-R} and 253J^{CisPt-R} were calculated using the software CompuSyn in order to determine synergistic (CI < 1), additive (CI = 1), or antagonistic (CI > 1) effects for the combination of cisplatin and SAR405. CompuSyn uses algorithms for a computerized simulation to show synergism, additivism, and antagonism at any effect level.

inhibitor Everolimus and cisplatin for UC. These discrepancies suggest that therapeutic approaches employing autophagy modulation might depend on the individual stage and grade of UC. In addition, the modes of action of chloroquine or mTOR inhibitors might include autophagy-independent effects. To our knowledge, specific inhibitors targeting the autophagy signaling pathway in general or the autophagy-inducing VPS34-Beclin 1 complex have not been evaluated for UCCs so far and would be worthwhile to be assessed in future preclinical or clinical studies.

Conflict of interest statement

The authors declare that there are no competing financial interests in relation to the work described.

Author contribution statement

DS designed the experiments, performed cell viability and caspase-3 activity assays, and performed immunoblot

analyses. MAS generated the cell lines and supported immunoblot analyses. NB, PB, JD, FS, NWH, WW, and CP gave technical support. DS, MAS, MJH, GN and BS analyzed and interpreted the data and wrote the manuscript. MJH, GN, and BS supervised the project. All authors discussed the results and commented on the manuscript.

Acknowledgments

We thank Wolfgang A. Schulz for helpful discussions and critical reading of the manuscript. This work was supported by the Deutsche Forschungsgemeinschaft STO 864/3-1, STO 864/4-1, STO 864/5-1, and GRK 2158 (to BS), the Research Committee of the Medical Faculty of the Heinrich Heine University Düsseldorf (22/2015 to BS), and the Düsseldorf School of Oncology (to GN and BS; funded by the Comprehensive Cancer Center Düsseldorf/Deutsche Krebshilfe and the Medical Faculty of the Heinrich Heine-University Düsseldorf).

Appendix A. Supporting information

Supplementary data associated with this article can be found in the online version at <https://doi.org/10.1016/j.urolonc.2017.11.021>.

References

- [1] Jemal A, Bray F, Center MM, Ferlay J, Ward E, Forman D. Global cancer statistics. *CA Cancer J Clin* 2011;61:69–90.
- [2] Knowles MA. Molecular subtypes of bladder cancer: jekyll and Hyde or chalk and cheese? *Carcinogenesis* 2006;27:361–73.
- [3] Stenzl A, Cowan NC, De Santis M, Kuczyk MA, Merseburger AS, Ribal MJ, et al. Treatment of muscle-invasive and metastatic bladder cancer: update of the EAU guidelines. *Eur Urol* 2011;59:1009–18.
- [4] Abida W, Bajorin DF, Rosenberg JE. First-line treatment and prognostic factors of metastatic bladder cancer for platinum-eligible patients. *Hematol Oncol Clin North Am* 2015;29:319–28:ix-x.
- [5] von der Maase H, Sengelov L, Roberts JT, Ricci S, Dogliotti L, Oliver T, et al. Long-term survival results of a randomized trial comparing gemcitabine plus cisplatin, with methotrexate, vinblastine, doxorubicin, plus cisplatin in patients with bladder cancer. *J Clin Oncol* 2005;23:4602–8.
- [6] Cohen SM, Lippard SJ. Cisplatin: from DNA damage to cancer chemotherapy. *Prog Nucleic Acid Res Mol Biol* 2001;67:93–130.
- [7] Ljungman M. The transcription stress response. *Cell Cycle* 2007;6:2252–7.
- [8] Galluzzi L, Senovilla L, Vitale I, Michels J, Martins I, Kepp O, et al. Molecular mechanisms of cisplatin resistance. *Oncogene* 2012;31:1869–83.
- [9] Olive PL, Banath JP. Kinetics of H2AX phosphorylation after exposure to cisplatin. *Cytometry B Clin Cytom* 2009;76:79–90.
- [10] Roos WP, Kaina B. DNA damage-induced cell death: from specific DNA lesions to the DNA damage response and apoptosis. *Cancer Lett* 2013;332:237–48.
- [11] Hohn A, Kruger K, Skowron MA, Bormann S, Schumacher L, Schulz WA, et al. Distinct mechanisms contribute to acquired cisplatin resistance of urothelial carcinoma cells. *Oncotarget* 2016;7:41320–35.
- [12] Skowron MA, Niegisch G, Fritz G, Arent T, van Roermund JG, Romano A, et al. Phenotype plasticity rather than repopulation from CD90/CK14+ cancer stem cells leads to cisplatin resistance of urothelial carcinoma cell lines. *J Exp Clin Cancer Res* 2015;34:144.
- [13] Chude CI, Amaravadi RK. Targeting autophagy in cancer: update on clinical trials and novel inhibitors. *Int J Mol Sci* 2017;18.
- [14] Rebecca VW, Amaravadi RK. Emerging strategies to effectively target autophagy in cancer. *Oncogene* 2016;35:1–11.
- [15] White E. The role for autophagy in cancer. *J Clin Invest* 2015;125:42–6.
- [16] Mizushima N, Yoshimori T, Ohsumi Y. The role of Atg proteins in autophagosome formation. *Annu Rev Cell Dev Biol* 2011;27:107–32.
- [17] Wesselborg S, Stork B. Autophagy signal transduction by ATG proteins: from hierarchies to networks. *Cell Mol Life Sci* 2015;72:4721–57.
- [18] Axe EL, Walker SA, Manifava M, Chandra P, Roderick HL, Habermann A, et al. Autophagosome formation from membrane compartments enriched in phosphatidylinositol 3-phosphate and dynamically connected to the endoplasmic reticulum. *J Cell Biol* 2008;182:685–701.
- [19] Geng J, Klionsky DJ. The Atg8 and Atg12 ubiquitin-like conjugation systems in macroautophagy. ‘Protein modifications: beyond the usual suspects’ review series. *EMBO Rep* 2008;9:859–64.
- [20] Amaravadi RK, Thompson CB. The roles of therapy-induced autophagy and necrosis in cancer treatment. *Clin Cancer Res* 2007;13:7271–9.
- [21] Petherick KJ, Conway OJ, Mpamhanga C, Osborne SA, Kamal A, Saxty B, et al. Pharmacological inhibition of ULK1 kinase blocks mammalian target of rapamycin (mTOR)-dependent Autophagy. *J Biol Chem* 2015;290:11376–83.
- [22] Ronan B, Flamand O, Vescovi L, Dureuil C, Durand L, Fassy F, et al. A highly potent and selective Vps34 inhibitor alters vesicle trafficking and autophagy. *Nat Chem Biol* 2014;10:1013–9.
- [23] Chou TC. Drug combination studies and their synergy quantification using the Chou-Talalay method. *Cancer Res* 2010;70:440–6.
- [24] Klionsky DJ, Abdelmohsen K, Abe A, Abedin MJ, Abeliovich H, Acevedo Arozena A, et al. Guidelines for the use and interpretation of assays for monitoring autophagy (3rd edition). *Autophagy* 2016;12:1–222.
- [25] King MA, Ganley IG, Flemington V. Inhibition of cholesterol metabolism underlies synergy between mTOR pathway inhibition and chloroquine in bladder cancer cells. *Oncogene* 2016;35:4518–28.
- [26] Wu YT, Tan HL, Shui G, Bauvy C, Huang Q, Wenk MR, et al. Dual role of 3-methyladenine in modulation of autophagy via different temporal patterns of inhibition on class I and III phosphoinositide 3-kinase. *J Biol Chem* 2010;285:10850–61.
- [27] Witjes JA, Comperat E, Cowan NC, De Santis M, Gakis G, Lebret T, et al. EAU guidelines on muscle-invasive and metastatic bladder cancer: summary of the 2013 guidelines. *Eur Urol* 2014;65:778–92.
- [28] Bago R, Malik N, Munson MJ, Prescott AR, Davies P, Sommer E, et al. Characterization of VPS34-IN1, a selective inhibitor of Vps34, reveals that the phosphatidylinositol 3-phosphate-binding SGK3 protein kinase is a downstream target of class III phosphoinositide 3-kinase. *Biochem J* 2014;463:413–27.
- [29] Dowdle WE, Nyfeler B, Nagel J, Elling RA, Liu S, Triantafellow E, et al. Selective VPS34 inhibitor blocks autophagy and uncovers a role for NCOA4 in ferritin degradation and iron homeostasis in vivo. *Nat Cell Biol* 2014;16:1069–79.
- [30] Egan DF, Chun MG, Vamos M, Zou H, Rong J, Miller CJ, et al. Small molecule inhibition of the autophagy kinase ULK1 and identification of ULK1 substrates. *Mol Cell* 2015;59:285–97.
- [31] Ma B, Liang LZ, Liao GQ, Liang YJ, Liu HC, Zheng GS, et al. Inhibition of autophagy enhances cisplatin cytotoxicity in human adenoid cystic carcinoma cells of salivary glands. *J Oral Pathol Med* 2013;42:774–80.

- [32] Liu D, Yang Y, Liu Q, Wang J. Inhibition of autophagy by 3-MA potentiates cisplatin-induced apoptosis in esophageal squamous cell carcinoma cells. *Med Oncol* 2011;28:105–11.
- [33] Zhao Z, Tao L, Shen C, Liu B, Yang Z, Tao H. Silencing of Barkor/ATG14 sensitizes osteosarcoma cells to cisplatin-induced apoptosis. *Int J Mol Med* 2014;33:271–6.
- [34] Fukuda T, Oda K, Wada-Hiraike O, Sone K, Inaba K, Ikeda Y, et al. The anti-malarial chloroquine suppresses proliferation and overcomes cisplatin resistance of endometrial cancer cells via autophagy inhibition. *Gynecol Oncol* 2015;137:538–45.
- [35] Zhao XG, Sun RJ, Yang XY, Liu DY, Lei DP, Jin T, et al. Chloroquine-enhanced efficacy of cisplatin in the treatment of hypopharyngeal carcinoma in xenograft mice. *PLoS One* 2015;10:e0126147.
- [36] Zhao J, Nie Y, Wang H, Lin Y. MiR-181a suppresses autophagy and sensitizes gastric cancer cells to cisplatin. *Gene* 2016;576:828–33.
- [37] Liu X, Sun K, Wang H, Dai Y. Knockdown of retinoblastoma protein may sensitize glioma cells to cisplatin through inhibition of autophagy. *Neurosci Lett* 2016;620:137–42.
- [38] Gaur S, Chen L, Yang L, Wu X, Un F, Yen Y. Inhibitors of mTOR overcome drug resistance from topoisomerase II inhibitors in solid tumors. *Cancer Lett* 2011;311:20–8.
- [39] Huang Y, Xi Q, Chen Y, Wang J, Peng P, Xia S, et al. A dual mTORC1 and mTORC2 inhibitor shows antitumor activity in esophageal squamous cell carcinoma cells and sensitizes them to cisplatin. *Anticancer Drugs* 2013;24:889–98.
- [40] Ma BB, Lui VW, Hui EP, Lau CP, Ho K, Ng MH, et al. The activity of mTOR inhibitor RAD001 (everolimus) in nasopharyngeal carcinoma and cisplatin-resistant cell lines. *Invest New Drugs* 2010;28:413–20.
- [41] Mabuchi S, Kawase C, Altomare DA, Morishige K, Sawada K, Hayashi M, et al. mTOR is a promising therapeutic target both in cisplatin-sensitive and cisplatin-resistant clear cell carcinoma of the ovary. *Clin Cancer Res* 2009;15:5404–13.
- [42] Tam KH, Yang ZF, Lau CK, Lam CT, Pang RW, Poon RT. Inhibition of mTOR enhances chemosensitivity in hepatocellular carcinoma. *Cancer Lett* 2009;273:201–9.
- [43] Wu C, Wangpaichitr M, Feun L, Kuo MT, Robles C, Lampidis T, et al. Overcoming cisplatin resistance by mTOR inhibitor in lung cancer. *Mol Cancer* 2005;4:25.
- [44] Garcia-Cano J, Ambroise G, Pascual-Serra R, Carrion MC, Serrano-Oviedo L, Ortega-Muelas M, et al. Exploiting the potential of autophagy in cisplatin therapy: a new strategy to overcome resistance. *Oncotarget* 2015;6:15551–65.
- [45] Chandrasekar T, Evans CP. Autophagy and urothelial carcinoma of the bladder: a review. *Investig Clin Urol* 2016;57(Suppl 1):S89–97.
- [46] Ojha R, Singh SK, Bhattacharyya S, Dhanda RS, Rakha A, Mandal AK, et al. Inhibition of grade dependent autophagy in urothelial carcinoma increases cell death under nutritional limiting condition and potentiates the cytotoxicity of chemotherapeutic agent. *J Urol* 2014;191:1889–98.
- [47] Mani J, Vallo S, Rakel S, Antonietti P, Gessler F, Blaheta R, et al. Chemoresistance is associated with increased cytoprotective autophagy and diminished apoptosis in bladder cancer cells treated with the BH3 mimetic (-)-Gossypol (AT-101). *BMC Cancer* 2015;15:224.
- [48] Li JR, Cheng CL, Yang CR, Ou YC, Wu MJ, Ko JL. Dual inhibitor of phosphoinositide 3-kinase/mammalian target of rapamycin NVP-BEZ235 effectively inhibits cisplatin-resistant urothelial cancer cell growth through autophagic flux. *Toxicol Lett* 2013;220:267–76.
- [49] Pinto-Leite R, Arantes-Rodrigues R, Palmeira C, Colaco B, Lopes C, Colaco A, et al. Everolimus combined with cisplatin has a potential role in treatment of urothelial bladder cancer. *Biomed Pharmacother* 2013;67:116–21.

Publication 2

Systematic analysis of ATG13 domain requirements for autophagy induction

Nora Wallot-Hieke, Neha Verma, David Schlütermann, Niklas Berleth, Jana Deitersen, Philip Böhler, Fabian Stuhldreier, Wenxian Wu, Sabine Seggewiß, Christoph Peter, Holger Gohlke, Noboru Mizushima, Björn Stork

Autophagy, volume 14, issue 5, pages 743-763, March 2018

DOI: 10.1080/15548627.2017.1387342

Systematic analysis of ATG13 domain requirements for autophagy induction

Nora Wallot-Hieke^a, Neha Verma ^b, David Schlütermann^a, Niklas Berleth^a, Jana Deitersen^a, Philip Böhler ^a, Fabian Stuhldreier^a, Wenxian Wu^a, Sabine Seggewiß^a, Christoph Peter ^a, Holger Gohlke ^b, Noboru Mizushima ^c and Björn Stork ^{a*}

^aInstitute of Molecular Medicine I, Medical Faculty, Heinrich Heine University Düsseldorf, Düsseldorf, Germany; ^bInstitute for Pharmaceutical and Medicinal Chemistry, Faculty of Mathematics and Natural Sciences, Heinrich Heine University Düsseldorf, Düsseldorf, Germany; ^cDepartment of Biochemistry and Molecular Biology, Graduate School and Faculty of Medicine, The University of Tokyo, Tokyo, Japan

ABSTRACT

Macroautophagy/autophagy is an evolutionarily conserved cellular process whose induction is regulated by the ULK1 protein kinase complex. The subunit ATG13 functions as an adaptor protein by recruiting ULK1, RB1CC1 and ATG101 to a core ULK1 complex. Furthermore, ATG13 directly binds both phospholipids and members of the Atg8 family. The central involvement of ATG13 in complex formation makes it an attractive target for autophagy regulation. Here, we analyzed known interactions of ATG13 with proteins and lipids for their potential modulation of ULK1 complex formation and autophagy induction. Targeting the ATG101-ATG13 interaction showed the strongest autophagy-inhibitory effect, whereas the inhibition of binding to ULK1 or RB1CC1 had only minor effects, emphasizing that mutations interfering with ULK1 complex assembly do not necessarily result in a blockade of autophagy. Furthermore, inhibition of ATG13 binding to phospholipids or Atg8 proteins had only mild effects on autophagy. Generally, the observed phenotypes were more severe when autophagy was induced by MTORC1/2 inhibition compared to amino acid starvation. Collectively, these data establish the interaction between ATG13 and ATG101 as a promising target in disease-settings where the inhibition of autophagy is desired.

Abbreviations: AMPK: AMP-activated protein kinase; ATG: autophagy-related; BafA1: bafilomycin A; EBSS: Earle's Balanced Salt Solution; GABARAP: gamma-aminobutyric acid A receptor-associated protein; HORMA: Hop1, Rev7 and MAD2; KO: knockout; LIR: LC3-interacting region; MAP1LC3/LC3: microtubule-associated protein 1 light chain 3; MEF: mouse embryonic fibroblast; MM-GB/SA: molecular mechanics Generalized Born solvent-accessible surface area; MTORC1/2: mechanistic target of rapamycin (serine/threonine kinase) complex 1/2; PAS: phagophore assembly site; PLPD: phospholipid-binding domain; RB1CC1/FIP200: RB1-inducible coiled-coil 1; RPS6KB1: ribosomal protein S6 kinase, polypeptide 1; SQSTM1/p62: sequestosome 1; ULK1/2: unc-51 like kinase 1/2; WIPI2: WD repeat domain, phosphoinositide interacting 2; WT: wild-type

ARTICLE HISTORY

Received 11 January 2017
Revised 24 August 2017
Accepted 28 September 2017

KEYWORDS

ATG13; ATG101; autophagy; RB1CC1; ULK1

Introduction

Autophagy is an intracellular degradation process mediating the clearance of misfolded or damaged proteins, protein aggregates, or entire organelles. During the course of autophagy, a phagophore forms from microdomains of the ER. This phagophore further engulfs the cargo to be removed. By addition of membrane compartments originating from different cellular sources, the phagophore closes into a mature autophagosome. This double-membraned vesicle then fuses with lysosomes, giving rise to an autolysosome in which the cargo becomes degraded by lysosomal hydrolases. This process is conserved from yeast to higher eukaryotes including mammals, and autophagy is essential for functional metabolism and cell integrity. Accordingly, the dysregulation of autophagy is implicated in various human diseases such as cancer, neurodegenerative diseases such as Alzheimer and Parkinson, myopathies, and heart and liver diseases.^{1–4}

Autophagy is executed on a basal level in most cell types, but can be actively induced by nutrient deprivation or other stress conditions. Autophagy-activating pathways all converge on the induction of the ULK1 complex, a central regulation node within the autophagy network. This protein complex comprises the Ser/Thr protein kinase ULK1 (unc-51 like kinase 1) and the interacting proteins ATG13, ATG101 and RB1CC1/FIP200 (RB1-inducible coiled-coil 1).^{5–8} Knockdown and knockout experiments revealed essential roles for each of these proteins in autophagy. Knockout of either *Atg13* or *Rb1cc1* leads to embryonic lethality,^{9,10} whereas *ulk1*^{-/-} or *ulk2*^{-/-} mice have rather mild autophagy phenotypes and *ulk1/2*^{-/-} mice are alive but die shortly after birth.^{11–13} Fibroblasts isolated from these *ulk1/2* double-knockout mice are responsive to glucose deprivation but do not display autophagy induction by amino acid withdrawal.¹¹ The ULK1 complex itself is regulated by upstream nutrient- and energy-sensing kinases, such as MTOR

CONTACT Björn Stork  bjoern.stork@uni-duesseldorf.de  Universitätsstr. 1, Building 23.12, 40225 Düsseldorf, Germany

 Supplemental data for this article can be accessed at:  <https://doi.org/10.1080/15548627.2017.1387342>

© 2018 The Author(s). Published by Informa UK Limited, trading as Taylor & Francis Group

This is an Open Access article distributed under the terms of the Creative Commons Attribution-NonCommercial-NoDerivatives License (<http://creativecommons.org/licenses/by-nc-nd/4.0/>), which permits non-commercial re-use, distribution, and reproduction in any medium, provided the original work is properly cited, and is not altered, transformed, or built upon in any way.

(mechanistic target of rapamycin [serine/threonine kinase]), AMPK (AMP-activated protein kinase), and AKT1 (reviewed in ref. 14–17). The individual subunits of the ULK1 complex have been investigated in detail over the past years, but still information about the relevance of the single protein-protein interactions within the complex is missing. Most reports suggest that ATG13 is the central subunit of this complex and recruits the remaining components,^{6,18–20} though one report indicates a direct interaction of ULK1 and RB1CC1 independent of ATG13.⁵ Along these lines, the modulation of protein-protein interactions involving ATG13 might be a valuable approach to regulate autophagy signaling pathways.

The N terminus of ATG13 comprises a HORMA domain functioning as an ATG101-interaction platform. This domain was first identified in the *Saccharomyces cerevisiae* proteins Hop1, Rev7, and Mad2, which display sequence similarities but no functional overlaps.²¹ Jao et al. are the first to identify a HORMA domain in ATG13.²² Mad2 can switch between an open (O-Mad2) and a closed (C-Mad2) conformation, and the ATG13 HORMA structure corresponds to the C-Mad2 state.²² This finding has been complemented by 3 other groups reporting the structure of ATG101 as O-Mad2-like and the HORMA-mediated dimerization of ATG13 and ATG101, respectively.^{20,23,24} Suzuki et al. show that an ATG101 version which cannot dimerize with ATG13 is not incorporated into the ULK1 complex, ultimately leading to impaired autophagy induction. The recruitment of the other subunits into the complex is unaffected.²⁰ Of note, additional binding partners of the Atg13/ATG13 HORMA domain have been reported, including ATG14 and yeast Atg9.^{22,25} Next to the HORMA domain, ATG13 contains a phospholipid-binding motif at its extreme N terminus.²⁶ Four amino acid residues conserved across species mediate its interaction with phosphatic acid (PA), phosphatidylinositol 3-phosphate (PtdIns3P), phosphatidylinositol 4-phosphate (PtdIns4P) and to a lesser extent with phosphatidylinositol 3,4,5-trisphosphate (PtdIns(3,4,5)P₃). Mutation of these 4 key residues severely decreases phospholipid binding, inhibits translocation of ATG13 to the autophagosome formation site and impedes autophagic flux upon starvation.²⁶

In contrast to the structured N terminus, the C-terminal part of ATG13 is intrinsically disordered.^{27,28} In yeast Atg13, the intrinsically disordered region (IDR) harbors the interaction sites for Atg1 and Atg17, representing the yeast orthologs for ULK1 and RB1CC1, respectively.^{29,30} In agreement with these data for yeast, Jung et al. have mapped the ULK1 and RB1CC1 interaction sites to the C terminus of human ATG13.¹⁹ Our group has fine-mapped these sites. We have observed an ATG13 isoform in the DT40 chicken B-lymphocyte cell line missing a 26-amino-acid stretch encoded by exon12. This isoform cannot bind to RB1CC1.³¹ With regard to ULK1, we have previously identified the last 3 amino acids of ATG13 to be indispensable for ULK1 binding.¹⁸ Notably, the deletion of this short peptide and correspondingly the disruption of the ATG13-ULK1 interaction had only minor effects on autophagy induction.¹⁸

Finally, a MAP1LC3/LC3-interacting region (LIR) motif was identified in ATG13. The LIR mediates interaction with members of the Atg8 family, and Alemu et al. have observed that the ATG13 LIR preferentially associates with the GABARAP

subfamily of Atg8 proteins.³² Suzuki et al. have determined the crystal structures of 3 MAP1LC3/LC3 isoforms in complex with a peptide containing the residues 436 to 447 of ATG13.³³ They also have performed mutational analysis of LC3A with either increased or decreased LIR-binding affinity and observe a defect in autophagosome formation.³³ However, since this defect might be caused by altered binding to other LIR-containing proteins and not necessarily to ATG13, the specific function of the ATG13 LIR remains elusive so far.

In the present work, we aimed at systematically investigating the individual importance of the ATG13 interaction sites for ULK1 complex formation, recruitment to the autophagosome formation site, and autophagy induction. For this, we made use of different proautophagic stimuli (i.e., amino acid starvation and MTOR inhibition) and different autophagy readouts (LC3 turnover; LC3, WIPI2, and ATG16L1 puncta formation). It appears that the association of ATG101 with ATG13 is central for autophagy induction. In contrast, binding of both ULK1 and RB1CC1 is not mandatory for this process. Generally, the observed effects were more pronounced upon MTOR inhibition, confirming the accepted model of MTOR-mediated regulation of the ULK1 complex and indicating that crude EBSS treatment might induce autophagy independently of the MTOR-ULK1 axis. We suggest that—next to the direct inhibition of ULK1 kinase activity—interference with the ATG13-ATG101 interaction might represent a promising approach to regulate autophagy induction.

Results

In order to comprehensively analyze the ATG13 domain requirements for autophagy, we performed a systematic analysis using specific ATG13 variants incapable of binding to phospholipids, ATG101, RB1CC1, Atg8 family members, or ULK1, respectively (Fig. 1A, B).

The amino acid sequence V348-M373 of ATG13 comprises the RB1CC1 interaction site

The ATG13-RB1CC1 interaction site was reported to be located at the C terminus of ATG13.¹⁹ We have previously identified an ATG13 isoform in the chicken B-lymphocyte cell line DT40, in which deletion of the amino acids encoded by exon 12 lead to inhibited interaction of ATG13 with RB1CC1.³¹ The amino acid sequence encoded by avian exon 12 corresponds to the amino acid sequence V348 to M373 of human ATG13 isoform 2, which is encoded by human exon 14. Deletion of this sequence disrupted the ATG13-RB1CC1 interaction, while binding of ATG13 to ULK1 and ATG101 was not affected. This was evident from immunopurification experiments and from increased protein levels of ATG101 and ULK1 following the expression of ATG13 variants in *atg13* KO MEFs (Fig. 2A). In order to exclude the possibility that the deletion of V348-M373 only results in a weakened interaction that is not detectable by immunopurification, we performed 2 additional assays to monitor protein interaction in vivo. First, we employed a proximity ligation assay that allows detection of single protein-protein interactions using antibody-recognition combined with exponential signal amplification by PCR.

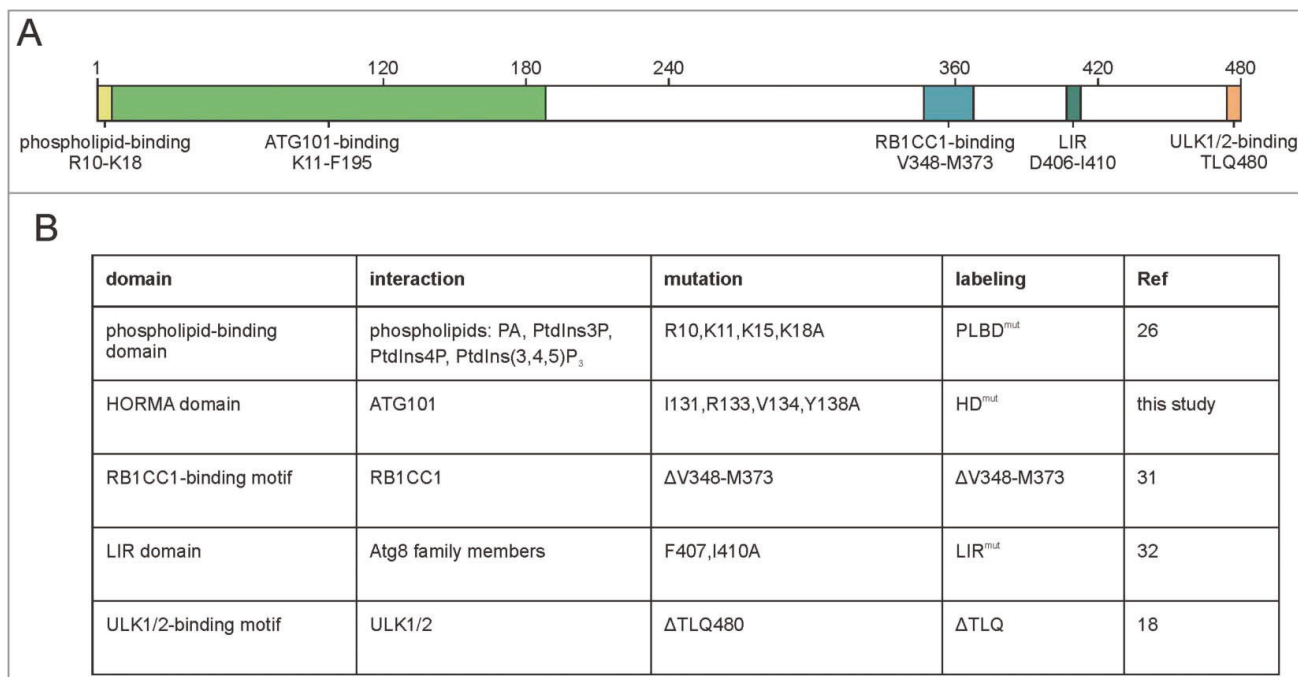


Figure 1. Interaction interfaces of human ATG13. (A) Schematic representation of human ATG13 (isoform 2; Uniprot identifier O75143-2). Amino acid sequences involved in binding to proteins and phospholipids are indicated.^{18,20,23,24,26,31–33,56} (B) List of ATG13 mutations investigated in this paper. Targeted domains, interaction partners, applied mutations and labelling used for this manuscript are given.

Visualization is mediated by fluorescent nucleotides. HA-tagged ATG13 variants were stained with mouse anti-HA antibodies and RB1CC1 with rabbit anti-RB1CC1 antibodies. As negative controls *Atg13* WT MEFs expressing untagged ATG13 and *atg13* KO MEFs expressing ATG13 lacking the entire C terminus (ΔC) were used. Cells reconstituted with full-length ATG13 displayed strong signals with significant difference to control cells (Fig. 2B). In contrast, MEFs expressing ATG13 (ΔV348-M373) revealed a signal count similar to control cells, indicating the disruption of the interaction with RB1CC1. Second, we used the *in vivo* biotin labeling assay developed by Ting and colleagues.^{34–36} In this assay, ATG13 variants were tagged with the ascorbate peroxidase derivative APEX2 and expressed in *atg13* KO MEFs. Upon activation of the peroxidase, the provided biotin-phenol is converted to biotin-phenoxyl radicals, which covalently react with nearby electron-rich amino acids and thereby label proteins with biotin. Since phenoxyl radicals are short-lived and have a small labeling radius, only proteins proximal to the APEX2 fusion protein become biotinylated.^{34–36} Subsequent cell lysis and enrichment of biotinylated proteins by streptavidine beads allow detection of interacting proteins. Immunoblotting revealed that RB1CC1 was only purified from cells expressing full-length ATG13 but was absent in all other samples (Fig. 2C). On the contrary, ATG101 was purified with all ATG13 variants. Note that ATG13 itself is biotinylated and purified; therefore, proteins might be purified due to biotinylation or interaction with ATG13. Nevertheless, both assays confirm that the ATG13 sequence V348-M373 mediates the interaction with RB1CC1.

Next we questioned if and how the assembly of the ULK1 complex might be affected by the inhibition of the ATG13-RB1CC1 interaction. For this, size-exclusion chromatography experiments were conducted. As has been reported

previously,¹⁰ *atg13* KO MEFs do not assemble the ULK1 complex (Fig. 2D, upper panels and black curve in diagrams). Whereas RB1CC1 is present in high-molecular mass fractions corresponding to complexes of approximately 3 MDa (Fig. 2D, fractions 18 to 21), ULK1 only distributes in lower-molecular mass fractions. ATG101 exists mainly as a monomer in fractions containing molecules lower than 43 kDa. Re-expression of wild-type ATG13 in these KO cells restores the assembly of the ULK1 complex, with all analyzed proteins being present in the high-molecular mass fractions (Fig. 2D, middle panels and blue curve in diagrams). Additionally, ATG101 and ATG13 display high protein amounts in fractions corresponding to a molecular mass of 400 to 200 kDa (Fig. 2D, middle panels, fractions 29 to 36). Finally, disruption of the RB1CC1 interaction with ATG13 by deleting the V348-M373 sequence resulted in a disassembled ULK1 complex and a shift of ATG13, ULK1 and ATG101 to lower-molecular mass fractions (Fig. 2D, lower panels and red curve in diagrams). Of note, ULK1 distribution resembles the *atg13* KO phenotype, whereas ATG101 accumulates in fractions corresponding to 400 to 200 kDa protein complexes, which is different from KO cells (Fig. 2D, compare black and red curve in diagrams). Similarly, ATG13 protein levels are almost completely depleted in high-molecular mass fractions and are mainly present in later fractions. These data indicate that ATG13-containing subcomplexes are formed in cells expressing the ATG13(ΔV348-M373) variant rather than the entire RB1CC1-dependent ULK1 complex. Besides ATG13, these complexes might harbor ULK1, ATG101, or both (Fig. 2A).

Because the ULK1 complex is not formed when the interaction of ATG13 and RB1CC1 is inhibited, we next asked if this has an effect on the recruitment of both proteins to the autophagosome formation site. Immunofluorescence experiments

Taken together, the sequence V348-M373 represents the RB1CC1 interaction site in ATG13, and this protein-protein interaction can be abolished by the deletion of this peptide. This in turn provokes disassembly of the ULK1 complex and inhibited recruitment to the phagophore.

The amino acids I131, R133, V134 and Y138 of ATG13 are mandatory for the interaction with ATG101

In addition to the RB1CC1 interaction, we were also interested in the binding of ATG13 to ATG101. We conducted a computational alanine scanning of the ATG13-ATG101 interface on the structure of the human ATG13-ATG101 HORMA heterodimer (PDB ID: 5C50; ref. 24) using the DrugScore^{PPI} web-server.³⁷ Interface residues resulting in a binding free energy change $\Delta\Delta G > 1$ kcal mol⁻¹ when mutated to alanine were considered binding hot spots (I131, R133, V134, Y138; Fig. 4A, upper panel). Isoleucine, arginine, and tyrosine are enriched in hot spot residues.³⁸ To independently validate the predicted hotspots, we performed MM-GB/SA calculations combined with a decomposition of the effective binding energy on a per-residue level.^{39,40} The MM-GB/SA calculations confirmed that R133, V134, Y138, and to a lesser extent I131, contribute most to the effective binding energy (Fig. 4A, middle panel). In addition, R139 and R142 were identified by MM-GB/SA but not by DrugScore^{PPI}, and Y115 *vice versa*. Furthermore, a cluster of

potential binding hot spots located in the connector loop (residues 33 to 58) of ATG13 was identified by MM-GB/SA but not by DrugScore^{PPI} (Fig. S1). The consensus hot spot residues in the ATG13 interface (Fig. 4A, lower panel) were then changed to alanine, and binding of ATG101 to these ATG13 variants was analyzed by a bimolecular fluorescence complementation assay.

For this analysis, ATG13 and ATG101 were fused to the N- or C-terminal part of the YFP variant Venus, respectively. Upon expression of VenusN-ATG13 and VenusC-ATG101 fusion proteins in *atg13* KO MEFs, Venus fluorescence was complemented by the interaction of wild-type ATG13 and ATG101. Mutations of single amino acids did not influence the interaction between ATG13 and ATG101 (data not shown). However, exchange of the 4 amino acids I131, R133, V134 and Y138 to alanine led to the disruption of the ATG13-ATG101 interaction as detected by decreased Venus fluorescence (Fig. 4B). When performing immunoblotting of ATG101, we detected low protein levels in cells transfected with the mutant ATG13 that were similar to the ones observed for *atg13* KO MEFs (Fig. 4B). This is due to the absence of the stabilizing effect of the ATG13-ATG101 protein-protein interaction on ATG101; the stabilizing effect is evident in cells expressing full-length ATG13 (Fig. 4B). We also performed immunopurification experiments of ATG101. Only wild-type ATG13 was copurified, while the 4 amino acid ATG13 variant (I131,R133,V134,Y138A; named HORMA

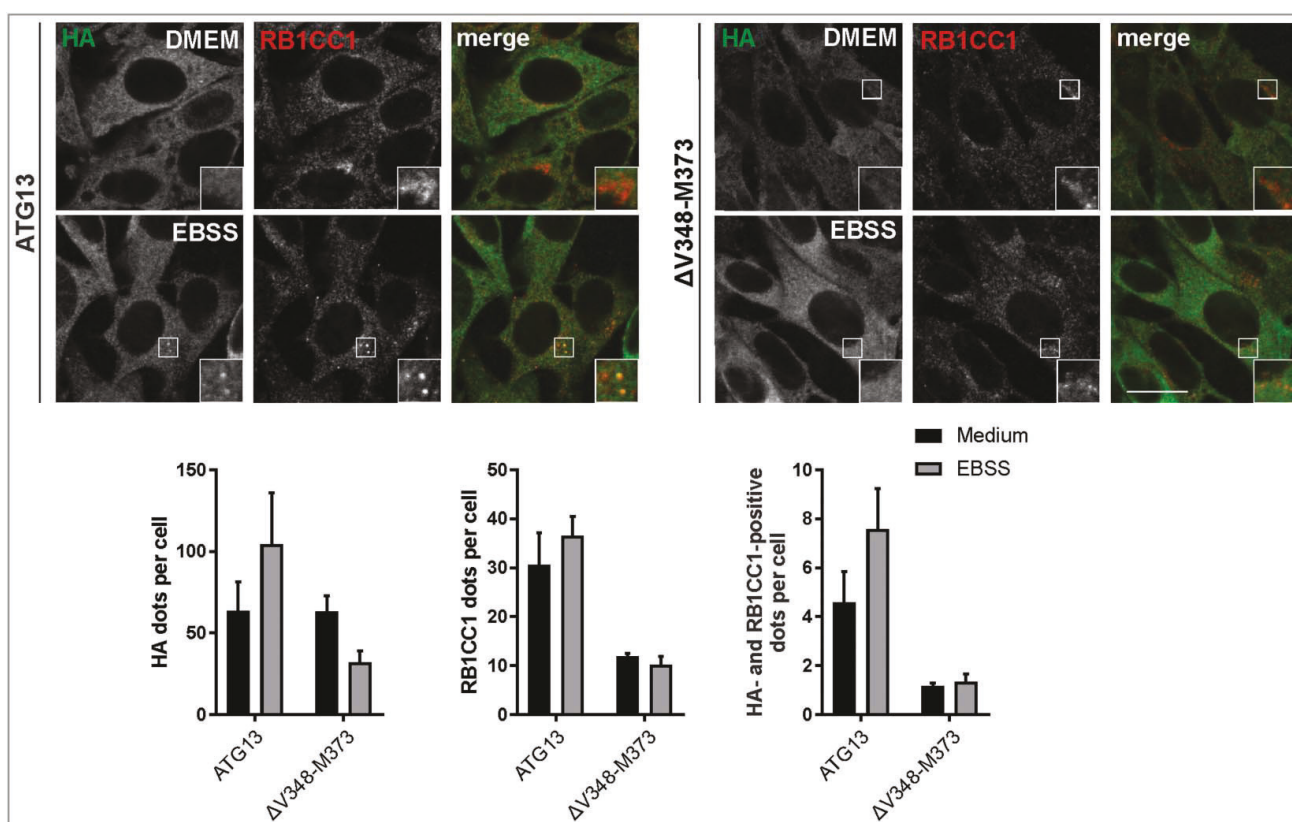


Figure 3. Disruption of the RB1CC1-binding region in ATG13 inhibits mutual recruitment to the phagophore. *atg13* KO MEFs retrovirally transfected with cDNA encoding either HA-ATG13 or HA-ATG13(ΔV348-M373) were seeded onto glass cover slips one day prior to stimulation with full medium (DMEM) or starvation medium (EBSS) for 1 h. Cells were fixed, permeabilized and stained for HA (covance MMS-101P) and RB1CC1. An inverse confocal laser scanning microscope was used for imaging. Puncta and colocalization per cell quantification was done using fiji software. Data represent mean + SEM. A minimum of 168 cells per stimulation was analyzed. Statistical analysis using the Student *t* test, 2-sample assuming unequal variances was performed comparing EBSS to DMEM for each individual cell line. No statistical significance with $P < 0.05$ was obtained. Columns for control (ATG13) are reused in figures 4, 6, and supplementary figure S9. Scale bar: 20 μ m.

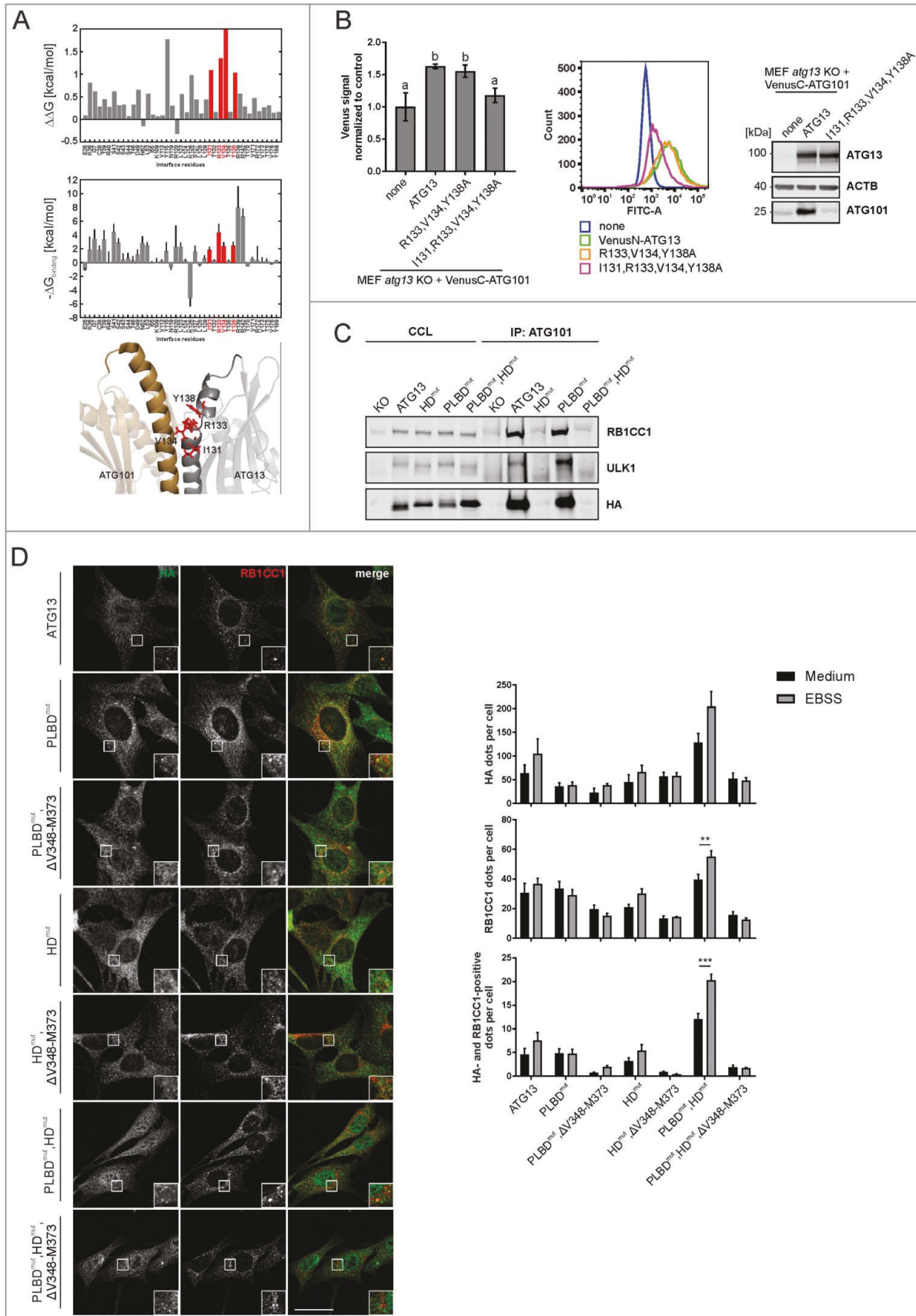


Figure 4. Mutation of residues I131, R133, V134 and Y138 in ATG13 is sufficient to inhibit its interaction with ATG101. (A) Computational alanine scanning of the ATG13-ATG101 interface was performed using the structure of the human ATG13-ATG101 HORMA heterodimer (PDB ID: 5C50, ref. 24) and the DrugScore^{PPI} webserver (ref. 37) (upper panel). $\Delta\Delta G$ denotes binding free energy differences for wild-type residue-to-Ala mutations; residues yielding $\Delta\Delta G > 1$ kcal mol⁻¹ are considered binding hot spots. In the middle panel, per-residue effective binding energies ($\Delta G_{\text{binding}}$) computed by the MM-GB/SA approach (ref. 39, 40) are shown. Residues considered hot spots according to both methods are colored in red. In the lower panel, the localization of these residues in the ATG13 interface is shown. (B) *atg13* KO MEFs stably expressing

domain mutant, HD^{mut}) was not capable of interacting with ATG101 (Fig. 4C). Furthermore, due to the missing ATG13 interaction, copurification of the other ULK1 complex members ULK1 and RB1CC1 was not possible. We also analyzed ATG13 harboring a mutated phospholipid-binding domain (PLBD^{mut}). This motif is very proximal to the HORMA domain, and mutation might unintentionally affect the HORMA domain function. In our purification experiments, the ATG13(PLBD^{mut}) variant was copurified with ATG101 indicating an intact HORMA domain (Fig. 4C, PLBD^{mut}). By combining the HD mutation with the PLBD variant (Fig. 4C, PLBD^{mut},HD^{mut}) the interaction with ATG101 was again inhibited. Importantly, the interaction with ATG14, which has recently been reported to bind to the HORMA domain of ATG13,⁴¹ was neither affected by the HD nor the PLBD mutation (Fig. S2). The interaction of ATG13 with ULK1 or RB1CC1, respectively, was not affected either (Fig. S2).

As described above for the RB1CC1-binding interface, we next investigated the ULK1 complex assembly by size-exclusion chromatography and recruitment to the phagophore by immunofluorescence. Mutation of the phospholipid-binding site did not affect the ULK1 complex assembly (Fig. 5A, PLBD^{mut}; red curve in diagrams). In contrast, mutation of the ATG101 interaction site severely altered complex assembly (Fig. 5B, HD^{mut}; red curve in diagrams). Distribution of ATG101 resembles the *atg13* KO phenotype as it is only present as a monomer in the low-molecular mass fractions, while it is completely absent from both the 3 MDa and 400 to 200 kDa protein complexes. ATG13 was present in low amounts in the early molecular mass fractions and concentrated in later fractions. Additional mutation of the phospholipid-binding domain did not exhibit an additive effect on the distribution of the ULK1 components (Fig. 5C, PLBD^{mut},HD^{mut}; red curve in diagrams). The described ATG13 variants were further analyzed in combination with a disrupted RB1CC1 interaction. Double mutation of the phospholipid- and RB1CC1-binding site (Fig. 5A, PLBD^{mut},ΔV348-M373; green curve in diagrams) induced a redistribution of ATG13, ATG101 and ULK1 into later fractions as was detected for the single ΔV348-M373 variant (see Fig. 2D). Combination of the RB1CC1 binding-deficient with the ATG101 binding-deficient mutant did not further impact ATG101 but promoted an additional reduction of ULK1 and ATG13 protein levels in early molecular mass fractions (Fig. 5B, HD^{mut},ΔV348-M373; green curve in diagrams). Finally, complex formation did not change in the triple mutant compared to the double mutant PLBD^{mut}, HD^{mut} (Fig. 5C, PLBD^{mut},HD^{mut},ΔV348-M373; compare red and green curves in diagrams).

The immunofluorescence experiments revealed that most ATG13 variants that are not capable of a proper ULK1 complex formation do not support ATG13 and RB1CC1 colocalization upon autophagy induction either (Fig. 4D, PLBD^{mut},ΔV348-M373; HD^{mut},ΔV348-M373; PLBD^{mut},HD^{mut},ΔV348-M373). The corresponding single mutations lacking either intact ATG101- or phospholipid-binding properties supported formation of ATG13- and RB1CC1-positive puncta, though their number appeared to be independent of autophagy induction by starvation (Fig. 4D, PLBD^{mut}; HD^{mut}). However, in cells expressing the ATG13 variant lacking both the ATG101 and phospholipid interaction site, a permanent accumulation of ATG13 and RB1CC1 was detected, which was even increased upon autophagy induction (Fig. 4D and S3, PLBD^{mut},HD^{mut}). This notable phenotype was reversed by additionally mutating the RB1CC1 interaction site (Fig. 4D, PLBD^{mut},HD^{mut},ΔV348-M373). Based on this observation, we hypothesize that the accumulation of ATG13 and RB1CC1 is potentially caused by inhibited signaling progression downstream of the recruitment of these proteins to the phagophore or a very early formation site. Since deletion of the RB1CC1 binding site abolished this accumulation, we suspect that the recruitment of ATG13 and RB1CC1 is dependent on their interaction and might occur earlier within the temporal hierarchy. In turn, ATG13-dependent binding to ATG101 and phospholipids are both important for the release of ATG13 and RB1CC1 from the phagophore. It is noteworthy that the disruption of one of the 2 interaction interfaces (PLBD^{mut} or HD^{mut}) does not affect signaling progression, indicating that interactions mediated by these interfaces might somehow compensate each other.

The ATG13-ULK1 interaction is required for ULK1 complex formation and recruitment to the autophagosome formation site while the LIR motif is dispensable

Two additional interaction interfaces have been reported for ATG13 proteins. The LC3-interacting region (LIR) domain mediates direct interaction of ATG13 with members of the Atg8 family. In agreement with the report on the LIR motif in ATG13 by Alemu et al.,³² we exchanged F407 and I410 to alanine (Fig. 1B) to effectively inhibit interaction with LC3s and GABARAPs. These mutations did not have an effect on ULK1 complex formation as shown by size-exclusion chromatography (Fig. 6A, LIR^{mut}; upper panels and red curve in diagrams), whereas a double mutant lacking both the LIR and the RB1CC1 interaction site showed disruption of the complex (Fig. 6A, LIR^{mut},ΔV348-M373; green curve in diagrams). Furthermore, we observed proper recruitment of ATG13 and

VenusC-ATG101 and VenusN-ATG13 (wild-type or the indicated mutants) were trypsinized and analyzed for Venus fluorescence using a flow cytometer. The median of fluorescence intensity for each sample was normalized to control cells lacking VenusN-ATG13 expression ("none") and was plotted in a bar diagram representing mean ± SEM. Samples without significant difference display identical letters (Student *t* test, 2-sample assuming unequal variances). Representative data are plotted in a histogram. Cell lysates were examined for expression of the indicated proteins by immunoblotting. (C) *atg13* KO MEFs retrovirally transfected with empty vector or cDNA encoding either HA-ATG13 or the indicated variants were lysed and cleared cellular lysates were subjected to immunoprecipitation with anti-ATG101 antibodies and a protein A/G-Sepharose mix. Purified proteins were subjected to SDS-PAGE and analyzed by immunoblotting for RB1CC1, ULK1, or HA. (D) *atg13* KO MEFs stably expressing the indicated HA-tagged ATG13 variants were grown on glass cover slips one day prior to incubation with starvation medium (EBSS) for 2 h, fixation and permeabilization. Immunofluorescence for HA (covance MMS-101P) and RB1CC1 was performed. An inverse confocal laser scanning microscope was used for imaging. Please note that we detected a high number of HA-positive puncta varying in size and intensity, of which only a minor portion colocalized with RB1CC1 puncta. This might be due to the exogenous expression of HA-ATG13 variants. Puncta and colocalization per cell quantification was done using Fiji software. A minimum of 89 cells per stimulation was analyzed. Data represent mean ± SEM. Statistical analysis using the Student *t* test, 2-sample assuming unequal variances was performed comparing EBSS to DMEM for each individual cell line. ***P* < 0.01, ****P* < 0.001. Scale bar: 20 μm.

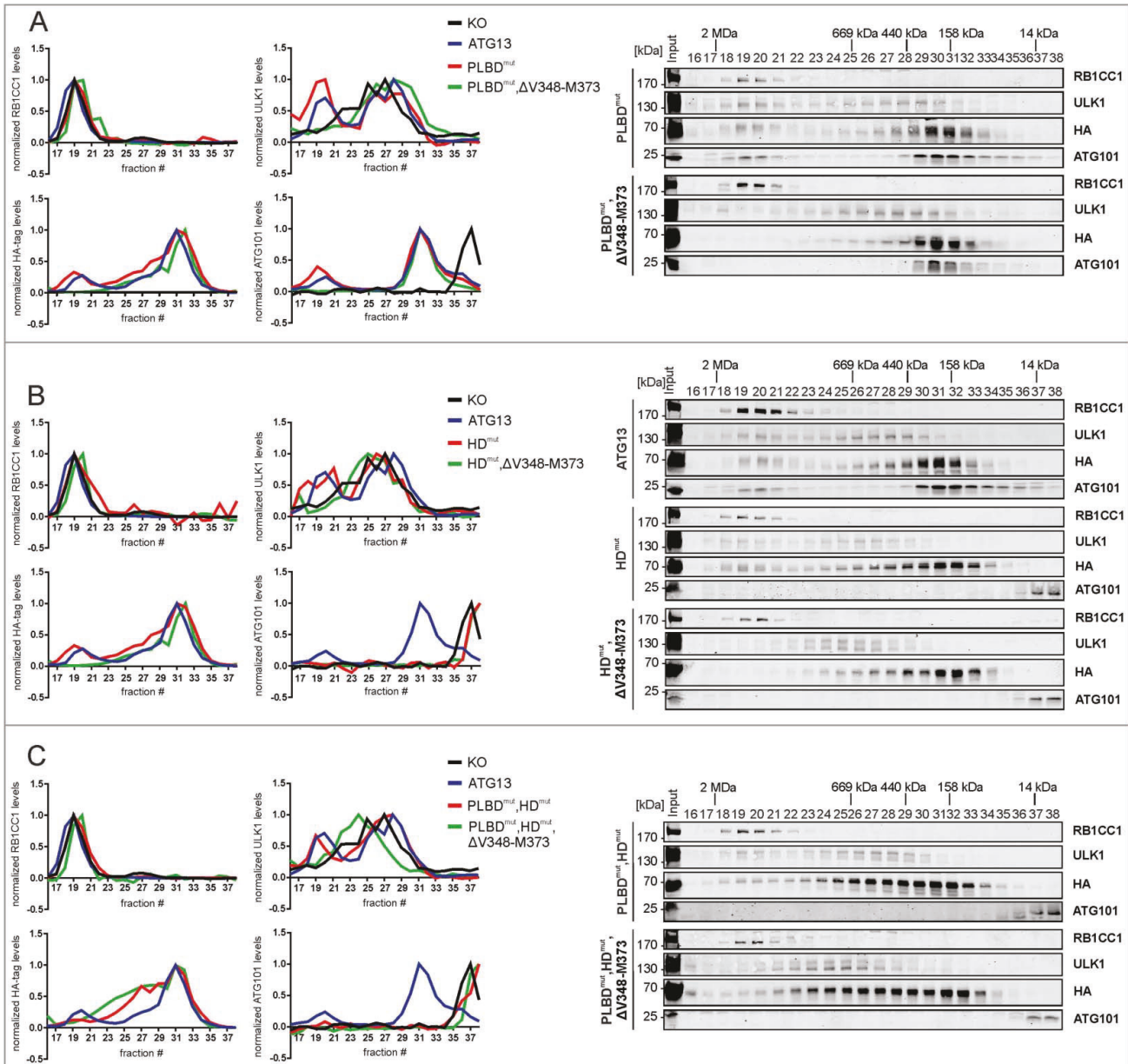


Figure 5. Mutation of the HORMA domain, but not of the phospholipid-binding domain leads to disintegration of the ULK1 complex. (A to C) S100 extracts of *atg13* KO MEFs stably expressing HA-ATG13 or the indicated mutants were separated by size-exclusion chromatography on a Superose 6 increase column. Fractions were analyzed by immunoblotting for the indicated proteins. Diagrams show protein levels for each fraction at a ratio of the input and normalized to the fraction containing the highest concentration of the analyzed protein. Curves for controls (KO and ATG13) are reused in figures 2 and 6.

RB1CC1 to the PAS after autophagy induction (Fig. 6B, LIR^{mut}), which again was abolished by additional deletion of the RB1CC1 binding site (Fig. 6B, LIR^{mut} Δ V348-M373). Interestingly, mutation of the LIR motif did not affect the colocalization of ATG13 with LC3 after autophagy induction by EBSS treatment (Fig. 6C, LIR^{mut}), which was also inhibited by deletion of the RB1CC1 interaction (Fig. 6C, LIR^{mut} Δ V348-M373). Of note, expression of this ATG13 double mutant led to increased localization of ATG13 to the nucleus despite autophagy induction.

Finally, we applied the Δ TLQ mutation, which has previously been validated for the inhibition of the ULK1-ATG13 interaction (Fig. 1B).¹⁸ Deletion of the minimal ULK1 interaction site in ATG13 resulted in a shift of ULK1 to later fractions in size-exclusion chromatography, while both ATG101 and

ATG13 were still present in high-molecular mass fractions (ref. 18 and Fig. 6A, Δ TLQ; lower panels and red curve in diagrams). Deletion of both the ULK1 and RB1CC1 interaction sites in ATG13 resulted in the depletion of ATG101 from early fractions (Fig. 6A, Δ V348-M373, Δ TLQ; green curve in diagrams). Despite the fact that the ATG13(Δ TLQ) variant still interacts with RB1CC1, recruitment of both proteins to the autophagosome formation site was inhibited (Fig. 6B, Δ TLQ).

Mutations of interaction sites in ATG13 partly affect amino acid starvation-induced autophagy

After mapping the interaction sites between ATG13 and its binding partners, we were next interested in their relevance

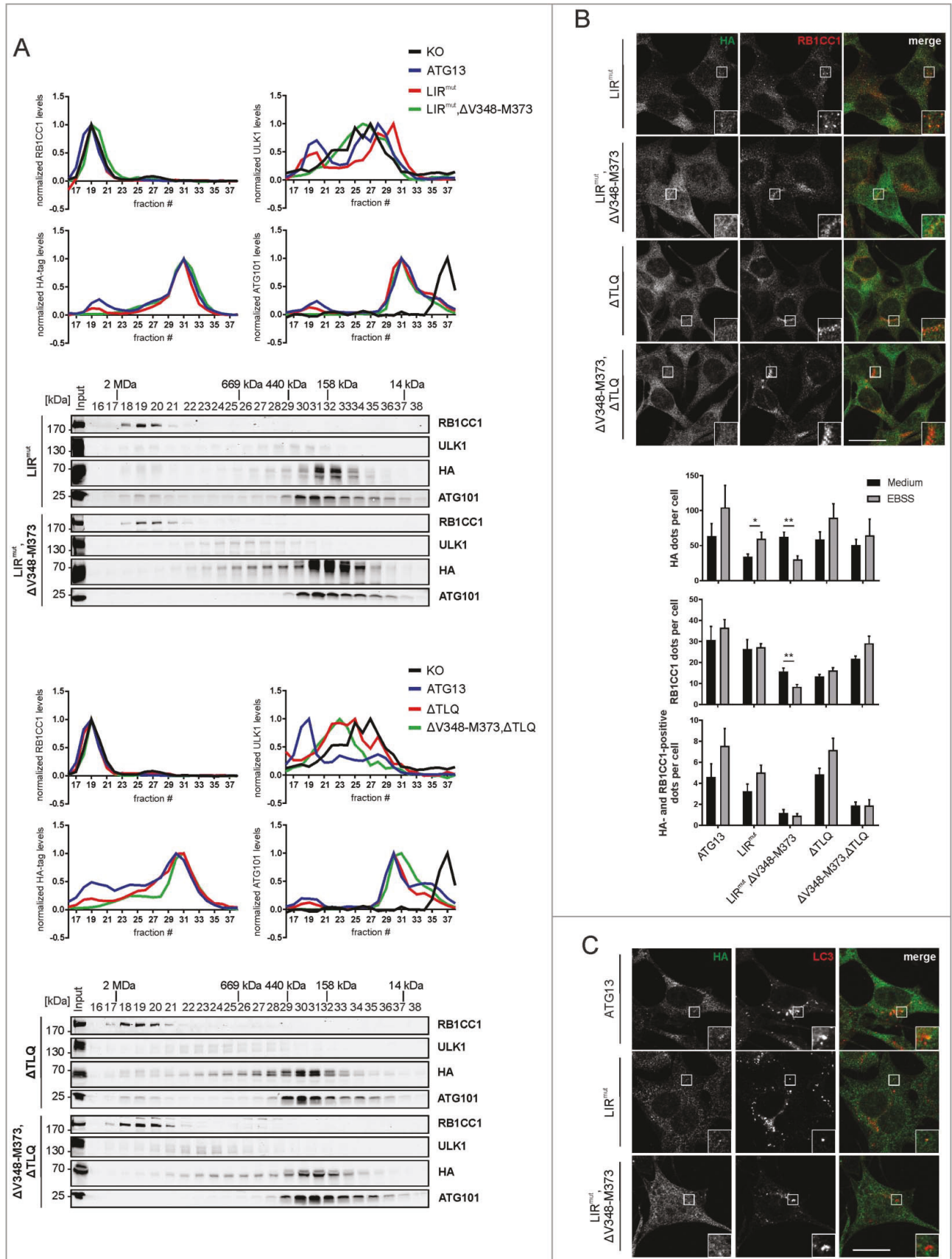


Figure 6. Composition of the ULK1 complex is influenced by the ATG13-ULK1 interaction but not by the LIR motif of ATG13. (A) S100 extracts of *atg13* KO MEFs stably expressing the indicated HA-ATG13 variants were separated by size-exclusion chromatography on a Superose 6 increase column. Fractions were analyzed by immunoblotting for the indicated proteins. Diagrams show protein levels for each fraction at a ratio of the input and normalized to the fraction containing the highest concentration of the analyzed protein. Curves for controls (KO and ATG13) are reused in figures 2 and 5. (B) Cells described in (A) were seeded onto glass cover slips one day prior to stimulation with full medium (DMEM) or starvation medium (EBSS) for 1 h. Cells were fixed, permeabilized and stained for HA (covance MMS-101P) and RB1CC1. An

for autophagy regulation. First, we investigated the requirement of the ATG13-RB1CC1 interaction, since this interaction is apparently essential for the formation of the 3 MDA ULK1 complex. In a first approach, we analyzed amino acid starvation-induced mCitricine-LC3B degradation by flow cytometry. Cells with an intact autophagy signaling machinery display low fluorescence after autophagy induction, and this effect can be reversed by adding bafilomycin A₁, as can be seen in *Atg13* WT MEFs as well as in *atg13* KO MEFs reconstituted with full-length ATG13 (Fig. 7A). Unexpectedly, expression of the ATG13 mutant Δ V348-M373 did not influence autophagy activity, since LC3B degradation as detected by a reduced fluorescence intensity was observed after treatment with EBSS (Fig. 7A). To further confirm this result, we performed immunofluorescence of endogenous LC3. This assay supported our previous observation, since the number of LC3-positive puncta increased in cells expressing either wild-type or ATG13(Δ V348-M373) upon bafilomycin A₁ treatment, and this effect was enhanced by inducing autophagy with EBSS (Fig. 7B). Finally, we performed an LC3 turnover assay by immunoblotting. Again *Atg13* WT MEFs and *atg13* KO MEFs reconstituted with either full-length ATG13 or the Δ V348-M373 variant displayed similar LC3-II levels in cells treated with bafilomycin A₁ alone (basal autophagy) or in combination with EBSS (induced autophagy) (Fig. 7C). Similar to the *atg13* KO MEFs, an ATG13 version lacking the entire C terminus (Δ C) did not reveal any detectable autophagic flux (Fig. 7C). Since the autophagy readouts employed so far rely on LC3 lipidation and/or degradation, we decided to check another autophagic marker. We chose the early autophagy protein WIPI2, which is recruited to the phagophore shortly after ULK1 complex activation. Immunofluorescence of WIPI2 in *atg13* KO MEFs expressing full-length ATG13 or the Δ V348-M373 mutant showed diffuse distribution in the cytoplasm under growing conditions, while WIPI2 puncta formation was induced by autophagy induction (Fig. 8, ATG13; and Δ V348-M373). Collectively, these data suggest that the interaction between ATG13 with RB1CC1 is not mandatory for autophagy induction.

As these findings were rather surprising, we further analyzed the other interaction motifs of ATG13. Mutation of the phospholipid-binding domain did not influence autophagy induction by amino acid starvation with EBSS either. LC3-II protein levels were similar in cells reconstituted with wild-type ATG13 or the PLBD mutant (Fig. 7D, PLBD^{mut}). Likewise, mutation of both the phospholipid- and the RB1CC1-binding site did not significantly affect autophagic activity (Fig. 7D, PLBD^{mut}, Δ V348-M373). In contrast, mutation of the ATG101 interaction site resulted in significantly reduced autophagic flux (Fig. 7D, HD^{mut}). Concomitant deletion of the RB1CC1 interaction site did not have an additional effect (Fig. 7D, HD^{mut},

Δ V348-M373). However, interference with both the phospholipid binding as well as the ATG101 interaction could further reduce the autophagic activity (Fig. 7D, PLBD^{mut},HD^{mut}). This was also evident from the analysis of SQSTM1/p62 levels, which are highly accumulated in *atg13* KO MEFs and in cells expressing the double mutant PLBD^{mut},HD^{mut} (Fig. 7E). These results were further supported by WIPI2 immunofluorescence. While we detected WIPI2 puncta formation upon autophagy induction in cells expressing the ATG13 variants PLBD^{mut}; and PLBD^{mut}, Δ V348-M373 (Fig. 8, PLBD^{mut}; and PLBD^{mut}, Δ V348-M373), inhibition of ATG101 binding to ATG13 severely inhibited WIPI2 puncta formation after autophagy induction (Fig. 8, HD^{mut}; HD^{mut}, Δ V348-M373; PLBD^{mut}, HD^{mut}; and PLBD^{mut},HD^{mut}, Δ V348-M373). Notably, these cells displayed very small WIPI2-positive structures, which were not regulated by autophagy induction.

As in our MEF cell lines the signal for LC3-II appeared to be very similar between full medium and EBSS in the presence of bafilomycin A₁, we hypothesized that the induction of autophagy is masked by high levels of basal autophagy. We therefore repeated the starvation experiments for cell lines displaying reduced autophagic activity (HD^{mut}; HD^{mut}, Δ V348-M373; PLBD^{mut},HD^{mut}; and PLBD^{mut},HD^{mut}, Δ V348-M373) with a shortened incubation time of 1 h (Fig S4). In this setup, differences in autophagic flux caused by ATG13 mutations were even more obvious and further confirmed our result that inhibition of the ATG13-ATG101 interaction has a tremendous impact on autophagy induction.

Next, mutation of the LIR motif was analyzed. Interestingly, we detected a slight increase of LC3-II levels in samples treated with starvation medium and bafilomycin A₁ compared to cells expressing wild-type ATG13 (Fig. 7F, LIR^{mut} and ATG13; Fig. S5). This effect was reversed when both the interaction with LC3s or GABARAPs, and RB1CC1 were inhibited, since cells expressing this ATG13 double mutant displayed autophagic activity similar to wild-type ATG13 expressing cells (Fig. 7F, LIR^{mut}, Δ V348-M373). WIPI2 staining also showed puncta formation upon autophagy induction (Fig. 8). However, with this readout, we did not observe significant differences between wild-type and LIR^{mut}- and/or LIR^{mut}, Δ V348-M373-expressing cells.

Finally, we investigated the mutation of both the ULK1 and the RB1CC1 interaction site. Our group has previously reported that inhibition of ATG13-ULK1 binding resulted in slightly but not significantly decreased autophagic activity.¹⁸ This reduced autophagic activity was further decreased by additional mutation of the RB1CC1 interaction site (Fig. 7F, Δ V348-M373, Δ TLQ). Consistently, WIPI2 puncta formation upon autophagy induction is present in cells expressing the ATG13(Δ TLQ) mutant; however, it appears severely decreased by further mutation of the RB1CC1 interaction site (Fig. 8, Δ TLQ; and Δ V348-M373, Δ TLQ).

inverse confocal laser scanning microscope was used for imaging. Puncta and colocalization per cell quantification was done using Fiji software. A minimum of 127 cells per stimulation was analyzed. Data represent mean \pm SEM. Statistical analysis using the Student *t* test, 2-sample assuming unequal variances was performed comparing EBSS to DMEM for each individual cell line. **P* < 0.05, ***P* < 0.01, ****P* < 0.001. Scale bar: 20 μ m. (C) *atg13* KO MEFs stably expressing HA-ATG13 or the indicated mutants were seeded onto glass cover slips one day prior to stimulation with starvation medium (EBSS) for 2 h. Cells were fixed, permeabilized and stained for HA (covance MMS-101P) and LC3. An inverse confocal laser scanning microscope was used for imaging. Scale bar: 20 μ m.

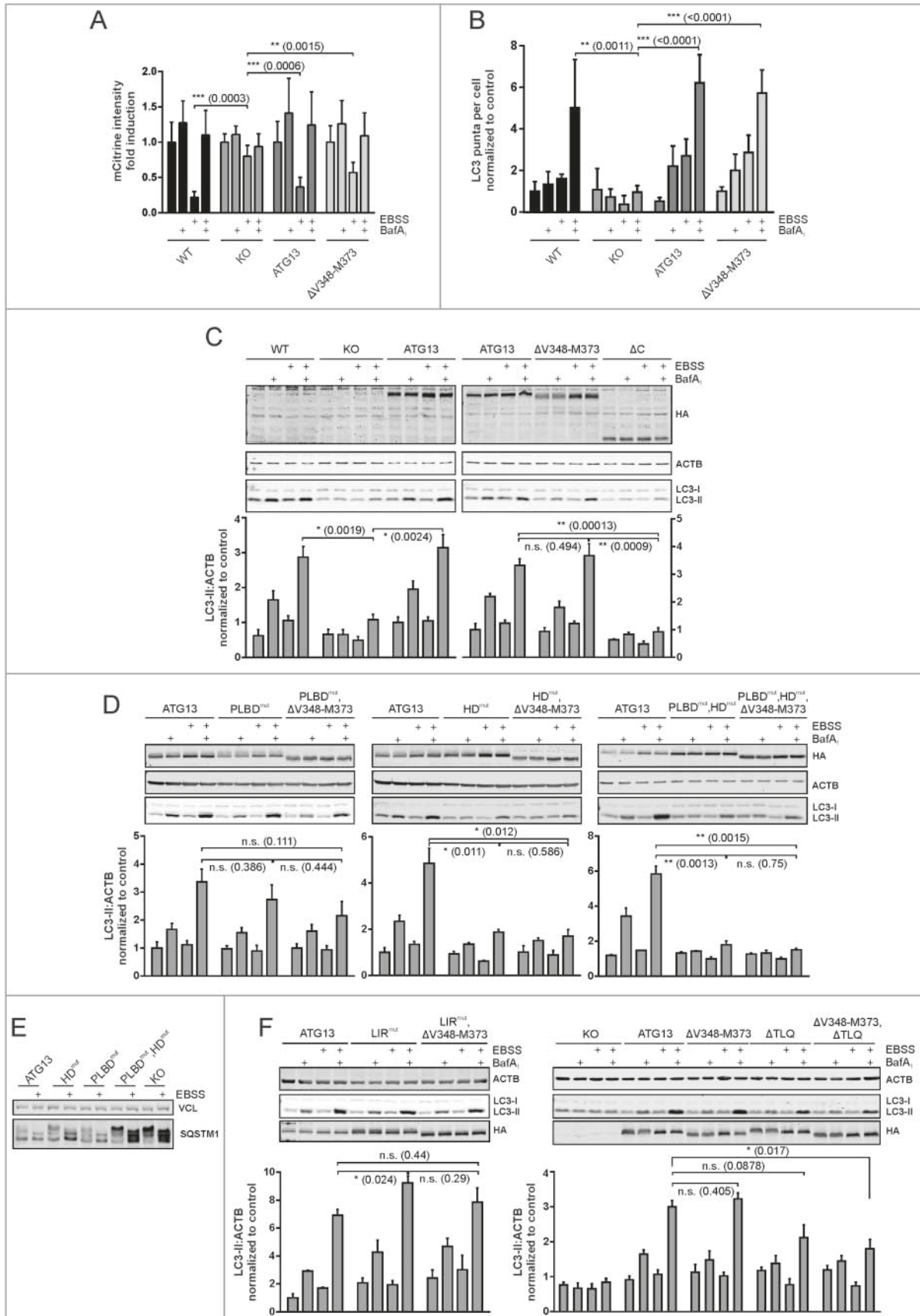


Figure 7. Differential requirement of ATG13 interaction interfaces for amino acid starvation-induced LC3 turnover. (A) *Atg13* wild-type MEFs (WT) or *atg13* KO MEFs stably expressing mCitrine-LC3B and the indicated ATG13 variants were cultured in growth medium or starvation medium (EBSS) with or without 40 nM bafilomycin A₁ (BafA₁) for 8 h. Total cellular mCitrine-LC3B signals were analyzed by flow cytometry. The median of fluorescence intensity for each sample was normalized to wild-type cells incubated in growth medium. Data represent mean + SEM. ***P* < 0.01, ****P* < 0.001 (Student *t* test, 2-sample assuming unequal variances). (B) Untransfected *Atg13* wild-type (WT) MEFs or *atg13* KO MEFs retrovirally transfected with empty vector (KO) or cDNA encoding the indicated ATG13 variants were grown on glass cover slips overnight

Mutations of interaction sites in ATG13 have severe effects on autophagy induction by MTORC1/2 inhibition

Because amino acid starvation by EBSS incubation is a rather crude treatment and ULK1/2-independent autophagy pathways have been described by several groups,^{11,31,42–44} we next wanted to selectively target ULK1 signaling by the modulation of MTOR activity. To do so, we used torin2, a member of the Tor kinase domain inhibitor family (TORKInibs), which inhibits both MTOR complex 1 and 2 (MTORC1/2). Furthermore, rapamycin was used, which interacts with FKBP1A and thereby inhibits interaction of MTOR with RPTOR and MTORC1 formation.

First, we analyzed the ability of the inhibitors to induce the autophagy signaling pathway via MTOR inhibition. We found that torin2, similar to EBSS treatment, inhibits ULK1 phosphorylation at T758 as well as RPS6KB1 phosphorylation at T389, both of which are well known MTOR phosphorylation sites (Fig. S6A to C). Rapamycin-induced effects on RPS6KB1 phosphorylation at T389 were similar, but the inhibition of ULK1 T758 phosphorylation appeared much weaker (Fig. S6B and S6C). Nevertheless, this site was not absolutely “rapamycin-resistant”.⁴⁵ Consistently, ULK1 kinase activity as monitored by immunoblotting for phospho-S318 in ATG13 was more prominently induced by torin2 than by rapamycin (Fig. S6B and S6C). Furthermore, torin2 induced the recruitment of the ULK1 complex to the phagophore similarly as starvation with EBSS (Fig. S7).

In *atg13* KO MEFs reconstituted with full-length ATG13 autophagy was induced following treatment with these inhibitors (Fig. 9A, ATG13). Interference with the RB1CC1-ATG13 interaction had only minor effects on autophagic activity (Fig. 9A, Δ V348-M373) as we have already detected for EBSS treatment.

Mutation of either the phospholipid-binding domain or the ATG101-interacting HORMA domain inhibited autophagy induction by torin2 and rapamycin (Fig. 9B, HD^{mut}; and PLBD^{mut}). Although this has been observed for the HD^{mut} variant upon EBSS treatment, the effect for the PLBD^{mut} is much more obvious for torin2 and rapamycin. It appears that cells expressing these ATG13 variants retain some autophagic activity, since we detected a slight increase of LC3-II levels in samples treated with bafilomycin A₁. This was totally erased by mutating both the phospholipid- and the ATG101-binding domain (Fig. 9C, PLBD^{mut}, HD^{mut}). In these cells, the addition of bafilomycin A₁ did not stimulate an accumulation of LC3-II compared to control cells. The subsequent deletion of the RB1CC1-binding domain did not have an additional effect (Fig. 9C, PLBD^{mut}, HD^{mut}, Δ V348-M373).

Next, the mutated LIR motif was investigated. In contrast to EBSS treatment, autophagy induction with torin2 or rapamycin neither increased nor inhibited autophagic activity in cells expressing the ATG13 variant (Fig. 9D, LIR^{mut}). We detected an additive effect for the ATG13 double mutant additionally lacking the RB1CC1 interaction site (Fig. 9D, LIR^{mut}, Δ V348-M373). In these cells, autophagic activity was significantly decreased when treated with torin2. These cells show increased levels when treated with bafilomycin A₁ but this effect was not further increased by torin2. These results indicate that basal autophagy is still active but autophagy induction by torin2 is not possible. This was not the case for rapamycin stimulation, since we detected only minor effects on autophagy induction.

At last, we studied the ATG13(Δ TLQ) mutant lacking ULK1 interaction. Similar to the LIR mutant, autophagy was not induced by torin2 treatment although basal activity was still detectable (Fig. 9E, Δ TLQ). Additional mutation of the RB1CC1 interaction site did not have any further effect (Fig. 9E, Δ V348-M373, Δ TLQ). Rapamycin induced autophagy in cells expressing the ATG13(Δ TLQ) variant (Fig. 9E, Δ TLQ) although this was significantly reduced compared to control cells. Again autophagy was not induced in cells expressing the double mutant Δ V348-M373, Δ TLQ (Fig. 9E, Δ V348-M373, Δ TLQ).

As has been done for EBSS experiments, we verified our results obtained for torin2-induced autophagy by immunofluorescence. Because we could not detect significant WIPI2 puncta formation upon torin2 treatment (Fig. S8), we monitored ATG16L1 puncta formation, another well-characterized marker for autophagosomes (Fig. S9). We observed a significant increase in puncta formation upon both EBSS and torin2 treatment for cells expressing wild-type ATG13 as well as ATG13 with a mutated LIR domain (Fig. S9, ATG13; LIR^{mut}). Cells expressing ATG13 with disrupted RB1CC1- or ULK1-binding sites depicted inducible ATG16L1 puncta formation as well (Fig. S9, Δ V348-M373; Δ TLQ). For all other cell lines, ATG16L1 puncta were not detectable. Taking all our observations together, it appears that targeting the interaction between ATG101 and ATG13 has the most severe effects on autophagy induction with regard to all applied stimuli and readouts (Fig. 10, HD^{mut}). LC3-II accumulation was blocked at least to ~50%, while WIPI2 dot formation was reduced to less than 20% and ATG16L1 to ~30%. These effects were even more pronounced when binding to both ATG101 and phospholipids was blocked (Fig. 10, PLBD^{mut}, HD^{mut}). In contrast, single interference with the binding to the other 2 ULK1 complex components, ULK1 and RB1CC1, respectively, did not or only weakly affect autophagy induction. However, the combination

and incubated for 2 h in growth medium or starvation medium (EBSS) in the presence or absence of 40 nM bafilomycin A₁ (BafA₁). Cells were fixed, permeabilized and stained for LC3. Imaging was performed using an inverse confocal laser scanning microscope and puncta per cell quantification was done using Fiji software. Data represent mean + SEM. Statistical analysis using the Student *t* test, 2-sample assuming unequal variances was performed comparing LC3 puncta accumulation during EBSS + BafA₁ treatment for depicted cell lines. ***P* < 0.01, ****P* < 0.001 (Student *t* test, 2-sample assuming unequal variances). (C, D, F) Untransfected *Atg13* wild-type MEFs (WT) or *atg13* KO MEFs retrovirally transfected with empty vector (KO) or cDNA encoding the indicated ATG13 variants were incubated as described in (B). Cleared cellular lysates were analyzed by immunoblotting for HA, LC3, ACTB, and VCL. Fold changes were calculated by dividing each normalized ratio (protein to loading control) by the average of the ratios of the control lane (ATG13 in medium). Results are mean + SEM **P* < 0.05, ***P* < 0.01, n.s., not significant (Student *t* test, 2-sample assuming unequal variances). (E) *atg13* KO MEFs retrovirally transfected with empty vector (KO) or cDNA encoding the indicated ATG13 variants were incubated in growth medium or starvation medium (EBSS) for 2 h. Cleared cellular lysates were analyzed by immunoblotting for SQSTM1 or VCL.

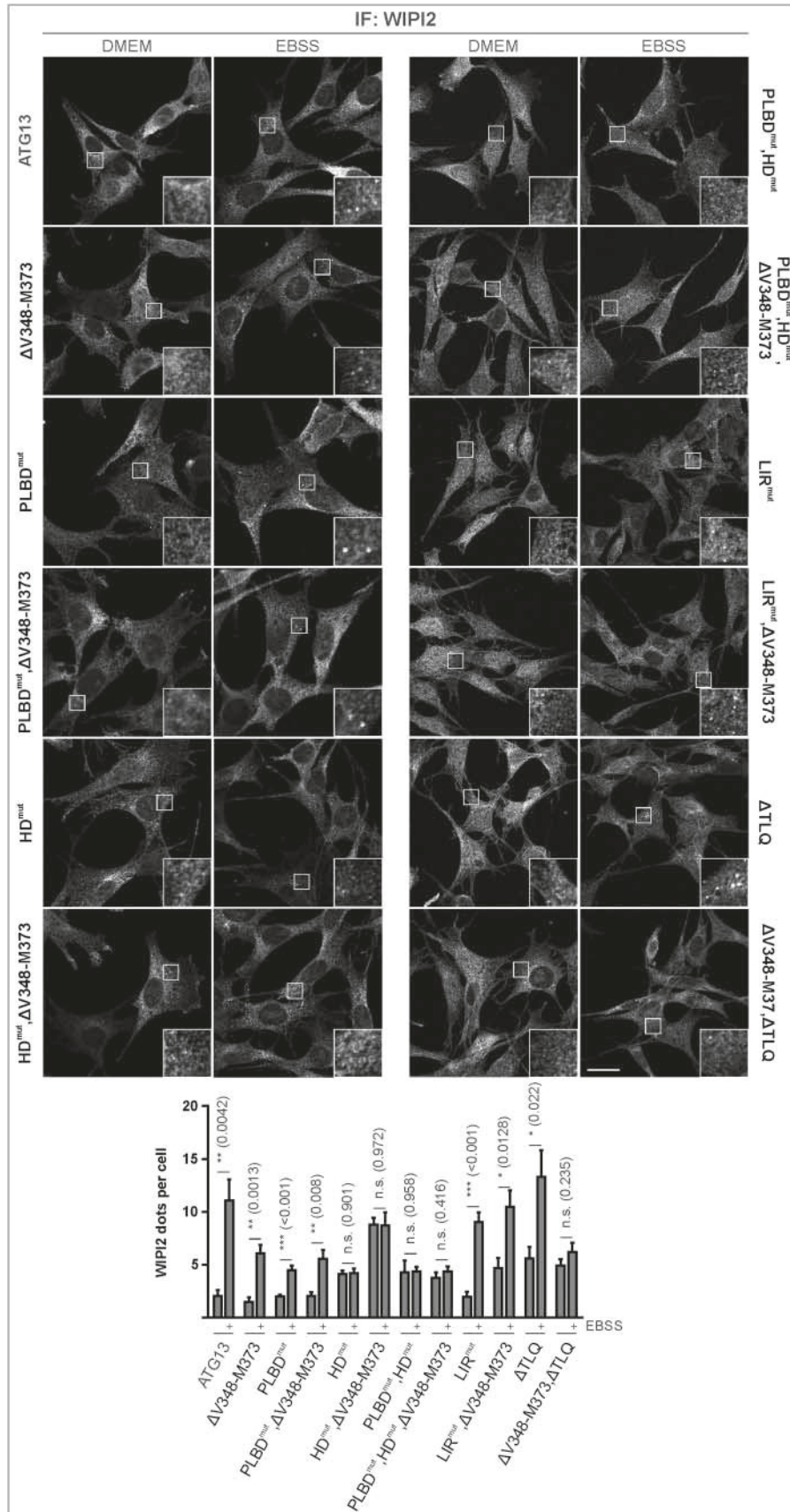


Figure 8. Differential requirement of ATG13 interaction interfaces for amino acid starvation-induced WIPI2 puncta formation. (A) *atg13* KO MEFs retrovirally transfected with cDNA encoding the indicated ATG13 variants were grown on glass cover slips overnight and incubated in growth medium (DMEM) or starvation medium (EBSS) for 2 h. Cells were fixed, permeabilized and stained for WIPI2. Imaging was performed using an inverse confocal laser scanning microscope. Puncta per cell quantification was done using Fiji software. Data represent mean + SEM. Statistical analysis using the Student *t* test, 2-sample assuming unequal variances was performed comparing EBSS to DMEM for each individual cell line. **P* < 0.05, ***P* < 0.01, ****P* < 0.001. Scale bar: 20 μm.

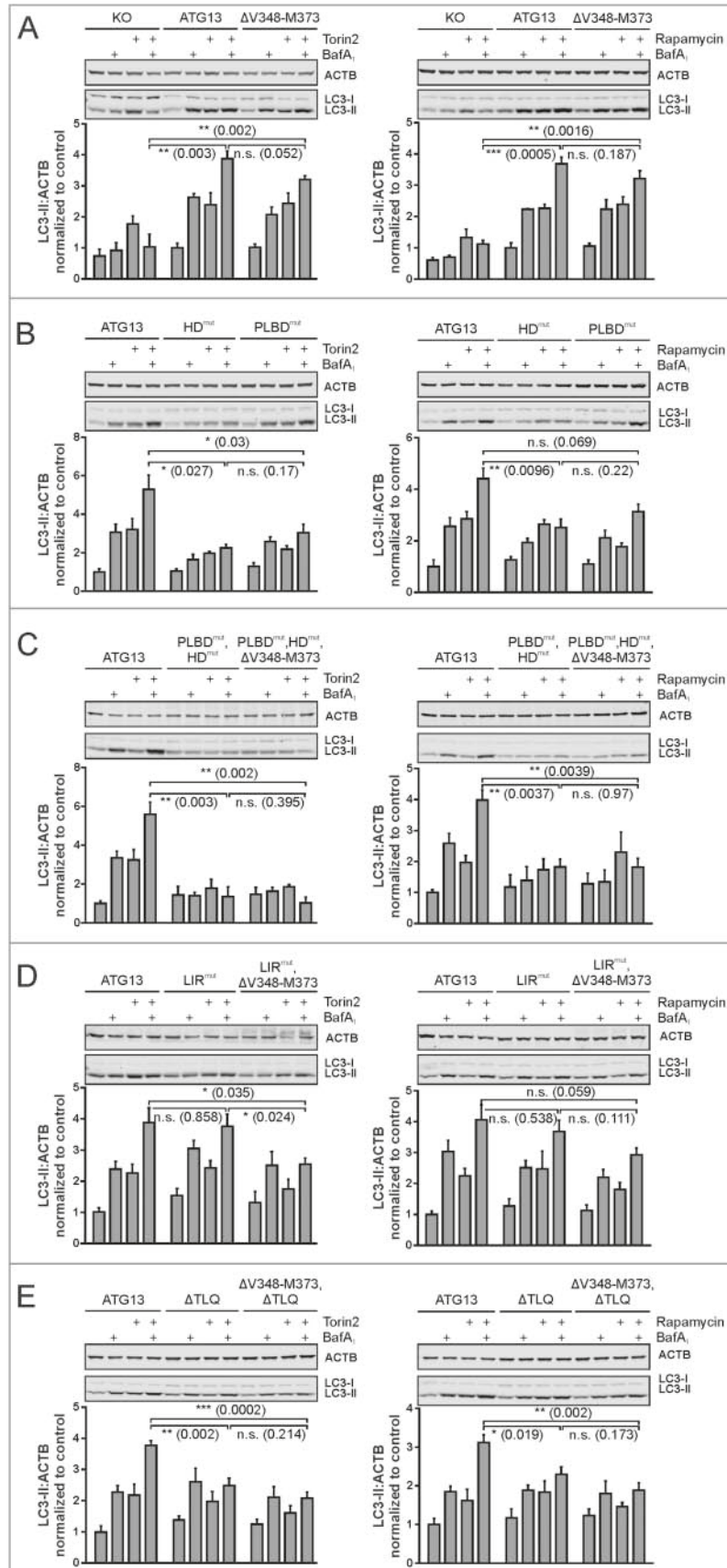


Figure 9. Differential requirement of ATG13 interaction interfaces for autophagy induced by MTOR inhibition. (**A to E**) *atg13* KO MEFs retrovirally transfected with empty vector (KO) or cDNA encoding the indicated ATG13 variants were incubated for 2 h in growth medium in the presence or absence of 250 nM torin2 (left panels) or 500 nM rapamycin (right panels) and 40 nM bafilomycin A₁ (BafA₁). Cleared cellular lysates were analyzed by immunoblotting for LC3 and ACTB. Fold changes were calculated by dividing each normalized ratio (protein to loading control) by the average of the ratios of the control lane (ATG13 in the medium). Results are mean + SEM **P* < 0.05, ***P* < 0.01, ****P* < 0.001 (Student *t* test, 2-sample assuming unequal variances).

of these 2 mutations clearly inhibited autophagy induction upon MTOR inhibition (Fig. 10, $\Delta V348$ -M373, Δ TLQ).

Discussion

In this study, we have systematically evaluated the relevance of the individual ATG13 interaction sites for the autophagic function of ATG13. In recent years, it became evident that the ULK1 protein kinase complex is an essential signaling node for the induction of autophagy. The core ULK1 complex consists of ULK1, ATG13, RB1CC1 and ATG101. Our analysis showed that targeting the ATG101-ATG13 protein interaction has the strongest effect on autophagy regulation. Though the remaining ATG13 interaction sites partially displayed functions during autophagy induction mediated by MTOR inhibition, mutations within the ATG13 HORMA domain clearly affected autophagy induced by amino acid starvation. In contrast, the interactions of ATG13 with ULK1 or RB1CC1 appeared to be rather dispensable for this type of autophagy induction.

The possibility to induce autophagy independently of ULK1/2 has been suggested by different groups. One might speculate that interference with the ATG13-ATG101 interaction targets both the ULK1 complex during canonical autophagy and potential ULK1-independent complexes that still rely on ATG13 and ATG101. These latter complexes might play a role in autophagy induction and/or during autophagy progression. Congruent to our observations, Suzuki et al. have reported that autophagy is defective in *atg101* KO MEFs expressing an ATG101 version that can no longer bind ATG13.²⁰ The authors have already suggested that ATG101 fulfills 2 proautophagic functions: i) the stabilization of ATG13 and ii) the recruitment of downstream factors via a

protruding loop termed WF finger.²⁰ Mutation of either the ATG13 interaction interface or the WF finger inhibited autophagy.²⁰ Future studies will have to reveal possible interacting molecules of the WF finger, and it remains to be shown that this motif is important for both ULK1-dependent and -independent processes.

Although the described observations suggest a central role for the ATG13-ATG101 interaction, we cannot entirely exclude that our ATG13 HORMA domain mutations simultaneously affect the binding to other reported interacting partners, i.e. ATG14 in higher eukaryotes and Atg9 in yeast.^{25,41} Recently, Park et al. reported that ATG14 is bound to a region between residues 1 to 198 in ATG13, which represents the HORMA domain.⁴¹ They show that this interaction enables ULK1-dependent phosphorylation of ATG14, which in turn stimulates the kinase activity of the class III phosphatidylinositol 3-kinase (PtdIns3K) complex.⁴¹ The observations by Park et al. are consistent with data obtained by Jao et al., who report that the HORMA domain of yeast Atg13 is important for the recruitment of the Atg14-containing class III PtdIns3K complex.²² However, at least our immunopurification experiments indicate that binding to ATG14 is not altered for our ATG13 HORMA domain variants. In *S. cerevisiae*, a second binding partner of the Atg13 HORMA domain has been identified: Suzuki et al. show that Atg9 vesicles are recruited to the PAS via the interaction with the Atg13 HORMA domain.²⁵ This model has been recently refined by Yamamoto et al. Apparently, Atg13 links Atg17-Atg29-Atg31 complexes with each other via 2 distinct regions, ultimately resulting in the self-assembly of the Atg1 complexes.³⁰ The supramolecular self-assembly of the Atg1 complexes then leads to the recruitment

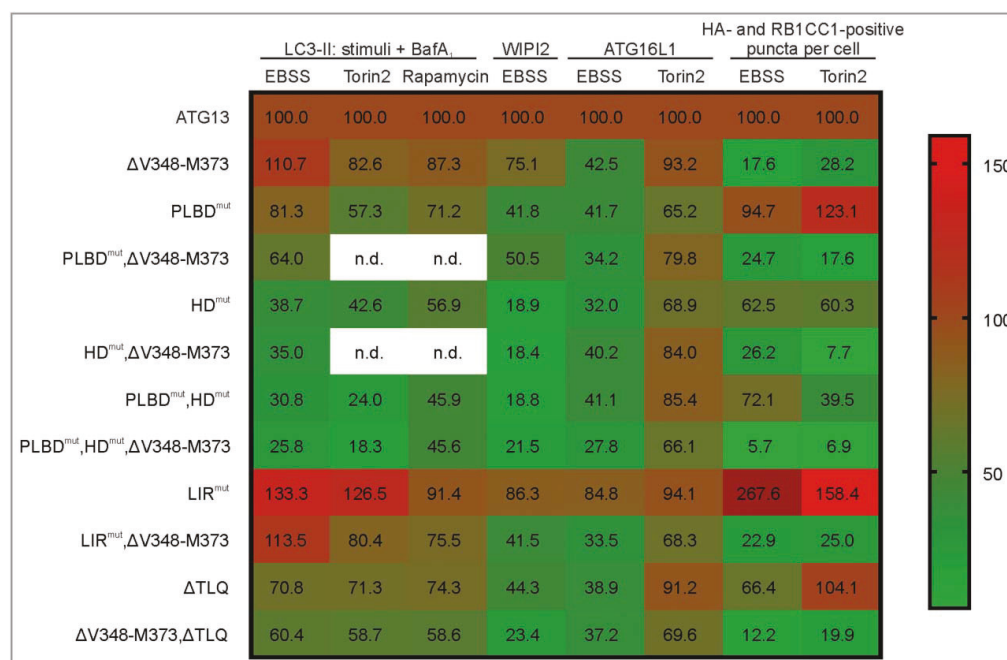


Figure 10. Summary of the effects of mutations in ATG13 interaction interfaces on autophagy induction by amino acid starvation or MTOR inhibition. The heat map shows i) the percentage of LC3-II signal detected by immunoblotting for the indicated stimuli in the presence of bafilomycin A₁ (columns 1 to 3), ii) the increase of WPI2 and ATG16L1 puncta formation after autophagy induction by the indicated stimuli (columns 4 to 6), or iii) the percentage of colocalization events of HA-ATG13 variants and RB1CC1 after treatment with the indicated stimuli (columns 7 and 8). All values were normalized to the control, which was set to 100% (ATG13, first row). The range for mapping was defined from 5.7 to 159. The value for LIR^{mut} under EBSS stimulation (267.6%) was set to out of range, and the color code dark red was manually assigned (n.d., not determined).

of Atg9 vesicles.³⁰ Ohsumi and colleagues have been able to generate an Atg9 binding-deficient Atg13 variant, and the residues of Atg13 mediating this interaction are located to β -strands 4 to 6 and the hinge loop.²⁵ In contrast, human ATG13 binds to human ATG101 via the α C and the α A- α B connector, including β 2'.²⁴ Furthermore, the interface between Atg101/ATG101 and Atg13/ATG13 is mostly conserved between fission yeast and human.^{20,24,46} In all, there are 2 aspects that arise from these observations. First, there is certainly crosstalk between the Atg1/ULK1 complex and Atg9/ATG9, both in yeast and mammalian model systems. In 2004, Reggiori et al. report that Atg9 cycles through the PAS in an Atg1-Atg13-dependent manner.⁴⁷ Sekito et al. have found that Atg9 interacts with Atg17 in *S. cerevisiae*.⁴⁸ This interaction appears to be essential for the recruitment of Atg9 to the PAS and requires Atg1.⁴⁸ Rao et al. also report the direct interaction of Atg9 with Atg17.⁴⁹ They observe that the Atg9-Atg17 interaction is inhibited by the regulatory Atg31-Atg29 subcomplex but restored by the association of the Atg1-Atg13 subcomplex.⁴⁹ Finally, Papinski et al. have characterized Atg1-dependent phosphorylation of Atg9.⁵⁰ With regards to higher eukaryotes, Young et al. observe that ULK1 regulates the starvation-induced redistribution of ATG9 from the trans-Golgi network to endosomes.⁵¹ Mack et al. report that the AMPK-dependent phosphorylation of ULK1 regulates ATG9 localization,⁵² and Weerasekera et al. observe that these 2 kinases mediate the phosphorylation of ATG9.⁵³ Recently, Karanasios et al. report that the nucleation of autophagosomes is initiated by the ULK1 complex on ER tubulo-vesicular regions marked by ATG9 vesicles.⁵⁴ Second, to our knowledge, there is no evidence so far that Atg13/ATG13 directly interacts with Atg9/ATG9 in Atg101/ATG101-positive cells, i.e. fission yeast or higher eukaryotes. Along these lines, a simultaneous interaction of ATG101 and ATG9 with the HORMA domain of ATG13 has not been described. Further studies are necessary to characterize the mutual influence of the known and potentially additional ATG13 HORMA domain interaction partners in mammalian model systems.

The phospholipid-binding motif is located proximal to the HORMA domain and has been shown to be important for the translocation of ATG13 to early autophagosomal structures.²⁶ The lipid-binding capabilities of yeast Atg13 were addressed by Rao et al. They observe that Atg13 does not bind to small unilamellar vesicles containing either 40 mol% phosphatidylserine or 30 mol% phosphatidylinositol or 25 mol% phosphatidylinositol supplemented with 2.5 mol% phosphatidylinositol-3-phosphate.⁴⁹ However, Atg13 is still recruited to small unilamellar vesicles composed of yeast polar lipids, indicating that other lipids than the mentioned ones are required for Atg13 binding.⁴⁹ In our experimental setup, mutation of the phospholipid-binding motif clearly inhibited autophagy induction by rapamycin or torin2 treatment but not by amino acid starvation. These data are partially similar to the findings reported by Karanasios et al. Notably, the inhibition of both binding to phospholipids and ATG101 enhanced the phenotypes of both individual mutations and resulted in accumulation of ATG13 and RB1CC1 within puncta independent of autophagy induction. We speculate that the components of the

ULK1 complex can be recruited to early autophagosomal structures possibly prior to phagophore formation, but that the subsequent release from this site is inhibited by blocked binding of phospholipids and ATG101. The observed accumulation of ATG13 and RB1CC1 was entirely abrogated by further inhibiting the ATG13-RB1CC1 interaction, hinting towards a hierarchical order of protein interactions. Nevertheless, neither the occurrence of these ATG13/RB1CC1 puncta nor their inhibition had implications for autophagy execution.

Generally, the data obtained for the RB1CC1-binding site are rather unexpected. Interference with the ATG13-RB1CC1 interaction resulted in disassembled ULK1 complexes and inhibited recruitment of ATG13 and RB1CC1 to the phagophore. However, we did not see any effect on autophagic activity. Our group has previously observed that deletion of the RB1CC1 interaction site in ATG13 results in inhibited autophagy in chicken DT40 B-lymphocytes.³¹ Furthermore, Chen et al. have identified the corresponding amino acids in RB1CC1 mediating the interaction with ATG13.⁵⁵ The ATG13-binding site in RB1CC1 is established by amino acids 582 to 585 (LQFL) in human RB1CC1.⁵⁵ The authors employ a knock-in mouse model expressing a RB1CC1 variant that cannot bind ATG13, and they observe that autophagy is completely blocked but that the nonautophagic functions of RB1CC1 fully support embryogenesis.⁵⁵ These observations are contradictory to our results. The usage of different model systems and/or autophagy readouts might contribute to this discrepancy. We suggest that the components of the ULK1 complex become recruited to the phagophore independently of a fully assembled ULK1 complex, ultimately resulting in regular autophagy progression. Since we observe that the interaction between ATG13 and RB1CC1 is important for their recruitment to the autophagosome formation site but not mandatory for autophagy induction, it also appears possible that they support autophagy execution remotely from the autophagosome formation site. Still, we cannot exclude that ATG13- and RB1CC1-positive puncta might still form but are not detectable due to reduced size or shortened half-life. Alternatively, other ULK1 complex components than ATG13 might directly interact with RB1CC1, or mammalian ATG13 possesses multiple RB1CC1-binding sites, as has been reported for yeast Atg13.³⁰ However, all these possibilities are clearly not supported by our immunopurifications, proximity ligation assays, biotin-phenol labelling experiments, or size-exclusion chromatographies.

The interaction of ATG13 and ULK1 is relevant for proper autophagy induction by EBSS stimulation as reported by our group,¹⁸ although the Δ TLQ-mutation-dependent reduction of the autophagic flux was not significant. In contrast, autophagic flux induced by rapamycin or torin2 was significantly decreased in cells expressing the ULK1 binding-deficient ATG13 variant, albeit basal autophagy levels were present. This is in accordance with the accepted model that autophagy induction by direct MTOR inhibition unequivocally relies on the ULK1 complex. At this point, we note that torin2 has a much stronger effect on ULK1 S758 and ATG13 S318 phosphorylation than rapamycin.

Although we would not state that ULK1 S758 phosphorylation is rapamycin-resistant as previously suggested,⁴⁵ the rapamycin-induced reduction of ULK1 phosphorylation is weaker than the one observed for torin2.

We also investigated the relevance of the LIR motif in ATG13. To date LIR motifs (alternatively termed Atg8-family interacting motif, AIM) have been identified for several components of the Atg1/ULK1 complexes, e.g. for yeast Atg1 or mammalian ULK1, ATG13, and RB1CC1.^{32,33,56–58} Kraft et al. report that mutation of the Atg1 LIR motif sensitizes cells for autophagy defects,⁵⁶ and Nakatogawa et al. observe that mutations in the Atg1 LIR cause a significant defect in autophagy, without affecting the functions of Atg1 during autophagosome formation.⁵⁷ With regard to mammalian ULK1, Kraft et al. show that the number of ULK1-positive structures upon starvation is significantly reduced for the LIR-mutated ULK1, whereas the total number of WIPI2 puncta is increased.⁵⁶ These data indicate that the ULK1 LIR motif is required for efficient recruitment to phagophores or autophagosomes and that WIPI2-positive autophagosomes or autophagosome precursors are stalled at an early stage during autophagy in cells expressing the ULK1 LIR mutant.⁵⁶ Similarly, Alemu et al. show that ULK1 needs the LIR motif to get recruited to WIPI2- and LC3-positive structures, again supporting the conclusion that ULK1 is located on phagophores and/or autophagosomes and might participate in later steps of autophagy.³² Two groups have identified a LIR motif within ATG13.^{32,33} Suzuki et al. have determined the crystal structures of 3 LC3 isoforms in complex with the Atg13 LIR.³³ However, so far an investigation of the ATG13-specific relevance of the LIR motif has not been reported. We did not observe any alterations of the recruitment of ATG13 or RB1CC1 to puncta upon mutation of the ATG13 LIR motif. Furthermore, WIPI2 puncta formation was not significantly affected by LIR mutation. However, LC3 turnover appeared to be rather increased than repressed. Notably, mutation of both the LIR motif and the RB1CC1 interaction site resulted in an enhanced nuclear localization of both ATG13 and LC3 following autophagy induction.

Huang et al. report that nuclear LC3 becomes deacetylated by SIRT1 and then traffics to the cytoplasm and enables autophagosome formation.⁵⁹ The association of deacetylated LC3 with autophagy factors shifts its distribution from the nucleus toward the cytoplasm.⁵⁹ Although a nuclear function of ATG13 has not been reported yet, it is tempting to speculate that ATG13 (possibly in combination with RB1CC1) participates in the regulation of the subcellular LC3 distribution. When ATG13 is released from the ULK1 complex by deletion of the RB1CC1 interaction site, LC3 is retained in the nucleus. Notably, nuclear functions and/or localization have been reported for ULK1, ULK2 and RB1CC1.^{60–62}

In summary, we suggest that the ATG13-ATG101 interaction represents one Achilles heel of autophagy induction and, accordingly, is an attractive target for therapeutic interventions in disease settings where the inhibition of autophagy is desired. Several ULK1 kinase inhibitors have been identified and characterized.^{63–66} However, these compounds neglect ULK1/2-independent autophagy pathways, which might still depend on the ATG13-ATG101 interaction. It is tempting to speculate that small-molecule compounds interfering with

this protein-protein interaction might be therapeutically valuable drugs.

Materials and methods

Antibodies and reagents

Antibodies against ACTB/ β -actin (clone AC-74, Sigma-Aldrich, A5316), ATG101 (Sigma-Aldrich, SAB4200175), ATG13 (Sigma-Aldrich, SAB4200100), ATG13 phospho (p)-S318 (Rockland Immunochemicals, 600-401-C49), ATG14 (MBL, PD026), ATG16L1 (MBL, PM040), HA (Covance, MMS-101R, now BioLegend, 901501), LC3 (for immunoblotting: Cell Signaling Technology, 2775 [detects endogenous levels of total LC3B protein; cross-reactivity may exist with other LC3 isoforms according to manufacturer specification]; for immunofluorescence: MBL International, PM036 [reacts with LC3A/LC3B/LC3C according to manufacturer specification]), RPS6KB1 phospho (p)-T389 (clone 1A5, Cell Signaling Technology, 9206), RB1CC1 (for immunoblotting: Bethyl Laboratories, A301-536A; for immunofluorescence: Proteintech, 17250-1-AP), SQSTM1/p62 (PROGEN Biotechnik, GP62-C), ULK1 (clone D8H5, Cell Signaling Technology, 8054), ULK1 phospho (p)-S757 (Cell Signaling Technology, 6888), VCL/Vinculin (Sigma-Aldrich, V9131), and WIPI2 (Serotec, MCA5780GA) were used. IRDye 800- or IRDye 680-conjugated secondary antibodies were purchased from LI-COR Biosciences (926-32210/11, 926-68070/71, 926-68024 and 926-32214), Alexa Fluor® 488-conjugated goat anti-mouse IgG and Alexa Fluor® 647-conjugated goat anti-rabbit or anti-mouse IgG antibodies from Jackson ImmunoResearch Laboratories (111-605-003 and 111-605-003). Other reagents used were bafilomycin A₁ (Sigma-Aldrich, B1793 and Alfa Aesar, J61835), torin2 (Selleckchem, S2817), rapamycin (Calbiochem, 553210), protein A/G Sepharose (GE Healthcare, 17-5280-01 and 17-0618-01) and HA-agarose (Sigma-Aldrich, A2095).

Cell lines and cell culture

Wild-type and *atg13* KO MEFs containing an insertion of a gene-trap cassette in the *Atg13* gene have previously been described.¹⁰ Cells were cultured in high glucose (4.5 g/l) DMEM supplemented with 10% FCS at 37°C in a 5% CO₂ humidified atmosphere. For amino acid starvation, cells were washed once with DPBS (Dulbecco's Phosphate-Buffered Saline, Gibco, 14190-094) and incubated for the indicated time points in EBSS (Earle's Balanced Salt Solution, Gibco, 24010-043).

Immunopurification, immunoblotting and size-exclusion chromatography

Immunopurification and immunoblotting were done as described previously.¹⁸ For size-exclusion chromatography, S100 extracts were prepared by resuspending cell pellets in RoederA buffer (10 mM HEPES, pH 7, 10 mM KCl, 1.5 mM MgCl₂, 0.5 mM DTT and protease inhibitor cocktail [Roche, 04693132001]), incubating at room temperature for 10 min and disruption with 10 strokes in a 1 ml tight Wheaton-dounce homogenizer (Wheaton, 357538). NaCl concentration was

adjusted to 150 mM and lysates were centrifuged at 17,000 x g for 30 min. Supernatants were filtered through a 45-nm PVDF filter unit and applied onto a Superose 6 increase 10/300 GL column (GE Healthcare, 29-0915-96). The column was calibrated with a Gel Filtration Calibration Kit (GE Healthcare, 28-4038-42, dextran blue [2 MDa], TG/thyroglobulin [669 kDa], ferritin [440 kDa], ALDO/aldolase [158 kDa] and RNaseA [14 kDa]). For quantification of protein levels in each fraction, immunoblotting was performed and densitometry was done using Image Studio Light Version 4 (LI-COR Biosciences). Protein ratios (fraction to input) were normalized to the fraction with highest signal intensity.

Immunofluorescence

Cells were grown on glass cover slips one day prior to stimulation, fixation with 4% formaldehyde-PBS for 15 min on ice, quenching with 50 mM NH₄Cl for 15 min and permeabilization with 50 μg/ml digitonin (Roth, 4005) for 5 min. Samples were blocked with 3% BSA (Roth, 8076)-PBS and incubated with primary antibodies for 1 h. After secondary antibody incubation, samples were washed 2 times with 0.2% Tween-20 (Sigma-Aldrich, P1379) in PBS. Cells were embedded in Mowiol-488 (Sigma-Aldrich, 81381) containing DAPI. Imaging was performed with a Zeiss LSM 710 or 780 confocal laser scanning microscope (Zeiss, Köln, Germany) with a Plan Aplanachromat 63x/1.4 oil objective (Zeiss, Köln, Germany). Quantification of images was performed with Fiji.⁶⁷ For that, signals and nuclei were counted per image and a signal-to-nuclei ratio was calculated.

Flow cytometry

Cells stably expressing mCitrine-LC3B were incubated in EBSS starvation medium for 8 h. Cells were trypsinized and analyzed for mCitrine fluorescence using an EC800 cell analyser (Sony, Tokyo, Japan).

Retroviral transfection

Generation of pMSCVpuro-HA-ATG13 based vectors has previously been described.¹⁸ Briefly, for the generation of cDNAs encoding ATG13 mutants mutagenesis PCRs were performed using the following primers: ΔV348-M373: CAAACCCATTAACCAGGTGAATCCTCCAGATTC, ΔC: GTAATATACCCGTCTGTAGAATAAGCGGCCGCTCGAAAC, phospholipid-binding domain (PLBD^{mut}): CTGATCTCAATTCCCA-GGACGCAGCGGACCTGGACGCGTTTATTGCATTTT-TTGCCCTCAAGACTG, HORMA domain (HD^{mut}): CTGAAGTCCCTTCTTGCTGCAACTGCGGCGACAC-CAGCCGCTAGGCTCTCCAGGAAAC, LIR domain (LIR^{mut}): CCATGATGACGCGTTATGGCAGACTTTAAAC, ΔTLQ: CCTTTGTGGAATAAGCGGCCGCTCGAAAC. Reverse complement sequences of forward primers were used as reverse primers. Plat-E cells (kindly provided by Toshio Kitamura, Institute of Medical Science, University of Tokyo, Japan) were used as packaging cell line. Transfection with retroviral expression vectors was performed with FuGENE[®] 6 (Roche, 11988387001). *atg13* KO MEF cells were incubated with

retroviral supernatant fractions containing 3 mg/ml polybrene (Sigma-Aldrich, H9268-106) and selected in medium containing 2.5 μg/ml puromycin (InvivoGen, ant-pr-1). Generation of MEFs stably expressing mCitrine-LC3B was performed as previously described.¹⁸

Bimolecular fluorescence complementation assay

Vectors containing the N- and C-terminal sequence of Venus were kindly provided by Michael Engelke.⁶⁸ Sequences encoding VAMP7 or ΔN-BLNK (also known as SLP-65) were excised by *Bam*HI and *Eco*RI or *Bgl*III and *Not*I digestion, respectively. Vector backbones were blunted and ligated generating pMSCVbleo-VenusC and pMSCVpuro-VenusN. VenusC cDNA was then cloned into the pBABEhygro vector (Addgene, 1765; deposited by Hartmut Land, Jay Morgenstern and Bob Weinberg). *ATG13* and *ATG101* cDNAs were inserted by sequence and ligation-independent cloning (SLIC; ref. 69) using the following primers: *ATG13* fwd: CAACTCAA-GATCCGCCACAACATCGAAGATCGGCCGCGAATT-GCGTGCAAAATTCGAATGATCTGAAACAGAAAGT-GATG, *ATG13* rev: GACTGCCTTGGGAAAAGCGCCT-CCCCTACCCGGTAGAATTTTACTGCAGGGTTTCCA-CAAAGGC, *ATG101* fwd: GCGTGCAAAATTCGAAT-GATCTCGAGCAGAAAGTGATGAACCATAACTGTC-GCTCGGAGGTGCTGGAG, and *ATG101* rev: GACACA-CATTCCACAGGGTTCGACTCAGAGGGCAAGGGTGT-CTTTGATG. As templates pMSCV-HA-ATG13 and CMV-FLAG-ATG101 (Addgene, 22877; deposited by Noboru Mizushima) were used, thereby generating pMSCVpuro-VenusN-ATG13 and pBABEhygro-VenusC-ATG101. The SLIC protocol (ref. 69) was performed with slight alterations, i.e., single strands were generated using the Klenow fragment at 37°C for 30 min, followed by heat inactivation at 75°C for 15 min. *atg13* KO MEFs stably expressing VenusC-ATG101 were generated by retroviral transfection. These cells were further incubated with VenusN-ATG13 viroid supernatant for 24 h. Cells were trypsinized and used for flow cytometric analysis or cleared cellular lysates were obtained for immunoblotting.

Biotin-phenol labeling in live cells

For the generation of pMSCV-HA-APEX2-ATG13, SLIC was performed with the primers ACGATGTGCCAGATTACGC-CGGATCCGGAAAGTCTTACCCAAGTGTGAGTG and AGCCCGAGGTTCGAGCCCGAGCCCTTGGCGGCATCAGCAAACCCAAGCTCGGAAAG using pcDNA3 Connexin43-GFP-APEX2 (Addgene, 49385; deposited by Alice Ting) as a template for APEX2 amplification and GGGCTCGGG-CTCGACCTCGGGCTCGGGCGAAACTGATCTCAATTCC-CAGGACAG and CCGGTAGAATTCGTTTCGAGCGGC-CGTTACTGCAGGG for *ATG13* amplification. pMSCV-HA-ATG13 was digested with *Bam*HI and *Not*I. Subsequently mutagenesis PCR was performed for *ATG13* mutants and stable cell lines were generated by retroviral transfection. The biotinylation protocol was performed as previously described.³⁵ For enrichment of biotinylated proteins, cells were lysed in RIPA buffer containing protease quenchers, and streptavidin

agarose (Sigma-Aldrich, S1638) was used for protein purification.

Proximity-ligation assay

In situ analysis of protein interaction was performed with the DuoLink® system from Sigma-Aldrich (Sigma-Aldrich, DUO92101). Cells were plated on glass cover slips 1 d prior to fixation with 4% formaldehyde-PBS for 15 min on ice, quenching with 50 mM NH₄Cl for 15 min and permeabilization with 50 µg/ml digitonin for 5 min. Samples were blocked with 3% BSA-PBS and incubated with primary antibodies for 1 h. Secondary antibody probing, ligation and amplification were performed according to the manufacturer's protocol. Imaging was performed on an inverse laser scanning confocal microscope in z stacks. Stacks were merged with average intensities. Signals and nuclei were counted per image and the signal-to-nuclei ratio was calculated.

Computational alanine scanning and MM-GB/SA calculations

The structure of the human ATG13-ATG101 HORMA heterodimer (PDB ID: 5C50, ref. 24) was prepared with the protein preparation wizard in Maestro.⁷⁰ A conformational ensemble was generated from 3 explicit solvent MD simulations of 250 ns length, performed with the Amber14 software package. All MD simulations and subsequent MM-GB/SA calculations were carried out as described previously.⁷¹ The same structure was used as input structure for the DrugScore^{PP1} webserver to perform computational alanine scanning.³⁷

Disclosure of Potential Conflicts of Interest

The authors declare that there are no competing financial interests in relation to the work described.

Acknowledgments

We thank Toshio Kitamura for providing Plat-E cells and Michael Engelke for providing vectors containing the N- and C- terminal sequence of Venus.

Funding

This work was supported by the Deutsche Forschungsgemeinschaft (DFG) (STO 864/3-1; to B.S.); Deutsche Forschungsgemeinschaft (DFG) (STO 864/4-1; to B.S.); Deutsche Forschungsgemeinschaft (DFG) (STO 864/5-1; to B.S.); Deutsche Forschungsgemeinschaft (DFG) (GRK 2158/1; to H.G. and to B.S.) and Research Committee of the Medical Faculty of the Heinrich Heine University (22/2015; to B.S.).

ORCID

Neha Verma  <http://orcid.org/0000-0002-3277-0937>
 Philip Böhler  <http://orcid.org/0000-0002-7792-8304>
 Christoph Peter  <http://orcid.org/0000-0002-0048-2279>
 Holger Gohlke  <http://orcid.org/0000-0001-8613-1447>
 Noboru Mizushima  <http://orcid.org/0000-0002-6258-6444>
 Björn Stork  <http://orcid.org/0000-0002-4167-7806>

References

- Dikic I, Johansen T, Kirkin V. Selective autophagy in cancer development and therapy. *Cancer Res.* 2010;70:3431–3434. doi:10.1158/0008-5472.CAN-09-4027. PMID:20424122
- Levine B, Kroemer G. Autophagy in the pathogenesis of disease. *Cell.* 2008;132:27–42. doi:10.1016/j.cell.2007.12.018. PMID:18191218
- Mizushima N, Levine B, Cuervo AM, Klionsky DJ. Autophagy fights disease through cellular self-digestion. *Nature.* 2008;451:1069–1075. doi:10.1038/nature06639. PMID:18305538
- Mowers EE, Sharifi MN, Macleod KF. Autophagy in cancer metastasis. *Oncogene.* 2017;36:1619–1630. doi:10.1038/onc.2016.333. PMID:27593926
- Ganley IG, Lam du H, Wang J, Ding X, Chen S, Jiang X. ULK1. ATG13.FIP200 complex mediates mTOR signaling and is essential for autophagy. *J Biol Chem.* 2009;284:12297–12305. doi:10.1074/jbc.M900573200. PMID:19258318
- Hosokawa N, Hara T, Kaizuka T, Kishi C, Takamura A, Miura Y, Iemura S, Natsume T, Takehana K, Yamada N, et al. Nutrient-dependent mTORC1 association with the ULK1-Atg13-FIP200 complex required for autophagy. *Mol Biol Cell.* 2009;20:1981–1991. doi:10.1091/mbc.E08-12-1248. PMID:19211835
- Hosokawa N, Sasaki T, Iemura S, Natsume T, Hara T, Mizushima N. Atg101, a novel mammalian autophagy protein interacting with Atg13. *Autophagy.* 2009;5:973–979. doi:10.4161/auto.5.7.9296. PMID:19597335
- Mercer CA, Kaliappan A, Dennis PB. A novel, human Atg13 binding protein, Atg101, interacts with ULK1 and is essential for macroautophagy. *Autophagy.* 2009;5:649–662. doi:10.4161/auto.5.5.8249. PMID:19287211
- Gan B, Peng X, Nagy T, Alcaraz A, Gu H, Guan JL. Role of FIP200 in cardiac and liver development and its regulation of TNFalpha and TSC-mTOR signaling pathways. *J Cell Biol.* 2006;175:121–133. doi:10.1083/jcb.200604129. PMID:17015619
- Kaizuka T, Mizushima N. Atg13 Is essential for autophagy and cardiac development in mice. *Mol Cell Biol.* 2015;36:585–595. doi:10.1128/MCB.01005-15. PMID:26644405
- Cheong H, Lindsten T, Wu J, Lu C, Thompson CB. Ammonia-induced autophagy is independent of ULK1/ULK2 kinases. *Proc Natl Acad Sci USA.* 2011;108:11121–11126. doi:10.1073/pnas.1107969108. PMID:21690395
- Kundu M, Lindsten T, Yang CY, Wu J, Zhao F, Zhang J, Selak MA, Ney PA, Thompson CB. Ulk1 plays a critical role in the autophagic clearance of mitochondria and ribosomes during reticulocyte maturation. *Blood.* 2008;112:1493–1502. doi:10.1182/blood-2008-02-137398. PMID:18539900
- Lee EJ, Tournier C. The requirement of uncoordinated 51-like kinase 1 (ULK1) and ULK2 in the regulation of autophagy. *Autophagy.* 2011;7:689–695. doi:10.4161/auto.7.7.15450. PMID:21460635
- Alers S, Löffler AS, Wesselborg S, Stork B. Role of AMPK-mTOR-Ulk1/2 in the regulation of autophagy: cross talk, shortcuts, and feedbacks. *Mol Cell Biol.* 2012;32:2–11. doi:10.1128/MCB.06159-11. PMID:22025673
- Papinski D, Kraft C. Regulation of autophagy by signaling through the Atg1/ULK1 complex. *J Mol Biol.* 2016;428:1725–1741. doi:10.1016/j.jmb.2016.03.030. PMID:27059781
- Wesselborg S, Stork B. Autophagy signal transduction by ATG proteins: from hierarchies to networks. *Cell Mol Life Sci: CMLS.* 2015;72:4721–4757. doi:10.1007/s00018-015-2034-8. PMID:26390974
- Wong PM, Puente C, Ganley IG, Jiang X. The ULK1 complex: sensing nutrient signals for autophagy activation. *Autophagy.* 2013;9:124–137. doi:10.4161/auto.23323. PMID:23295650
- Hieke N, Löffler AS, Kaizuka T, Berleth N, Böhler P, Driessen S, Stuhldreier F, Friesen O, Assani K, Schmitz K, et al. Expression of a ULK1/2 binding-deficient ATG13 variant can partially restore autophagic activity in ATG13-deficient cells. *Autophagy.* 2015;11:1471–1483. doi:10.1080/15548627.2015.1068488. PMID:26213203
- Jung CH, Jun CB, Ro SH, Kim YM, Otto NM, Cao J, Kundu M, Kim DH. ULK-Atg13-FIP200 complexes mediate mTOR signaling to the autophagy machinery. *Mol Biol Cell.* 2009;20:1992–2003. doi:10.1091/mbc.E08-12-1249. PMID:19225151

20. Suzuki H, Kaizuka T, Mizushima N, Noda NN. Structure of the Atg101-Atg13 complex reveals essential roles of Atg101 in autophagy initiation. *Nat Struct Mol Biol.* 2015;22:572–580. doi:10.1038/nsmb.3036. PMID:26030876
21. Aravind L, Koonin EV. The HORMA domain: a common structural denominator in mitotic checkpoints, chromosome synapsis and DNA repair. *Trends Biochem Sci.* 1998;23:284–286. doi:10.1016/S0968-0004(98)01257-2. PMID:9757827
22. Jao CC, Ragusa MJ, Stanley RE, Hurley JH. A HORMA domain in Atg13 mediates PI 3-kinase recruitment in autophagy. *Proc Natl Acad Sci USA.* 2013;110:5486–5491. doi:10.1073/pnas.1220306110. PMID:23509291
23. Michel N, Schwarten M, Decker C, Nagel-Steger L, Willbold D, Weiergraber OH. The mammalian autophagy initiator complex contains two HORMA domain proteins. *Autophagy.* 2015;11:2300–2308. doi:10.1080/15548627.2015.1076605. PMID:26236954
24. Qi S, Kim do J, Stjepanovic G, Hurley JH. Structure of the Human Atg13-Atg101 HORMA Heterodimer: an Interaction Hub within the ULK1 Complex. *Structure.* 2015;23:1848–1857. doi:10.1016/j.str.2015.07.011. PMID:26299944
25. Suzuki SW, Yamamoto H, Oikawa Y, Kondo-Kakuta C, Kimura Y, Hirano H, Ohsumi Y. Atg13 HORMA domain recruits Atg9 vesicles during autophagosomal formation. *Proc Natl Acad Sci United States America.* 2015;112:3350–3355. doi:10.1073/pnas.1421092112. PMID:25737544
26. Karanasios E, Stapleton E, Manifava M, Kaizuka T, Mizushima N, Walker SA, Ktistakis NT. Dynamic association of the ULK1 complex with omegasomes during autophagy induction. *J Cell Sci.* 2013;126:5224–5238. doi:10.1242/jcs.132415. PMID:24013547
27. Fujioka Y, Suzuki SW, Yamamoto H, Kondo-Kakuta C, Kimura Y, Hirano H, Akada R, Inagaki F, Ohsumi Y, Noda NN. Structural basis of starvation-induced assembly of the autophagy initiation complex. *Nat Struct Mol Biol.* 2014;21:513–521. doi:10.1038/nsmb.2822. PMID:24793651
28. Mei Y, Su M, Soni G, Salem S, Colbert CL, Sinha SC. Intrinsically disordered regions in autophagy proteins. *Proteins.* 2014;82:565–578. doi:10.1002/prot.24424. PMID:24115198
29. Chew LH, Lu S, Liu X, Li FK, Yu AY, Klionsky DJ, Dong MQ, Yip CK. Molecular interactions of the *Saccharomyces cerevisiae* Atg1 complex provide insights into assembly and regulatory mechanisms. *Autophagy.* 2015;11:891–905. doi:10.1080/15548627.2015.1040972. PMID:25998554
30. Yamamoto H, Fujioka Y, Suzuki SW, Noshiro D, Suzuki H, Kondo-Kakuta C, Kimura Y, Hirano H, Ando T, Noda NN, et al. The intrinsically disordered protein atg13 mediates supramolecular assembly of autophagy initiation complexes. *Dev Cell.* 2016;38:86–99. doi:10.1016/j.devcel.2016.06.015. PMID:27404361
31. Alers S, Löffler AS, Paasch F, Dieterle AM, Keppeler H, Lauber K, Campbell DG, Fehrenbacher B, Schaller M, Wesselborg S, et al. Atg13 and FIP200 act independently of Ulk1 and Ulk2 in autophagy induction. *Autophagy.* 2011;7:1423–1433. doi:10.4161/auto.7.12.18027. PMID:22024743
32. Alemu EA, Lamark T, Torgersen KM, Birgisdottir AB, Larsen KB, Jain A, Olsvik H, Overvatn A, Kirkin V, Johansen T. ATG8 family proteins act as scaffolds for assembly of the ULK complex: sequence requirements for LC3-interacting region (LIR) motifs. *J Biol Chem.* 2012;287:39275–39290. doi:10.1074/jbc.M112.378109. PMID:23043107
33. Suzuki H, Tabata K, Morita E, Kawasaki M, Kato R, Dobson RC, Yoshimori T, Wakatsuki S. Structural basis of the autophagy-related LC3/Atg13 LIR complex: recognition and interaction mechanism. *Structure.* 2014;22:47–58. doi:10.1016/j.str.2013.09.023. PMID:24290141
34. Hung V, Zou P, Rhee HW, Udeshi ND, Cracan V, Svinikina T, Carr SA, Mootha VK, Ting AY. Proteomic mapping of the human mitochondrial intermembrane space in live cells via ratiometric APEX tagging. *Mol Cell.* 2014;55:332–341. doi:10.1016/j.molcel.2014.06.003. PMID:25002142
35. Lam SS, Martell JD, Kamer KJ, Deerinck TJ, Ellisman MH, Mootha VK, Ting AY. Directed evolution of APEX2 for electron microscopy and proximity labeling. *Nat Methods.* 2015;12:51–54. doi:10.1038/nmeth.3179. PMID:25419960
36. Rhee HW, Zou P, Udeshi ND, Martell JD, Mootha VK, Carr SA, Ting AY. Proteomic mapping of mitochondria in living cells via spatially restricted enzymatic tagging. *Science.* 2013;339:1328–1331. doi:10.1126/science.1230593. PMID:23371551
37. Krüger DM, Gohlke H. DrugScorePPI webserver: fast and accurate in silico alanine scanning for scoring protein-protein interactions. *Nucleic Acids Res.* 2010;38:W480–W486. doi:10.1093/nar/gkq471. PMID:20511591
38. Moreira IS, Fernandes PA, Ramos MJ. Hot spots—a review of the protein-protein interface determinant amino-acid residues. *Proteins.* 2007;68:803–812. doi:10.1002/prot.21396. PMID:17546660
39. Gohlke H, Kiel C, Case DA. Insights into protein-protein binding by binding free energy calculation and free energy decomposition for the Ras-Raf and Ras-RalGDS complexes. *J Mol Biol.* 2003;330:891–913. doi:10.1016/S0022-2836(03)00610-7. PMID:12850155
40. Homeyer N, Gohlke H. Free energy calculations by the molecular mechanics Poisson-boltzmann surface area method. *Mol Inform.* 2012;31:114–122. doi:10.1002/minf.201100135. PMID:27476956
41. Park JM, Jung CH, Seo M, Otto NM, Grunwald D, Kim KH, Moriarity B, Kim YM, Starker C, Nho RS, et al. The ULK1 complex mediates MTORC1 signaling to the autophagy initiation machinery via binding and phosphorylating ATG14. *Autophagy.* 2016;12:547–564. doi:10.1080/15548627.2016.1140293. PMID:27046250
42. Choi H, Merceron C, Mangiavini L, Seifert EL, Schipani E, Shapiro IM, Risbud MV. Hypoxia promotes noncanonical autophagy in nucleus pulposus cells independent of MTOR and HIF1A signaling. *Autophagy.* 2016;12:1631–1646. doi:10.1080/15548627.2016.1192753. PMID:27314664
43. Gao Y, Liu Y, Hong L, Yang Z, Cai X, Chen X, Fu Y, Lin Y, Wen W, Li S, et al. Golgi-associated LC3 lipidation requires V-ATPase in noncanonical autophagy. *Cell Death Dis.* 2016;7:e2330. doi:10.1038/cddis.2016.236. PMID:27512951
44. Manzoni C, Mamais A, Roosen DA, Dihanich S, Soutar MP, Plun-Favreau H, Bandopadhyay R, Hardy J, Tooze SA, Cookson MR, et al. mTOR independent regulation of macroautophagy by Leucine Rich Repeat Kinase 2 via Beclin-1. *Sci Rep.* 2016;6:35106. doi:10.1038/srep35106. PMID:27731364
45. Kang SA, Pacold ME, Cervantes CL, Lim D, Lou HJ, Ottina K, Gray NS, Turk BE, Yaffe MB, Sabatini DM. mTORC1 phosphorylation sites encode their sensitivity to starvation and rapamycin. *Science.* 2013;341:1236566. doi:10.1126/science.1236566. PMID:23888043
46. Noda NN, Mizushima N. Atg101: Not just an accessory subunit in the Autophagy-initiation complex. *Cell Struct Funct.* 2016;41:13–20. doi:10.1247/csf.15013. PMID:26754330
47. Reggiori F, Tucker KA, Stromhaug PE, Klionsky DJ. The Atg1-Atg13 complex regulates Atg9 and Atg23 retrieval transport from the pre-autophagosomal structure. *Dev Cell.* 2004;6:79–90. doi:10.1016/S1534-5807(03)00402-7. PMID:14723849
48. Sekito T, Kawamata T, Ichikawa R, Suzuki K, Ohsumi Y. Atg17 recruits Atg9 to organize the pre-autophagosomal structure. *Gen Cell.* 2009;14:525–538. doi:10.1111/j.1365-2443.2009.01299.x. PMID:19371383
49. Rao Y, Perna MG, Hofmann B, Beier V, Wollert T. The Atg1-kinase complex tethers Atg9-vesicles to initiate autophagy. *Nat Commun.* 2016;7:10338. doi:10.1038/ncomms10338. PMID:26753620
50. Papinski D, Schuschnig M, Reiter W, Wilhelm L, Barnes CA, Maiolica A, Hansmann I, Pfaffenwimmer T, Kijanska M, Stoffel I, et al. Early steps in autophagy depend on direct phosphorylation of Atg9 by the Atg1 kinase. *Mol Cell.* 2014;53:471–483. doi:10.1016/j.molcel.2013.12.011. PMID:24440502
51. Young AR, Chan EY, Hu XW, Kochl R, Crawshaw SG, High S, Hailey DW, Lippincott-Schwartz J, Tooze SA. Starvation and ULK1-dependent cycling of mammalian Atg9 between the TGN and endosomes. *J Cell Sci.* 2006;119:3888–3900. doi:10.1242/jcs.03172. PMID:16940348
52. Mack HI, Zheng B, Asara JM, Thomas SM. AMPK-dependent phosphorylation of ULK1 regulates ATG9 localization. *Autophagy.* 2012;8:1197–1214. doi:10.4161/auto.20586. PMID:22932492
53. Weerasekara VK, Panek DJ, Broadbent DG, Mortenson JB, Mathis AD, Logan GN, Prince JT, Thomson DM, Thompson JW, Andersen JL. Metabolic-stress-induced rearrangement of the 14-3-3zeta interactome promotes autophagy via a ULK1- and AMPK-regulated 14-3-3zeta interaction with phosphorylated

- Atg9. *Mol Cell Biol.* 2014;34:4379–4388. doi:10.1128/MCB.00740-14. PMID:25266655
54. Karanasios E, Walker SA, Okkenhaug H, Manifava M, Hummel E, Zimmermann H, Ahmed Q, Domart MC, Collinson L, Ktistakis NT. Autophagy initiation by ULK complex assembly on ER tubulovesicular regions marked by ATG9 vesicles. *Nat Commun.* 2016;7:12420. doi:10.1038/ncomms12420. PMID:27510922
55. Chen S, Wang C, Yeo S, Liang CC, Okamoto T, Sun S, Wen J, Guan JL. Distinct roles of autophagy-dependent and -independent functions of FIP200 revealed by generation and analysis of a mutant knock-in mouse model. *Gen Dev.* 2016;30:856–869. doi:10.1101/gad.276428.115. PMID:27013233
56. Kraft C, Kijanska M, Kalie E, Siergiejuk E, Lee SS, Semplicio G, Stoffel I, Brezovich A, Verma M, Hansmann I, et al. Binding of the Atg1/ULK1 kinase to the ubiquitin-like protein Atg8 regulates autophagy. *EMBO J.* 2012;31:3691–3703. doi:10.1038/emboj.2012.225. PMID:22885598
57. Nakatogawa H, Ohbayashi S, Sakoh-Nakatogawa M, Kakuta S, Suzuki SW, Kirisako H, Kondo-Kakuta C, Noda NN, Yamamoto H, Ohsumi Y. The autophagy-related protein kinase Atg1 interacts with the ubiquitin-like protein Atg8 via the Atg8 family interacting motif to facilitate autophagosome formation. *J Biol Chem.* 2012;287:28503–28507. doi:10.1074/jbc.C112.387514. PMID:22778255
58. Okazaki N, Yan J, Yuasa S, Ueno T, Kominami E, Masuho Y, Koga H, Muramatsu M. Interaction of the Unc-51-like kinase and microtubule-associated protein light chain 3 related proteins in the brain: possible role of vesicular transport in axonal elongation. *Brain Res Mol Brain Res.* 2000;85:1–12. doi:10.1016/S0169-328X(00)00218-7. PMID:11146101
59. Huang R, Xu Y, Wan W, Shou X, Qian J, You Z, Liu B, Chang C, Zhou T, Lippincott-Schwartz J, et al. Deacetylation of nuclear LC3 drives autophagy initiation under starvation. *Mol Cell.* 2015;57:456–466. doi:10.1016/j.molcel.2014.12.013. PMID:25601754
60. Chano T, Ikegawa S, Kontani K, Okabe H, Baldini N, Saeki Y. Identification of RB1CC1, a novel human gene that can induce RB1 in various human cells. *Oncogene.* 2002;21:1295–1298. doi:10.1038/sj.onc.1205178. PMID:11850849
61. Joshi A, Iyengar R, Joo JH, Li-Harms XJ, Wright C, Marino R, Winborn BJ, Phillips A, Temirov J, Sciarretta S, et al. Nuclear ULK1 promotes cell death in response to oxidative stress through PARP1. *Cell Death Differ.* 2016;23:216–230. doi:10.1038/cdd.2015.88. PMID:26138443
62. Shin SH, Lee EJ, Chun J, Hyun S, Kang SS. ULK2 Ser 1027 phosphorylation by PKA regulates its nuclear localization occurring through karyopherin beta 2 recognition of a PY-NLS motif. *PLoS One.* 2015;10:e0127784. doi:10.1371/journal.pone.0127784. PMID:26052940
63. Egan DF, Chun MG, Vamos M, Zou H, Rong J, Miller CJ, Lou HJ, Raveendra-Panickar D, Yang CC, Sheffler DJ, et al. Small molecule inhibition of the autophagy kinase ULK1 and identification of ULK1 substrates. *Mol Cell.* 2015;59:285–297. doi:10.1016/j.molcel.2015.05.031. PMID:26118643
64. Lazarus MB, Novotny CJ, Shokat KM. Structure of the human autophagy initiating kinase ULK1 in complex with potent inhibitors. *ACS Chem Biol.* 2015;10:257–261. doi:10.1021/cb500835z. PMID:25551253
65. Lazarus MB, Shokat KM. Discovery and structure of a new inhibitor scaffold of the autophagy initiating kinase ULK1. *Bioorg Med Chem.* 2015;23:5483–5488. doi:10.1016/j.bmc.2015.07.034. PMID:26275681
66. Petherick KJ, Conway OJ, Mpamhanga C, Osborne SA, Kamal A, Saxty B, Ganley IG. Pharmacological inhibition of ULK1 kinase blocks mammalian target of rapamycin (mTOR)-dependent autophagy. *J Biol Chem.* 2015;290:11376–11383. doi:10.1074/jbc.C114.627778. PMID:25833948
67. Schindelin J, Arganda-Carreras I, Frise E, Kaynig V, Longair M, Pietzsch T, Preibisch S, Rueden C, Saalfeld S, Schmid B, et al. Fiji: an open-source platform for biological-image analysis. *Nat Methods.* 2012;9:676–682. doi:10.1038/nmeth.2019. PMID:22743772
68. Engelke M, Pirkuliyeva S, Kuhn J, Wong L, Boyken J, Herrmann N, Becker S, Griesinger C, Wienands J. Macromolecular assembly of the adaptor SLP-65 at intracellular vesicles in resting B cells. *Sci Signal.* 2014;7:ra79. doi:10.1126/scitranslmed.2005104. PMID:25140054
69. Li MZ, Elledge SJ. Harnessing homologous recombination in vitro to generate recombinant DNA via SLIC. *Nat Methods.* 2007;4:251–256. doi:10.1038/nmeth1010. PMID:17293868
70. Sastry GM, Adzhigirey M, Day T, Annabhimoju R, Sherman W. Protein and ligand preparation: parameters, protocols, and influence on virtual screening enrichments. *J Comput Aided Mol Des.* 2013;27:221–234. doi:10.1007/s10822-013-9644-8. PMID:23579614
71. Ciglia E, Vergin J, Reimann S, Smits SH, Schmitt L, Groth G, Gohlke H. Resolving hot spots in the C-terminal dimerization domain that determine the stability of the molecular chaperone Hsp90. *PLoS One.* 2014;9:e96031. doi:10.1371/journal.pone.0096031. PMID:24760083

Publication 3

FIP200 controls TBK1 activation threshold at SQSTM1/p62-positive condensates

David Schlütermann, Niklas Berleth, Jana Deitersen, Nora Wallot-Hieke, Olena Friesen, Wenxian Wu, Fabian Stuhldreier, Yadong Sun, Lena Berning, Annabelle Friedrich, María José Mendiburo, Christoph Peter, Constanze Wiek, Helmut Hanenberg, Anja Stefanski, Kai Stühler, Björn Stork

Manuscript in preparation

FIP200 controls TBK1 activation threshold at SQSTM1/p62-positive condensates

AUTHORS/AFFILIATIONS

David Schlütermann¹, Niklas Berleth¹, Jana Deitersen¹, Nora Wallot-Hieke¹, Olena Friesen¹, Wenxian Wu¹, Fabian Stuhldreier¹, Yadong Sun¹, Lena Berning¹, Annabelle Friedrich¹, María José Mendiburo¹, Christoph Peter¹, Constanze Wiek², Helmut Hanenberg^{2,3}, Anja Stefanski⁴, Kai Stühler^{1,4}, Björn Stork^{1,*}

¹*Institute of Molecular Medicine I, Medical Faculty, Heinrich Heine University, 40225 Düsseldorf, Germany*

²*Department of Otorhinolaryngology & Head/Neck Surgery, Medical Faculty, Heinrich Heine University, 40225 Düsseldorf, Germany*

³*Department of Pediatrics III, University Hospital Essen, University of Duisburg-Essen, 45122 Essen, Germany*

⁴*Molecular Proteomics Laboratory, Biologisch-Medizinisches Forschungszentrum (BMFZ), Heinrich Heine University, 40225 Düsseldorf, Germany*

CONTACT

*Corresponding author:

Björn Stork, Universitätsstr. 1, Building 22.03, 40225 Düsseldorf, Germany,

Tel.: +49 (0)211 81 11954, Fax: +49 (0)211 81 14103, E-mail: bjoern.stork@hhu.de

RUNNING TITLE: FIP200 controls TBK1 activation

KEYNOTES: autophagy, TBK1, FIP200, TAX1BP1, SQSTM1/p62

ABBREVIATIONS: ALS, amyotrophic lateral sclerosis; ATG, autophagy-related; AZI2/NAP1, 5-azacytidine induced 2; cGAS, cyclic GMP-AMP synthase; FIP200, focal adhesion kinase (FAK)-interacting protein of 200 kDa; FTD, frontotemporal dementia; HSE, herpes simplex encephalitis; IFN, interferon; IRF3/7, interferon regulatory factor 3/7; (MAP1)LC3, (microtubule-associated proteins 1A/1B) light chain 3; MAVS, mitochondrial antiviral signaling protein; MyD88, myeloid differentiation primary response 88; NBR1, neighbor of BRCA1 gene 1; NDP52, nuclear dot protein 52 kDa; NRBF2, nuclear receptor-binding factor 2; NTG, normal tension glaucoma; OPTN, optineurin; PIK3C3/VPS34, phosphatidylinositol 3-kinase catalytic subunit type 3; PIK3R4/VPS15, phosphoinositide 3-kinase regulatory subunit 4; PRR, pattern recognition receptor; RIG-I, retinoic acid-inducible gene I; RLR, RIG-I-like receptor; SAR, selective autophagy receptor; SQSTM1/p62, sequestosome 1; STING, stimulator of interferon genes; TAX1BP1, Tax1 binding protein 1; TBK1, TANK-binding kinase 1; TBKBP1/SINTBAD, TBK1 binding protein 1; TLR3/4, toll-like receptor 3/4; TRIF, TIR-domain-containing adapter-inducing interferon- β ; ULK1/2, UNC-51 like autophagy activating kinase 1/2

ABSTRACT

The protein kinase TBK1 is a central regulator of innate immune responses and autophagy, and ablation of either function has been linked to neuroinflammatory or -degenerative diseases. Autophagy is an intracellular process recycling long-lived or damaged proteins and organelles. In recent years, the TBK1-dependent regulation of autophagy pathways has been characterized. However, the autophagy-dependent regulation of TBK1 activity awaits further clarification. Here, we observe that TBK1 becomes recruited to SQSTM1/p62-containing aggregates via the selective autophagy receptor TAX1BP1. In these aggregates, TBK1 phosphorylates SQSTM1/p62 at serine 403 and thus presumably regulates the efficient engulfment and clearance of these structures. We find that TBK1 activation is strongly increased if FIP200, a component of the autophagy-inducing ULK1 complex, is not present or cannot bind to TAX1BP1. Collectively, we hypothesize that FIP200 ensures the inducible activation of TBK1 at SQSTM1/p62 condensates.

1. INTRODUCTION

(Macro-)autophagy is an intracellular recycling process that maintains cellular homeostasis by degrading long-lived or damaged proteins and organelles. Autophagy can be either non-selective or selective with regard to its cargo. Non-selective autophagy occurs at basal levels in most cell types but is also inducible under conditions of nutrient depletion. The process is initiated with the nucleation of a phagophore, which engulfs bulk cargo and expands into double-membraned vesicles called autophagosomes. Autophagosomes transport the cargo to lysosomes, in which the cargo ultimately becomes degraded. The initiation of autophagic processes is centrally regulated by two kinase complexes: (1) the ULK1 protein kinase complex containing the Ser/Thr kinase UNC-51 like autophagy activating kinase 1 (ULK1) and the adapter proteins autophagy-related protein 13 (ATG13), ATG101 and focal adhesion kinase (FAK)-interacting protein of 200 kDa (FIP200), and (2) the class III phosphatidylinositol 3-kinase (PtdIns3K) lipid kinase complex containing the phosphatidylinositol 3-kinase catalytic subunit type 3 (PIK3C3/VPS34) and the associated proteins phosphoinositide 3 kinase regulatory subunit 4 (PIK3R4/VPS15), Beclin 1, ATG14, and nuclear receptor-binding factor 2 (NRBF2)^{1,2}. Both kinase complexes are also involved in the regulation of selective autophagy processes. During selective autophagy the cargo is specifically targeted by selective autophagy receptors (SARs)^{3,4}. Selective autophagy is classified based on the degraded cargo, for example damaged mitochondria (mitophagy), protein aggregates (aggrephagy), or intracellular pathogens (xenophagy)³. The SARs sequestosome 1 (SQSTM1/p62), neighbor of *BRCA1* gene 1 (NBR1), nuclear dot protein 52 kDa (NDP52), Tax1 binding protein 1 (TAX1BP1), and optineurin (OPTN) all belong to the SQSTM1/p62-like receptor (SLR) family and represent the best-studied family of SARs⁵. They simultaneously bind ubiquitin moieties on the cargo and phosphatidylethanolamine (PE)-conjugated ATG8 family proteins⁵, which are attached to the membrane of forming autophagosomes⁶. Recently, NDP52 was shown to attract the ULK1 complex to damaged mitochondria⁷ or cytosolic pathogens⁸ via binding to a C-terminal region of FIP200. Once recruited, ULK1 initiates the formation of the phagophore directly at the cargo⁹. The recruitment of the ULK1 complex is facilitated by TANK binding kinase 1 (TBK1)^{7,8}. The

Ser/Thr kinase TBK1 is a central regulator of innate immune responses, but in recent years its involvement in autophagy signaling pathways has been discovered. Next to the facilitated recruitment of the ULK1 complex to mitochondria or intracellular pathogens, TBK1 directly regulates other components of the autophagy signaling cascade, including AMPK¹⁰, syntaxin 17¹¹, or various SARs^{7,8,12-17}. TBK1-dependent phosphorylation frequently modulates the binding affinities of the SARs, e.g. it has been reported that TBK1-catalyzed phosphorylation of SQSTM1/p62 at serine 403 enhances ubiquitin binding^{13,14,18}.

The innate immune response is the first line of defense during viral infections. Pattern recognition receptors (PRRs) detect specific bacterial or viral components finally leading to type I interferon (IFN) and pro-inflammatory cytokine production to prevent viral invasion and replication¹⁹. PRRs include toll-like receptors (TLRs), retinoic acid-inducible gene I (RIG-I)-like receptors (RLRs), and cytosolic DNA receptors like cyclic GMP-AMP synthase (cGAS). Upon ligand binding, TLR3/4, RIG-I, and cGAS mediate the recruitment of TBK1 to the adaptor proteins TIR-domain-containing adapter-inducing interferon- β (TRIF), mitochondrial antiviral signaling protein (MAVS), or stimulator of interferon genes (STING), respectively²⁰. Local clustering leads to trans-autophosphorylation at serine 172 and thus activation of TBK1^{21,22}. Once activated, TBK1 phosphorylates interferon regulatory factor 3 (IRF3) and IRF7, thereby inducing their dimerization and nuclear translocation. In the nucleus, IRF3 and IRF7 activate type I IFN gene expression²³. TLR signaling also induces autophagy, e.g. via binding of the adaptor proteins TRIF and myeloid differentiation primary response 88 (MyD88) to Beclin 1^{24,25}. On the other hand, autophagy can exert anti-inflammatory effects²⁶, e.g. by targeting the RIG-I-MAVS axis²⁷ or by TAX1BP1-mediated selective degradation of TRIF²⁸. Furthermore, TAX1BP1 and the ubiquitin-editing enzyme A20 target TBK1 to inhibit the immune response by disrupting the TRAF3-TBK1 signaling complex²⁹.

Mutations of the *TBK1* gene are connected to several diseases including childhood herpes simplex encephalitis (HSE), amyotrophic lateral sclerosis (ALS), frontotemporal dementia (FTD), and normal tension glaucoma (NTG) (reviewed in³⁰). These diseases are caused either by dysregulated autophagy

or by impaired IFN production³⁰. Loss of function mutations in the *TBK1* gene could be linked to ALS and FTD^{31,32}. In turn, gain of function *TBK1* mutations (i.e. gene duplication) were reported in patients with NTG. Therefore, TBK1 must be tightly regulated to maintain cellular homeostasis. Although the involvement of TBK1 in the regulation of autophagy is undoubted, the regulation of TBK1 itself during autophagic processes awaits further clarification.

In this study, we show that TBK1-TAX1BP1-SQSTM1/p62 aggregates develop in cells deficient for autophagy in general and for FIP200 in particular. TBK1 gets activated in those aggregates and phosphorylates SQSTM1/p62 at serine 403. These aggregates are likely caused by the proteotoxic stress induced by inhibited autophagy. The recruitment of TBK1 to these aggregates is mediated by TAX1BP1. The activation of TBK1 is clearly increased in cells if FIP200 is not present or cannot bind to TAX1BP1, indicating that the presence of FIP200—next to its function for the recruitment of the downstream autophagy machinery—inhibits the aberrant activation of TBK1. We propose that FIP200 controls the TBK1 activation threshold and ensures the inducibility of TBK1 activity.

2. RESULTS

Loss of autophagy in general and loss of components of the ULK1 complex in particular lead to an increased focal accumulation and activation of TBK1

In a search for novel FIP200-interacting proteins, we performed mass spectrometric analysis using GFP-FIP200 as bait. Amongst the identified binding partners were TBK1, TBKBP1/SINTBAD, and several autophagy receptors (TAX1BP1, SQSTM1/p62, and NBR1) (Table **S1**). The interaction between GFP-FIP200 and TBK1 was confirmed by immunopurification (Figure **S1A**). Recent reports show that TBK1 binds to the autophagy receptor NDP52 and facilitates ULK1 complex recruitment via FIP200^{7,8}. In our immunopurifications, we observe that GFP-FIP200 binds the autophagy receptors TAX1BP1 and NDP52 (Figure **S1A**). Accordingly, we assume that FIP200 interacts with TBK1 via TAX1BP1 and/or NDP52. Since the cells used for mass spectrometry or immunopurification were cultured in full medium, it is likely that these interactions are constitutive.

It has been previously reported that the C terminus of FIP200 mediates binding to the autophagy receptors NDP52 and/or SQSTM1/p62^{7,8,33}. The interaction between the C terminus of FIP200 (aa 1352-1441) and NDP52 was shown to be mandatory for the recruitment of the ULK1 complex to damaged mitochondria or intracellular bacteria, respectively^{7,8}, whereas the binding of the C-terminal FIP200 claw domain (aa 1494-1594) to SQSTM1/p62 promotes autophagosome formation at SQSTM1/p62-ubiquitin condensates³³. To analyze a potential role of FIP200 and in particular its C terminus in TBK1 activation, we made use of *fip200* knockout (KO) mouse embryonic fibroblasts (MEFs) that were transfected with an empty vector or cDNA encoding wild type FIP200 or a variant lacking the C-terminal part of FIP200 (amino acids 1369-1594, Δ CT). Notably, we observed that loss of FIP200 leads to an aberrant accumulation of activated TBK1, as determined by immunofluorescence using antibodies specific for phospho-Ser172 of TBK1 (Figure **1A**). This is in accordance with a report by Goodwin et al. investigating ferritinophagy³⁴. Expression of wild type FIP200 in *fip200* KO MEFs blocks the accumulation of phospho-TBK1. In contrast, the C-terminally truncated version of FIP200

reduced the focal localization of phospho-TBK1, but was not able to completely prevent it (Figure **1A**). For comparison, phospho-TBK1 positive dots per cell were counted and the size and intensity of each dot were determined. Loss of FIP200 led to an increase of the number of dots per cell. Moreover, these phospho-TBK1-positive structures were larger and exhibited a higher intensity. Removal of the FIP200 C-terminal domain increased the number of TBK1 aggregates by the factor 3. These structures were also larger (~5x) and had a higher intensity (~9x) (Figure **1B**). Since autophagy is blocked in FIP200-deficient MEFs ³⁵, we also investigated the influence of generally defective autophagy on TBK1 regulation. For that, we examined the phospho status of TBK1 in MEFs deficient for ATG3 by immunoblotting and immunofluorescence (Figure **1A** and **1B**, Figure **S1B**). ATG3 mediates the E2-like conjugation of LC3 to phosphatidylethanolamine (PE), which is an essential step during autophagy ⁶. *Atg3* KO cells showed an increased TBK1 activation compared to wild type MEFs (Figure **1A** and **1B**, Figure **S1B**). We observed that the blockage of autophagy by the lysosomal V-ATPase inhibitor bafilomycin A₁ only increases TBK1 activation in wild type cells, but not in *atg3* KO cells (Figure **S1B**). Interestingly, the phospho-TBK1 aggregates in *atg3* KO cells are fewer, smaller and less intense than the ones observed in *fip200* KO MEFs (Figure **1A** and **1B**).

Next, we aimed at investigating whether the depletion of other components of the ULK1 complex affects TBK1 activation. For that, MEFs deficient for either ATG13 or ULK1/ULK2 were transfected with cDNAs encoding wild type ATG13 or ULK1, respectively. As determined by immunoblotting, loss of ATG13 also increases TBK1 activation, while loss of ULK1/2 only led to a slight increase. Nevertheless, the absence of FIP200 had the strongest effect on TBK1 activation (Figure **1C**). Interestingly, immunofluorescence analysis revealed that both TBK1 and FIP200 form dot structures in *atg13* KO cells (Figure **1D**). Transient expression of GST-TBK1 showed that the observed TBK1 and FIP200 puncta co-localize, and partially circular structures were detectable (Figure **1E**). Next, we analyzed whether FIP200 also influences TBK1 activation in human cell lines. Therefore, siRNA was used to reduce FIP200 levels in HeLa cells or differentiated THP-1 cells. Reduction of FIP200 by three different siRNAs increased TBK1 activation in both cell lines indicating a general validity of our observations (Figure

S1C). Collectively, these data suggest that autophagy in general and the ULK1 complex in particular are important for the regulation of TBK1 activation. Within the ULK1 complex, FIP200 seems to be the main effector controlling TBK1 activation.

Phospho-TBK1 aggregates are positive for the autophagy receptors TAX1BP1 and SQSTM1/p62

We observed that loss of FIP200 or deletion of its C terminus results in aberrant TBK1 accumulation. Normally, protein aggregates are cleared by autophagy. Since autophagy receptors recognize the cargo during selective autophagy and connect them to the autophagy machinery, we analyzed whether the receptors TAX1BP1, NDP52, OPTN and SQSTM1/p62 localize to TBK1 aggregates. As determined by immunofluorescence, TAX1BP1 and SQSTM1/p62 co-localize with TBK1 aggregates caused by loss of FIP200, while NDP52 and OPTN do not (Figure **2A**). Similar observations were made for cells expressing the C-terminally truncated version of FIP200 (Figure **2B**). It has previously been described that TBK1 phosphorylates SQSTM1/p62 at Ser403, and that this phosphorylation ensures an efficient autophagosomal engulfment of ubiquitinated mitochondria¹³. This phospho-SQSTM1/p62 is highly abundant within the TBK1-TAX1BP1-SQSTM1/p62 aggregates (Figure **2A** and **2B**). We also analyzed whether the C-terminally truncated variant of FIP200 gets recruited to the TBK1 aggregates. The expression of FIP200 Δ CT showed a cytosolic distribution and no co-localization with TBK1 aggregates (Figure **2B**). Additionally, some of the TBK1 positive aggregates caused by loss of FIP200 were positive for the autophagy marker LC3, and some were not. Similar observations were made for cells expressing FIP200 Δ CT (Figure **S2A**). It has been previously reported that the Golgi apparatus acts as platform for TBK1 activation³⁶. Thus, we aimed at investigating whether the TBK1 aggregates occur at specific organelles. Antibodies against ERGIC-53/p58, ERp72 and Golgin97 were used to stain the ER-Golgi intermediate compartment (ERGIC), the ER, or the Golgi complex, respectively. As determined by immunofluorescence, TBK1 aggregates do not co-localize with any of these organelles (Figure **S2B**).

Taken together, these data suggest that TBK1 accumulates together with TAX1BP1 and SQSTM1/p62 in large aggregates/condensates when binding to FIP200 is abolished.

TBK1 aggregation depends on TAX1BP1

Since we observed that TAX1BP1 co-localizes with TBK1 aggregates, we next asked whether the TBK1-SQSTM1/p62 aggregate formation itself depends on TAX1BP1. Therefore, we decreased TAX1BP1 expression by RNAi in *fip200* KO, FIP200 WT and FIP200 Δ CT cells and analyzed TBK1 activation and SQSTM1/p62 phosphorylation at Ser403 by immunoblotting. Although we clearly detected focal localization of TBK1 in FIP200 Δ CT cells (Figure **1A** and **1B**), the phospho-Ser172 signal detected by immunoblotting rather resembled the status of FIP200 WT cells. Knock-down of TAX1BP1 decreased TBK1 activation and SQSTM1/p62 phosphorylation in all cell lines (Figure **3A-C**). Interestingly, we observed that SQSTM1/p62 migrates at a higher molecular weight in *fip200* KO MEFs and in cells expressing the C-terminally truncated FIP200 variant, presumably reflecting increased phosphorylation of SQSTM1/p62, albeit not necessarily only at Ser403 (Figure **3A**). These results indicate that TBK1-SQSTM1/p62 aggregate formation and the phosphorylation of SQSTM1/p62 at Ser403 in those aggregates depend on the autophagy receptor TAX1BP1.

*Impaired autophagy in *fip200* KO MEFs contributes to aberrant TBK1 aggregation and activation*

Since defective autophagy increased TBK1 activation in *atg3* KO MEFs (Figure **S1B**), we next asked whether non-functional autophagy is the only mechanism leading to increased TBK1 activation in *fip200* KO MEFs. For that, we analyzed starvation-induced bulk autophagy. We performed an LC3 turnover assay in *fip200* KO, FIP200 WT and FIP200 Δ CT-expressing cells. Upon autophagy induction, lipidated LC3-II is increasingly generated and then degraded in autolysosomes³⁷. The V-ATPase inhibitor bafilomycin A₁ blocks lysosomal degradation leading to the accumulation of LC3-II³⁷. In *fip200*

KO MEFs, we observed LC3-II accumulation neither under normal nor under starvation conditions, again confirming defective autophagy signaling. However, expression of FIP200 WT and FIP200 Δ CT restored basal and starvation-induced autophagy (Figure **4A** and **4B**). Similar to *Atg3* WT cells (Figure **S1B**), TBK1 activation was increased in FIP200 WT and FIP200 Δ CT MEFs after inhibition of autophagy by bafilomycin A₁. Additionally, starvation led to reduced SQSTM1/p62 levels and decreased TBK1 phosphorylation. However, TBK1 and SQSTM1/p62 phosphorylation was increased in *fip200* KO cells and stayed unaffected under all treatment conditions (Figure **4A**). Again, FIP200 Δ CT cells rather resemble FIP200 WT cells during bulk autophagy with regard to TBK1 phosphorylation (see also Figure **3A**), whereas FIP200 Δ CT cells rather represent an intermediate status between *fip200* KO and FIP200 WT cells with regard to SQSTM1/p62 phosphorylation. Collectively, we conclude that the TBK1 accumulation in FIP200 Δ CT as detected by immunofluorescence (Figure **1A**) cannot solely be attributed to impaired autophagy signaling, since bulk autophagic flux appears rather normal in these cells.

Loss of FIP200 further enhances TBK1 accumulation and activation caused by defective autophagy

Since we observed a clear difference between *atg3* KO and *fip200* KO MEFs with regard to phospho-TBK1 accumulation by immunofluorescence (Figure **1A**) and a rather regular autophagic flux in FIP200 Δ CT cells (Figure **4A**), we speculated that inhibited autophagy cannot be the sole cause for this aberrant TBK1 activation. Accordingly, we next aimed at investigating whether loss of FIP200 in autophagy-deficient cells can further increase TBK1 accumulation and activation. We performed FIP200 knock-down experiments in *atg3* KO cells and analyzed TBK1 activation and SQSTM1/p62 phosphorylation by immunoblotting. siRNA-mediated reduction of FIP200 led to an increased TBK1 activation and SQSTM1/p62 phosphorylation in *atg3* KO MEFs (Figure **5A**). We also investigated TBK1 accumulation by immunofluorescence. Upon transfection of non-targeting or *Fip200* siRNA, we observed dot-like or circular TBK1 positive structures (Figure **5B** and **5C**). *Fip200* siRNA led to the removal of FIP200 from

those aggregates and to an increased size of these ring-shaped structures. Like in *fip200* KO cells, the TBK1 structures also contain phosphorylated SQSTM1/p62 (Figure 5C). Collectively, these data show that the combination of defective autophagy with the loss of FIP200 leads to an aberrant accumulation of TBK1-TAX1BP1-SQSTM1/p62 aggregates. It appears that the presence of FIP200 at these aggregates ensures the inducibility of TBK1 activation.

*The IFN- β response upon TLR3/TLR4 stimulation is not significantly affected in *fip200* KO or FIP200 Δ CT-expressing cells*

Since TBK1 is not only involved in autophagy signaling but also in the regulation of innate immune responses, we examined whether loss of FIP200 influences TLR3/TLR4-induced IFN- β production through TBK1-TAX1BP1-SQSTM1/p62 aggregate formation. Therefore, *fip200* KO, FIP200 WT and FIP200 Δ CT MEFs were either transfected with poly I:C or treated with LPS, and IFN- β gene expression was analyzed by RT-qPCR. In all three cell lines, poly I:C treatment resulted in a clear upregulation of IFN- β mRNA expression, whereas the response to LPS was rather weak (Figure 6A). Although TBK1 is highly activated in *fip200* KO MEFs, this did not result in increased IFN- β production under basal or stimulated conditions compared to FIP200 WT cells (Figure 6A). In contrast, IFN- β production appeared rather impaired in *fip200* KO and FIP200 Δ CT MEFs after poly I:C treatment, but these differences were statistically not significant (Figure 6A). Additionally, the receptors STING and TRIF, which recruit TBK1 during innate immune responses, do not co-localize with TBK1-TAX1BP1-SQSTM1/p62 aggregates (Figures S3A and S3B). Next to IFN- β production, we also examined TBK1 and SQSTM1/p62 phosphorylation by immunoblotting. Both poly I:C and LPS could not induce major changes in the (increased) phosphorylation status of TBK1 and SQSTM1/p62 in *fip200* KO MEFs (Figure 6B and 6C), whereas expression of wild-type FIP200 restored inducibility of TBK1 phosphorylation upon these treatments. In FIP200 Δ CT MEFs, poly I:C and LPS treatment also result in an increased TBK1 phosphorylation, accompanied by a simultaneous decrease of SQSTM1/p62 phosphorylation (Figure

6B and **6C**). Collectively, FIP200 deficiency seems to desensitize cells for TLR3/TLR4-engaging stimuli with regard to TBK1 activation. However, this does not result in increased IFN- β production under basal or TLR3/TLR4-stimulated conditions. If FIP200 is present but not capable of interacting with TAX1BP1 and/or SQSTM1/p62 (as in FIP200 Δ CT MEFs), the inducibility of TBK1 activation upon TLR3/TLR4 engagement is restored.

3. DISCUSSION

As component of the autophagy-inducing ULK1 complex, FIP200 is centrally involved in bulk and selective autophagy. However, FIP200 participates in several additional cellular signaling pathways³⁸. TBK1 is a central regulator of both autophagic and inflammatory signaling³⁹. Here, we observe that TBK1, TAX1BP1 and SQSTM1/p62 form protein aggregates in MEFs lacking FIP200. Within these structures, TBK1 becomes activated by trans-autophosphorylation and in turn phosphorylates SQSTM1/p62 at S403, thus further promoting SQSTM1/p62-ubiquitin condensates. TBK1 activation and SQSTM1/p62 phosphorylation depend on TAX1BP1, indicating that this autophagy receptor mediates the recruitment of TBK1 to SQSTM1/p62 condensates. We observed that TBK1 activation is strongly enhanced in cells lacking FIP200. On the one hand, this might be caused by the inhibition of autophagy and thus generally inhibited/reduced clearance of SQSTM1/p62 condensates. On the other hand, our data suggest that the constitutive binding of FIP200 to TBK1 via TAX1BP1 keeps TBK1 in an inducible status. Accordingly, FIP200 controls the TBK1 activation threshold at SQSTM1/p62-positive protein aggregates. Collectively, we hypothesize that the TAX1BP1-TBK1-phospho-SQSTM1/p62 axis represents a positive feedforward regulation of autophagy that is controlled by the recruitment of FIP200 (scheme depicted in Figure **S4**).

In 2008, it has been reported that FIP200 binds to ULK1/2 and is required for autophagosome formation³⁵. Since then, several reports have confirmed its central role for autophagy signaling, including selective autophagic processes. Studies using conditional *fip200* KO mice showed that loss of FIP200 leads to an accumulation of SQSTM1/p62 positive protein aggregates in osteoblasts⁴⁰, retinal pigment epithelium cells⁴¹, and mammary tumor cells⁴² due to an impairment of autophagy. Recent reports indicate that the recruitment of the ULK1 complex to damaged mitochondria or invading bacteria is mediated by the binding of FIP200 to the autophagy receptor NDP52^{7,8}. Furthermore, it has been described that the C-terminal claw domain of FIP200 binds to the autophagy receptor SQSTM1/p62 and thus promotes autophagosome formation at SQSTM1/p62-ubiquitin condensates³³. We observe that FIP200 also associates with the autophagy receptor TAX1BP1, also resulting in the

association of FIP200 with SQSTM1/p62-positive condensates. Furthermore, it appears that NDP52 and/or OPTN are not recruited to these structures. Generally, our observations are in line with a recent manuscript describing that the clearance of protein aggregates is mediated by TAX1BP1⁴³. Apparently, both SQSTM1/p62 and TAX1BP1 are present in protein aggregates and can recruit FIP200. The binding of FIP200 to these two autophagy receptors does not have to be mutually exclusive, since binding of TAX1BP1 (and NDP52) has been reported to occur outside the claw domain⁸. However, TAX1BP1 is clearly responsible for TBK1 activation and SQSTM1/p62 phosphorylation within these structures.

There exist several crosstalks between TBK1 and autophagy. On the one hand, TBK1 regulates several components of the autophagy signaling cascade, including AMPK¹⁰, syntaxin 17¹¹, or various autophagy receptors^{7,8,12-17}. We observe that the TBK1-dependent phosphorylation of SQSTM1/p62 at Ser403 is increased in *fip200* KO MEFs. This phosphorylation has been implicated in the SQSTM1/p62-dependent phase separation/clustering of polyubiquitinated proteins and the selective autophagic clearance of these protein aggregates^{18,44,45}. Furthermore, it has been confirmed that TBK1 can catalyze this phosphorylation^{13,14}. We think that the TAX1BP1-dependent recruitment of TBK1 to protein aggregates and the subsequent phosphorylation of SQSTM1/p62 at Ser403 represents a feedforward loop that ensures efficient phase separation, engulfment, and clearance of the cargo. Apparently, this function needs to be controlled by FIP200, since otherwise TBK1 might increase the size of the protein aggregates and potentially their insolubility by uncontrolled SQSTM1/p62 phosphorylation. This is in line with the observations by Turco et al., who reported that knockdown of FIP200 increases both numbers and volume of SQSTM1/p62 puncta³³. As mentioned above, SQSTM1/p62-positive protein aggregates have already been reported for different cell lines obtained from conditional *fip200* KO mice⁴⁰⁻⁴². Additionally, the generation of insoluble protein aggregates was prevented by TBK1 inhibition in hepatocytes⁴⁶. Interestingly, we observed that the phospho-Ser403 variant of SQSTM1/p62 shifted to a higher molecular weight. Phospho-Ser403 itself might contribute to this phenomenon; however, we cannot exclude that additional phosphorylation events are involved. Turco et al. reported that phosphorylation of the FIP200-interacting region in SQSTM1/p62

(i.e. Ser349/Thr350, Ser365, Ser366, Ser370/Thr375) increases its affinity to the FIP200 claw domain⁴⁷. It is possible that these phosphorylations are increased as a compensatory mechanism in order to counteract FIP200 deficiency and thus contribute to the altered molecular weight.

On the other hand, TBK1 activation is controlled by autophagy, and this is confirmed by our observations. We showed that inhibition of autophagy by targeting various autophagy-related genes (e.g. ATG3, FIP200, ATG13, ULK1) or by treatment with bafilomycin A₁ increase TBK1 activation. Furthermore, starvation-induced autophagy decreased TBK1 activation, while starvation did not have any effect on TBK1 activation in autophagy-incompetent cells. Yang et al. also observed that starvation-induced autophagy represses TBK1 activation, while inhibition increases its activity⁴⁸. The authors suggest that NDP52 and SQSTM1/p62 promote autophagy of phospho-TBK1 complexes⁴⁸. It has also been reported that TBK1 is directly targeted by ULK1¹⁰. Finally, Goodwin et al. analyzed TBK1 activation during lysosomal ferritin flux in cells deficient for either one of the ULK1 complex subunits. Similar to our results, they observed that FIP200 depletion had the highest impact on TBK1 activation, and they also observed TAX1BP1-TBK1-positive structures³⁴. In this case the authors suggest a compensatory relationship between the ULK1/2 complex and TBK1 activation at least for lysosomal ferritin flux³⁴. We think that FIP200 exerts an additional, specific function during aggrephagy/selective autophagy that cannot be compensated for by the other subunits of the ULK1 complex. Furthermore, we think that this additional function of FIP200 is independent of its autophagy-regulating function. This is supported by two observations. First, we detected increased phospho-TBK1 levels in cells deficient for ULK1/2, ATG13, or ATG3. However, these levels were still lower compared to *fip200* KO MEFs. We think that number and/or size of protein aggregates are increased in all these autophagy-incompetent/impaired cell lines, and that this effect certainly contributes to TBK1 activation. However, these data simultaneously suggest that the recruitment of the ULK1 complex is not the sole function of FIP200 during aggrephagy. Of note, Turco et al. reported that ULK1 is still recruited to SQSTM1/p62 condensates in cells lacking FIP200, but that ATG16L1 recruitment is abolished³³. This observation was recently substantiated by a preprint of the same group, reporting that FIP200 is dispensable for the

recruitment of the upstream autophagy machinery to the condensates, but it is necessary for phosphatidylinositol 3-phosphate formation, WIPI2 recruitment, and activation of the ULK1 kinase ⁴⁹. Second, we observed increased p-TBK1 levels in cells expressing the Δ CT variant of FIP200. However, in these cells starvation-induced autophagy occurred regularly. It has been reported that the ULK1 complex is organized by a C-shaped FIP200 N-terminal domain dimer ⁵⁰. Accordingly, it might be possible that the C-terminal domain of FIP200 exerts some additional functions that might be independent of its canonical autophagy function. Of note, Jun-Lin Guan's group has recently reported that FIP200 can limit AZI2/NAP1-TBK1-IRF signaling independent of its canonical autophagy function ^{51,52}. They propose that—in *fip200* KO cells—phospho-TBK1-containing phase condensates accumulate, resulting in TBK1 hyperactivation and sustained pro-inflammatory signaling ^{51,52}. This is in line with a report describing that cellular stress leads to the incorporation of the TBK1 adaptors TBKBP1/SINTBAD and AZI2/NAP1 into membraneless organelles that control the threshold of TBK1 activation ⁵³. It remains to be investigated whether the TBKBP1/SINTBAD-AZI2/NAP1-membraneless organelles and the SQSTM1/p62-aggregates represent different or overlapping phase condensates. We detect TBKBP1/SINTBAD in our mass spectrometric analyses of anti-FIP200 immunopurificates (see Table S1), but we do not observe differences in TBKBP1/SINTBAD puncta formation in FIP200 WT, FIP200 Δ CT or *fip200* KO cells (data not shown). It is tempting to speculate that different compositions of phase condensates can regulate different TBK1 signaling outcomes in different cellular systems. Here, we do not observe an effect on IFN- β production, but on SQSTM1/p62 phosphorylation. Generally, the relative contribution of the different protein-protein interactions for the heterotrimeric control of TBK1 activation at phase condensates awaits further clarification, i.e. between FIP200 and TAX1BP1 (this report and ⁸), between TAX1BP1 and TBKBP1/SINTBAD or AZI2/NAP1 ¹⁶, and between FIP200 and TBKBP1/SINTBAD or AZI2/NAP1 ^{8,51}. Furthermore, it has been suggested that TAX1BP1 can directly associate with TBK1 ¹², adding another level of complexity. Currently, we speculate that the binding of FIP200 to TAX1BP1 and/or TBKBP1/SINTBAD-AZI2/NAP1 is sufficient for the control of TBK1 activation, either by mediating the selective removal of TBK1 or by steric hindrance of TBK1 trans-autophosphorylation.

The involvement of LC3 in this process (removal of SQSTM1/p62 condensates and/or regulation of TBK1 activation) awaits further clarification. In the above mentioned study of TBK1 hyperactivation at phase condensates, the authors make use of a FIP200 variant that cannot bind ATG13 anymore⁵¹. In cells expressing this mutant, LC3 lipidation is blocked⁵⁴. The authors speculate that FIP200 can—through its ability to bind cargo receptors—bypass the need for LC3 and initiate phagophore formation at the cargo during selective autophagy⁵². However, alternative recruitment mechanisms might also play a role. It has been reported that the deletion of the FIP200 claw domain does not completely prevent the targeting of SQSTM1/p62-positive cargo to lysosomes³³, and that there is residual LC3 lipidation in cells expressing a FIP200 claw domain mutant that cannot bind to SQSTM1/p62⁴⁹. We clearly observe partial co-localization of LC3 and TBK1 in both *fip200* KO cells and cells expressing our Δ CT variant that is lacking both the interaction site with TAX1BP1 and the claw domain. So far, we cannot differentiate whether this is caused by an alternative recruitment of the LC3 lipidation machinery or perhaps by a lipidation-independent recruitment of LC3 molecules.

Protein aggregates are a hallmark of neurodegenerative diseases. Additionally, several mutations in *TBK1* have been identified that underlie neuroinflammatory diseases and dysregulation of TBK1 is strongly connected to them (reviewed in³⁰). For example, treatment with the TBK1 inhibitor BX795 abrogated the aberrant insolubility of an optineurin mutant (E50K) that can be found in patients suffering from normal-tension glaucoma (NTG)⁵⁵. Additionally, amyotrophic lateral sclerosis (ALS)-associated *TBK1* mutations affect phosphorylation of different autophagy receptors⁵⁶. Similarly, FIP200 has been assigned a role in neuronal homeostasis. Liang et al. reported that neural-specific loss of FIP200 resulted in cerebellar degeneration accompanied by progressive neuronal loss, spongiosis, and neurite degeneration⁵⁷. The authors also reported the accumulation of SQSTM1/p62 and ubiquitinated protein aggregates⁵⁷. Interestingly, the authors also state that the observed phenotypes were earlier and partially more severe in neural-specific FIP200 conditional KO mice compared to Atg5 or Atg7 conditional KO mice⁵⁷. We speculate that the FIP200-dependent regulation of TBK1 activity at SQSTM1/p62 condensates might contribute to these observations, establishing the enforced

recruitment of FIP200 to these condensates—next to the pharmacological regulation of TBK1 activity—
as a promising therapeutic approach.

4. MATERIAL & METHODS

Antibodies and reagents

Antibodies against β -Actin (WB: 1:20000, clone AC-74, Sigma-Aldrich, #A5316), ATG13 (1:1000, Sigma-Aldrich, #SAB4200100), ATG3 (WB: 1:1000, Cell Signaling Technology, #3415), ERGIC-53/p58 (IF: 1:25, Sigma-Aldrich, #E1031), ERp72 (IF: 1:100, clone D70D12, Cell Signaling Technology, #5033), FIP200 (IF: 1:500, Proteintech, #17250-1-AP or WB: 1:1000, Bethyl Laboratories, #A301-536A or WB: 1:1000, Bethyl Laboratories, #A301-574A, used for THP-1 and HeLa cells), FLAG (WB: 1:1000, clone M2, Sigma-Aldrich, #F1804), GAPDH (WB: 1:5000, clone 6C5, Abcam, #ab8245), GFP (WB: 1:1000, clone 3H9, ChromoTek, #3H9), Golgin97 (IF: 1:100, clone D8P2K, Cell Signaling Technology, #13192), GST (IF: 1:800, clone 26H1, Cell Signaling Technology, #2624), LC3B (WB: 1:1000, IF: 1:200, Cell Signaling Technology, #2775), NDP52 (IF: 1:50, Proteintech, #12229-1-AP), OPTN (IF: 1:50, Proteintech, #10837-1-AP), SQSTM1/p62 (WB: 1:1000, PROGEN, #GP62-C), SQSTM1/p62 pS403 (WB: 1:1000, IF: 1:400, clone D8D6T, Cell Signaling Technology, #39786), STING (IF: 1:100, Proteintech, #19851-1-AP), TAX1BP1 (IF: 1:50, Proteintech, #14424-1-AP or WB: 1:1000, Bethyl Laboratories, #A303-792A), TBK1 (IF: 1:50, WB: 1:1000, clone A-6, Santa Cruz Biotechnology, #sc-398366 or WB: 1:1000, clone D1B4, Cell Signaling Technology, #3504, used for THP-1 and HeLa cells), TBK1 pS172 (IF: 1:50, WB: 1:1000, clone D52C2, Cell Signaling Technology, #5483), TRIF (IF: 1:100, clone E-7, Santa Cruz Biotechnology, #sc-514384), ULK1 (1:1000, clone D8H5, Cell Signaling Technology, #8054), Vinculin (WB: 1:2000, clone hVIN-1, Sigma-Aldrich, #V9131) were used. For immunoblot analyses IRDye[®]800- or IRDye[®]680-conjugated secondary antibodies were used (LI-COR Biosciences, #926-68070, #926-68071 and #926-32211). The secondary antibodies for immunofluorescence analyses were purchased from Jackson ImmunoResearch (Alexa Fluor 488-AffiniPure Goat Anti-Rabbit IgG, 1:500, #111-545-003 and Alexa Fluor 647-AffiniPure Goat Anti-Mouse IgG, 1:500, #115-605-003). Other reagents used were bafilomycin A₁ (BafA₁; Sigma-Aldrich, #B1793), lipopolysaccharides from Escherichia coli O55:B5 (LPS; Sigma-Aldrich, #L4524), PMA (Sigma-Aldrich, #P1585), polyinosinic–polycytidylic acid (poly I:C; Sigma-

Aldrich, #P9582), puromycin (InvivoGen, #ant-pr). Dimethyl sulfoxide (DMSO; AppliChem, #A3672) was used to dissolve BafA₁.

Constructs and siRNAs

Human cDNA encoding FLAG-tagged full-length FIP200 (isoform 1) was amplified from p3xFLAG-CMV10-hFIP200 (kindly provided by Noboru Mizushima and previously described in ³⁵; Addgene plasmid #24300; <http://n2t.net/addgene:24300>; RRID:Addgene_24300) and cloned into the multiple cloning site of the oncoretroviral vector S9112Pco. This vector expressed the FIP200 cDNA and also an internal ribosomal entry site (IRES)-puromycin resistance gene (*paca*) cassette, optimized for human codon usage using the GeneArt online tool (Thermo Fisher Scientific), under control of the SFFV promoter in the 5'LTR. The codons encoding the C terminus of FIP200 (aa1369-1594, CT) were removed by site-directed mutagenesis using Q5 High-Fidelity 2X Master Mix (New England BioLabs, #M0492). Sequences of oligonucleotides used for mutagenesis PCRs were TAAAATTCTGCAGTCGAC (FIP200 Δ1369-1594 fwd) and TATCAAATCTTTATCCCGTTC (FIP200 Δ1369-1594 rev). The FIP200-encoding S9112Pco vectors (both full length and ΔCT) harbor cDNAs that encode the amino acid exchange D818Y. Human cDNA encoding FLAG-tagged full-length ULK1 was cloned into pMSCVpuro. Mouse Fip200 (ON-TARGETplus siRNA SMARTpool, #L-041191-01-0005), mouse Tax1bp1 (ON-TARGETplus siRNA SMARTpool, #L-055360-01-0005) and negative control (ON-TARGETplus non-targeting pool, #D-001810-10-20) siRNAs were obtained from Dharmacon (Horizon Discovery Group). Human FIP200 (#HSS114818 [#1], #HSS114819 [#2] and #HSS190643 [#3]), human GAPDH (#12935-140, RNAi Positive Control) and negative control (#12935-300, Medium GC Duplex) Stealth siRNAs were obtained from Thermo Fisher Scientific. Lipofectamine RNAiMAX (Thermo Fisher Scientific, #13778-150) was used as transfection reagent to knockdown Fip200 and Tax1bp1 in MEF cells and Viromer Blue (Biozym Scientific, #230005) to knockdown FIP200 and GAPDH in HeLa and THP-1 cells. 72 h after transfection, cells were harvested for immunoblotting or fixed and stained for immunofluorescence.

Cell lines

Fip200 KO MEFs were kindly provided by Jun-Lin Guan (Department of Cancer Biology, University of Cincinnati College of Medicine, Cincinnati, Ohio, USA) and have been described previously⁵⁸. *Ulk1/2* DKO MEFs were kindly provided by Tullia Lindsten (Memorial Sloan Kettering Cancer Center, New York City, New York, USA) and have been described previously⁵⁹. Plat-E cells were kindly provided by Toshio Kitamura (Institute of Medical Science, University of Tokyo, Japan) and have been described previously⁶⁰. Plat-E cells were transfected with 1.9 µg of the S9112Pco- or pMSCV-based retroviral vectors using FuGENE® 6 Transfection Reagent (Promega, #E2692) to produce recombinant retroviruses. After 48 h, retroviral supernatant was collected and added together with 3 µg/ml polybrene (Sigma, #9268) to *fip200* KO or *ulk1/2* DKO MEFs expressing mCit-hLC3, respectively. After 72 h, cells were selected in puromycin-containing medium (2.5 µg/ml). *Atg13* KO MEFs were kindly provided by Noboru Mizushima (Department of Biochemistry and Molecular Biology, Graduate School and Faculty of Medicine, University of Tokyo, Japan), and their reconstitution has been described previously⁶¹. Wild type and *atg3* KO MEFs were kindly provided by Masaaki Komatsu (Department of Physiology, Juntendo University Graduate School of Medicine, Tokyo, Japan) and have been described previously⁶². Wild type HeLa cells were kindly provided by Richard J. Youle (National Institute of Neurological Disorders and Stroke, Bethesda, Maryland, USA). THP-1 cells were obtained from Leibniz Institute DSMZ-German Collection of Microorganisms and Cell Cultures (#ACC 16). The procedure how to generate Flp-In™ T-REx™ 293 cells inducibly expressing a protein of interest has been previously described⁶³. Briefly, full-length human FIP200 cDNA was amplified and cloned into the vector pcDNA5/FRT/TO-GFP. The expression constructs (GFP or GFP-FIP200) were then co-transfected with pOG44 into Flp-In™ T-REx™ 293 cells (Invitrogen, R780-07). Stable transfectants were selected with 200 µg/ml hygromycin B (Invitrogen, 10687-010) and 5 µg/ml blasticidin (Invitrogen, A11139-02). MEFs, HeLa and Flp-In™ T-REx™ 293 cells were cultured in high D-glucose Dulbecco's Modified Eagle's Medium (DMEM, Thermo Fisher Scientific, #41965-039) supplemented with 10% FCS (GE Healthcare,

#A15-101 or Thermo Fisher Scientific, #10270-106), 100 U/ml penicillin and 100 µg/ml streptomycin at 37°C and 5% CO₂. THP-1 cells were cultured in Roswell Park Memorial Institute (RPMI) 1640 Medium (Thermo Fisher Scientific, #61870-010) supplemented with 10% FCS, 100 U/ml penicillin, 100 µg/ml streptomycin and 10 mM HEPES solution (Sigma-Aldrich, #H0887). For amino acid starvation, cells were washed once with PBS and starved in EBSS (Thermo Fisher Scientific, #24010043) for 2 h. For the induction of GFP or GFP-FIP200 expression, Flp-In™ T-REx™ 293 cells were incubated in full medium including 0.1 doxycycline (Clontech Laboratories, #631311) for 16 h.

Immunofluorescence

For immunofluorescence microscopy, MEFs were seeded on glass coverslips (Marienfeld). For staining of total TBK1, cells were fixed in cold methanol for 15 min at 4°C. Whenever total TBK1 was not stained, cells were fixed in 4% paraformaldehyde for 15 min at 4°C, quenched with 50 mM NH₄Cl for 15 min and permeabilized with 50 µg/ml digitonin (Sigma-Aldrich, #D141) for 5 min. Fixed samples were blocked with 3% BSA (Roth, #8076) for 30 min and incubated with primary antibodies diluted in 3% BSA for 1-2 h. Afterwards, samples were washed three times with PBS, incubated with secondary antibodies diluted in 3% BSA for 30 min, washed once with 0.2% Tween-20 (Sigma-Aldrich, #P1379) and three times with PBS. Finally, cells were embedded in ProLong Glass Antifade Mountant (Thermo Fisher Scientific, #P36980) containing 1 µg/ml DAPI (Roth, #6335.1). Representative images were collected with an Axio Observer 7 fluorescence microscope (Carl Zeiss Microscopy) using a 40x/1,4 Oil DIC M27 Plan-Apochromat objective (Carl Zeiss Microscopy) and an ApoTome 2 (Carl Zeiss Microscopy). A lateral shift of the channel 647 was corrected using ZEN 2.3 (Carl Zeiss Microscopy) as follows: $x = -0.82 \text{ px}$ (63.5 nm) and $y = 0.52 \text{ px}$ (40.3 nm). Estimation of the average displacement values was determined by five images of multispectral beads (FocalCheck™ fluorescence microscope test slide #1 A5, Invitrogen, # F36909) and the analysis is based on the channel registration tool of the NanoJ toolbox for ImageJ using a single block to obtain linear displacement values⁶⁴. The pixel intensities of

the areas indicated by dashed red arrows were measured with ZEN 2.3 lite (Carl Zeiss microscopy) and depicted in histograms.

Immunoblotting and immunopurification

For immunoblotting, cells were harvested following the indicated treatment, pelleted, flash frozen and lysed in lysis buffer (50 mM Tris-HCl, pH7.5, 150 mM NaCl, 1 mM EDTA, 1 mM EGTA, 10 μ M Na₂MoO₄, 1 mM Na₃VO₄, 50 mM NaF, 5 mM Na₄P₂O₇, 1% [v/v] TritonX-100 [Carl Roth, #3051.2], and protease inhibitor cocktail [Sigma-Aldrich, #P2714]) for 30 min on ice. Lysates were clarified by centrifugation at 18,000 rcf and 4°C for 15 min. Equal protein amounts were determined by Bradford method, prepared by addition of sample buffer (125 mM Tris-HCl, pH 6.8, 17.2% [v/v] glycerol, 4.1% [w/v] SDS [AppliChem GmbH, #A7249], 200 μ g/ml bromophenol blue, 2% [v/v] β -mercaptoethanol), heated to 95°C for 5 min and subjected to SDS-PAGE. Afterwards, proteins were transferred to PVDF membranes (Merck Millipore, #IPFL00010) and analyzed using the indicated primary antibodies and appropriate secondary antibodies (LI-COR Biosciences). Signals were detected using an Odyssey® Infrared Imaging system (LI-COR Biosciences) and quantified by Image Studio 5.25 (LI-COR Biosciences). For affinity purification of GFP-tagged proteins, cells were flash frozen and lysed in lysis buffer containing 0.3% CHAPS (Roth, #1479.2) as detergent. Lysates were clarified and incubated with GFP-trap® beads (ChromoTek, #gta-200) overnight with rotation. Purified proteins were washed three times with lysis buffer and analyzed by immunoblotting.

Reverse transcription quantitative PCR (RT-qPCR)

Total RNA was isolated from approximately 1×10^6 cells using the NucleoSpin® RNA II Kit (Macherey-Nagel, #740955.250) according to the manufacturer's instructions. Isolated RNA was either directly used for reverse transcription reaction or stored at -80 °C. First strand cDNA was generated using the

High-Capacity cDNA Reverse Transcription Kit (Thermo Fisher Scientific, # #4368814) according to the manufacturer's instructions. For that, 1 µg of isolated total RNA plus additional RNase inhibitor (Thermo Fisher Scientific, #10777019) were used in standard cycling conditions (10 min at 25 °C, 120 min at 37 °C, 5 min at 85 °C). Generated cDNAs were directly used for qPCR or stored at -20 °C. Quantitative PCR analysis was performed using the Applied Biosystems 7300 Real Time PCR System (Thermo Fisher Scientific) and GoTaq® qPCR Master Mix (Promega, #A6001). Sequences of oligonucleotides used for RT-qPCRs were TGACAGGATGCAGAAGGAGA (β-Actin left), CGCTCAGGAGGAGCAATG (β-Actin right), CAGGCAACCTTTAAGCATCAG (IFN-β left), and CCTTTGACCTTCAAATGCAG (IFN-β right). For each gene, technical triplicates were prepared, each containing 25 ng of total cDNA and a primer concentration of 500 nM. Amplification was done by a standard temperature profile (2 min at 50 °C, 10 min at 95 °C, 40 cycles of 15 s at 95 °C and 1 min 60 °C) followed by a dissociation run (15 s at 95 °C, 1 min at 60 °C, gradual increase of 1 °C/min up to 95 °C). Threshold (CT) values were computed automatically. Relative gene expression was calculated by the 2- $\Delta\Delta$ CT method and β-Actin was used as a reference gene. Additionally, values were normalized to control samples. Experiments were performed in triplicates.

In-Gel Digestion and Mass Spectrometry

For MS analysis, gel pieces were reduced and alkylated followed by digestion with trypsin as described elsewhere. Peptides were extracted with 0.1% trifluoroacetic acid and subjected to liquid chromatography. For peptide separation over a 130 min LC gradient, an Ultimate 3000 Rapid Separation liquid chromatography system (Dionex/Thermo Scientific, Idstein, Germany) equipped with an Acclaim PepMap 100 C18 column (75 µm inner diameter, 25 cm length, 2 µm particle size from Thermo Scientific, Bremen, Germany) was used. MS analysis was carried out on an Orbitrap Elite mass spectrometer (Thermo Scientific, Bremen, Germany) operating in positive mode and equipped with a nano electrospray ionization source. Capillary temperature was set to 275°C and source voltage to

1.4 kV. Survey scans were carried out in the Orbitrap mass analyzer over a mass range from 350 to 1700 m/z at a resolution of 60 000 (at 400 m/z). The target value for the automatic gain control was 1 000 000, and the maximum fill time was 200 ms. The 20 most intense peptide ions (minimal signal intensity 500, excluding singly charged ions and ions with a charge state of four and up) were isolated, transferred to the linear ion trap (LTQ) part of the instrument and fragmented using collision-induced dissociation. Peptide fragments were analyzed using a maximal fill time of 200 ms and automatic gain control target value of 100 000 with the mass range set in dependency of parent mass using normal scan mode. Already fragmented ions were excluded for fragmentation for 45 s.

Computational mass spectrometric data analysis

Peptide and protein identification and quantification was done using MaxQuant (version 1.5.0.3, MPI for Biochemistry, Planegg, Germany) applying standard parameters. Searches were carried out based on 20183 *Homo sapiens* protein entries downloaded from the UniProtKB on 26th November 2014. Methionine oxidation and acetylation at protein N-termini were set as variable modification and carbamidomethylations at cysteines were considered as fixed modification. Peptides and proteins were accepted with a false discovery rate set to 1%. Unique and razor peptides were used for label-free quantification. The minimal ratio count was set to two and the matched between runs option was enabled. The normalized intensities as provided by MaxQuant were analyzed using Perseus framework (version 1.5.0.15, MPI for Biochemistry, Planegg, Germany). Only proteins with a minimum of 3 valid values in total were taken into consideration for protein quantification. Proteins which were identified only by site or marked as contaminant (from the MaxQuant contaminant list) were excluded from the analysis. For the calculation of enriched proteins in the two groups a Student's t-test was applied. The significance analysis was applied on log₂ transformed values after replacing missing values from a normal distribution (Width 0.3, Down shift 1.5) using a S0 constant = 0 and a 5% false discovery rate

based cutoff. The mass spectrometry proteomics data has been deposited to the ProteomeXchange Consortium via the PRIDE partner repository with the data set identifier PXD022563.

Statistical analysis

For immunoblotting, the density of each protein band was divided by the average of the densities of all bands from the same protein on the membrane. The resulting ratios of the proteins of interest were normalized to the ratio of the corresponding loading control and fold changes were calculated by dividing each normalized density ratio by the average of the density ratios of the indicated control lane (control lane: fold change = 1.00, $n \geq 3$). For immunofluorescence analyses, dots and nuclei were quantified and analyzed using ImageJ 1.53c. A dot-to-nuclei ratio was calculated to determine the number of dots per cell. Macros used for quantifications are provided in Table **S2**. At least 50 cells per experiment were analyzed in three biological replicates. For comparisons between different groups a two-way ANOVA was performed using GraphPad Prism 7 (GraphPad Software).

ACKNOWLEDGMENTS

We thank Jun-Lin Guan for providing *fip200* KO MEFs. We thank Tullia Lindsten for providing *ulk1/2* DKO MEFs. We thank Masaaki Komatsu for providing *atg3* KO MEFs. We thank Noboru Mizushima for providing *atg13* KO MEFs. We thank Toshio Kitamura for providing Plat-E cells. We thank Richard J. Youle for providing wild-type HeLa cells. We thank Antje Löffler, Maria Deak and Dario Alessi for generating the Flp-In™ T-REx™ 293 cells inducibly expressing GFP or GFP-FIP200. We thank Stefanie Scheu and Shafaqat Ali for providing IFN- β primer sequences. This work was supported by the Deutsche Forschungsgemeinschaft STO 864/4-1, STO 864/5-1, STO 864/6-1 and GRK 2158 (to BS), and the Düsseldorf School of Oncology (to BS; funded by the Comprehensive Cancer Center Düsseldorf/Deutsche Krebshilfe and the Medical Faculty of the Heinrich-Heine-University Düsseldorf).

CONFLICT OF INTEREST STATEMENT

The authors declare that there are no competing financial interests in relation to the work described.

DATA AVAILABILITY STATEMENT

Further information and requests for resources and reagents should be directed to and will be fulfilled by the corresponding author. Plasmids generated in this study are available from the corresponding author without restriction upon request. The mass spectrometry proteomics data have been deposited to the ProteomeXchange Consortium ⁶⁵ via the PRIDE ⁶⁶ partner repository with the dataset identifier PXD022563.

AUTHOR CONTRIBUTION STATEMENT

DS designed the experiments, performed mutagenesis, and generated cell lines (FIP200+ULK1). DS performed immunofluorescence and immunoblot analyses, and supported RT-qPCR analyses. NB performed RT-qPCR analyses. JD performed cloning of cDNA constructs (FLAG-ULK1) and provided expertise on statistics. NWH performed cloning of cDNA constructs and generated cell lines (ATG13). CW and HH supported retroviral infections. OF, AS and KS performed mass spectrometric analyses and initial validation experiments. WW, FS, YS, LB, AF, MJM, and CP gave technical support. DS and BS analyzed and interpreted the data and wrote the manuscript. BS supervised the project. All authors discussed the results and commented on the manuscript.

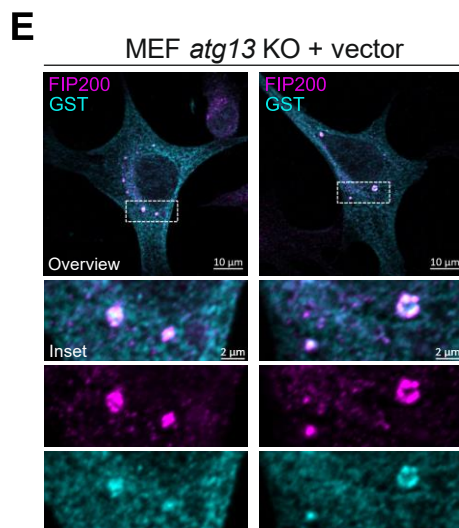
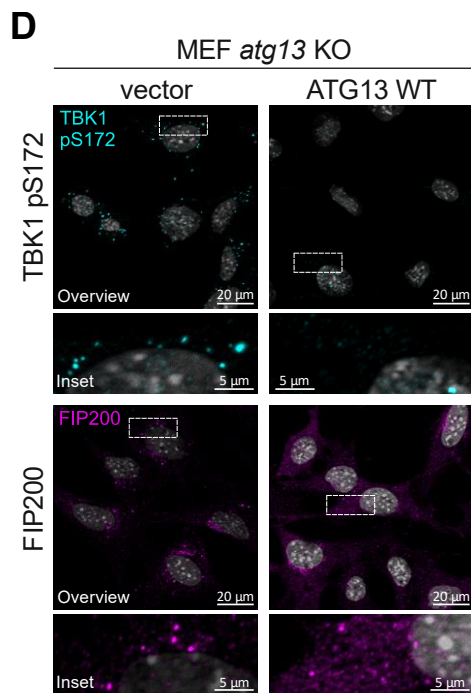
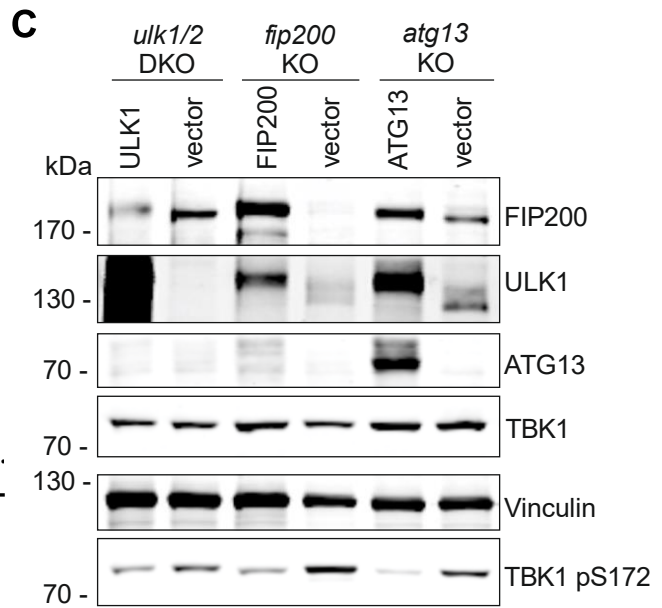
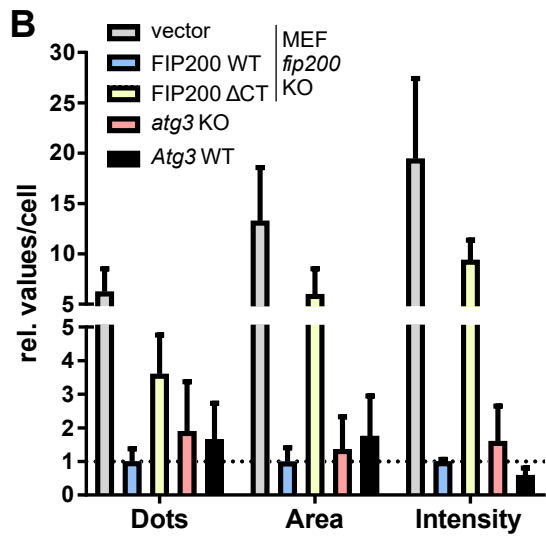
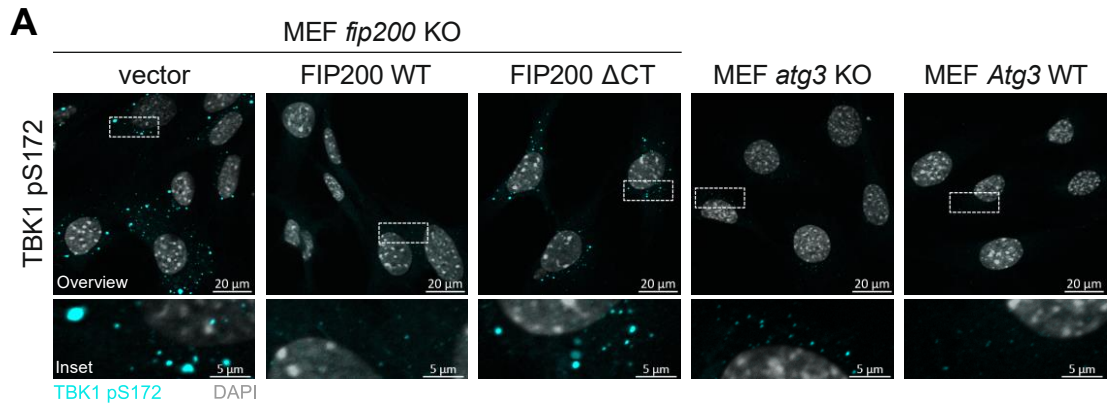


Figure 1: Loss of components of the ULK1 complex leads to an aberrant accumulation and increased activation of TBK1. (A+B) *fip200* KO MEFs were transfected with empty vector or with cDNA encoding full length FIP200 (FIP200 WT) or a C-terminally truncated FIP200 (aa 1369-1594, FIP200 ΔCT). These transfectants, *atg3* KO and *Atg3* WT MEFs were fixed in 4% PFA and immunostained for TBK1 pS172. (A) Representative sections are depicted and (B) the number, area, and intensity of TBK1 pS172 positive structures of at least 198 cells per cell line were quantified using ImageJ 1.53c and normalized to FIP200 WT cells. The means + SD of three independent experiments are shown. (C) Cleared cellular lysates of MEF *ulk1/2* DKO, *fip200* KO and *atg13* KO MEFs transfected with an empty vector or the respective wild type cDNA (ULK1, FIP200 or ATG13) were immunoblotted for the indicated proteins. (D) *atg13* KO MEFs transfected with an empty vector or cDNA encoding wild type ATG13 were fixed in 4% PFA and immunostained for TBK1 pS172 and FIP200. Representative sections are depicted. (E) For co-staining of TBK1 and FIP200, *atg13* KO MEFs were transiently transfected with cDNA encoding GST-TBK1, fixed in 4% PFA, and immunostained for FIP200 and GST. Representative sections are depicted. For immunofluorescence imaging, DAPI was used to stain nuclei.

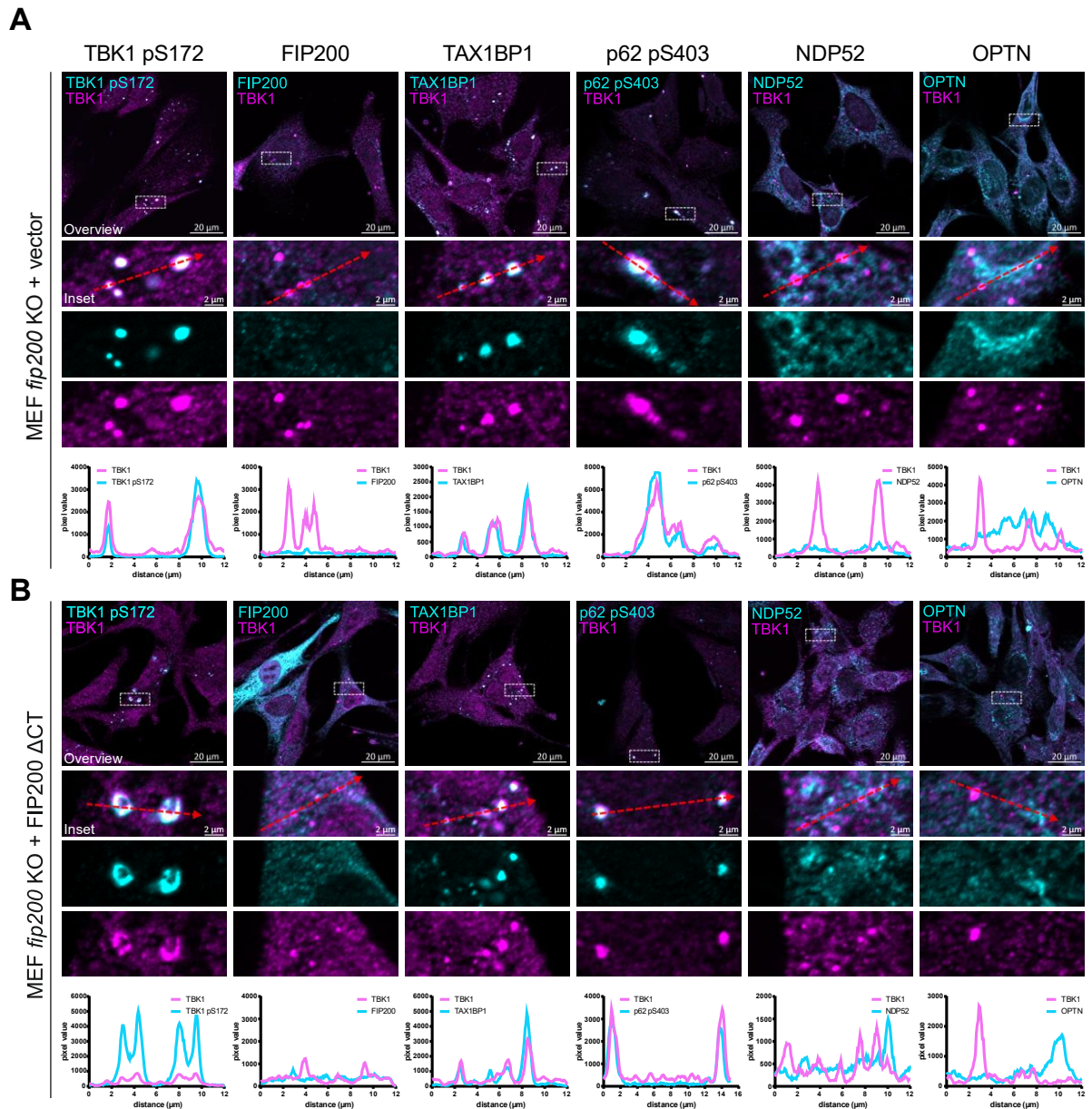


Figure 2: TBK1 aggregates are positive for the autophagy receptors TAX1BP1 and SQSTM1/p62 pS403. (A+B) *fip200* KO MEFs transfected with empty vector (A) or cDNA encoding FIP200 Δ CT (B) were fixed in 100% MeOH and immunostained for TBK1 in combination with either TBK1 pS172, FIP200, SQSTM1/p62 pS403, NDP52, or OPTN. Representative sections of three independent experiments are depicted. Histograms represent pixel intensities of the areas indicated by the respective dashed red arrow shown in the insets.

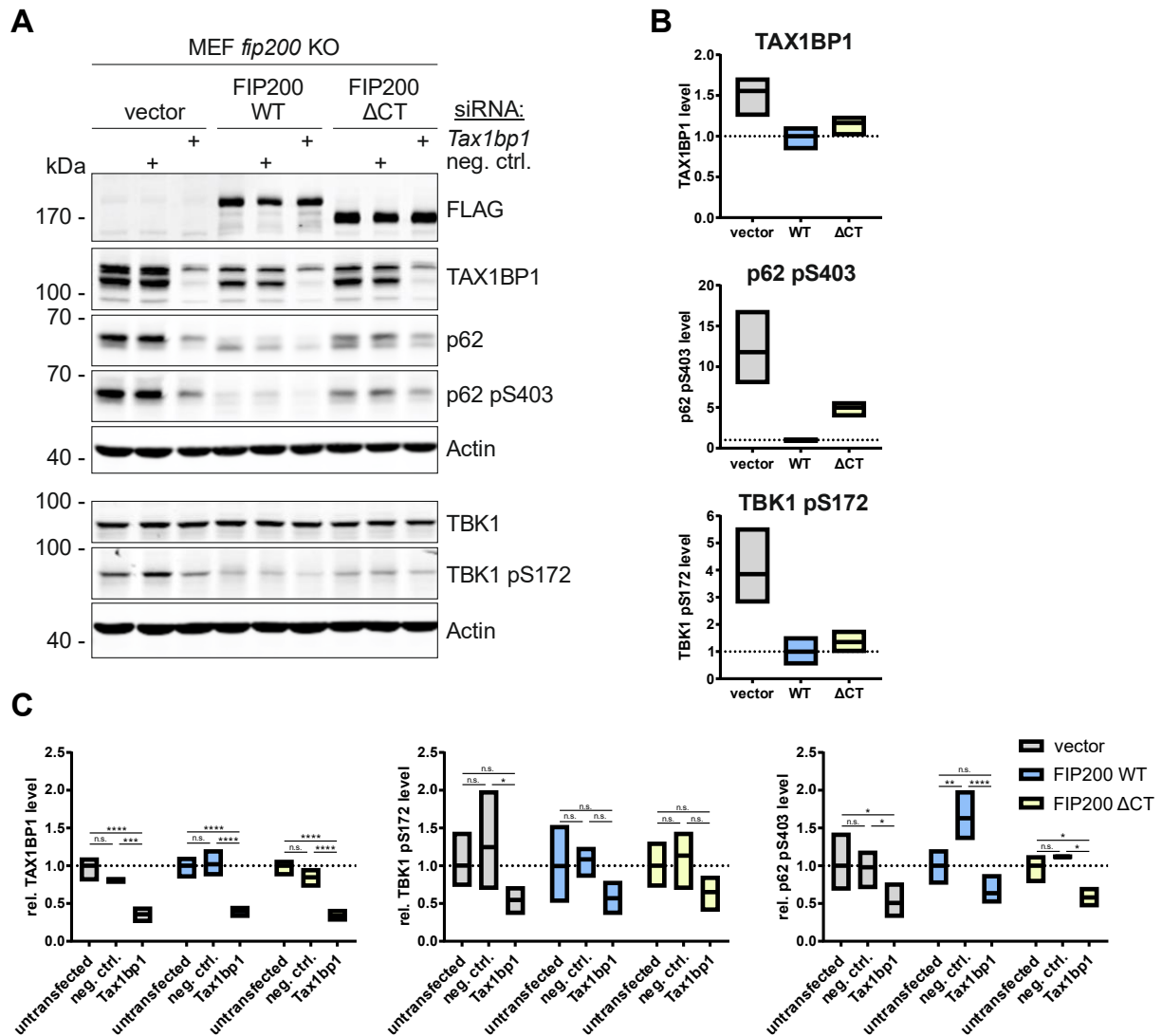


Figure 3: Aberrant TBK1 accumulation depends on TAX1BP1. (A) *fip200* KO, FIP200 WT, and FIP200 ΔCT MEFs were transfected with either 20 nM negative control siRNA or *Tax1bp1* siRNA for 72 h and cleared cellular lysates were immunoblotted for the indicated proteins. The FIP200 cDNAs used for the reconstitution of *fip200* KO MEFs encode an N-terminal FLAG peptide. Densities of bands on immunoblots of three independent experiments were quantified and normalized to Actin. (B) To compare basal expression levels between the used cell lines, the normalized densities of the untransfected samples were normalized to the signal of FIP200 WT MEFs. (C) To analyze the influence of siRNA transfection, the normalized densities of all samples of each cell line were normalized to the corresponding untransfected sample. Only relative levels of TAX1BP1, TBK1 pS172, and SQSTM1/p62 pS403 are shown. Boxes represent the highest and the lowest value, while the centerline shows the

mean. Two-way ANOVA with uncorrected Fisher's LSD test was used to determine differences between treatments. n.s. = not significant; * $p < 0.05$; ** $p < 0.01$; *** $p < 0.001$; **** $p < 0.0001$.

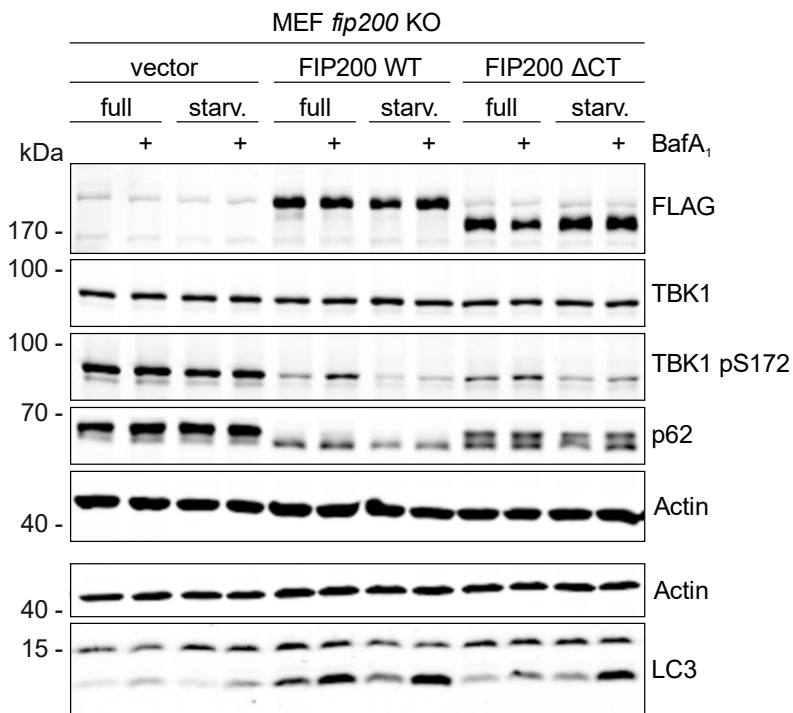
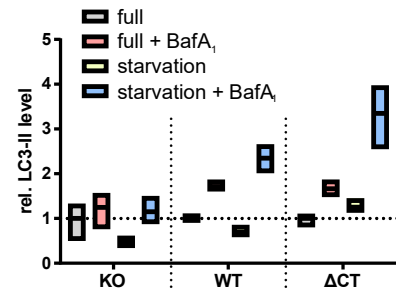
A**B**

Figure 4: The C-Terminus of FIP200 is dispensable for starvation-induced autophagy. (A) *fip200* KO, FIP200 WT, and FIP200 ΔCT MEFs were cultured in full or starvation (EBSS) medium either in the absence or presence of 10 nM bafilomycin A₁ (BafA₁) for 2 h. Cleared cellular lysates were immunoblotted for the indicated proteins. The FIP200 cDNAs used for the reconstitution of *fip200* KO MEFs encode an N-terminal FLAG peptide. (B) Densities of bands on immunoblots of three independent experiments were quantified and normalized to Actin. The normalized densities of all samples of each cell line were then normalized to the respective untreated control sample. Only relative levels of LC3-II are shown. Boxes represent the highest and the lowest value, while the centerline shows the mean.

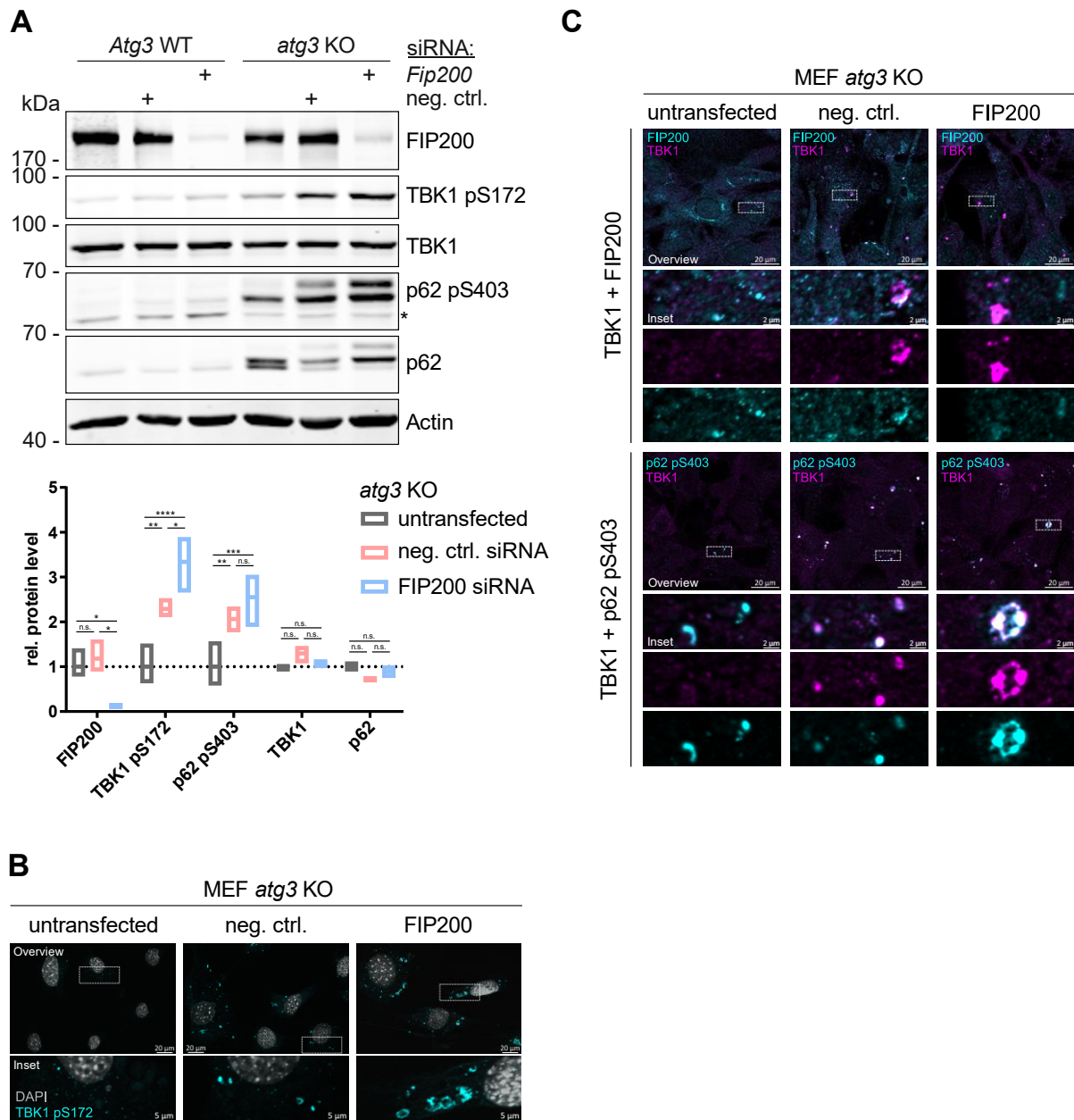


Figure 5: Loss of FIP200 further enhances TBK1 accumulation and activation caused by defective autophagy. (A) *Atg3* WT and *atg3* KO MEFs were transfected with either 20 nM negative control siRNA or *Fip200* siRNA for 72 h and cleared cellular lysates were immunoblotted for the indicated proteins. The asterisk indicates a non-specific band. Densities of bands on immunoblots of three independent experiments were quantified and normalized to Actin. For each protein, the normalized densities of *atg3* KO samples were normalized to the respective untransfected sample. Boxes represent the highest and the lowest value, while the centerline shows the mean. Two-way ANOVA with Tukey's multiple comparisons test was used to determine differences between treatments. n.s. = not significant;

* $p < 0.05$; ** $p < 0.01$; *** $p < 0.001$; **** $p < 0.0001$. (**B+C**) *atg3* KO MEFs were transfected with either 20 nM negative control siRNA or Fip200 siRNA for 72 h, and immunostained for TBK1 pS172 (B; fixed in 4% PFA) or TBK1 in combination with either FIP200 or SQSTM1/p62 pS403 (C; fixed in 100% MeOH).

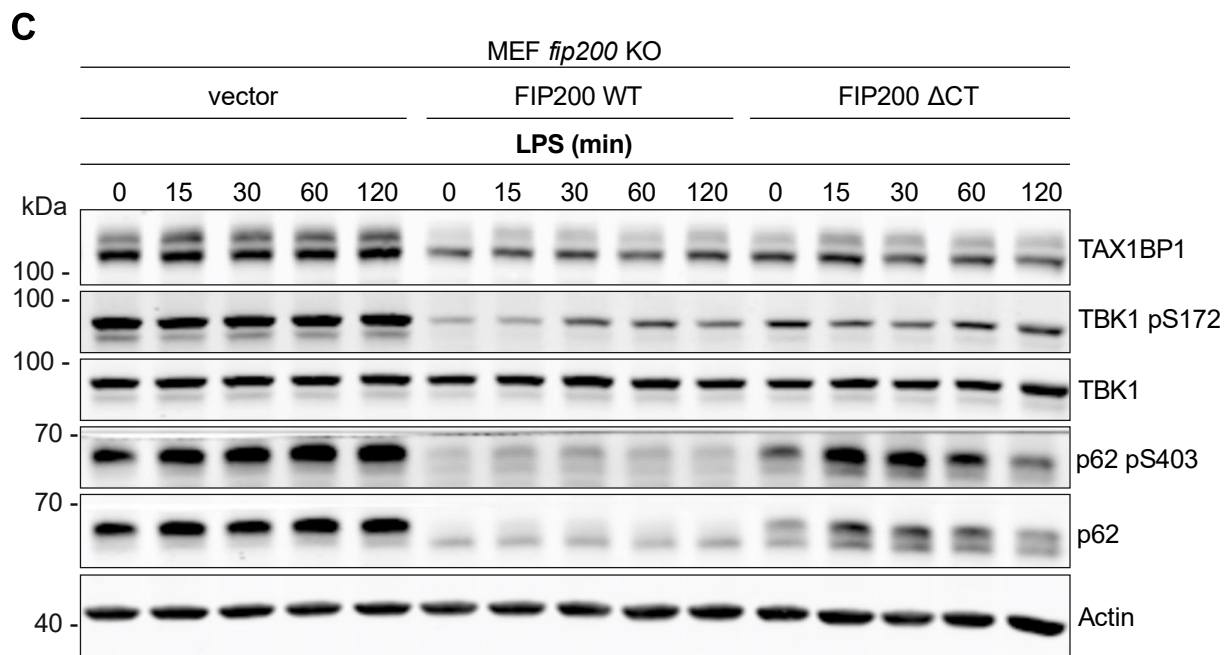
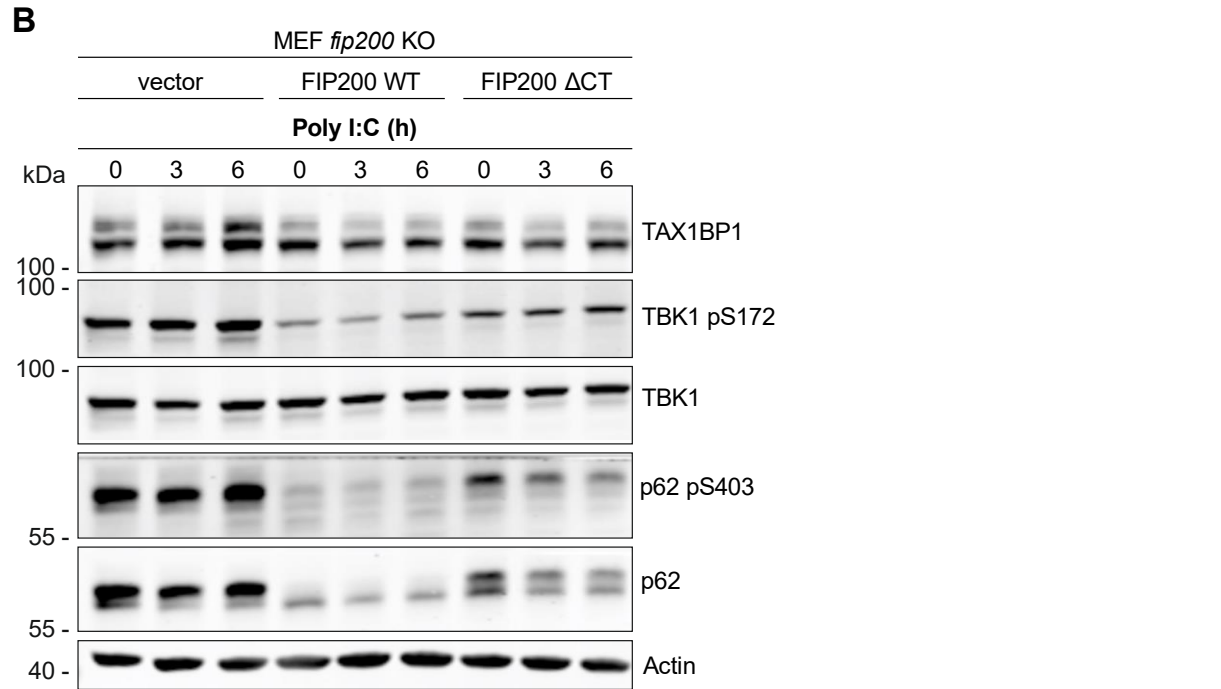
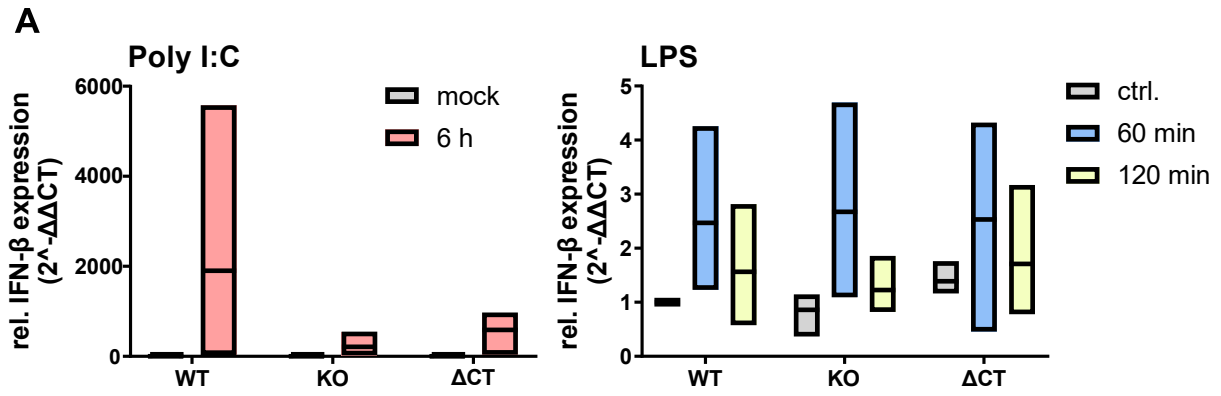


Figure 6: FIP200 deficiency desensitizes cells for TLR3/TLR4-engaging stimuli. (A-C) *fip200* KO, FIP200 WT, and FIP200 Δ CT MEFs were transfected with 2 μ g/ml poly I:C or treated with 1 μ g/ml LPS for the indicated time points. dH₂O was used for mock transfection. (A) RT-qPCR analyses were performed to determine the relative IFN- β expression. All values were normalized to control samples of FIP200 WT MEFs. Boxes represent the highest and the lowest value, while the centerline shows the mean of three independent experiments. Additionally, lysates of poly I:C transfected (B) or LPS treated cells (C) were immunoblotted for the indicated proteins. Representative immunoblots of three independent experiments are depicted.

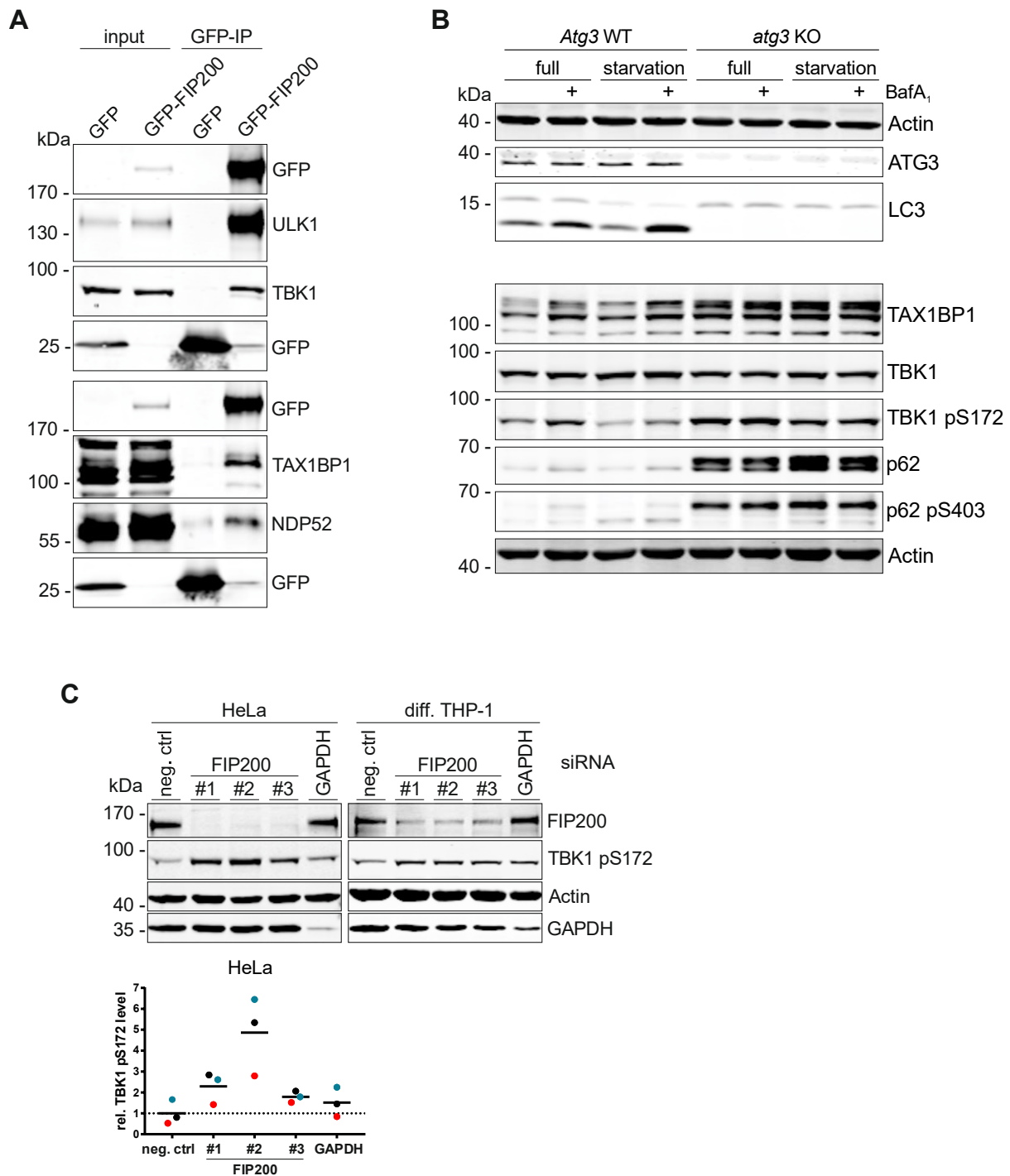
REFERENCES

- 1 Wesselborg, S. & Stork, B. Autophagy signal transduction by ATG proteins: from hierarchies to networks. *Cellular and Molecular Life Sciences*, doi:10.1007/s00018-015-2034-8 (2015).
- 2 Mizushima, N., Yoshimori, T. & Ohsumi, Y. The role of Atg proteins in autophagosome formation. *Annu Rev Cell Dev Biol* **27**, 107-132, doi:10.1146/annurev-cellbio-092910-154005 (2011).
- 3 Rogov, V., Dotsch, V., Johansen, T. & Kirkin, V. Interactions between autophagy receptors and ubiquitin-like proteins form the molecular basis for selective autophagy. *Mol Cell* **53**, 167-178, doi:10.1016/j.molcel.2013.12.014 (2014).
- 4 Johansen, T. & Lamark, T. Selective Autophagy: ATG8 Family Proteins, LIR Motifs and Cargo Receptors. *J Mol Biol* **432**, 80-103, doi:10.1016/j.jmb.2019.07.016 (2020).
- 5 Kirkin, V. & Rogov, V. V. A Diversity of Selective Autophagy Receptors Determines the Specificity of the Autophagy Pathway. *Molecular Cell* **76**, 268-285, doi:10.1016/j.molcel.2019.09.005 (2019).
- 6 Mizushima, N. The ATG conjugation systems in autophagy. *Current Opinion in Cell Biology* **63**, 1-10, doi:10.1016/j.ceb.2019.12.001 (2020).
- 7 Vargas, J. N. S. *et al.* Spatiotemporal Control of ULK1 Activation by NDP52 and TBK1 during Selective Autophagy. *Molecular Cell* **74**, 347-362.e346, doi:10.1016/j.molcel.2019.02.010 (2019).
- 8 Ravenhill, B. J. *et al.* The Cargo Receptor NDP52 Initiates Selective Autophagy by Recruiting the ULK Complex to Cytosol-Invading Bacteria. *Molecular Cell* **74**, 320-329.e326, doi:10.1016/j.molcel.2019.01.041 (2019).
- 9 Walker, S. A. & Ktistakis, N. T. Autophagosome Biogenesis Machinery. *Journal of Molecular Biology*, doi:10.1016/j.jmb.2019.10.027 (2019).
- 10 Zhao, P. *et al.* TBK1 at the Crossroads of Inflammation and Energy Homeostasis in Adipose Tissue. *Cell* **172**, 731-743.e712, doi:10.1016/j.cell.2018.01.007 (2018).
- 11 Kumar, S. *et al.* Phosphorylation of Syntaxin 17 by TBK1 Controls Autophagy Initiation. *Developmental Cell* **49**, 130-144.e136, doi:10.1016/j.devcel.2019.01.027 (2019).
- 12 Fu, T. *et al.* Mechanistic insights into the interactions of NAP1 with the SKICH domains of NDP52 and TAX1BP1. *Proceedings of the National Academy of Sciences of the United States of America* **115**, E11651-E11660, doi:10.1073/pnas.1811421115 (2018).
- 13 Matsumoto, G., Shimogori, T., Hattori, N. & Nukina, N. TBK1 controls autophagosomal engulfment of polyubiquitinated mitochondria through p62/SQSTM1 phosphorylation. *Human molecular genetics* **24**, 4429-4442, doi:10.1093/hmg/ddv179 (2015).
- 14 Pilli, M. *et al.* TBK-1 Promotes Autophagy-Mediated Antimicrobial Defense by Controlling Autophagosome Maturation. *Immunity* **37**, 223-234, doi:10.1016/j.immuni.2012.04.015 (2012).
- 15 Richter, B. *et al.* Phosphorylation of OPTN by TBK1 enhances its binding to Ub chains and promotes selective autophagy of damaged mitochondria. *Proceedings of the National Academy of Sciences*, 201523926-201523926, doi:10.1073/pnas.1523926113 (2016).
- 16 Thurston, T. L., Ryzhakov, G., Bloor, S., von Muhlinen, N. & Randow, F. The TBK1 adaptor and autophagy receptor NDP52 restricts the proliferation of ubiquitin-coated bacteria. *Nature immunology* **10**, 1215-1221, doi:10.1038/ni.1800 (2009).
- 17 Wild, P. *et al.* Phosphorylation of the autophagy receptor optineurin restricts Salmonella growth. *Science* **333**, 228-233, doi:10.1126/science.1205405 (2011).
- 18 Matsumoto, G., Wada, K., Okuno, M., Kurosawa, M. & Nukina, N. Serine 403 phosphorylation of p62/SQSTM1 regulates selective autophagic clearance of ubiquitinated proteins. *Mol Cell* **44**, 279-289, doi:10.1016/j.molcel.2011.07.039 (2011).
- 19 Koyama, S., Ishii, K. J., Coban, C. & Akira, S. Innate immune response to viral infection. *Cytokine* **43**, 336-341, doi:10.1016/j.cyto.2008.07.009 (2008).
- 20 Liu, S. *et al.* Phosphorylation of innate immune adaptor proteins MAVS, STING, and TRIF induces IRF3 activation. *Science* **347**, aaa2630-aaa2630, doi:10.1126/science.aaa2630 (2015).
- 21 Helgason, E., Phung, Q. T. & Dueber, E. C. Recent insights into the complexity of Tank-binding kinase 1 signaling networks: The emerging role of cellular localization in the activation and

- substrate specificity of TBK1. *FEBS Letters* **587**, 1230-1237, doi:10.1016/j.febslet.2013.01.059 (2013).
- 22 Ma, X. *et al.* Molecular basis of Tank-binding kinase 1 activation by transautophosphorylation. *Proceedings of the National Academy of Sciences* **109**, 9378-9383, doi:10.1073/pnas.1121552109 (2012).
 - 23 Tamura, T., Yanai, H., Savitsky, D. & Taniguchi, T. The IRF family transcription factors in immunity and oncogenesis. *Annu Rev Immunol* **26**, 535-584, doi:10.1146/annurev.immunol.26.021607.090400 (2008).
 - 24 Shi, C. S. & Kehrl, J. H. MyD88 and Trif target Beclin 1 to trigger autophagy in macrophages. *J Biol Chem* **283**, 33175-33182, doi:10.1074/jbc.M804478200 (2008).
 - 25 Pattingre, S. *et al.* Bcl-2 antiapoptotic proteins inhibit Beclin 1-dependent autophagy. *Cell* **122**, 927-939, doi:10.1016/j.cell.2005.07.002 (2005).
 - 26 Galluzzi, L. & Green, D. R. Autophagy-Independent Functions of the Autophagy Machinery. *Cell* **177**, 1682-1699, doi:10.1016/j.cell.2019.05.026 (2019).
 - 27 Jounai, N. *et al.* The Atg5 Atg12 conjugate associates with innate antiviral immune responses. *Proc Natl Acad Sci U S A* **104**, 14050-14055, doi:10.1073/pnas.0704014104 (2007).
 - 28 Yang, Q. *et al.* TRIM32-TAX1BP1-dependent selective autophagic degradation of TRIF negatively regulates TLR3/4-mediated innate immune responses. *PLoS Pathogens* **13**, 1-21, doi:10.1371/journal.ppat.1006600 (2017).
 - 29 Parvatiyar, K., Barber, G. N. & Harhaj, E. W. TAX1BP1 and A20 inhibit antiviral signaling by targeting TBK1-IKKi kinases. *J Biol Chem* **285**, 14999-15009, doi:10.1074/jbc.M110.109819 (2010).
 - 30 Ahmad, L., Zhang, S. Y., Casanova, J. L. & Sancho-Shimizu, V. Human TBK1: A Gatekeeper of Neuroinflammation. *Trends in Molecular Medicine* **22**, 511-527, doi:10.1016/j.molmed.2016.04.006 (2016).
 - 31 Freischmidt, A. *et al.* Haploinsufficiency of TBK1 causes familial ALS and fronto-temporal dementia. *Nature Neuroscience* **18**, 631-636, doi:10.1038/nn.4000 (2015).
 - 32 Cirulli, E. T. *et al.* Exome sequencing in amyotrophic lateral sclerosis identifies risk genes and pathways. *Science* **347**, 1436-1441, doi:10.1126/science.aaa3650 (2015).
 - 33 Turco, E. *et al.* FIP200 Claw Domain Binding to p62 Promotes Autophagosome Formation at Ubiquitin Condensates. *Molecular Cell* **74**, 330-346.e311, doi:10.1016/j.molcel.2019.01.035 (2019).
 - 34 Goodwin, J. M. *et al.* Autophagy-Independent Lysosomal Targeting Regulated by ULK1/2-FIP200 and ATG9. *Cell Reports* **20**, 2341-2356, doi:10.1016/j.celrep.2017.08.034 (2017).
 - 35 Hara, T. *et al.* FIP200, a ULK-interacting protein, is required for autophagosome formation in mammalian cells. *J Cell Biol* **181**, 497-510, doi:10.1083/jcb.200712064 (2008).
 - 36 Pourcelot, M. *et al.* The Golgi apparatus acts as a platform for TBK1 activation after viral RNA sensing. *BMC Biol* **14**, 69, doi:10.1186/s12915-016-0292-z (2016).
 - 37 Klionsky, D. J. *et al.* Guidelines for the use and interpretation of assays for monitoring autophagy (3rd edition). *Autophagy* **12**, 1-222, doi:10.1080/15548627.2015.1100356 (2016).
 - 38 Gan, B. & Guan, J. L. FIP200, a key signaling node to coordinately regulate various cellular processes. *Cellular Signalling* **20**, 787-794, doi:10.1016/j.cellsig.2007.10.021 (2008).
 - 39 Louis, C., Burns, C. & Wicks, I. TANK-Binding Kinase 1-Dependent Responses in Health and Autoimmunity. *Frontiers in immunology* **9**, 434, doi:10.3389/fimmu.2018.00434 (2018).
 - 40 Liu, F. *et al.* Suppression of autophagy by FIP200 deletion leads to osteopenia in mice through the inhibition of osteoblast terminal differentiation. *Journal of Bone and Mineral Research* **28**, 2414-2430, doi:10.1002/jbmr.1971 (2013).
 - 41 Yao, J. *et al.* Deletion of autophagy inducer RB1CC1 results in degeneration of the retinal pigment epithelium. *Autophagy* **11**, 939-953, doi:10.1080/15548627.2015.1041699 (2015).
 - 42 Wei, H. *et al.* Suppression of autophagy by FIP200 deletion inhibits mammary tumorigenesis. *Genes & Development*, doi:10.1101/gad.2051011 (2011).
 - 43 Sarraf, S. A. *et al.* Loss of TAX1BP1-Directed Autophagy Results in Protein Aggregate Accumulation in the Brain. *Mol Cell*, doi:10.1016/j.molcel.2020.10.041 (2020).

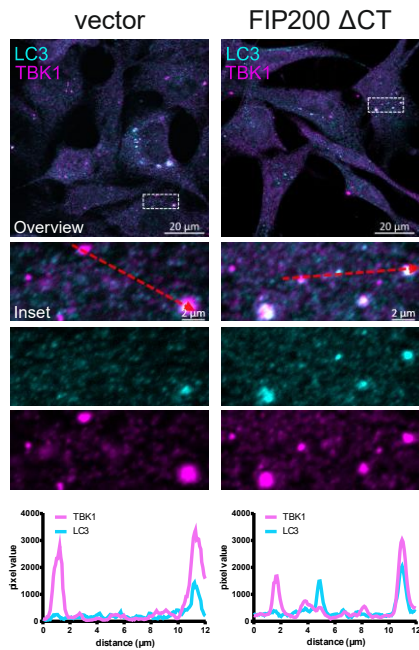
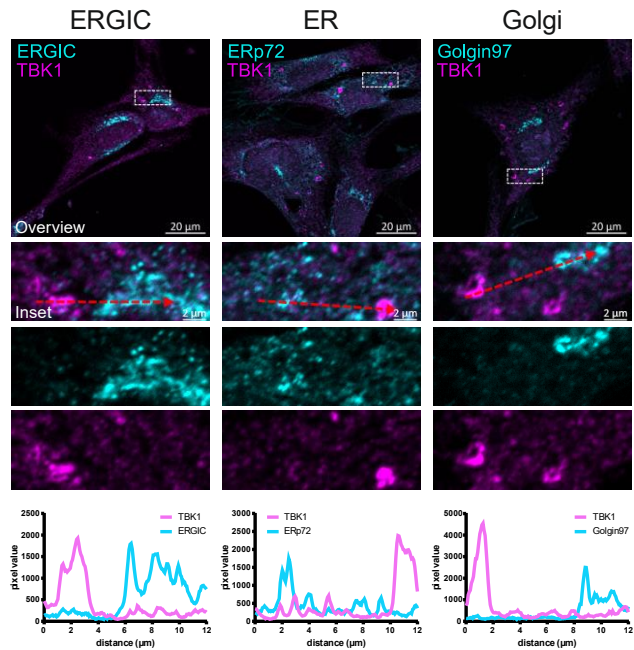
- 44 Sun, D., Wu, R., Zheng, J., Li, P. & Yu, L. Polyubiquitin chain-induced p62 phase separation drives autophagic cargo segregation. *Cell Res* **28**, 405-415, doi:10.1038/s41422-018-0017-7 (2018).
- 45 Zaffagnini, G. *et al.* P62 Filaments Capture and Present Ubiquitinated Cargos for Autophagy. *The EMBO Journal* **37**, 1-21, doi:10.15252/emj.201798308 (2018).
- 46 Cho, C. S. *et al.* Lipotoxicity induces hepatic protein inclusions through TANK binding kinase 1-mediated p62/sequestosome 1 phosphorylation. *Hepatology* **68**, 1331-1346, doi:10.1002/hep.29742 (2018).
- 47 Turco, E., Fracchiolla, D. & Martens, S. Recruitment and Activation of the ULK1/Atg1 Kinase Complex in Selective Autophagy. *Journal of Molecular Biology* **432**, 123-134, doi:10.1016/j.jmb.2019.07.027 (2020).
- 48 Yang, S. *et al.* Autophagy Inhibition Dysregulates TBK1 Signaling and Promotes Pancreatic Inflammation. *Cancer Immunology Research* **4**, 520-530, doi:10.1158/2326-6066.CIR-15-0235 (2016).
- 49 Turco, E., Fischer, I. & Martens, S. FIP200 organizes the autophagy machinery at p62-ubiquitin condensates beyond activation of the ULK1 kinase. *bioRxiv*, 2020.2007.2007.191189, doi:10.1101/2020.07.07.191189 (2020).
- 50 Shi, X. *et al.* ULK complex organization in autophagy by a C-shaped FIP200 N-terminal domain dimer. *J Cell Biol* **219**, doi:10.1083/jcb.201911047 (2020).
- 51 Okamoto, T. *et al.* FIP200 Suppresses Immune Checkpoint Therapy Responses in Breast Cancers by Limiting AZI2/TBK1/IRF Signaling Independent of Its Canonical Autophagy Function. *Cancer research* **80**, 3580-3592, doi:10.1158/0008-5472.CAN-20-0519 (2020).
- 52 Yeo, S. K., Wang, C. & Guan, J. L. Role of FIP200 in inflammatory processes beyond its canonical autophagy function. *Biochemical Society transactions* **48**, 1599-1607, doi:10.1042/BST20191156 (2020).
- 53 Saul, V. V. *et al.* ULK1/2 Restricts the Formation of Inducible SINT-Speckles, Membraneless Organelles Controlling the Threshold of TBK1 Activation. *iScience* **19**, 527-544, doi:10.1016/j.isci.2019.08.001 (2019).
- 54 Chen, S. *et al.* Distinct roles of autophagy-dependent and -independent functions of FIP200 revealed by generation and analysis of a mutant knock-in mouse model. *Genes Dev* **30**, 856-869, doi:10.1101/gad.276428.115 (2016).
- 55 Minegishi, Y. *et al.* Enhanced optineurin E50K-TBK1 interaction evokes protein insolubility and initiates familial primary open-angle glaucoma. *Hum Mol Genet* **22**, 3559-3567, doi:10.1093/hmg/ddt210 (2013).
- 56 Ye, J. *et al.* Effects of ALS-associated TANK binding kinase 1 mutations on protein-protein interactions and kinase activity. *Proc Natl Acad Sci U S A* **116**, 24517-24526, doi:10.1073/pnas.1915732116 (2019).
- 57 Liang, C. C., Wang, C., Peng, X., Gan, B. & Guan, J. L. Neural-specific deletion of FIP200 leads to cerebellar degeneration caused by increased neuronal death and axon degeneration. *J Biol Chem* **285**, 3499-3509, doi:10.1074/jbc.M109.072389 (2010).
- 58 Gan, B. *et al.* Role of FIP200 in cardiac and liver development and its regulation of TNFalpha and TSC-mTOR signaling pathways. *J Cell Biol* **175**, 121-133, doi:10.1083/jcb.200604129 (2006).
- 59 Cheong, H., Lindsten, T., Wu, J., Lu, C. & Thompson, C. B. Ammonia-induced autophagy is independent of ULK1/ULK2 kinases. *Proc Natl Acad Sci U S A* **108**, 11121-11126, doi:10.1073/pnas.1107969108 (2011).
- 60 Morita, S., Kojima, T. & Kitamura, T. Plat-E: an efficient and stable system for transient packaging of retroviruses. *Gene therapy* **7**, 1063-1066, doi:10.1038/sj.gt.3301206 (2000).
- 61 Wallot-Hieke, N. *et al.* Systematic analysis of ATG13 domain requirements for autophagy induction. *Autophagy* **14**, 743-763, doi:10.1080/15548627.2017.1387342 (2018).
- 62 Sou, Y. S. *et al.* The Atg8 conjugation system is indispensable for proper development of autophagic isolation membranes in mice. *Molecular biology of the cell* **19**, 4762-4775, doi:10.1091/mbc.E08-03-0309 (2008).
- 63 Löffler, A. S. *et al.* Ulk1-mediated phosphorylation of AMPK constitutes a negative regulatory feedback loop. *Autophagy* **7**, 696-706, doi:10.4161/auto.7.7.15451 (2011).

- 64 Laine, R. F. *et al.* NanoJ: a high-performance open-source super-resolution microscopy toolbox. *Journal of physics D: Applied physics* **52**, 163001, doi:10.1088/1361-6463/ab0261 (2019).
- 65 Deutsch, E. W. *et al.* The ProteomeXchange consortium in 2020: enabling 'big data' approaches in proteomics. *Nucleic acids research* **48**, D1145-D1152, doi:10.1093/nar/gkz984 (2020).
- 66 Perez-Riverol, Y. *et al.* The PRIDE database and related tools and resources in 2019: improving support for quantification data. *Nucleic acids research* **47**, D442-D450, doi:10.1093/nar/gky1106 (2019).

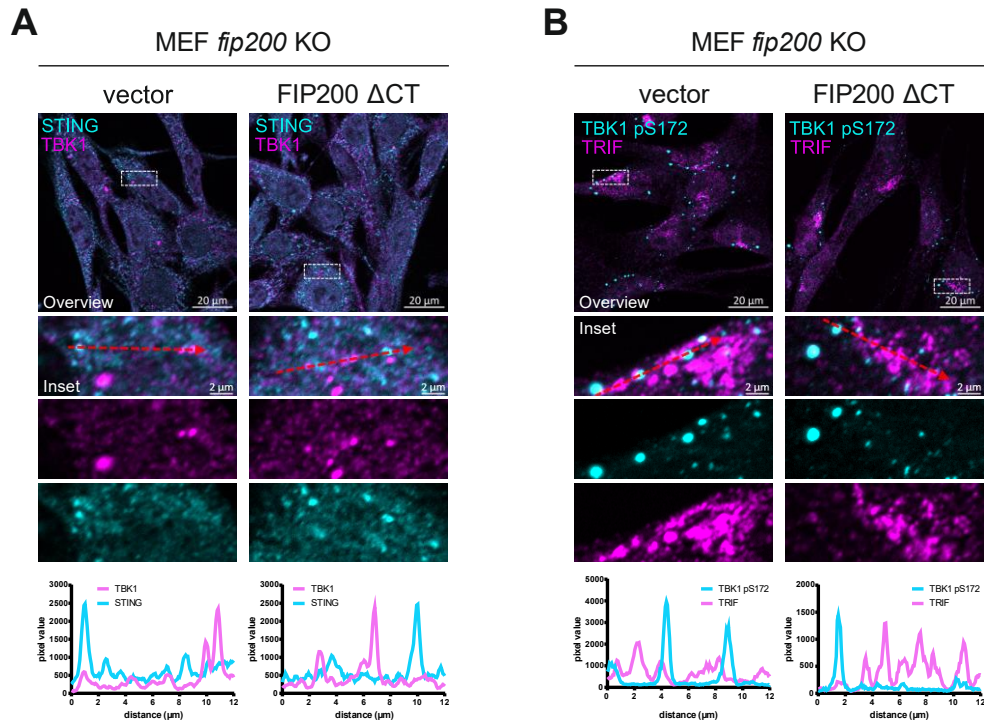


Supplementary Figure S1: FIP200 interacts with TBK1, and TBK1 activation is increased in *atg3* KO MEFs or in human cells treated with *FIP200* siRNA. (A) Flp-In™ T-REx™ 293 cells inducibly expressing GFP or GFP-FIP200 were treated with 0.1 µg/ml doxycycline for 16 h to induce expression. Afterwards, GFP proteins were purified overnight using GFP-trap® beads. Cleared cellular lysates (input) and purified proteins were immunoblotted for the indicated proteins. **(B)** *Atg3* WT and *atg3* KO MEFs were cultured in full or starvation (EBSS) medium either in the absence or presence of 10 nM bafilomycin A₁

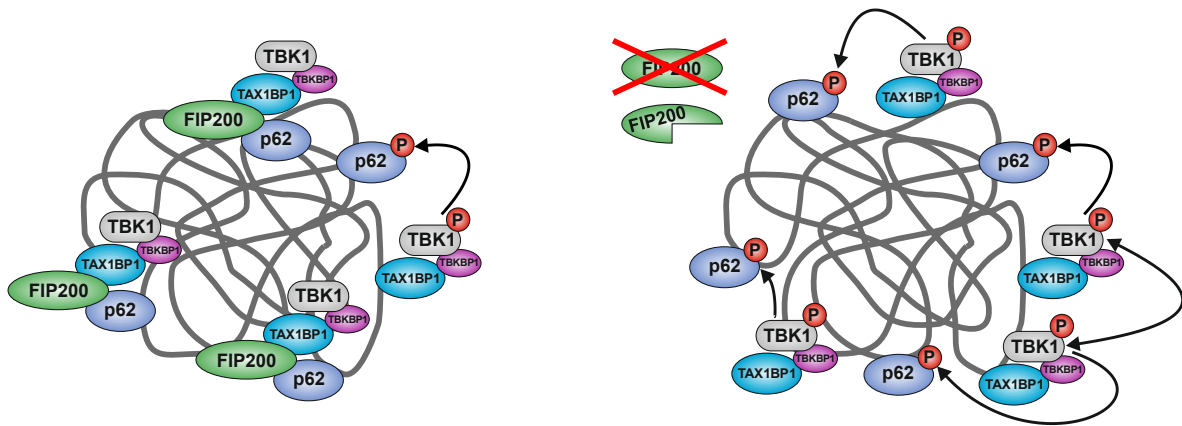
(BafA₁) for 2 h. Cleared cellular lysates were immunoblotted for the indicated proteins. (C) THP-1 cells were incubated with 100 ng/ml PMA for 72 h to induce differentiation. HeLa and differentiated THP-1 cells were transfected with either 20 nM negative control siRNA, FIP200 siRNA (#1, #2 or #3), or GAPDH siRNA for 72 h. Cleared cellular lysates were immunoblotted for the indicated proteins. For HeLa cells, densities of bands on immunoblots of three independent experiments were quantified and normalized to Actin. All values were then normalized to the samples transfected with the negative control siRNA. Dots represent the relative TBK1 pS172 levels of each experiment and each color indicates one experiment. Lines show the mean of the three independent experiments.

AMEF *fip200* KO**B**MEF *fip200* KO + vector

Supplementary Figure S2: TBK1 aggregates partially co-localize with LC3 but do not localize at the Golgi, the ER or the ERGIC. (A) *fip200* KO MEFs transfected with empty vector or cDNA encoding FIP200 Δ CT were fixed in 100% MeOH and immunostained for TBK1 and LC3. (B) Empty vector-transfected *fip200* KO MEFs were fixed in 100% MeOH and immunostained for TBK1 in combination with either ERGIC, ERp72, or Golgin97. Histograms represent pixel intensities of the areas indicated by the respective dashed red arrow shown in the insets.



Supplementary Figure S3: TBK1 aggregates do not co-localize with STING or TRIF. (A) *fip200* KO MEFs transfected with empty vector or cDNA encoding FIP200 Δ CT were fixed in 100% MeOH and immunostained for TBK1 and STING. (B) MEFs described in (A) were fixed in 4% PFA and immunostained for TBK1 pS172 and TRIF. Histograms represent pixel intensities of the areas indicated by the respective dashed red arrow shown in the insets.



Supplementary Figure S4: FIP200 controls TBK1 activation threshold at SQSTM1/p62-positive condensates. In FIP200-expressing cells (left), TBK1 activation at SQSTM1/p62-positive aggregates is kept at basal levels. TBK1-dependent phosphorylation of SQSTM1/p62 at Ser403 presumably contributes to the efficient engulfment of protein aggregates. In cells deficient for FIP200 or expressing a C-terminally truncated variant of FIP200 (right), TBK1 auto-transphosphorylation and TBK1-dependent phosphorylation of SQSTM1/p62 is increased, likely contributing to the increased formation of insoluble protein aggregates. FIP200, focal adhesion kinase (FAK)-interacting protein of 200 kDa; SQSTM1/p62, sequestosome 1; TAX1BP1, Tax1 binding protein 1; TBK1, TANK-binding kinase 1; TBKBP1/SINTBAD, TBK1 binding protein 1